OCEANIC NITROUS OXIDE DISTRIBUTION AND PRODUCTION
A STABLE ISOTOPIC APPROACH

Muhammed Nayeem Mullungal

A thesis submitted for the degree of
DOCTOR OF PHILOSOPHY
UNIVERSITY OF OTAGO

Dunedin, New Zealand.

June 2017

Abstract

Nitrous oxide (N_2O) is a biogenic trace gas that has a significant role in global climate change, stratospheric chemistry and in the ocean nitrogen cycle. Its concentration in the ambient air has increased to the current value of 330 ppbv from 275 ppbv (pre-industrial period). The oceans are thought to account for 25-30 % of global N_2O emissions. However, the biogeochemical pathways resulting in its formation are not well known. Two microbial pathways, nitrification and denitrification, dominate N_2O production with their N_2O source product varying with oxygen availability. There is a paucity of N_2O data for many oceanic regions, and hence the global budget of N_2O is not fully closed. This thesis describes the N_2O distribution and its changes with AOU and nutrients along the selected regions in the Southwest Pacific Ocean (SWP) and Northeastern Arabian Sea (NEAS).

The comparison of the oxygen minimum zones (OMZs) in NEAS with minimum oxygen concentrations of > 10 μM and the SWP Ocean with minimum oxygen concentrations > 130 μM reveals significant differences in the N_2O cycling of both the regions, which is reflected in N_2O saturations, dual isotope ratios and isotopomers.

At coastal Otago Continental Shelf, N_2O distribution was the highest during spring; [N_2O], and saturations varied with MSTW > Neritic > SASW. In late autumn, an inverse trend in the distribution of N_2O was observed. At the surface, saturations varied between 110 % - 130 % in spring, and it decreased below 100 % during autumn. The results indicate that the Otago coastal region is a source of atmospheric N_2O. At the SWP open ocean stations, the minimum [N_2O] was always found in the surface layer, with average N_2O saturation values of 101 ± 1 % (winter), and 103 ± 1 % (spring) in the STSW, and 102.5 ± 0.5 % in the SASW. These values are similar to the global oceanic mean values (103.5%), derived by Bange *et al.* (2008).

At the NAES, surface mixed layers were poorly oxygenated (20 – 120 μM) relative to the SWP, with a strong oxygen minimum zone (OMZ) present below the mixed layer (25 - 1000 m). The N_2O water column distribution showed a single peak structure, with only one broad maximum at mid-depths. The surface saturations are 2 - 4 times higher than the SWP saturations at NAES. N_2O sea to air (F_{s-a}) fluxes indicates that the SWP and NEAS is

a source of N_2O to the atmosphere, though the extent of the fluxes varies regionally and seasonally.

In SWP, below the surface mixed layer [N_2O] varied with depth. In the upper thermocline [DO] decreased below that of the surface water whereas [N_2O] increased. Beneath the upper thermocline [N_2O] in the AAIW increased coincident with an increase in [DO] except at the subantarctic SWP. The maximum [N_2O] was found in the CPDW where DO was the minimum. At NEAS N_2O saturation were 220 - 630 % in intermediate water (ICW) and 330-390 % in AAIW.

A [DO] *vs* [N_2O] inverse relationship and ΔN_2O *vs* AOU positive correlation observed in the SWP as evidence for nitrification as the major formation pathway of N_2O. Positive correlations between ΔN_2O and nitrate (NO_3^-) provides further evidence for the nitrification process being the primary source of N_2O. For the NAES, ΔN_2O vs AOU and ΔN_2O vs nitrate suggests formation primarily via nitrification.

Stable isotopes and isotopomers of N_2O provided more insight into the N_2O formation pathways. The depletions in $\delta\,^{15}N_{bulk}$ and $\delta^{18}O$ in the SWP surface mixed layer, minima in the subsurface, and enrichment at the bottom suggest nitrification, except in the subsurface 200-500 m. The NAES dual isotopes reflect the major role of nitrification especially in the surface and in the OMZ. These different oxygen isotope results suggest oxidation of hydroxylamine (NH_2OH) followed by nitric oxide (NO) oxidation (during nitrification) at all depths in the SWP (except at 200-500 m) and NEAS. To examine the formation processes, $\Delta^{18}O$ was also determined ($\delta^{18}O_{N2O}$ - $\delta^{18}O$ of DO). $\Delta^{18}O$ was almost constant at all depths for SWP waters, while it showed a minimum (roughly 9 ‰ lower than waters above and below) at 200-500 m except in subantarctic SWP waters. This observation proves the additional contribution to N_2O source from nitrifier denitrification at 200-500m in the SWP (except in the subantarctic) and throughout the OMZ in the NEAS. The intramolecular distribution of isotopomers of ^{15}N in N_2O and S.P were also supportive of these findings. ^{15}N isotope labelled incubation experiments using $^{15}NH_4Cl$ and $K^{15}NO_3$ for the selected stations of Otago Continental Shelf transect also indicated that ammonium oxidation is the major process responsible for the production of N_2O.

Acknowledgement

I would like to express my special thanks to my advisors Professor Russell D Frew, Dr Robert Van Hale and Professor Cliff S Law. You have been tremendous supervisors for me. I would like to thank you for encouraging my research and for allowing me to grow as a research scientist. Your advice on both research as well as on my career have been priceless. The support and care you provided as supervisors especially during the second half of my research voyage when the boat was experiencing a lot of hardships will remain immortal.

I am very lucky to have been able to study the isotopes under Rob, who always provided helpful advice even in the most frantic of times. Rob has not only advised me on a daily basis but has been my mentor and research assistant. The care and support you and Hazel provided me during the very first week in New Zealand, or later during the demise of my father is priceless.

I am very grateful to Russell for always pushing me to my fullest potential and for also providing support (even when he was at IAEA, Austria) in all of my research pursuits. I am truly privileged to have had such a great supervision during my PhD, and have gained a lot of professional and personal experiences.

This research wouldn't have been possible without Cliff's valuable advice. The time we have had at NIWA or Otago were the key to success on many occasions. I also want to thank you for your brilliant comments and suggestions.

Special thanks to Professor Philip Boyd for being my supervisor when Russell was away and also for helping me to get samples from the GEOTRACES and Bloom 2 cruises. I am grateful to Dr Scott Nodder for giving me an opportunity to take part in NIWA Biophysical Mooring Cruise Program and to collect the samples.

Dr Kim Currie (NIWA) was the leader of all my cruises aboard the *Polaris II*. I could not have completed sampling without her help, especially during those days with terrible weather. Thanks to Bill Dixon and Phil Heseltine, the captain and crewman of the RV *Polaris II*. My sincere gratitude goes to Andrew Marriner (NIWA) who helped me a lot during my NIWA, Wellington visits and also Bloom 2 sampling. I am thankful to Yoshitaka Uchida at the National Institute for Agro-Environmental Sciences (NIAES), Japan and Brian Popp, the USA for their

support in the isotope analysis. Thanks a lot to Murray Smith (NIWA) for the wind speed data. Thanks to the Department of Botany for conducting nutrient analyses for me.

I would like to thank Dr Kurian Sajan (CUSAT, India) and Dr Sherine Cubalio, Chief scientist, Sagar Sampada, 2012 Monsoon Cruise (CMLRE, India) for the priceless supports during the Arabian Sea research cruise. Also, would like to thank Manish T P for his services during the Indian cruise and post-cruise data collection.

The opportunity to study in New Zealand, to attend SOLAS Summer School, Xiamen, China, to participate in the ISOECOL Conference, Brest, France, to be a part of AGU Conference, San Francisco, USA and to conduct sampling in Arabian Sea, would never have been possible without the funding provided by the University of Otago Divisional Postgraduate Scholarship, support from the Department of Chemistry, funding provided by the New Zealand Marine Sciences Society and SOLAS. Let me also show my gratitude to NIWA for their assistance and guidance to support my research.

Thanks to all my friends within the Water World, Isotrace research groups and the Department of Chemistry (past and present). I also want to thank the administrative, technical, and general staff within the department for always being helpful and cheerful.

A special thanks to my family. Words cannot express how grateful I am to my mother, father, brother and sister for all of the sacrifices that you've made on my behalf. Your prayer for me was what sustained me thus far. At the end, I would like to express appreciation to my beloved wife and our new family member four months old little Alaan. I would not have been able to complete this thesis without their continuous love and encouragement.

Dedication

This thesis is dedicated in memory of my father, Erassutty Mullungal. I miss him every day and his love and life continues to inspire me today.

.

Table of Contents

List of Figures

List of Tables

Chapter 1

Introduction

1.1. Overview

The heat-trapping, which keeps the surface of our planet warm enough to sustain us, is called the natural greenhouse effect. The trace gases responsible are known as greenhouse gases. These gases are responsible for maintaining the current mean temperature of the Earth's surface at 15°C. In the absence of greenhouse gases, the Earth's surface would have an average temperature of -18 °C (Intergovernmental Panel on Climate Change IPCC, 2001). Though the three gases nitrogen (78.09 %), oxygen (20.95%), and argon (0.93%) make up 99.9%, by volume, of the Earth's atmosphere the greenhouse gases have a significant role in climate because of their high radiative forcing (Rodhe 1990; Whiting and Chanton 2001; Ramaswamy *et al*., 2001).

Water vapour is the principal greenhouse gas and accounts for nearly 60 % of the greenhouse effect. Besides water vapour, the IPCC's Fourth Assessment Report differentiates four principal greenhouse gases (Forster *et al*., 2007). They are carbon dioxide (CO_2), methane (CH_4), nitrous oxide (N_2O) and the halocarbons. The efficiency of the different greenhouse gases is assessed using the concept of Global Warming Potentials (GWP). The GWP is defined as the ratio of the time-integrated radiative forcing from a pulse emission of 1 kg of some compound X relative to that of 1 kg of the reference gas CO_2 (Houghton *et al*., 1990). On a molar basis, CH_4 and N_2O have 23 and 296-340 times higher global warming potential (GWP) relative to CO_2 (Jain *et al*., 2001; IPCC., 2007). Modified (higher) concentrations of these gases in the Earth's atmosphere will lead to increased trapping of infrared radiation. As a result, the troposphere will get warm, changing the weather and climate. This suggests that the changes in the weather will add to the natural greenhouse effect, producing an enhanced or induced greenhouse effect.

Although climate change is still a hot topic of scientific and political debate, almost all the scientists now accept the argument that the anthropogenic or enhanced greenhouse effect is real. The majority of the observed warming over the last 50 years is likely to have been due to the increase in greenhouse gas concentrations (IPCC., 2001). The atmospheric concentrations of the principal greenhouse gases have increased significantly since the industrial revolution (Table 1.1). Global trace gas concentrations before the industrial revolution (1750) were relatively unaffected by anthropogenic activities, IPCC, 2001 (Table 1.1 and Figure 1.1). Fossil fuel burning, nitrogenous fertilizers, deforestation and rice fields are identified as major anthropogenic sources of greenhouse gases in the atmosphere (Forster *et al*., 2007). The global average concentrations of CO_2, CH_4 and N_2O, increased from the pre-industrial period to the current year (IPCC, 2001; IPCC., 2013; NOAA., 2016).

Table 1.1: Global N_2O Concentrations and climatic importance; Source: IPCC, 2001, 2013 and NOAA-Mauna Loa Observatory data 2016.

Trace gas	Pre-1750 concentration	Tropospheric concentration (2016)	% Increase	GWP (100 year)	Atmospheric life time(years)
CO_2 (ppmv)	280	403	(31 ± 4 %)	1	5-200
CH_4 (ppmv)	0.730	1.85	(151 ± 25%)	23	12
N_2O (ppbv)	270	329	(20 %)	296-340	114

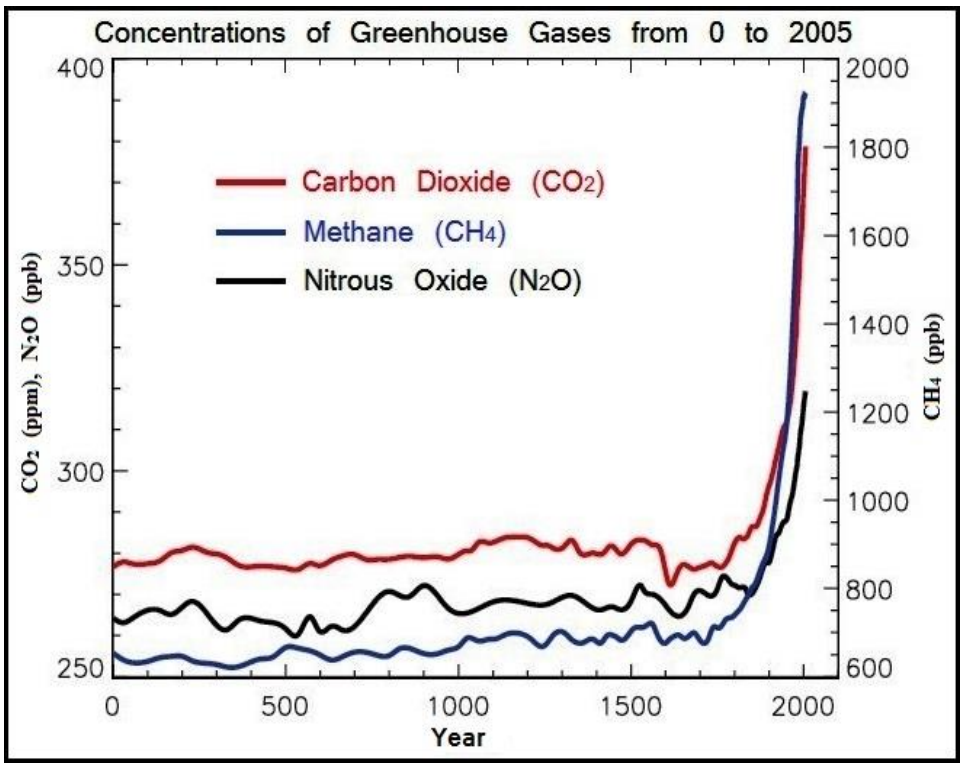

Figure 1.1: Global atmospheric trace gas concentrations, IPCC 2013.

Greenhouse gases (GHG) are also emitted naturally from various sources, including water bodies (IPCC, 2001). The contribution of marine sources, including open oceans, estuaries and coastal zones to the global budgets of trace gases is still uncertain due to the spatial and temporal variations and limited database available especially from tropical regions which can be subject to intense anthropogenic input (IPCC, 2001). The coastal ocean may act as a source or sink for atmospheric species of importance to global biogeochemical cycles and climate (Naqvi *et al*., 2010). Coastal zones can influence atmospheric chemistry through the transfer of biogenic trace gases and sea salt aerosols to the atmosphere which can influence the Earth's radiative balance. Biogeochemical processes that influence coastal regions include riverine and groundwater inputs, atmospheric inputs, benthic interactions of nutrients (including denitrification), suspension of sediments, upwelling, and sediment burial. Rivers carry terrestrial soil particles, litters from land and domestic loads (sewage) (Wollast, 1983; Meybeck, 1993; Abril *et al*., 2002) and intensively exchange nutrients, inorganic and organic carbon in the open ocean across marginal boundaries (Thomas *et al*., 2004).

1.2. Nitrous oxide (N_2O) and its climatological importance

Nitrous oxide (N_2O, dinitrogen monoxide) is a colourless, non-toxic gas with an asymmetrical linear structure (N=N=O). It has a boiling point of -88.5 °C, molecular weight of 44.01 $gmol^{-1}$ and is commonly known as "laughing gas". The physical properties of this molecule, like solubility and diffusion in water, are similar to that of CO_2. After molecular nitrogen, it is the most abundant nitrogen compound in the atmosphere, and its concentration in the atmosphere is currently at trace levels.

N_2O has an average atmospheric lifetime of about 114 years (IPCC, 2007) and generates a significant radiative forcing (Rodhe 1990). When century-long effects are considered, the global warming potential of N_2O is 296-340 times greater than that of CO_2 on a molecular basis (Albritton *et al*., 1996; Ramaswamy *et al*., 2001; Jain *et al*., 2001; IPCC, 2001 and 2007). Although N_2O only accounts for around 0.03 % of the total greenhouse gas emissions (Bates *et al*., 2008), when considered in terms of GWP, N_2O accounts for approximately 10 % of GWP (IPCC, 2007).

In 1970, Paul Crutzen identified the importance of N_2O for the atmospheric chemistry. Due to a relatively long atmospheric lifetime of 114 years (Forster *et al*., 2007), N_2O can mix up to the stratosphere, where it acts as the major source of nitric oxide radicals (NO). NO radicals are involved in one of the primary ozone (O_3) reaction cycles (Forster *et al*., 2007) resulting in ozone depletion (Ravisankara *et al*., 2009). Therefore, N_2O influences the Earth's climate both directly and indirectly by acting as a greenhouse gas and destructor of ozone or precursor of ozone depletion in the stratosphere.

Since the industrial revolution, the concentration of N_2O in the atmosphere has increased by 18 - 20 % (Forster *et al*., 2007; Bates *et al*., 2008, IPCC 2013). The historical development of atmospheric N_2O is illustrated in Figure 1.1 and 1.2. The Northern Hemisphere has a higher N_2O concentration than the Southern Hemisphere since the majority of the sources of atmospheric N_2O are located in the Northern Hemisphere (Prinn *et al*., 2000; Prather *et al*., 2001; Khalil *et al*., 2002). As all other GHG's changing the concentration of N_2O in the atmosphere both by natural or anthropogenic forces will affect the climate by altering the radiative balance of the Earth. Based on its radiative forcing, N_2O is ranked fourth among long-lived greenhouse gases. The atmospheric

N_2O concentration shows a continuing increase at a constant rate of 0.2 to 0.3 % annually (0.7- 0.8 $ppby^{-1}$) (Khalil and Rasmussen, 1992; Bates *et al*., 2008; Montzka *et al*., 2011). The atmospheric concentrations of important halocarbons are slowly decreasing so N_2O is expected to take third place in this ranking (Forster *et al*., 2007) as the contribution of N_2O to both the greenhouse effect and ozone depletion becomes more pronounced in the twenty-first century (IPCC, 2001; Ravisankara *et al*., 2009). Human activities enhance the N_2O budget through direct emissions and also influence N_2O production in both terrestrial and aquatic ecosystems (Mosier *et al*., 1998).

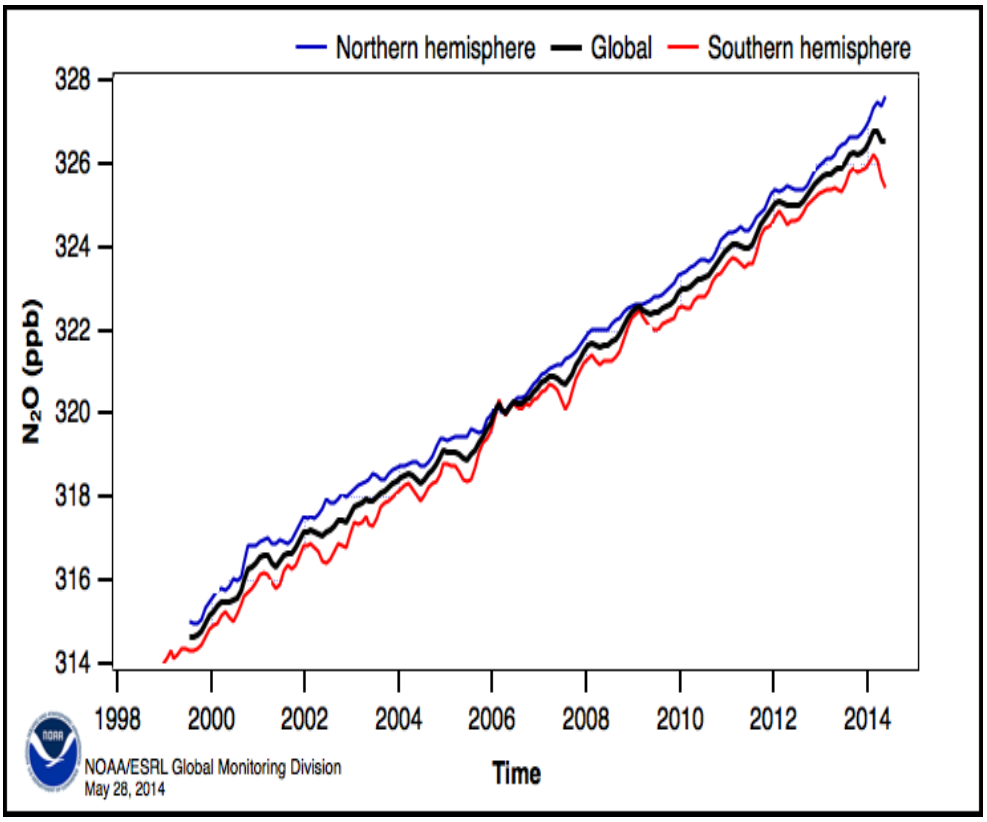

Figure 1.2: Increase in global and hemispheric atmospheric N_2O measured at Mauna Loa Observatory, NOAA, USA (1998-2014).

1.3. Global N_2O: Sources and sinks

The dominant natural sources of N_2O are soils and oceans. The most important anthropogenic sources are agricultural and industrial activities. The main pathways of N loss from soils are erosion, leaching, ammonia volatilization, ammonia oxidation and denitrification through which N_2O will be both produced and consumed. The stratosphere also acts as a sink for N_2O. Approximately, 60 % of total global N_2O emissions is thought to be released from soils (Skiba and Smith, 2000; Smith *et al*., 2008), with oceans contributing the other one-third of emissions (Bange *et al*., 2010). Anthropogenic sources of N_2O include the production of nitric acid, power plants and vehicle emissions (IPCC, 2001). The two pathways of the nitrogen cycle, nitrification and denitrification are the major processes responsible for N_2O production in marine (Seitzinger, 1990; Suntharalingam and Sarmiento, 2000; Codispoti *et al*., 2005) as well as terrestrial environments (Bouwman, 1996). Figure 1.3 illustrates the proportions of total global nitrous oxide emitted by various sources, including human activities.

The known sources of N_2O, with the estimates of their emission rates and ranges, are listed (Table 1.2). It is challenging to assess total global emissions from individual sources that vary greatly over small spatial and temporal scales. Total annual N_2O global emissions of 16.4 TgN y^{-1} have been calculated from the N_2O global sink strength (IPCC, 2001). In current budgets global sinks, N_2O exceed sources by 40 % (Mathews, 1994). According to the latest estimates, the global emissions vary widely from 8.1 – 30.7 TgN y^{-1} (IPCC, 2013). This budgetary discrepancy in the sources and sinks implies that there exist some unknown sources of N_2O. It can also be due to the underestimation of existing sources. Oceans are thought to be net sources of atmospheric N_2O. However depending upon the seasonal changes and resulting temperature induced solubility variations some oceanic regions, such as the North Atlantic, may act as a temporary source or sink (Nevison *et al*., 2003). Areas of deep convection are also temporary sinks for N_2O (Bange and Andreae, 1999; Walter *et al*., 2006). Anoxic regions are identified as permanent sinks for N_2O since in those regions the prevailing microbial process is denitrification.

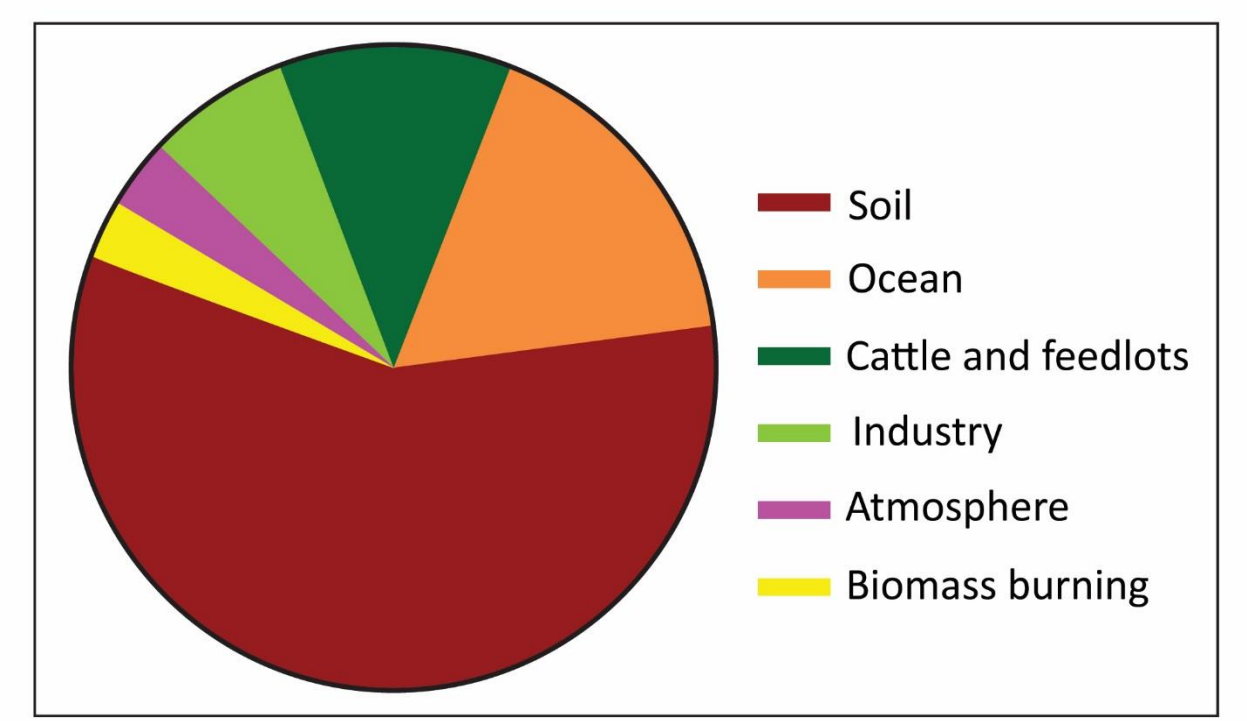

Figure 1.3: Proportions of total global N_2O emitted by natural sources and anthropogenic activities (Metz *et al*., 2007).

Table 1.2: Global N_2O estimates (in TgN yr-1) from different sources.*SAR Second Assessment Report, IPCC (1996); #TAR Third Assessment Report, IPCC (2001).

References	**Mosier *et al* (1998) Kroeze *et al* (1999)**		**Oliver *et al* (1998)**		**SAR***	**TAR#**
Base year	**1994**	**range**	**1990**	**range**	**1980s**	**1990s**
Sources						
Ocean	3.0	1-5	3.6	2.8-5.7	3	
Atmosphere (NH_3 oxidation)	0.6	0.3 -1.2	0.6	0.3 -1.2		
Wet forest	3.0	2.2 -3.7			3	
Dry savannas	1.0	0.5 -2.0			1	
Temperate soils						

Forests	1.0	1.0-2.0			1	
Grasslands	1.0	0.5 -2.0			1	
All soils			6.6	3.3 -9.9		
Natural sub-total	9.6	4.6 -15.9	10.8	6.4 -16.8	9	
Agricultural soils	4.2	0.6 -14.8	1.9	0.7 -4.3	3.5	
Biomass burning	0.5	0.2 -1.0	0.5	0.2 -0.8	0.5	
Industrial sources	1.3	0.7 -1.8	0.7	0.2 -1.1	1.3	
Cattle and feedlots	2.1	0.6 -3.1	1.0	0.2 -2.0	0.4	
Anthropogenic Sub-total	8.1	2.1 -20.7	4.1	1.3 -7.7	5.7	6.9
Total sources	17.7	6.7 - 36.6	14.9	7.7 - 24.5	14.7	
Imbalance (trend)	3.9	3.1 -4.7			3.9	3.8
Total sinks (stratospheric)	12.3	9 -16			12.3	12.6
Implied total source	16.2				16.2	16.4

1.4. N_2O in the oceans

The oceans play an essential role in the global N_2O distribution and atmospheric N_2O budget (Bange, 2006). Hence the role of N_2O in the ocean chemistry and its formation pathways during the nitrogen cycle has been studied widely over the last three decades. The ocean is considered as the second largest natural source of N_2O to the atmosphere (Denman *et al*., 2007) (Table 1.2). Total marine contribution to the global source of tropospheric N_2O estimates ranges from 17 % to 35 % (Cline *et al*., 1987; Mosier *et al*., 1998; Kroeze *et al*., 1999; Naqvi *et al*., 2010, Freing *et al*., 2012; IPCC 2013). Tropical ecosystems are currently an important source of N_2O (and NO). Industrial activities and the addition of fertiliser will generate NO and N_2O fluxes that are 10 to 100 times greater than the same N-limited ecosystems (Hall and Matson., 1999). Large-scale

additions of fixed nitrogen to the natural inventory of bio-available N as a result of industrial and agricultural activities has fuelled an increase in nitrogen turnover as well as N_2O production (Gruber and Galloway., 2008). Along with other human activities, it will increase the atmospheric N_2O inventory.

1.4.1. Oceanic pathways of N_2O Production: Nitrogen cycle

All biological organisms need nitrogen to synthesize amino acids, proteins, nucleic acids and many additional cofactors. This nitrogen originates from the atmosphere via N fixation to where it is ultimately returned as the gas, N_2. Due to the presence of one of the most stable chemical triple bond in N_2 that has a very high energy barrier towards breaking the bond demand the use of highly effective catalysts, or enzymes, to speed up the chemical processes. The conversion of N_2 to bio-available N forms such as nitrate (NO_3^-) and ammonium (NH_4^+) and subsequent transformations between these during nitrogen fixation are central to the functioning of the nitrogen cycle. The marine nitrogen cycle is principally driven by organisms, of which the vast majority are microbes. The nitrogen cycle involves a series of biological processes such as; nitrogen fixation, nitrification, and Dissimilatory Nitrate Reduction to Ammonia (DNRA, or nitrate ammonification), anaerobic ammonia oxidation (anammox) and denitrification. The oceans are the most extensive planetary reservoir of bio-available nitrate (NO_3^-), which is the largest marine source of fixed N (Owens N P J., 1993). Increasing anthropogenic activities tends to transform the global nitrogen cycle (Galloway *et al*., 2008). Much of this human-induced nitrogen will cause an increase in freshwater and coastal water nitrate levels which will lead to increased N_2O production (Duce *et al*., 2008).

The dissolved oxygen concentration in the water column controls mainly the nitrogen transformations within the oceanic N cycle. N_2O is microbially produced through two major microbial processes, nitrification and denitrification (Seitzinger and Kroeze., 1998; Naqvi *et al*., 2010; Bange *et al*., 2010b). In oxic conditions, it is mainly nitrification during which N_2O is evolved as a by-product that accumulates in the sub-surface and deep layers of the water column whereas a consumption of N_2O is not observed (Bange H W., 2008). In suboxic conditions, N_2O will be formed as an intermediate during denitrification. In anoxic regions, N_2O will be mainly consumed by denitrification, and during anammox it becomes dominant (Canfield *et al*., 2010). During denitrification and anammox fixed nitrogen is respired to N_2, with different pathways for

both processes. However, the exact mechanism of nitrification and denitrification, as well as their individual contributions towards the global flux, still remains unclear due to the lack of studies and available data (Codispoti *et al*., 2001; Popp *et al*., 2002; Punshon and Moore, 2004; Yamagishi *et al*., 2005). Figure 1.7 shows the various steps and transformations involved in the nitrogen cycle including the nitrous oxide formation pathways.

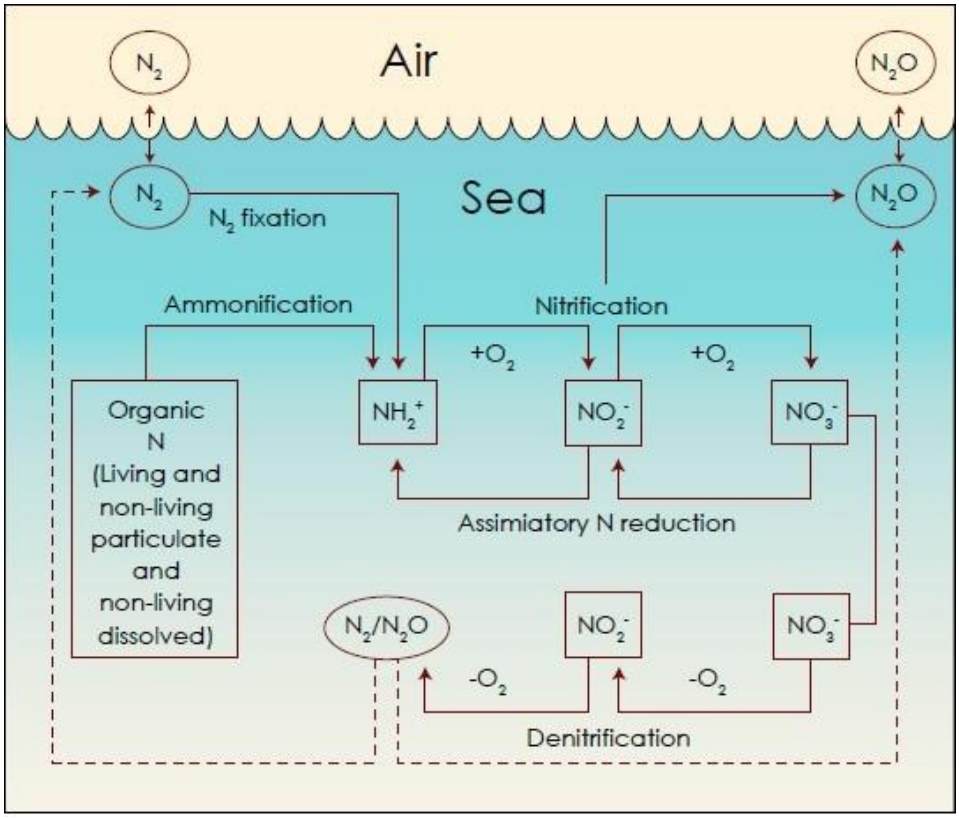

Figure 1.4: Simplified sketch of the oceanic nitrogen cycle, Source: Karl *et al*., 2002.

1.4.1.1 Nitrification

Nitrification is the primary process by which N_2O is produced in most of the ocean and was reported first by Yoshinari in 1976. It involves the oxidation of ammonium (NH_4^+) to nitrate (NO_3^-) which involves hydroxylamine (NH_2OH) and nitrite (NO_2^-) as intermediates (Ostrom *et al*., 2000). It has been suggested that these intermediate molecules are the major precursors of N_2O during nitrification. (Ritchie and Nicholas, 1972; Kim and Craig, 1990; Naqvi and Noronha, 1991). N_2O is produced as a by-product of nitrification (Yoshida and Alexander., 1970; Goreau *et al*., 1980; Frame and Casciotti., 2010). Nitrification is carried out both by heterotrophic and

autotrophic bacteria, although the latter is thought to be of higher importance (Bremnar and Blackmer., 1981) and use the classical nitrification pathway. Recent studies indicate that archaea also contribute to the oceanic N_2O production through nitrification (Loscher *et al*., 2012). The third nitrification pathway is called nitrifier–denitrification pathway which is predominant in low-oxygen conditions (Poth and Focht., 1985; Arp and Stein., 2003). The exact mechanism of the N_2O formation through nitrification is not yet clear. However, a series of mechanisms have been proposed and are explained below (Ritchie and Nicholson., 1972; Groffman., 1991; Naqvi and Noronha., 1991).

1.4.1.1.1. Classical Nitrification (Bacterial Nitrification)

Autotrophic nitrification is considered as the final step of remineralization of nitrogen-containing organic matter. It is a two-step process involving AOB (Ammonium Oxidizing Bacteria) and NOB (Nitrite Oxidizing Bacteria) and occurs in oxygenated ocean waters and sediments (Kaplan and Wofsy., 1985) as shown below.

Step 1: $2\,NH_4^+ \rightarrow 2\,NH_2OH \rightarrow 2(NOH) \rightarrow 2NO \rightarrow 2NO_2^-$

Pathway 1 ↓ N_2O Pathway 2 ↓ N_2O

Step 2: $NO_2^- \rightarrow NO_3^-$ (Ostrom *et al* 2000)

N_2O is an obligate intermediate during ammonium oxidation. The first step is carried out by *Nitrosomonas* spp and *Nitrosospira* spp, which are ammonia-oxidising bacteria (AOB). AOB produce N_2O during autotrophic process via $NH_2OH \rightarrow N_2O$ (pathway 1) and $NO \rightarrow N_2O$ (pathway 2) (Ostrom *et al*., 2000; Arp and Stein., 2003; Stein and Yung., 2003). The third pathway is part of the nitrifier-denitrification process. In the oceans, nitrification-denitrification occur during nitrification by $NO_2^- \rightarrow NO \rightarrow N_2O$, when there is reduced oxygen conditions (Poth and Focht., 1985; Wrage *et al*., 2001; Shaw *et al*., 2006) or due to the presence of nitrite (pathway 3) (Frame and Casciotti., 2010).

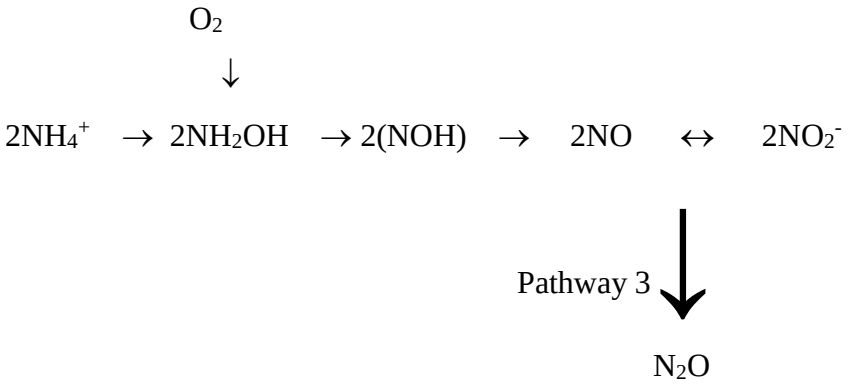

An alternate pathway is predicted to produce N_2O through the heterotrophic nitrification process during aerobic denitrification. Heterotrophic nitrification is performed using different enzymes to those of autotrophic production. Heterotrophic nitrification proceeds through the same mechanism to that of nitrifier-denitrification ($NO_2^- \rightarrow NO \rightarrow N_2O$). (Shoda. M., 2017)

Nitrification is generally an aerobic process. However, studies (Goreau *et al*., 1980, De Bie *et al*., 2002) indicate that the production of N_2O is enhanced under suboxic conditions. The second NO_2^- oxidation step is strong evidence for nitrification as a source for N_2O, when a negative correlation between N_2O and O_2, and a positive correlation between N_2O and NO_3^- is observed (Yoshinari., 1976; Cohen and Gordon., 1979; Naqvi *et al*., 1994; de Wilde and Helder., 1997; Patra *et al*., 1999; Oudot *et al*., 2002; Nevison *et al*., 2003).

1.4.1.1.2. Archaeal nitrification

Archaeal nitrification is an aerobic process which involves the same nitrogen transformation processes as that of autotrophic nitrification which involves a two-step process. Nevertheless, there are significant differences in the structure and regulation of some enzymes involved in this process (Cabello *et al*., 2004). During the first step of nitrification in the former process, nitrifiers are Proteobacteria, while it will be Ammonia-Oxidizing Archaea (AOA) in archaeal nitrification that has only been recently discovered. Schleper *et al*. (2005) detected genes of NH_3 oxidizing Archaea in environmental metagenomic libraries. It was later confirmed by Konnecke *et al.* (2005) with the cultivation of the AOA strains that oxidise NH_3 to NO_2^-. It now seems likely that AOA make up a significant fraction of prokaryotic cells (Archaean group crenarchaeotal) in the marine environment and AOA are more abundant than AOB (Wuchter *et al*., 2006). The enzyme ammonia monooxygenase similar to that of Proteobacteria has been found in archaea (Treusch *et al*., 2005; Nicol and Schleper., 2006). Archaea capable of ammonia oxidation have been detected in various oceanic regions throughout the water column and in sediments (Wuchter *et al*., 2006; Lam *et al*., 2009; Santoro *et al*., 2010; 2011). Martens-Habbena *et al.* in 2009 identified Archaea that can oxidize ammonia even under the oligotrophic conditions that dominate in large parts of the open ocean. Archaeal N_2O production is highly sensitive to dissolved O_2 concentration and production is optimal at lowest O_2 concentrations (Loscher *et al*., 2012). Therefore with the predicted expansion of OMZs in the future, in many parts of the ocean archaeal nitrification may lead to an enhanced N_2O production in the ocean (Stramma *et al*., 2008; Naqvi *et al*., 2010)

1.4.1.2. Denitrification

Denitrification is the reduction of combined nitrogen (eg, NO_3^-) to gaseous end products N_2O and N_2, by oxidising organic compounds using NO_3^- as the terminal electron acceptor agent in the absence of oxygen, as shown in Figure 1.4. It results in the loss of bio-available (fixed) nitrogen in the form of gaseous products such as N_2O and N_2 (Devol *et al*., 2008). Most of the denitrifiers are facultative anaerobes, and N_2O is produced as an obligate intermediate (Smith and Zimmerman., 1981; Knowles., 1982; Firestone and Davidson., 1989) and is also consumed during denitrification (Hattori *et al*., 1978).

The N- oxide reduction pathway during denitrification involves the sequential reduction of nitrate to nitrite, followed by nitric oxide, nitrous oxide and finally to nitrogen gas. This reduction is facilitated by four enzyme systems, nitrate reductase, nitrite reductase, nitric oxide reductase and nitrous oxide reductase (Zumft and Korner., 1997). The sequential processes involved in denitrification processes can be represented as follows:-

$$2NO_3^- \rightarrow 2NO_2^- \rightarrow 2NO \rightarrow N_2O \rightarrow N_2$$ (Payne., 1973; Knowles., 1982)

Water column suboxic and anoxic events are observed in the coastal areas, the Baltic Sea, the Black Sea, the OMZs of eastern tropical Pacific Ocean and in the Arabian Sea (Naqvi *et al*., 2010). The presence of oxygen will have an inhibitory influence on denitrification (Knowels., 1982; Payne., 1973). N_2O production and consumption by denitrification are known to become dominant as oxygen concentrations decrease to suboxic conditions, $0 < O_2 < 10$ µM (Codispoti *et al*., 1992; Codispoti *et al*., 2005). In anoxic environments, i.e. $O_2 = 0$ µM due to the presence of hydrogen sulphide and lack of nitrite, N_2O production will not take place. However, in oxic water column, the interior of sinking particles have been proposed as the sites for denitrification (Yoshinari and Koike., 1994). Denitrification is believed to influence climate both directly through N_2O production and indirectly via modification of the marine $NO_3^{-\,a}$ pool which has consequences for the biological CO_2 pump (Altabet *et al*., 2002; Falkowski, 1997).

In marine sediments, rates of denitrification, and the extent to which they are coupled are controlled by a combination of environmental variables. They are the direct supply of NO_3^- by diffusion from bottom waters (Christensen *et al.*, 1990; Law and Owens., 1990) and the oxygen status of the sediments (Owens., 1993). Sediments with high organic carbon content, typically estuarine and coastal sediments, have higher bacterial activity and lower oxygen concentrations and hence higher rates of denitrification than open ocean sediments with low organic carbon.

1.4.1.3. Anaerobic Ammonia Oxidation (Anammox)

Anaerobic ammonium oxidation (anammox) is a recently recognized (Strous *et al*., 1999) as a significant loss process of fixed nitrogen in the ocean (Francis *et al*., 2007; Devol, 2008) that mainly takes place in the open ocean denitrification zones (Codispoti *et al*., 2001). During

anammox molecular nitrogen is produced by reducing nitrite and oxidising ammonia. The mechanism can be summarised as shown below:-

$$NO_2^- + NH_4^+ \rightarrow N_2 + 2H_2O$$

Anammox is carried out by anaerobic chemoautotrophic bacteria that fix CO_2 using NO_2^- as the electron donor (Guven *et al*., 2005). The proposed mechanism of anammox involves hydrazine hydrolase, which catalyzes the combination of hydroxylamine and ammonium to form hydrazine. The hydrazine is subsequently oxidized to N_2 by a hydrazine-oxidizing enzyme (Jetten *et al*., 2003). N_2O is formed in only small amounts during nitric oxide detoxification ($NO_2 \rightarrow NO \rightarrow N_2O$). This NO oxidation is performed by the anammox bacterium *Kuenenia stuttgartiensis* as a side reaction of the anammox reaction (Kartal *et al*., 2007). Anammox has been found in the sub-oxic zones of eastern tropical South Pacific Ocean, in the upwelling off Namibia (Kuypers *et al*., 2005; Thamdrup *et al*., 2006; Hamersley *et al*., 2007) as well as in the central Baltic Sea (Hannig *et al*., 2007). The role of anammox in N_2O production is a topic of further investigation.

Of the various processes outlined above, denitrification and nitrification are the two principal bacterial pathways that alter fixed nitrogen from the biosphere by changing its oxidation state. There is a debate on whether the main process of N_2O formation is nitrification or denitrification (Naqvi *et al*., 2010). Both processes rely on N substrates, and the availability or lack of O_2. Both nitrification and denitrification are described as sources of N_2O production, while denitrification is a sink of N_2O in the water column, sediments and in suspended particles (Schropp and Schwarz., 1983; Seitzinger., 1990; Michotey and Bonin., 1997; Nevison *et al*., 2003; Codispoti *et al*., 2005) (Figure 1.4). However, most of the above studies agree that nitrification dominates the formation of oceanic N_2O.

1.4.2. Factors affecting oceanic N_2O concentration

1.4.2.1. Dissolved oxygen and N_2O

The relationship of dissolved oxygen with N_2O is already mentioned in the earlier sections. The influence of O_2 N_2O production can be explained regarding redox potentials. NO_3^- respiration

(denitrification) is favoured under reduced O_2 concentrations (Falkowski *et al*., 2008) and the enzyme involved in N_2O consumption, N_2O reductase, is sensitive to O_2 concentrations (Firestone and Tiedje., 1979). There is a lack of mechanistic explanation on the effect of O_2 concentrations on N_2O formation through nitrification is still lacking a mechanistic explanation. The [O_2] versus [N_2O] relationship is well documented in oceanic provinces with well-defined and persistent O_2 minima such as the Arabian Sea and the Eastern Tropical North Pacific (Cohen and Gordon., 1978; Codispoti and Christensen., 1985; Naqvi., 1987; Law and Owens., 1990; Upstill Goddard *et al*., 1999). Similar relationships are also observed in near-shore regions characterised by seasonal anoxia and high nitrogen loading (Howarth *et al*., 1996).

The variation in N_2O production with oxygen saturation is presented below (Figure 1.5). The Apparent oxygen utilization (AOU) is a measure of the amount of O_2 consumed during organic matter remineralization (oxidation) in the ocean and nitrification is part of the organic matter oxidation sequence. Plots of ΔN_2O versus AOU have been used to identify the prevailing formation and consumption processes of N_2O in the water column. Positive linear ΔN_2O/AOU relationships suggest that nitrification is the main N_2O formation process in most parts of the oceans ((Yoshinari., 1976; Cohen and Gordon., 1979). Moreover, in most oxic water columns, N_2O is positively correlated with dissolved nitrate (NO_3^-), the final product of nitrification (Yoshinari., 1976; Cohen and Gordon., 1979; Naqvi *et al*., 1994; de Wilde and Helder., 1997; Patra *et al*., 1999; Oudot *et al*., 2002; Nevison *et al*., 2003; Walter *et al*., 2006). Nevertheless, there are arguments against the interpretation of the linear ΔN_2O/AOU relationship as an indicator for N_2O formation via nitrification. ΔN_2O/AOU positive relationship may happen during denitrification as well (Yamagishi *et al*., 2005). A linear ΔN_2O/AOU relationship is observed in case of isopycnal mixing of water masses with different preformed N_2O and O_2 concentrations, which can mask the 'true' biological N_2O production (Nevison *et al*., 2003). A linear ΔN_2O/AOU relationship does not exist in sub-oxic and anoxic water. This is due to the complex processes leading to N_2O formation and consumption during denitrification and/or a coupling of nitrification and denitrification at the upper boundary of the sub-oxic zones (Bange *et al*., 2005; Walter *et al*., 2006b; Westley *et al*., 2006; Farías *et al*., 2007; Yamagishi, H., 2007). Under extreme oxygen depletion conditions, there is a net N_2O consumption leading to a decrease in its concentration. The threshold concentration of oxygen for the transition from the oxic to anoxic N cycling is not well defined yet. Several

studies found a co-occurrence of nitrification and denitrification or anammox under suboxic conditions (Bange *et al*., 2005; Farias *et al*., 2009). For more details see sections 1.2.5.

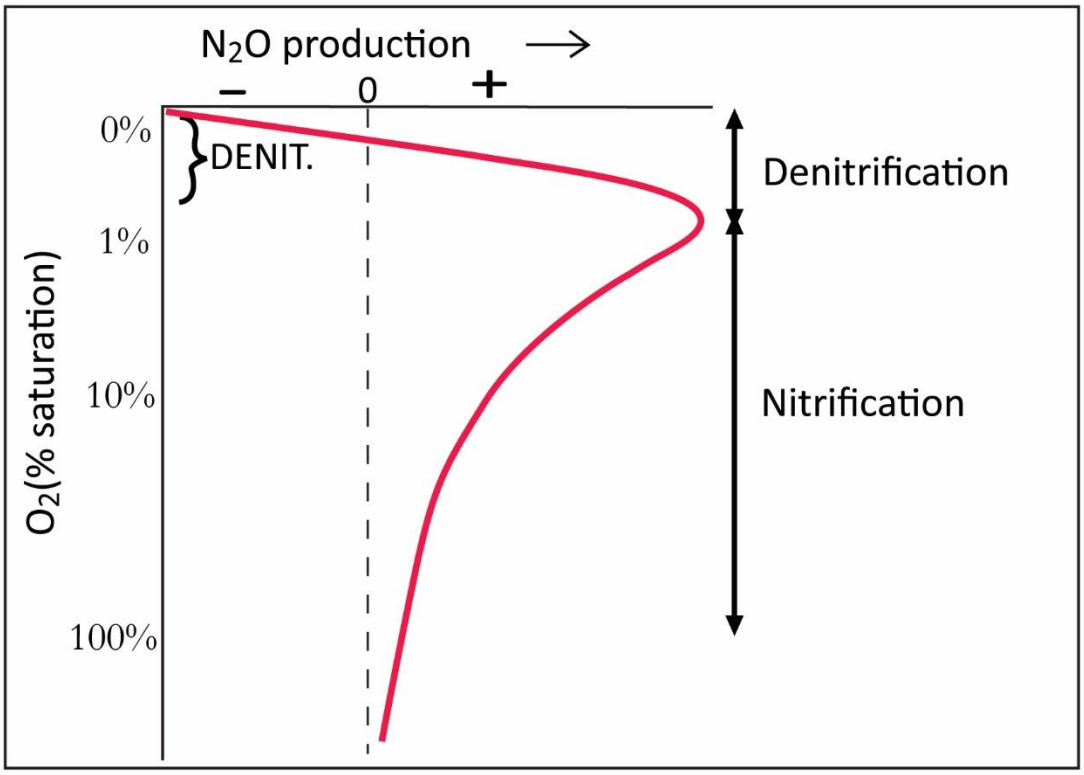

Figure 1.5: N_2O production *vs* O_2 saturation in the ocean: (Source: Bange *et al*., 2010)

1.4.2.2. Wind and N_2O

The release or uptake of N_2O across the ocean/atmosphere interface depends on physical processes such as wind-driven air-sea gas exchange and wind-driven oceanic circulation (Wanninkhof *et al*., 1992) or mixing processes such as coastal upwelling and storm events. A storm can deepen the mixed layer considerably, thereby entraining N_2O from the subsurface maximum to the surface layer, from where it escapes to the atmosphere (Naik *et al*., 2008). N_2O emissions triggered by high wind events may contribute significantly to both regional and global oceanic N_2O emissions (Patra *et al*., 2004; Bange *et al*., 2008). Thus any long-term changes of the atmospheric circulation

that alter wind speeds and the wind field patterns might lead to changes in N_2O emissions (Bange *et al*., 2010).

Other important factors include large-scale ocean fertilisation (Suntharalingam *et al*., 2000), atmospheric nitrogen deposition (Devol *et al*., 2008), increasing volume of hypoxic zones (Stramma *et al*., 2008), ocean warming, eutrophication of the coastal zones and ocean acidification.

1.4.3. N_2O distribution in the ocean

1.4.3.1. N_2O oceanic surface distribution and fluxes

Table 1.3: N_2O Fluxes from various oceanic environments, **a** Bange *et al.* (1996), **b** Seitzinger and Kroeze (1998), **c** de Wilde and de Bie (2000), d Capone (1996).

Sources	Percentage of the world ocean's Area	N_2O emission (Tg yr^{-1})	Percentage of the global oceanic N_2O
Estuaries	0.4	0.2-1.5[c]	10
Coastal Upwelling	0.2	3 .0-4.7[d]	35
Continental Shelves	17.9	0.6-2.7[a]	15[b]
Open Ocean	81.5	4.2-5.8[d]	40

The open oceans are the most significant contributors to the total oceanic N_2O flux; however, a study by Bange *et al.* (1996) showed that estuarine and coastal regions contribute a considerable portion of the global marine N_2O flux (Table 1.3). Estuaries are a globally significant source of N_2O, emitting approximately one-third of the total oceanic N_2O flux (Bange *et al*., 1996) and contribute significantly to the anthropogenic source (Mosier *et al*., 1998; Robinson *et al*., 1998;

Seitzinger and Kroeze., 1998). A detailed estimate of N_2O budget from various marine environments with their contribution to the global oceanic N_2O fluxes are presented in Table 1.3. There exists considerable uncertainty (up to 50 %) for the estimates of the global N_2O budget and is due to different methodological approaches, the use of different air-sea gas exchange parameterisations and differences in classifications for coastal areas (Bange *et al*., 2008).

Craig and Gordon conducted the first study on oceanic N_2O in the South Pacific Ocean in 1963. Junge and Hahn first quantified the oceanic source of nitrous oxide in the late 1960's. For the first time, Yoshinari reported the inverse relationship between dissolved N_2O and O_2 concentrations (Yoshinari, 1976). Global maps of [N_2O] in the upper 10 m of the world's oceans have been computed based on the extensive [N_2O] dataset collected by Weiss *et al* from 1977 to 1992 with additional data from Butler *et al* (1988) and Lobert *et al* (1996) (Nevison *et al*., 2004). In 1995 Nevison suggested that global average N_2O surface ocean saturation is 103.5 % which indicates the ocean as a net source of N_2O to the atmosphere. This saturation of the surface layer may vary with season (Nevison *et al*., 1995); however, present data are insufficient to depict this seasonal variability (Bange *et al*., 2010). In coastal areas, enhanced concentrations of N_2O are observed in upwelling areas and nitrogen-rich estuaries, but as for open ocean emissions, seasonal variation makes the flux values less certain (Bange *et al*., 2010). Positive N_2O anomalies (the N_2O anomaly, $\Delta pN_2O = pN_2O_{measured} - pN_2O_{equilibrium}$ indicate the ocean as a source of N_2O to the atmosphere). High anomalies are reported from a narrow band of coastal upwelling systems of Arabian Sea and off central Chile (Naqvi *et al.* 2005., Corenjo *et al*., 2006). The global distribution of N_2O surface anomalies is shown in Figure 1.6. The main feature of the maps in Figure 1.6 is enhanced N_2O anomalies in the equatorial upwelling regions of the eastern Pacific and Atlantic Oceans, along coastal upwelling regions such as along the west coasts of North and Central America, off Peru, off Northwest Africa and the North Western Indian Ocean (Arabian Sea). North and South Atlantic Ocean, the South Indian Ocean and the central gyres of the North and South Pacific Ocean exhibited N_2O anomalies close to zero.

Based on [N_2O] measurements on the shelf of the west coast of India, Naqvi *et al.* (2000) suggested increased N_2O emissions from shallow suboxic or anoxic coastal systems in the future. It is because the number of coastal regions with severely depleted dissolved oxygen concentrations is currently

increasing worldwide (UNEP., 2004; Diaz and Rosenberg., 2008). Eutrophication is also supposed to enhance the sedimentary N_2O formation significantly by denitrification (Seitzinger and Nixon., 1985). Future N_2O emissions may increase in shallow sub-oxic and anoxic coastal systems (including mangrove ecosystems) due to excessive nutrient inputs caused by continuing industrialization and intensification of agricultural activities arising from the anthropogenic activities.

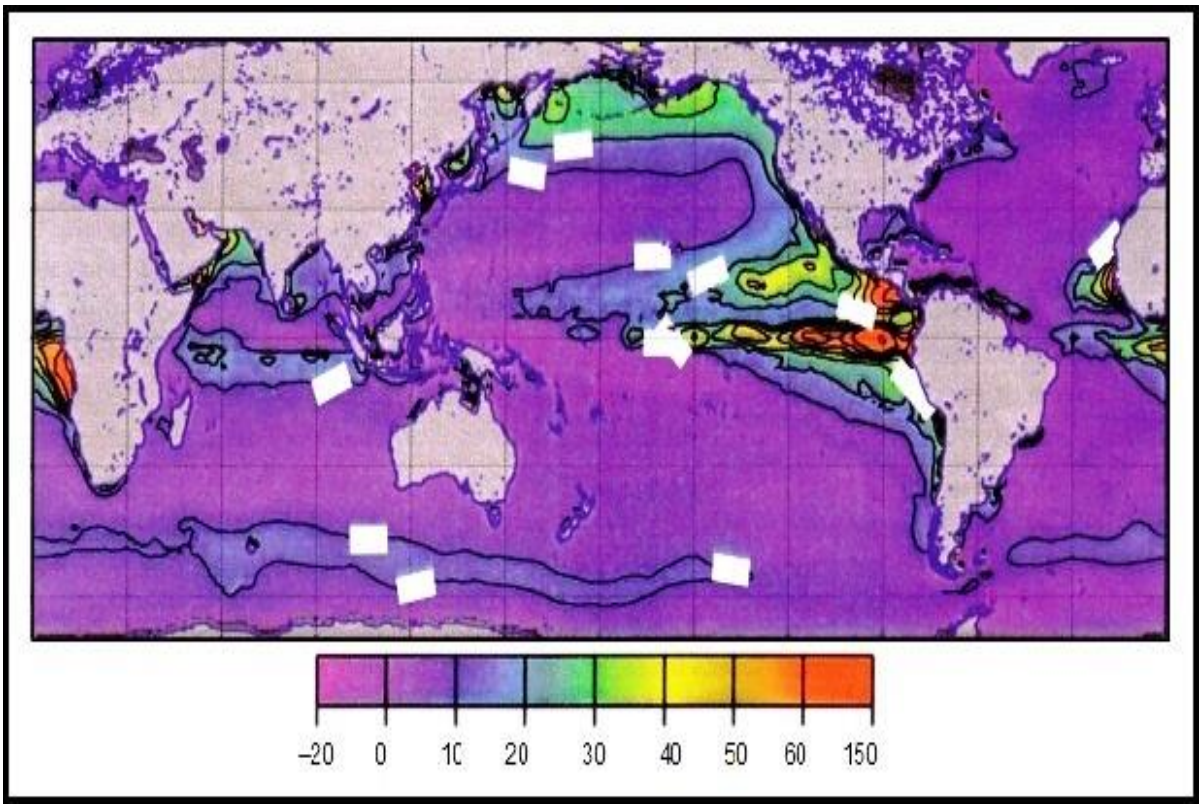

Figure 1.6: Δp N_2O (in natm) in the surface layer of the world's oceans, map by Suntharalingam and Sarmiento (2000). NB: The colour coding is non-linear.

In the open ocean, Stramma *et al.* (2008) recently showed that the oxygen minimum zones of the intermediate layers (300 to 700 m water depth) in various regions of the ocean are expanding and have been losing oxygen. These changes will also cause an addition of N_2O to the open ocean in the future. Nevertheless, N_2O accumulation at intermediate water depths in the open ocean will not lead to an immediate release of N_2O to the atmosphere since these waters are not in direct contact with the atmosphere. When the water masses are transported to the ocean surface, a major fraction of the accumulated N_2O will be subsequently released to the atmosphere. This emission

will depend upon the circulation and age of the water mass. A future increase in N_2O emissions may occur as an indirect result of the increased productivity through the increases in oceanic nitrogen or iron (Fe) (Fuhrman and Capone., 1991; Jin and Gruber., 2003; Duce *et al*., 2008), N_2 fixation (Karl., 1999) and riverine nutrient inputs (Naqvi *et al*., 2000). CO_2 emission scenarios indicate that the oceanic suboxic regions and N_2O production in the open oceans are not likely to change significantly during the next 100 years. However, in next 4000 years, a 64 % increase in oceanic N_2O production because of decreasing O_2 concentration in the open ocean is predicted (Schmittner *et al*., 2008). Also, a short-term expansion of the open ocean sub-oxic areas ($[O_2] < 5$ µM) during the next 90 years is predicted (Oschlies *et al*., 2008). We can expect that this will also change near-future N_2O production and emission. Ocean acidification could lead to a counteracting effect because it shifts the oceanic NH_3/NH_4^+ equilibrium towards NH_4^+ (Ward., 2008). Therefore, an overall decrease of the oceanic NH_3 concentrations might lead to a decrease in nitrification since AOB preferably take up NH_3 and not NH_4^+ (Huesemann *et al*., 2002).

1.4.3.2 Water column distribution of N_2O

N_2O water column distributions can be divided into three types depending on the ambient water column oxygen distribution. N_2O depth profiles from major oxic waters of Pacific, Atlantic and Indian Oceans are characterised by a single peak structure as shown in Figure 1.7 (Elkins *et al*., 1978; Cohen and Gordon., 1979; Butler at al., 1989; Outdot *et al*., 1990, 2002; Naqvi and Noronha., 1991). The subsurface N_2O maximum at the oxygen minimum is accompanied by a nitrate (NO_3^-) maximum concentration (Elkins *et al*., 1978; Cohen and Gordon., 1979). This distribution pattern varies with the age of the water masses. An increase in deep water N_2O concentration relative to the surface water was observed from North Atlantic Ocean to North Pacific waters (Bange and Andrea., 1999) because of the age difference.

Suboxic regions have a different water column distribution for N_2O with a double maxima structure. The major suboxic regions having denitrification zones are seen in the Arabian Sea and eastern tropical North Pacific Ocean (Cohen and Gordon., 1978; Law *et al*., 1990; Naqvi and Noronha., 1991; Bange *et al*., 2001b; Bange *et al*., 2005). The double peak structure observed for central Arabian Sea [N_2O] (Figure 1.8a, data of Bange *et al*., 2005). The maximum N_2O values

were seen at the upper and lower boundaries of the Oxygen Minimum Zone (OMZ), where oxygen concentrations were 2.5 - 3 µmol/L^{-1}. At lower DO at the core of the OMZ, having least DO concentrations (DO below 2.5 µmol/L^{-1}), there is an [N_2O] minimum. It is due to the occurrence of active denitrification processes in the OMZ and resulting partial consumption of the N_2O when the system was shifted from oxic to suboxic conditions (Punshon and Moore., 2004). N_2O concentrations were not detectable in anoxic water masses such as central Baltic Sea, Cariaco Basin or Saanich Inlet (Cohen and Gordon., 1978, Hashimoto *et al*., 1983, Brettar and Rheinheimer., 1991, Walter *et al*., 2006). Denitrification will be absent in anoxic regions due to the presence of hydrogen sulphide and lack of nitrite (Codispoti *et al*., 2005). Figure 1.8 b illustrates the water column distribution of N_2O in Baltic Sea. In anoxic Baltic, as shown in Figure, apart from the surface oxic zone, N_2O was not detectable due to the consumption from denitrification accompanied by anoxic conditions. Therefore, the above distributional patterns indicate that the oceanic N_2O concentrations vary according to the ambient DO concentrations in the water column.

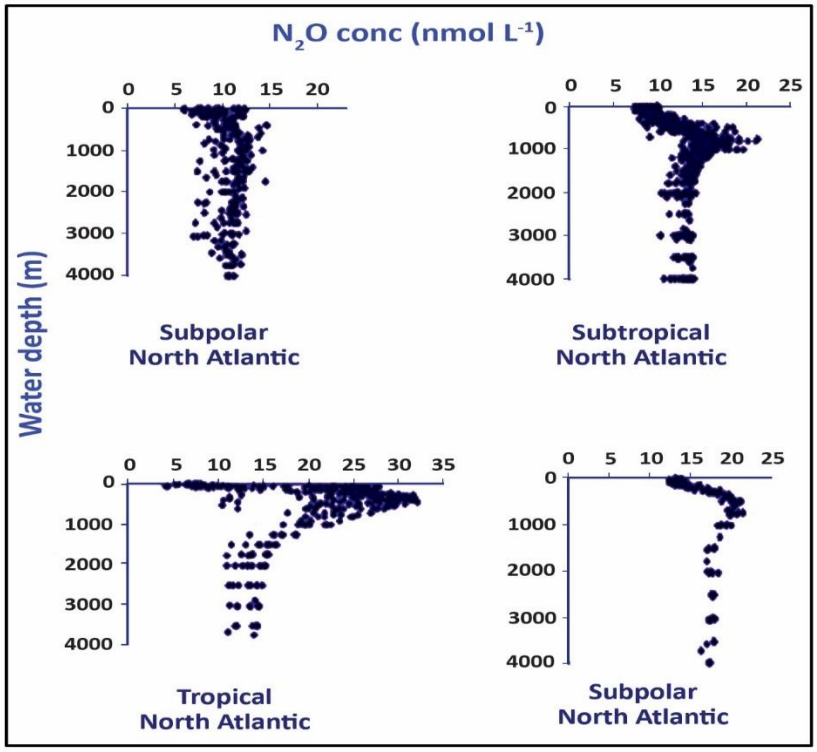

Figure 1.7: Water column distribution of N_2O in the oxic water of Atlantic, Walter *et al*., 2006.

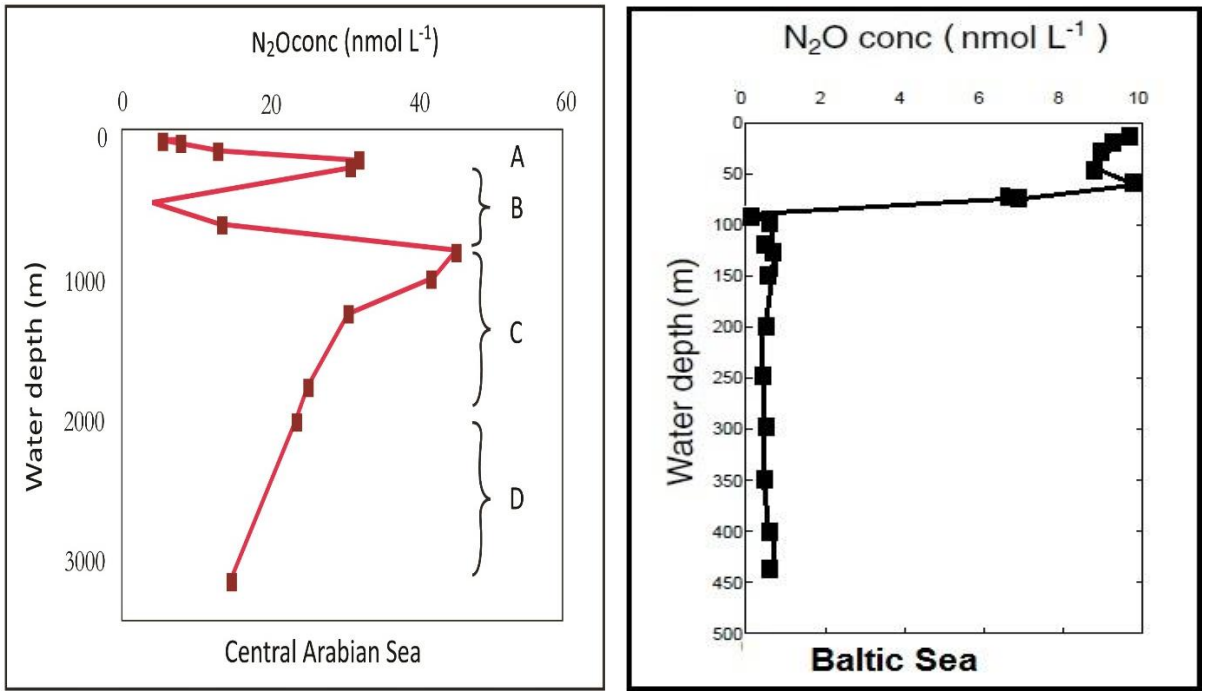

Figure 1.8: a) Water column distribution of N_2O in the suboxic waters of Central Arabian Sea, Bange *et al*., 2005. A, B, C and D represent four compartments according to the depth and N_2O formation processes. A <150 m, N_2O maximum derived from nitrification, B, 150–1000 m, N_2O reduction to N_2 during denitrification, C, 1000–2000 m, N_2O maximum derived from nitrification and D >2000 m, N_2O formation during nitrification combined with consumption during denitrification. b) Water column distribution of N_2O in the anoxic waters of Baltic sea, Walter at al., 2006.

1.5. Stable isotopes of N_2O and their applications

The use of the stable nitrogen and oxygen isotopes of N_2O, ^{15}N and ^{18}O, as a tracer, is central to the study of N_2O biogeochemistry in marine ecosystems. The distribution of these dual isotopes within the marine ecosystems can identify the sources of different N substrates of and the major pathways and mechanisms are moving nitrogen through the biota. In general, the isotopic composition of N_2O is useful in deciphering the relative importance of different sources that are isotopically distinct. This will help to identify the processes that add or remove N_2O with a characteristic pattern of isotopic discrimination (Yoshida *et al*., 1984; Yamazaki *et al*., 1987; Kim

and Craig., 1990, 1993; Yoshinari *et al*., 1997; Dore *et al*., 1998; Naqvi *et al*., 1998; Barford *et al*., 1999; Ostrom *et al*., 2000). The serious challenges in using this biogeochemical isotopic approach are of the complexity of the marine nitrogen cycle and the potential influence of multiple processes. Henceforth to unravel the marine N_2O processes using stable isotopes, an understanding of the general distribution of nitrogen isotopes in marine systems, the nature of isotopic fractionation and a careful consideration of the processes are essential.

Yoshida *et al.* first documented distributions and water column variations in the natural abundance of ^{15}N-N_2O ($\delta^{15}N$-N_2O) in marine systems in 1984. However, a decade later in 1990 and in 1993 the first method for the dual isotopic signatures of N_2O was presented by Kim and Craig. These and subsequent studies of the distribution of dual isotopes in marine systems suggested that the natural abundance of ^{15}N and ^{18}O of N_2O in marine systems could be used as an indicator of the sources or sinks of N_2O in an ecosystem.

There are two stable isotopes of nitrogen, ^{14}N and ^{15}N. The average ratio is very constant with $^{15}N/^{14}N$=1/272 (Junk and Svec., 1958). Oxygen has three stable isotopes, and they are ^{16}O, ^{17}O and ^{18}O, with a relative abundance of 99.76 %, 0.04 % and 0.20 % respectively. The stable isotopes of N_2O are measured using Isotope Ratio Mass Spectrometry (IRMS). The detailed techniques adopted for the measurements are given in Chapter 2. 1. In IRMS after exiting the source, the ion beam is deflected by the magnetic field and will be directed into Faraday cups. Beam currents for masses 44 ($^{14}N^{14}N^{16}O$), 45 ($^{15}N^{14}N^{16}O$, $^{14}N^{15}N^{16}O$, $^{14}N^{14}N^{17}O$) and 46 ($^{14}N^{14}N^{18}O$) are measured at Faraday cups. The nitrogen isotope data are reported as δ values relative to AIR-N_2 and represented using units per mille (‰).

The isotope ratio $^{15}N/^{14}N$ of N_2O is expressed as $\delta^{15}N_{AIR}$ relative to atmospheric N_2:

$$\delta^{15}N_{AIR} \text{ (sample) [‰]} = (((^{15}N/^{14}N) \text{ sample} / (^{15}N/^{14}N) \text{ std} - 1)$$

In the same way, the isotope ratio $^{18}O/^{16}O$ of N_2O is usually expressed as $\delta^{18}O_{VSMOW}$ relative to Vienna standard mean ocean water (VSMOW).

$$\delta^{18}O_{VSMOW} \text{ (sample) [‰]} = (^{18}O/^{16}O) \text{ sample} / (^{18}O/^{16}O) \text{ std} - 1$$

Therefore, $\delta^{15}N_{bulk}$-N_2O is obtained from 45/44 ratio and $\delta^{18}O$-N_2O from 46/44 ratio. In some cases, $\delta^{18}O_{ATM}$ relative to O_2 in the atmosphere is reported. $\delta^{18}O_{VSMOW}$ can be converted to $\delta^{18}O_{ATM}$ using the equation:

$$^{18}O_{ATM} = -23.0 + {}^{18}O_{VSMOW} / 1.0235 \qquad \text{(Kim and Craig., 1993)}$$

Mean $\delta^{15}N_{AIR}$ and $\delta^{18}O_{VSMOW}$ of N_2O in the troposphere are 6.72 ± 0.12 ‰ and 44.62 ± 0.21 ‰, respectively (Kaiser *et al*., 2003). The isotopic signal resulting from the air-sea exchange is small compared to the biological processes (Kim and Craig., 1990) and hence biological N_2O formation will yield a clear and distinct isotopic signature in oceanic N_2O. Chemical reactions and physical processes mainly control the isotopic compositions of N_2O during biogeochemical cycles. The light isotopes (^{14}N or ^{16}O) are preferentially taken up over the heavier isotopes (^{15}N and ^{18}O) by microbes and will be transferred to the reaction products (Kim and Craig., 1990). It is because during the microbial process the molecules with heavier isotopes will react slowly. Therefore, the substrates will become enriched in the heavy isotope and the products depleted with respect to the dual isotopes as reactions proceed (Kroopnick and Craig., 1976). N_2O being a product of both nitrification and denitrification, so marked depletions in ^{15}N occur to the substrates NH^+_4 and NO^-_3 (Ostrom *et al*., 2000). Denitrification also results in consumption of nitrous oxide which results in the residual N_2O having enriched ^{15}N and ^{18}O (Yoshinari., 1976; Yamazaki *et al*., 1987; Barford *et al*., 1999). Dual isotopic depletions are indicative of production by nitrification or denitrification, and enrichments attributes to consumption by denitrification. However, understanding N_2O formation pathways strongly depends on the information of the initial isotopic signatures of the substrates, which will vary both temporally and spatially.

Therefore, the earlier studies suggested that in oxic waters N_2O is mainly produced through nitrification. All these studies are incapable of differentiating the importance of pathway 1 (hydroxylamine), pathway 2 (nitric oxide) or pathway 3 (nitrifier-denitrification). Clarification of pathway may be attained through the isotopic studies of the $\delta^{18}O$ value of dissolved O_2 and H_2O and N_2O. The isotopic signal of oxygen in N_2O produced during nitrification is introduced by the $\delta^{18}O$ value of both dissolved O_2 and H_2O, where the first oxygen atom is added from dissolved oxygen and second from the water. So knowledge of the source of O in N_2O and understanding

the isotopic shifts and its direction will help to differentiate between nitrification and denitrification more precisely (Ostrom *et al*., 2000).

Some studies have been conducted in different parts of the oceans on N_2O dual isotopes and the major findings are summarised in Table 1.4. The table also gives a review of the significant works conducted so far in the marine environment. Water column distribution of N_2O dual isotopes from some of the oceanic regions revealed that $\delta^{15}N$ and $\delta^{18}O$ of N_2O are in equilibrium with tropospheric N_2O at the ocean surface. The isotope variations with depth were different for different environments and biological conditions. The depletion of both ^{15}N and ^{18}O with depth from the ocean surface was due to nitrification, and large-scale enrichment was due to denitrification and related consumption (Dore *et al*., 1998; Ostrom *et al*., 2000; Popp *et al*.; 2002). A more detailed study of $\delta^{18}O$ in dissolved O_2 and H_2O revealed that N_2O might be formed by three different pathways; first, by nitrification via NH_2OH or NO at most depths and, second, by nitrification via NO at most depths and, third, by nitrifier-denitrification via reduction of NO_2^- at subsurface depths with reduced oxygen concentrations (Ostrom *et al*., 2000).

Table 1.4: Summary of stable isotopic and isotopomeric studies conducted at various oceanic regions and inference from the results on the prevailing major pathways of the N_2O formation.

Oceanic region	Measured isotopic parameters	Suggested main formation pathways	References
Eastern tropical N Pacific	$\delta^{15}N$	Nitrification in oxic waters, denitrification in suboxic waters	Yoshida *et al*., 1984.
Western tropical N Pacific	$\delta^{15}N$	Denitrification in oxic waters	Yoshida *et al*., 1989.
N and S Pacific	$\delta^{15}N$, $\delta^{18}O$	Nitrification or coupled nitrification / denitrification	Kim and Craig., 1990.
Subtrop. N Pacific	$\delta^{15}N$, $\delta^{18}O$,SP_{N2O}	Nitrification via two different pathways Nitrification, nitrifier-denitrification and denitrification	Dore etal., 1998; Fujii et al, 2013.

Stat. ALOHA	$\delta^{15}N$, $\delta^{18}O$ SP_{N2O}	Nitrification via two different pathways	Popp *et al*., 2002
Arabian Sea	$\delta^{15}N$, $\delta^{18}O$	Coupled nitrification/ denitrification in oxic waters, denitrification in suboxic waters	Naqvi *et al*., 1998
South Atlantic	$\delta^{15}N$, $\delta^{18}O$, SP_{N2O}	nitrifier-denitrification in shallow waters, denitrification in suboxic waters	Frame *et al*., 2014.
Western N Pacific, stat. KNOT	$\delta^{15}N$, $\delta^{18}O$, SP_{N2O}	Nitrification	Toyoda *et al*., 2002.
Western N Pacific, Stat. KNOT	$\delta^{15}N$, $\delta^{18}O$, SP_{N2O}	Denitrification in oxic waters	Yamagishi *et al*., 2005.

1.6. Isotopomers of N_2O

N_2O is an asymmetrical linear molecule and analyses of the intramolecular distribution of ^{15}N in N_2O (isotopomers) could offer additional information to more tightly constrain sources and sinks of this greenhouse gas (Toyoda and Yoshida., 1999. Yoshida and Toyoda., 2000). Isotopomers are one of a set of molecules having isotopically substituted atoms. N_2O can have 12 isotopomers, though only five of them are significant at natural abundance level. They are $^{14}N^{14}N^{16}O$, $^{15}N^{14}N^{16}O$, $^{14}N^{15}N^{16}O$, $^{14}N^{14}N^{17}O$ and $^{14}N^{14}N^{18}O$. The nitrogen atoms at the centre and end positions are designated as N^{α} and N^{β}.

Quantification of the relative abundances of ^{15}N in the central (α) and terminal (β) positions of the linear N_2O molecule relies on the fragmentation of N_2O^+ to NO^+ within the ion source of a mass spectrometer (Brenninkmeijer *et al*., 1999. Toyoda *et al*., 2005). The intramolecular distribution of ^{15}N is often expressed as the site preference ($SP = \delta^{15}N^{\alpha} - \delta^{15}N^{\beta}$, Toyoda and Yoshida., 1999). Measurements of SP N_2O should allow for the identification of the mechanisms of N_2O formation by the different microbial pathways (Sutka *et al*., 2003, 2004) since it is characteristic of each production and consumption process (Yamulki *et al*., 2001. Toyoda *et al*., 2002; Sutka *et al*., 2003) and is independent of the nitrogen isotope ratio of the starting material. Based on the results of a

study with cultures of AOB, nitrifier–denitrifiers and denitrifiers, Sutka *et al.* (2006) concluded that the characteristic SP of denitrification (including nitrifier denitrification) is approximately 33 ‰ lower than that produced by nitrification. They also suggested that SP of N_2O is a robust indicator of the microbial origins of N_2O and most importantly SP is not affected by isotopic fractionation. Thus, isotopomers might be used to distinguish between N_2O produced during oxidation (nitrification) and reduction (denitrification and nitrifier-denitrification) processes. However, it seems that isotopomers cannot be used to differentiate between nitrifier-denitrification and denitrification processes (Schmidt *et al*., 2004; Sutka *et al*., 2006). There exist only limited number of studies for SP, in the North and South Pacific Oceans (Popp *et al*., 2002; Toyoda *et al*., 2002; Yamagishi *et al*., 2005; Charpentier *et al*., 2007), in the eastern tropical North Pacific Ocean and Gulf of California (Yamagishi *et al*., 2005), and in the anoxic Black Sea (Westley *et al*., 2006).

1.7. Significance of the study and thesis outline

The long-lived greenhouse gas N_2O has a significant role in global climate change and stratospheric chemistry. It may be affected by potential increases in coastal hypoxia and extent of OMZ's in the world oceans along with the ocean warming and acidification in the future. There exists a severe lack of oceanic data on the N_2O distribution. Still, the debates continue on whether the formation of N_2O is dominated by nitrification or denitrification. The present study focuses on N_2O water column distribution, sea to air flux and elucidation of formation pathways using concentration, stable isotopic and isotopomeric methods for the first time in the regions of Southwest Pacific Ocean around New Zealand and Sub-Antarctic regions of the Southern Ocean. A comparative study of the well-studied Northeast Arabian Sea waters is also included, and during this, isotopomeric methods were used for the first time in Arabian Sea water column. This thesis compiles some studies to produce a large dataset of N_2O, its stable isotope and isotopomer measurements to investigate the oceanic N_2O production pathways.

Comprehensive information on the regional studies including sampling transects and stations, and sampling techniques are described in Chapter 2. The development of a purging and trapping system connected to the IRMS to measure N_2O concentration, isotopic and isotopomeric ratios are detailed in the chapter. The analytical procedures adapted for the measurement of auxiliary hydrographic

parameters and other stable isotopes ($\delta^{18}O$ of dissolved O_2 and H_2O) are also defined in this chapter.

A detailed description of N_2O distribution and its variations with dissolved oxygen and nutrients for Southwest Pacific and Sub-Antarctic regions are detailed in Chapter 3. ΔN_2O/AOU and $\Delta N_2O/NO_3^-$ relationships for these regions are also presented in this chapter. Seasonal and decadal variations of N_2O in these oceanic regions are also described in this chapter.

In Chapter 4, nitrous oxide sea to air (F_{s-a}) and cross thermocline (F_{c-t}) flux measurements based on three different parameterizations (F_{s-a}) and one (F_{c-t}) for the study areas are explained. These results are also used to determine the role of the mixed layer in N_2O formation processes. Based on these estimates, the contribution of the Southwest Pacific and Subantarctic regions to the global N_2O budget were also studied and is reported in the same chapter.

The most important objective of the thesis is to understand the different formation pathways in this Southwest Pacific water masses using stable isotopes. The water column distributions of the dual isotopes of N_2O, $\delta^{18}O$ of dissolved O_2 and H_2O and isotopomeric signatures of N_2O (SP, $\delta^{15}N^{\alpha}$, $\delta 15N^{\beta}$) are described in Chapter 5. These results are used to explain and differentiate between different formation pathways of N_2O.

The Arabian Sea region is one of the most studied and largest marine sources with regard to N_2O. All measurements described in Chapter 3, 4 and 5 were applied to examine N_2O distribution and production in the Arabian Sea for comparison. There are few studies on N_2O stable isotopes in the Arabian Sea, and isotopomeric studies have not yet been conducted in a comprehensive way for Arabian Sea regions. All the above studies conducted for Arabian Sea waters as a part of the thesis is explained in Chapter 6. A summary and conclusions from the whole study are given in chapter 7 to establish the role and contribution of the Southwest Pacific to N_2O cycling and global budget with future research plans into the topic.

Chapter 2

Study Area and Experimental Methodologies

2.1. Introduction

This chapter explains in detail the study area, sampling methods and analytical techniques adopted for the current project. A large number of studies on N_2O and its various aspects have been conducted in Indian Ocean, Atlantic Ocean, North Pacific Ocean and South East Pacific Ocean. The similar kinds of studies on N_2O are not extended to South West Pacific Ocean. Besides its growing importance in present century oceanography, N_2O in the Southern Ocean is also very poorly studied. There is a lack of sufficient data for the surficial and water column distribution of world ocean N_2O as compared to the other greenhouse gases. The stable isotopic and isotopomeric measurements of N_2O in these waters will provide more insight into the processes and production mechanisms of the trace gas. N_2O stable isotopic and isotopomeric studies are available for restricted regions of world ocean only. So to fulfil the overall aim of the thesis, measurements of the concentration and stable isotopic composition of N_2O from South West Pacific (SWP) and Arabian Sea water samples were required. The study of the relationship between [N_2O] and basic biogeochemical features like nutrients and dissolved oxygen (DO) was also a part of the work. There are insufficient studies that look into all the above-mentioned parameters together. So the development of a new analytical system for [N_2O] and its isotope and isotopomer measurements were the most significant part of this project. There exist few analytical techniques which allow the measurements of all these N_2O parameters effectively on time. Among the available methodologies, a fully automated technique developed by McIlvin and Casciotti (2010) proved to be effective for the present work. To achieve this an automated sparging and trapping system connected to an Isotope Ratio Mass Spectrometer (IRMS) was constructed adopting the McIlvin and Casciotti (2010) method. The instrumental and analytical procedures used for the measurements of other hydrographic parameters are also detailed in this chapter.

2.2. Objectives

1. To collect seawater samples from different oceanic regions including the Southwest Pacific Ocean and the Indian Ocean according to the spatial, temporal requirements and sampling protocols of the project.

2. To successfully adopt a new analytical system for the precise determination of the concentration, stable isotope and isotopomer characteristics of N_2O with accuracy enabling an increased spatial and temporal coverage of [N_2O] and its isotopic signatures for the Oceans using the above methods and measurements.

2.3. Study area

The ocean contributes about 30% to the atmospheric N_2O budget, so there is strong interest in the oceanic N_2O cycle. While coastal regions are well-studied, there are limited data available for open ocean N_2O especially in the subantarctic sector of SWP, and very few South West Pacific Ocean studies in the literature report on the relative contribution of different bacterial processes that influence N_2O cycling such as nitrification and denitrification. Stations and transects from various cruises were selected to address the lack of information in these regions.

The sub-tropical Pacific surrounding New Zealand is of particular interest for N_2O studies due to many reasons. There exist water masses of contrasting physical, chemical and biological characteristics in Southwest Pacific and Sub Antarctic waters surrounding New Zealand (Heath. R. A., 1976, 1985; Stanton and Ridgway., 1988; Vincent *et al*., 1991; Chiswell *et al*., 2014). The availability of background information from studies such as Munida time series transect (http://www.iopan.gda.pl/IOCCP/images/03TimeSeries/IOCCP%20Time%20Series%20Stations_201109_Pacific.pdf) (Currie and Hunter., 1999; Baer Jones., K. N., 2012), Fe Cycle cruise programs (http://www.geotraces.org/cruises/cruises-completed) and NIWA'S Biophysical Mooring(http://www.epa.govt.nz/eez/EEZ000006/EEZ000006_Appendix07_Summary_Other_Voyages_Overview.pdf) program is valuable to N_2O studies in this region. In order to study the sub-tropical Pacific characteristics along with latitudinal and longitudinal variations samples were

collected from Geotraces GP-13 cruise programme (http://www.geotraces.org/cruises/cruises-completed) and NIWA's Biophysical Mooring voyage (http://www.epa.govt.nz/eez/EEZ000006/EEZ000006_Appendix07_Summary_Other_Voyages_Overview.pdf) in 2011. The Spring Bloom II voyage (TAN1212, conducted by NIWA during the spring bloom period) sampling conducted to compare the annual variations in the N_2O in the same oceanic regions. Sub-tropical frontal and sub-Antarctic waters having contrasting biogeochemistry with that of sub-tropical Pacific were also sampled concerning spatial and temporal variations from Otago Continental Shelf transect and Southern Mooring stations. For a comparative study, sampling was also conducted in the Indian Ocean, one of the world's most significant N_2O sources (Law *et al*., 1990; Naqvi. S. W. A., 1991) and a widely studied ocean with respect to N_2O (Bange *et al*., 2005).

So, in summary, this thesis involves studies in three main regions:

1. Subtropical SWP
2. Subantarctic SWP
3. North-eastern Arabian Sea (Indian Ocean)

2.3.1. Sampling Locations

Water and air samples were collected both spatially and seasonally for the quantification of trace gases and all other parameters**.** Spatial sampling was carried out by taking samples from 15 different locations; Indian Ocean (3 sites) and subtropical (9) and subantarctic (3) SWP (for more information see Table 2.1). The study regions are named after the respective cruises as shown below in Figures 2.1, 2.2 and 2.3 for the sake of representation. They are NZ Geotraces transect (Geotraces GP-13 cruise, TAN 1109), Bloom voyage II (Spring Bloom II Voyage ,TAN 1212), NIWA Mooring September 2011 (Biophysical Moorings 22 cruise conducted by NIWA, TAN 1113), Otago Continental Shelf Transect (Polaris II time series transect starting from Taiaroa Head to Subantarctic water) and Indian Monsoon upwelling transect (Southwest Monsoon Upwelling cruise, FORV-SS 302).

The NZ Geotraces transect is named after the cruise GP-13 under Geotraces programme (http://www.geotraces.org/). The study regions are fully in the SWP, North of New Zealand in oligotrophic subtropical waters, with sampling conducted during the winter, June 2011. The four stations are designated as GA, GB, GC and GD (Figure 2.1). In early spring September 2012, during Bloom II voyage TAN 1212 samples were collected from two stations. These stations east of North Island of New Zealand were in SW Pacific. The two stations are B_2A and B_2B (Figure 2.1). NIWA has two long-term time stations SBM (Southern Biophysical Mooring) and NBM (Northern Biophysical Mooring) (Figure 2.1), with biennial surveys conducted at these two stations for a decade. During September-October 2011 mooring samples were collected for current work. NBM is located in subtropical SWP east of New Zealand while SBM is located south of New Zealand in subantarctic SWP waters. For all sampling the voyages were conducted onboard the RV-Tangaroa, NIWA owned research Vessel. The detailed information about the sampling dates and geographic locations of the sampling stations are given below in Table 2.1 and Figure 2.1.

The Otago Continental Shelf transect (Figure 2.2) is a 60 km long time series transect formerly called Munida time series transect (Currie *et al*., 2009). This transect will be referred as Otago Continental Shelf Transect (OCS) from hereafter. The sampling was conducted in University of Otago research vessel Polaris II. From 1998 pCO_2 measurements were collected bimonthly along this transect which starts at the tip of Otago Peninsula at Taiaroa Head (-45º 46' 20" N, 171º 43' 20" E) and goes offshore. The transect crosses neritic, subtropical frontal and Sub-Antarctic waters in an east-southeasterly direction (Curie *et al*., 2009; Baer Jones, K. N., 2012). For the present study, sampling was conducted three times over 14 months from September 2011-November 2012; in September 2011, May 2012 and November 2012 respectively. The stations were named as PA, PB, PC and PD where PA and PB correspond to the neritic waters and PC represents the STF regions. The Sub-Antarctic station is PD. More about sampling dates and geographic locations of the stations are given below in Table 2.1 and Figure 2.2.

Indian Ocean samples were taken during Southwest Monsoon Upwelling Cruise SS-302 conducted by Central Marine and Living Resources and Ecology (CMLRE), Kochi, Kerala, India in FORV-Sagar Sampada. The three selected stations are SC, SK and SU among which two of

them were open ocean stations (SC-Cape and SK-Kochi) and SU belonged to the shallow coastal upwelling regions of Cape Kanyakumari. More details about these stations are given in table 2.1, Figure 2.3 and Chapter 6.

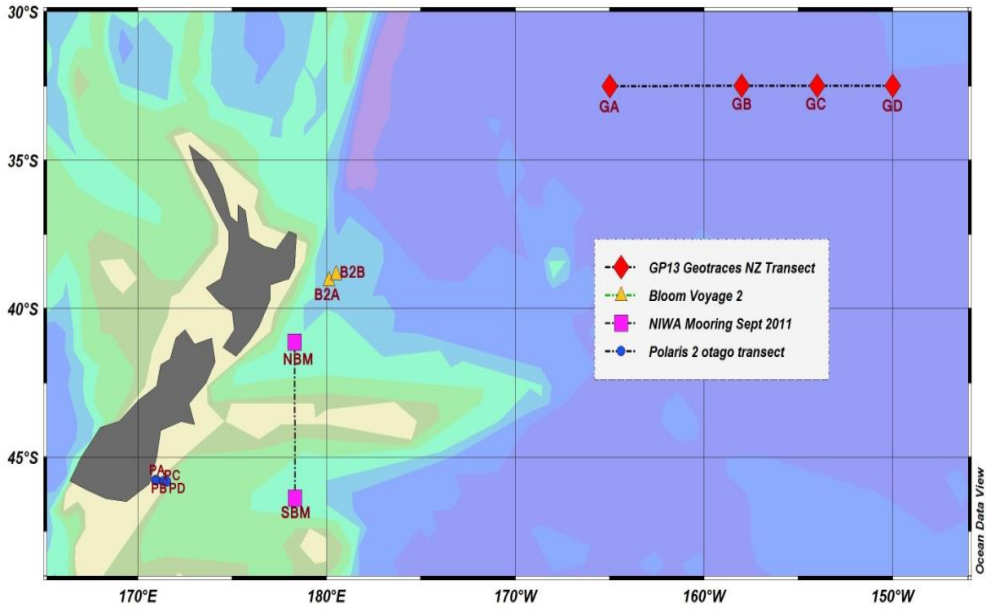

Figure 2.1: The sampling area map for the SWP

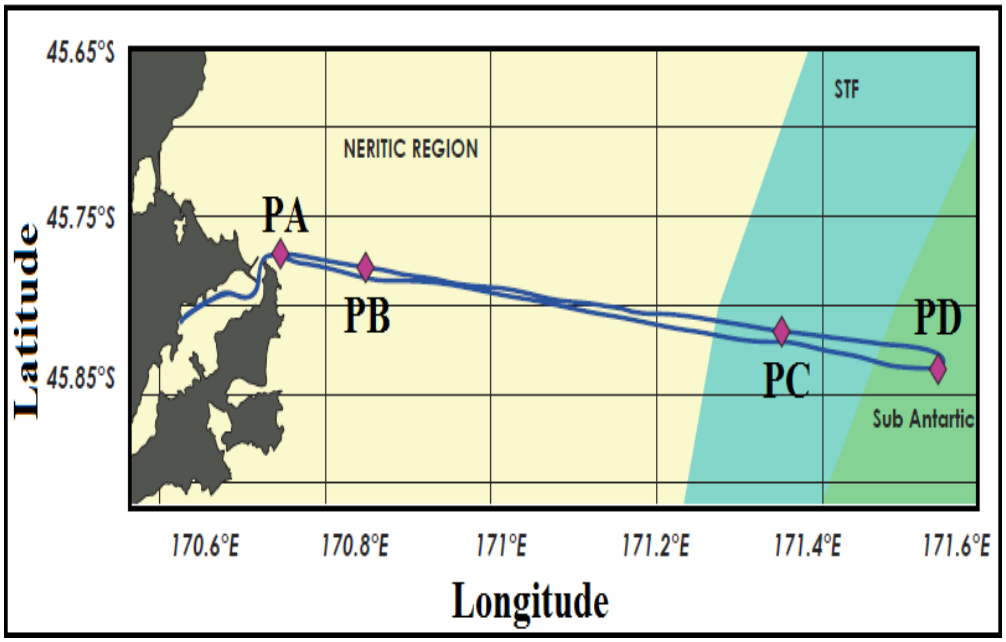

Figure 2.2: The area map for the Polaris transect. From coastal to the open ocean the three different water masses are shown by different colour codes. Yellow Neritic, blue STF and green Sub-Antarctic waters respectively.

Table 2.1. The sampling locations and their respective geography

Station ID	Sampling date	Oceanic Region	Latitude (degree East)	Longitude (degree North)
Geotraces Transect				
GA	14-06-2011	SW Pacific	195.005	-32.501
GB	18-06-2011	SW Pacific	202.005	-32.495
GC	20-06-2011	SW Pacific	205.995	-32.494
GD	22-06-2011	SW Pacific	209.998	-32.486
Bloom II Voyage				
B_2A	27-09-2012	SW Pacific	180.495	-38.834
B_2B	04-10-2012	SW Pacific	180.119	-39.042
NIWA –Mooring Transect				
NBM	21-10-2011	SW Pacific	178.312	-41.132
SBM	29-09-2011	Sub-Antarctic	178.325	-46.386
Polaris II transect				
PA	23-09-11,24-05-13 and 10-11-13	Neritic	170.910	-45.786
PB	23-09-11,24-05-13 and 10-11-13	Neritic	170.992	-45.790
PC	23-09-11,24-05-13 and 10-11-13	Sub-Tropical Front	171.342	-45.811
PD	23-09-11,24-05-13 and 10-11-13	Sub-Antarctic	171.546	-45.836
Indian Ocean Transect				
SU	10-06-2012	Indian	8.000	77.660
SC	11-06-2012	Indian	7.380	77.530
SK	18-06-2012	Indian	9.930	75.480

.

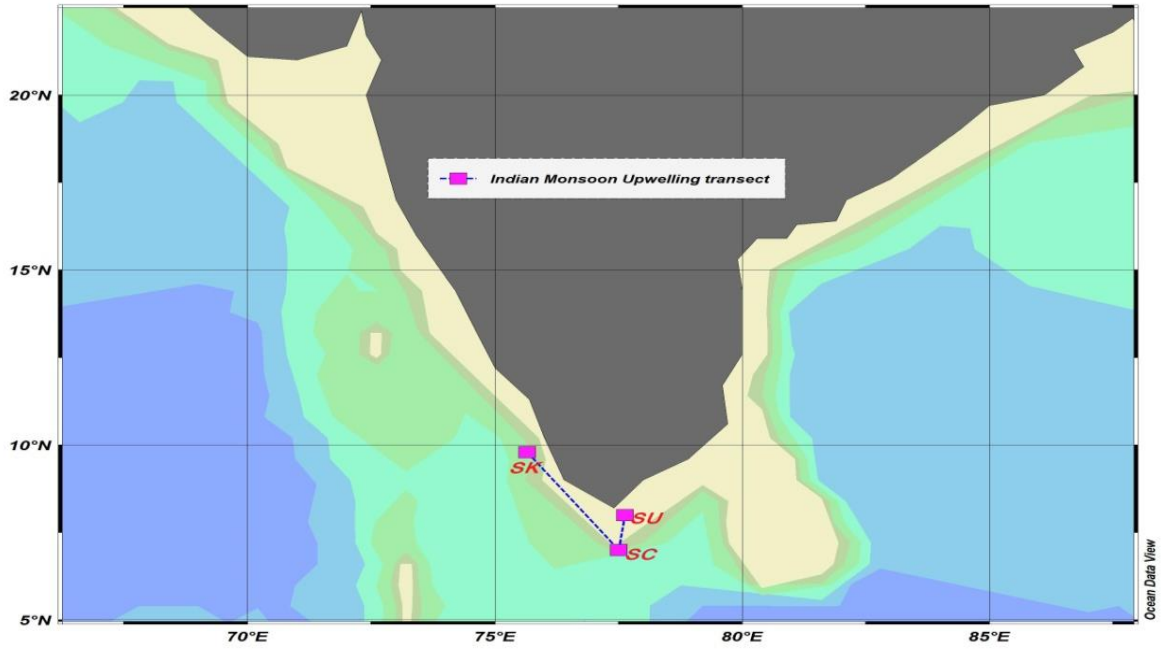

Figure 2.3: Sampling sitemap of Indian Ocean transect

2.3.2. The general oceanographic features of the study area

2.3.2.1. South West Pacific Ocean (SWP)

The Pacific Ocean is the largest ocean basin in the world with the lowest salinity, little input of terrigenous sediments and receives less freshwater input than the other oceans (Nunn. P. D., 1999). The SWP (Figure 2.4a) has a complicated geography with sizeable temporal variability in bathymetry (Pickard and Emery., 1990) and active narrow currents (Figure 2.4b) (Heath. R. A., 1976) in a complex bathymetry. These factors pose severe challenges for *in situ* sampling and measurements. The dynamic nature of these complex bathymetry through time and space usually makes it very difficult to interpret biological, physical and chemical data collected from discrete locations. Hence this area is poorly documented despite its importance in the climate system (Ganachaud *et al*., 2007). New Zealand, due to its geographic location that is ideally located for studying the oceanography of the SWP and is the gateway to the Southern Ocean, the most remote and least studied of the world's oceans. The coastal waters of this region contain areas of strong boundary forcing, wind-induced upwelling, sharp gradients in mixed-layer depth induced through

river inflows, fronts, gyres, plumes (Heath. R. A., 1985) which are likely to create a diverse range of biological conditions. Moreover, the South Island lies adjacent to a Subtropical Convergence (STC) which separates subtropical water in the north from Subantarctic water to the south (Heath. R. A., 1976) and is accompanied by strong physical and nutrient gradients which have major implications for the biology of the regions.

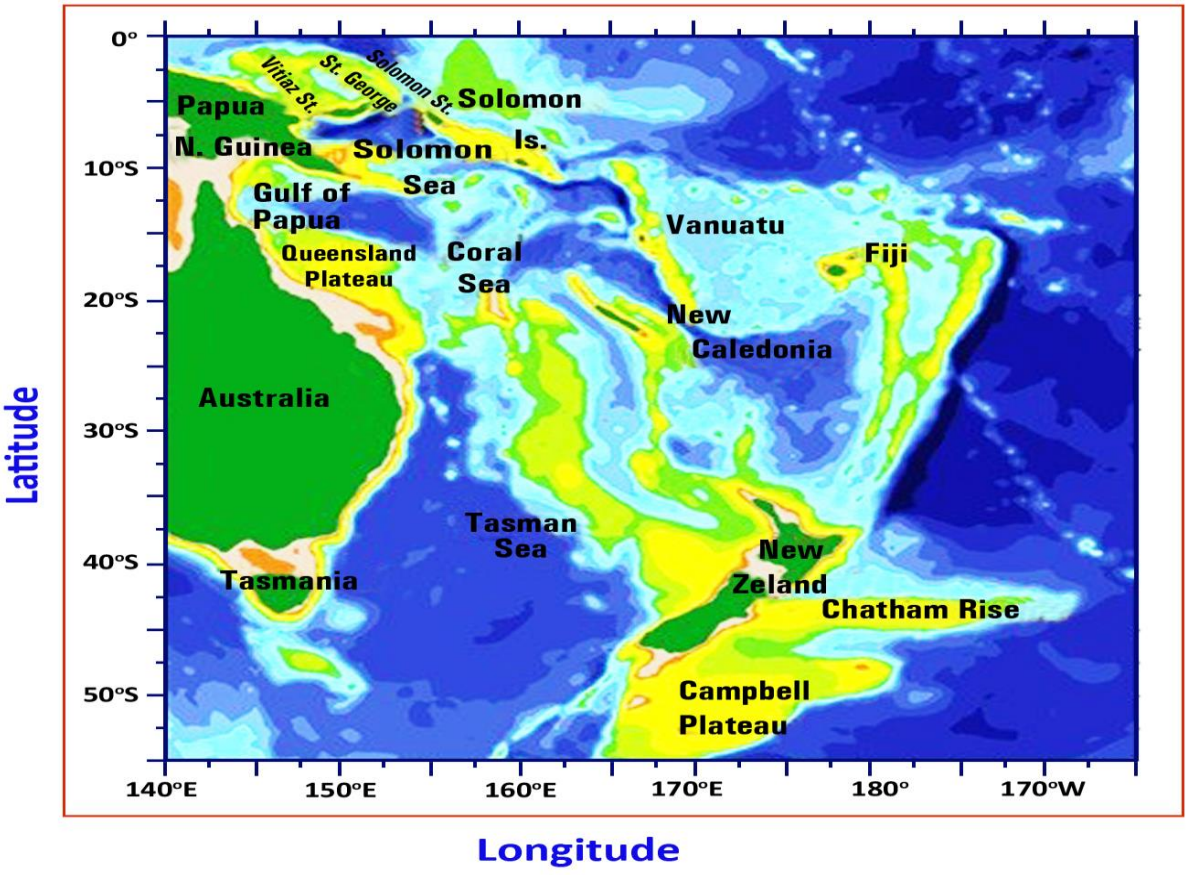

Figure 2.4 a: The general topography of the study regions including SWP (reproduced from Tomczak and Godfrey., 2003).

The major oceanographic features in the South West Pacific regions around New Zealand are shown in Fig 2.4b. SWP waters are transported in the westward flowing South Equatorial Current from the subtropical gyre centre toward the SWP - a major circulation pathway that redistributes water from the subtropics to the equator and to the Southern Ocean. The eastward flow of warm water splits around the country with the Tasman Front current flowing south-eastwards around the North Island, and north-westwards around the South Island's east coast in the Southland Current.

To the south of New Zealand, the SAF and associated cold Antarctic Circumpolar Current (ACC) hug the deep ocean floor to the east of the Campbell Plateau and Chatham Rise (Jillet. J. B., 1969; Heath. R. A., 1976., 1985a, 1985b). The ACC is a large current which is driven by the strong westerly's in the high latitudes of the southern hemisphere that encircle Antarctica unimpeded (Heath. R. A., 1976).

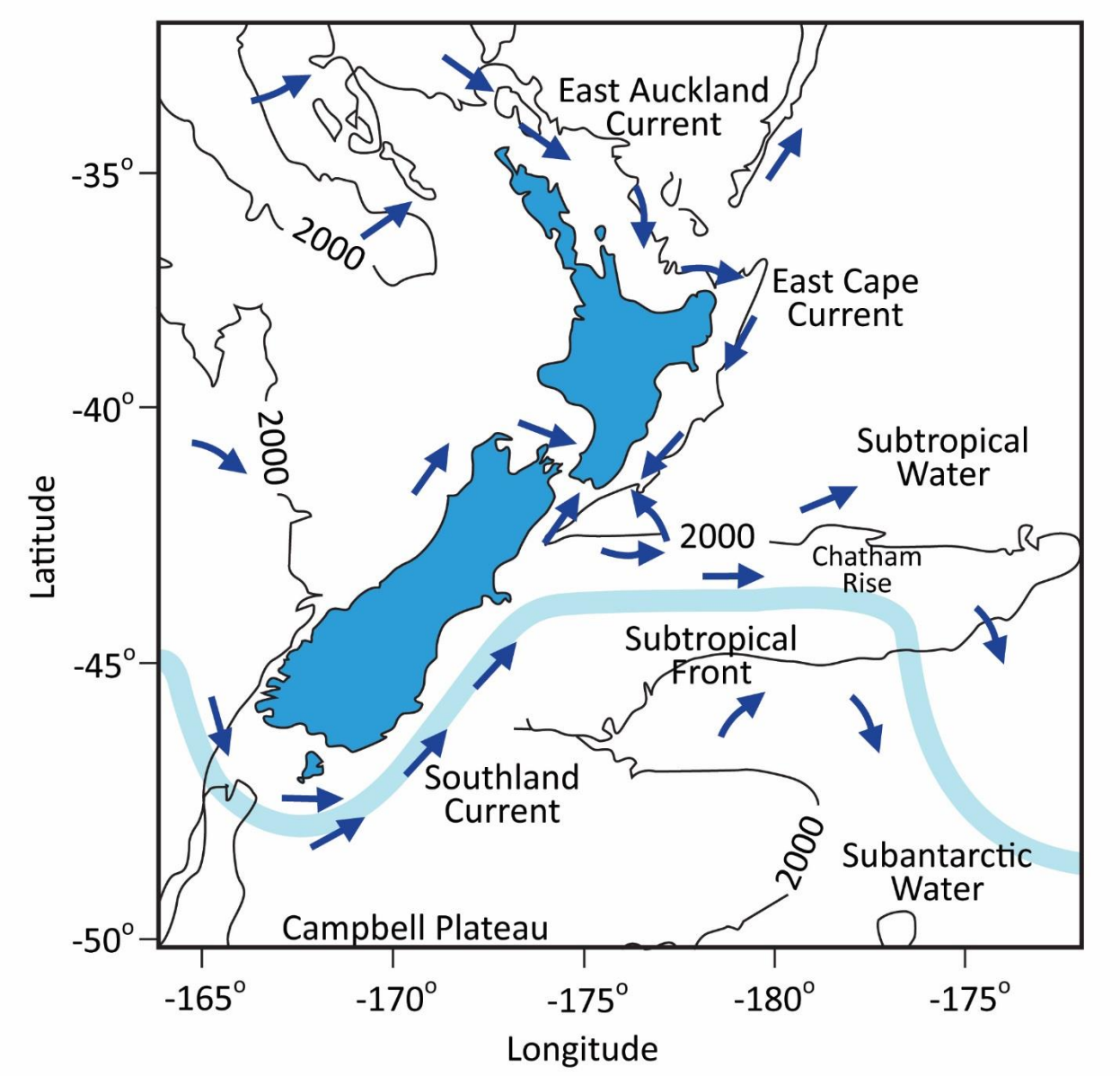

Figure 2.4 b: The prevailing water currents in the study region (Currie *et al*., 1998)

In the SWP region the Tasman Current (TC), characterized by high salinity and high temperature indicative of its subtropical origin, flows eastward in the south Tasman Sea towards New Zealand. Sub Antarctic Surface Water (SASW), low in both salinity and temperature, is driven northward in the West Wind Drift within the Circumpolar Current south of New Zealand (Heath. R. A., 1985). The subtropical frontal zone (STF) that separates these sub-tropical and sub-Antarctic water masses and is characterized at the surface by steep horizontal gradients of temperature and salinity (Garner. D.M., 1959). The STF passes to the south of the New Zealand land mass (see Figure 2.4b), where mixing of the water from the two sources results in modification of the subtropical water by slightly decreasing its temperature and salinity (Butler *et al*., 1992). The modified subtropical water then flows northward along the southern portion of the east coast of the South Island, where it is known as the Southland Current (SC). The portion of the STF separating the SC and SASW is termed the Southland Front (SF). The convergence turns eastward at the Chatham Rise, with one portion of the SC flowing offshore and the remainder flowing further northwards. These fronts, as the Tasman Front (TF), Subtropical Front (STF) and Sub-Antarctic Front (SAF) are shown in Figure 2.4. The TF and STF are relatively warm surface currents (Sutton., 2003).

The subantarctic and subtropical water masses are distinctive in both their chemical and biological characteristics, the subtropical waters being generally depleted in macronutrients, higher in chlorophyll *a* (Bradford and Taylor., 1980; Vincent *et al*., 1991) and having different species of zooplankton (Jillett *et al*., 1976). The convergence zone-STF, being the site of interaction of these two different water masses, exhibits highly variable chemical and biological behaviour, in both spatial and seasonal sense (Heath R A., 1976; Heath R A., 1985).

The term the Southern Ocean is sometimes used for the whole region including Antarctic, Subantarctic and south of South West Pacific Ocean. The Southern Ocean is crucial to the understanding of global N_2O studies as it has been identified as the largest area of anthropogenic CO_2 sequestration of all major oceans. Most of the Southern Ocean is described as High Nitrate Low Chlorophyll (HNLC) due to very low iron concentrations that limit the extent of primary productivity (Boyd *et al*., 1999, 2001; de Jong *et al*., 1998). Consequently, the supply of Fe is the primary parameter determining biological activity, nutrient utilization and therefore can act a major role in the production of biogenic gases such as N_2O in the Southern Ocean.

2.3.2.2. Indian Ocean

Arabian Sea regions of Indian Ocean were also made a part of this study. Suboxic regions in the Arabian Sea regions of the Indian Ocean are the largest oceanic N_2O source to the atmosphere through upwelling and denitrification processes occurring in these regions (Naqvi *et al*., 2010). All the other above study regions are well oxygenic. Moreover, the Indian Ocean is one of the world's best studied oceanic regions with respect to N_2O. The Indian Ocean can be subdivided into the Northern Indian Ocean and Southern Indian Ocean. The present study involves the northwest Arabian Sea regions of the Northern Indian Ocean.

The oceanography of North Indian Ocean is very different from that of the Southern Ocean, and Southwest Pacific Ocean as the North Indian Ocean is land-locked on three sides. The increased stratification of the surface ocean as a result of the warmer temperature of the tropical climate and monsoon rain-induced freshening of the waters makes large changes in biogeochemical cycles in these regions (Naqvi and Unnikrishnan., 2009; Shenoy *et al*., 2011). The two dominant seasons are the Southwest Monsoon (Summer Monsoon) and Northeast Monsoon (Winter Monsoon). The Monsoons are climate events and hence are predicted to make these regions vulnerable to the global climate change (Mantoura *et al*., 1993; Naqvi *et al*., 2010; Shenoy *et al*., 2011). Indian Summer Monsoon is a part of Asian Monsoon, and these regions are responsible for the transport of global atmospheric heat and moisture to a significant extent (Schulz *et al*., 1998). During Southwest monsoon events nutrient-rich subsurface waters are upwelled to the surface which will give rise to the high productivity of Arabia, Somalia and Southwest India. Wind and surface currents will act as the primary drivers of upwelling (Qasim *et al*., 1977).

The Ocean currents during the sampling season are shown in Figure 2.5. During Summer Monsoon surface waters become fresher along the Southwest coast of India as a result of higher precipitation, and run-off carried into the Northeast Arabian surface which is along the Southwest Indian coast (Kessarkar *et al*., 2010). Upwelling, driven by Ekman transport, brings nutrient-enriched waters to the surface and enhance productivity (Gupta *et al*., 2003). The moderate water removal rate due to increased residence time and high productivity leads to high remineralisation, which supports a significant Oxygen Minimum Zone (OMZ) below the surface mixed layer down to ~1200 m. This

region forms the world's largest natural coastal hypoxic zone (Naqvi *et al*., 1994, 2009). OMZ's serve as sites for water column denitrification (Naqvi *et al*., 1987), which makes the Arabian Sea a unique place to study N_2O production. In contrast, the Southern Ocean and Southwest Pacific waters are very well oxygenated with prevailing strong nitrification processes (Ward *et al*., 2008). Therefore this will allow a significant comparison of oceanic N_2O in different regions and originate from different processes.

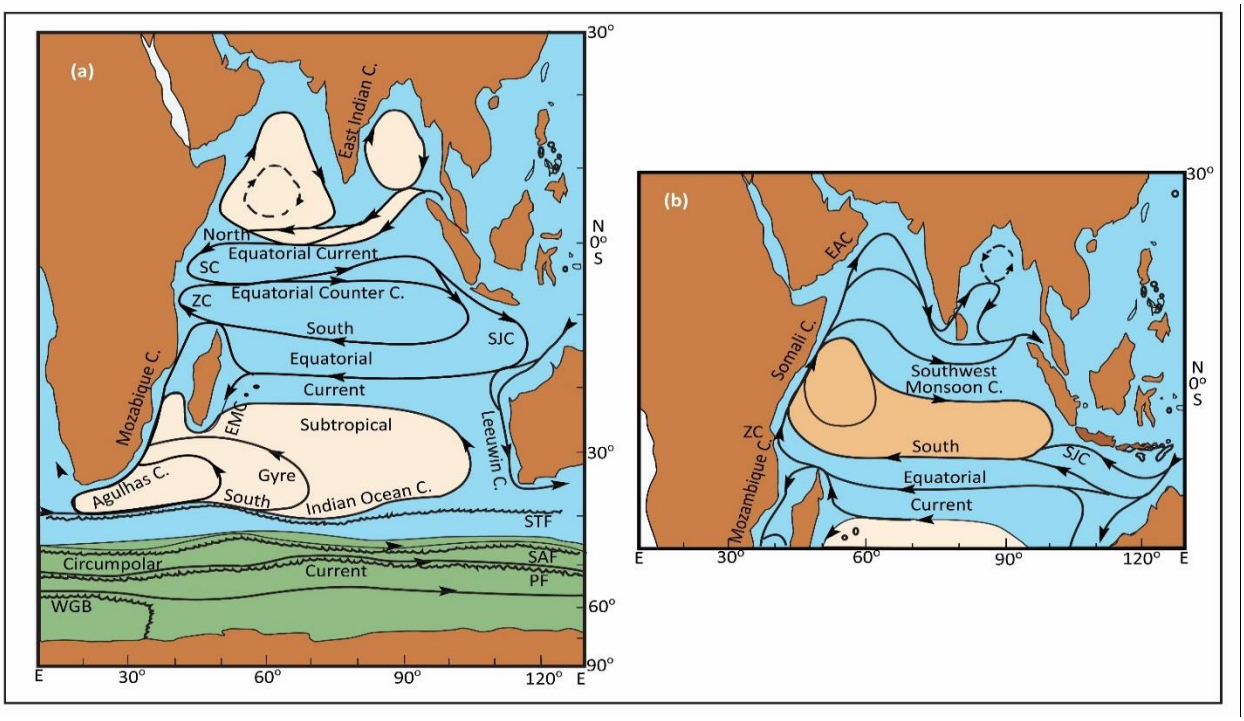

Figure 2.5: The surface currents In Indian Ocean during a) Winter (Northeast) and b) Summer (Southwest) Monsoons. EAC-East Arabian, SJC-South Java, ZC-Zan Zibar, EMC-East Madagascar, SC-Somali currents. STF-Sub-Tropical Front, SAF-Sub Antarctic Front, PF-Antarctic Polar Front and WGB-Weddell Gyre Boundary (Modified from Mathias Tomczack., 1994).

2.4. Sampling methods

2.4.1. Collection of Water Samples

Water samples for the measurement of dissolved N_2O concentration, nutrients, incubation experiments, stable isotopes and isotopomers were collected using a CTD sampler. A series of five 12 L Niskin bottles configured on the CTD rosette were deployed to collect water samples from

various depths on the Munida transect. While on Tangaroa, CTD of 24 bottles was configured on the rosette.

Table 2.2: Sampling equipment used for different voyages

Cruise Name	Number of Stations	Number of Depth Profiles	Ship Name	Water Sampler and type	CTD-Bottle Type
Geotraces-GP13	4	15(Duplicates)	RV-Tangaraoa	CTD-SBE*911plus*-NIWA Ocean CTD Facility (NOCF)	24 x 10-L SBE-32 Carousel Niskin Bottles
Bloom II	2	14 (Duplicates)	RV-Tangaraoa	CTD-SBE*911plus*-NIWA Ocean CTD Facility (NOCF)	24 x 10- L SBE-32 Carousel Niskin Bottles
Mooring-22	2	12 (Duplicates)	RV-Tangaraoa	CTD-SBE*911plus*-NIWA Ocean CTD Facility (NOCF)	24 x 10- L SBE-32 Carousel Niskin Bottles
Polaris II	4	5/6/10/11 (Triplicates or duplicates)	RV-Polaris II	CTD-SBE 19*plus* V2 SEACAT	5*12 L Niskin Bottles
Indian Southwest Monsoon Upwelling	3	4 /14 (triplicates)	FORV-Sagar Sampada	CTD-SBE*911plus*-NORINCO	12x10- L SBE-32 Carousel Niskin Bottles

Water samples were drawn from the Niskin bottles via Tygon tubes. Sampling bottles were pre-rinsed with dilute acid (5 % HCl) and Milli-Q (Millipore Corp; conductivity ~18.2 MΩ·cm, bacterial rejection >99%) water and stored according to the protocols as described in the subsequent sections. All bottles were rinsed at least three times with the collection water prior to

the respective samples. A Garmin GPS76 recorded the exact locations of high-resolution sampling, and the position data were appended to the SBE21 thermosalinograph data. Data acquisition instrumentation combined a Seabird Electronics Inc. (SBE) 911plus in Tangaroa and FORV-Sagar Sampada. More details of the sampling equipment used for cruises are given below in Table 2.2. Water samples from Geotraces GP-13 cruise were collected by C. Law & A. Marriner, and Bloom II by A. Marriner.

2.4.1.1 Dissolved N_2O, $\delta^{15}N_{bulk}$, $\delta^{18}O$, site preference (SP) of N_2O and $\delta^{18}O$ of dissolved oxygen

Water samples were collected for the measurements of dissolved N_2O ($[N_2O]$), $\delta^{15}N_{bulk}$, $\delta^{18}O$, site preference (SP) of N_2O and $\delta^{18}O$ of dissolved oxygen. The samples were transferred from the CTD water sampler via Tygon tubing into serum bottles (240 ml). Samples were overfilled by at least three times the volume of the bottles to minimise the impact of sample contact with air. Care was taken to ensure no bubbles were trapped. The collected samples were poisoned immediately using 0.1 ml of saturated $HgCl_2$ to prevent biological activities and then sealed with a butyl rubber septa crimped on with aluminium caps. Samples were stored in the dark at room temperature and analysed within six months of collection. Water samples for $\delta^{18}O$ of DO were collected in 12.1 ml Exetainer® vials in a similar way to that of dissolved N_2O samples. The Exetainers were sealed with butyl rubber septa and polypropylene screw caps.

2.4.1.2. Nutrients

Samples for the analysis of dissolved nutrients nitrate (NO_3^-), ammonium (NH_4^+) and phosphate (PO_4^-) were collected from the CTD water sampler after filtering through Whatman GF/C glass fibre filters (45 mm) and stored in 50 ml polycarbonate autosampler (AA) vials. Before use the AA vials were pre-rinsed in 0.1 M, HCl followed by Milli-RO® water. Filtrates were stored in dry ice during transport and subsequently frozen at -20 °C prior to the analysis.

2.4.1.3. Samples for $\delta^{18}O$ water

Samples for the measurement of $\delta^{18}O$ of water were collected from the water sampler directly to a 20 ml screw-cap glass bottle with rubber seals. Upon return to the laboratory, these were subsampled to a 2 ml GC vials suitable for the Picarro autosampler tray. All vials were pre-rinsed in 0.1 M HCl followed by Milli-RO® and thoroughly dried before sampling.

2.4.1.4. Samples for Labelled Isotope Incubation experiments

For incubation experiments, water samples were collected for measuring dissolved N_2O ([N_2O]), $\delta^{15}N_{bulk\text{-}}$ N_2O, nutrients nitrate (NO_3^-) and ammonia (NH_4^+). Initially, the seawater samples were transferred directly from the CTD sampler via Tygon tubing into incubation vessels Cubitainer® (5L). Cubitainers were acid cleaned, and samples were overfilled by at least three times the volume of the bottles to minimise the impact of sample contact with air. Care was taken to ensure no bubbles were trapped. Required labelled isotope tracers of $^{15}NH_4Cl$ and $K^{15}NO_3$ were added to the incubation vessels as needed. The control samples were poisoned immediately using 0.1 ml of saturated $HgCl_2$. The Cubitainers were capped with modified caps which allows subsampling without air contamination. Samples were kept for incubation around 12 hours in a temperature regulated water bath maintained at ± 1° C of the in situ temperature. Subsamples were collected from the incubation vessels according to the experimental set up for dissolved N_2O ([N_2O]), $\delta^{15}N_{bulk\text{-}}$ N_2O, nutrients nitrate (NO_3^-) and ammonia (NH_4^+) as explained in the earlier sections and were poisoned with $HgCl_2$. The collected samples were stored in the dark at room temperature and analysed for the required parameters. Samples with $^{15}NH_4Cl$ tracers were wrapped in black polyethylene film to prevent potential photoinhibition of Ammonia-Oxidizing Bacteria (AOB). The detailed experimental set up is explained in section 2.6.

2.5. Analytical methods and Calibrations

2.5.1. Basic Hydrographical parameters

In ORV-Tangaroa a calibrated SBE 19plus V2 SEACAT Profiler was used to measure conductivity, temperature and depth (CTD) profiles at depth cast at each sampling station. All data acquisition and data processing followed NOCF protocols and performance of all instrumentation were within nominal limits. Dissolved oxygen (DO) was measured using a DO probe fitted to the CTD which were calibrated during each sampling. ORV-Tangaroa CTD Calibrations were done by M. Walkington and N. Barr. For CTD calibration dissolved oxygen samples were drawn and measured aboard ship while salinity samples were drawn and returned

for shore-based measurement all according to NOCF protocols. These results were used to calibrate and correct the CTD sensor measurements at bottle fire.

FORV-Sagara Sampada calibrations were performed by Arun George, NORINCO (Norinco.Pvt.Ltd). The dissolved oxygen calibrations were done by Winkler titration experiments as explained in Grasshoff *et al*., 1999. For POLARIS II the uncalibrated dissolved oxygen values were used. The CTD sensor configuration consisted of primary temperature (SBE 3plus), primary conductivity (SBE 4), and primary dissolved-oxygen (SBE 43) sensors. The sensors were ducted horizontally and pumped by SBE 5T pumps.

2.5.2. Macro nutrients

Nitrate, ammonium and phosphate concentrations for the POLARIS II samples were determined using UV-Visible spectrophotometry with a flow-injection analysis Lachat Auto-analyser in the Department of Botany at the University of Otago. While for all other samples from above-mentioned cruises nutrients data were obtained from the respective cruise data. M. Woodward measured nutrients for Geotraces- GP-13 TAN 1109 using micro-molar Bran and Luebbe AAIII segmented flow, colourimetric, auto analyser. Bloom voyage nutrients were measured by Van Kooten and for Indian Ocean samples by Maneesh TP. The basic principles behind all the above methods for nutrients are explained below.

2.5.2.1. Nitrate (NO_3^-)

Keeney and Nelson (1982) indicated that the preferred method, based on sensitivity, reproducibility, and accuracy, is to reduce nitrate (NO_3^-) to nitrite (NO_2^-) by passing through a copperized cadmium column, followed by the determination of nitrite (NO_2^-) by common colourimetric diazotization reaction. Nitrite was then estimated using the standard procedure suggested by Grasshoff *et al.* in 1999, in which the nitrite formed reddish-purple azo dye, with sulphanilamide and N-(1-naphthyl) ethylenediamine dihydrochloride (NED), which was then quantified spectrophotometrically at 540 nm followed by standardisation. The absorbance at 540

nm was linearly proportional to the concentration of nitrate+nitrite in the sample according to the Beer-Lambert's Law. Nitrite concentrations in almost all stations were very small, so the measured concentrations were always the sum of nitrate plus nitrite ($[NO_3^-]+[NO_2^-]$).

2.5.2.2. Ammonium (NH_4^+)

Ammonium ions are often determined by indophenol blue method. Here phenate and ammonium ion react in the presence of hypochlorite and nitroprusside as a catalyst to produce the indophenol blue compound (Bremner and Mulvaney., 1982; Keeney and Nelson., 1982; Catalano., 1987). Absorbance is measured using an Ultraviolet-visible spectrophotometer at 630 nm after standardization.

2.5.2.3. Phosphate (PO_4^{3-})

Phosphate is determined by spectrophotometry. The sample first treated with a mixed reagent containing molybdic acid and trivalent antimony to form an antimony-phosphomolybdate complex (Grasshoff *et al*., 1999). This complex was further reduced to a blue-coloured complex using ascorbic acid and absorbance of this product measured at a wavelength 885 nm .Standard calibration was conducted to before the sample analysis.

2.5.3. Nitrous Oxide (N_2O)

2.5.3.1. Construction of sparge and trap apparatus for pre-concentration of N_2O from seawater

Increased spatial and temporal data coverage for dissolved [N_2O] is needed to improve our understanding of the production and distribution of N_2O in a variety of marine environments to overcome the difficulties associated with the paucity of the data. Greater understanding of isotopic data of [N_2O] can provide valuable information about the mechanisms of production and consumption of this climatically important trace gas. The intramolecular nitrogen isotope distribution of N_2O (Site Preference) will give detailed insight into the sources and cycling of N_2O

in the aquatic environment. The preliminary task was to develop a working method for automated measurement of dissolved nitrous oxide concentration, $\delta^{15}N\text{-}N_2O$, $\delta^{18}O\text{-}N_2O$ and site preference of ^{15}N in dissolved N_2O in natural waters. Yoshida *et al.* in 1984 introduced the first techniques used for isotopic analysis of oceanic N_2O which required large volumes of seawater (100 L) and 15 hours of sample processing time per sample. However, with the introduction of continuous flow techniques and use of N_2O itself as the analyte, sample size requirement and analysis time was reduced, but the analysis is still labour intensive (Yoshinari *et al*., 1997). The N_2O dual isotopic analytical techniques involve loading the sample into a sparging vessel, collecting the N_2O using a liquid nitrogen trap, and subsequent release into an IRMS (Dore *et al*., 1998). In this methods trap and release portion of this procedure has been automated for quite some time, the sample transfer to and from the sparging column, which involves many steps, has been done manually. Automating the whole technique would save laboratory time and will increase sample throughput, which will allow more detailed examination of N_2O processes in the ocean. Therefore recently developed fully automated apparatus developed by McIlvin and Casciotti (2010) is adopted for the study. The setup (Fig. 2.6) consists of a GC-Pal autosampler (CTC analytics, LEAP Technologies), a degassing flask to sparge N_2O from water, a trapping system to isolate and purify N_2O, and an Isotope Ratio Mass Spectrometer (IRMS, Isoprime® EA-Micromass). The system is capable of analyzing 30 samples in 20 h without user attention after the start of the run. The automated purge and trap analytical system are shown below with its schematic diagram (Figure 2.6 and 2.7).

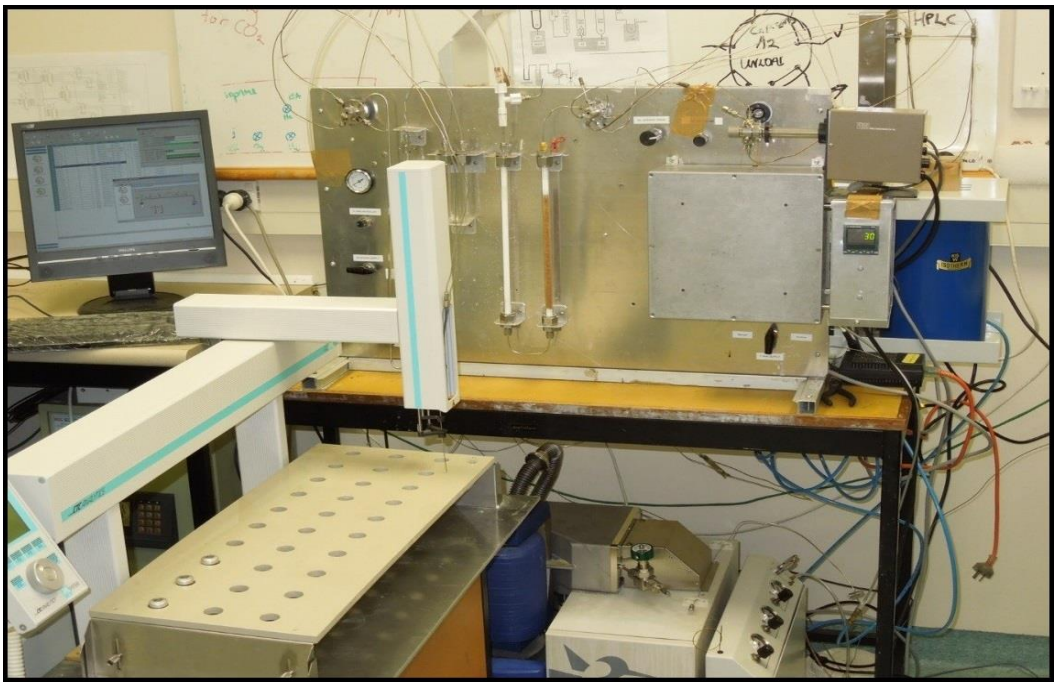

Figure 2.6: Automated purge and trap system connected to IRMS (Isotrace Lab)

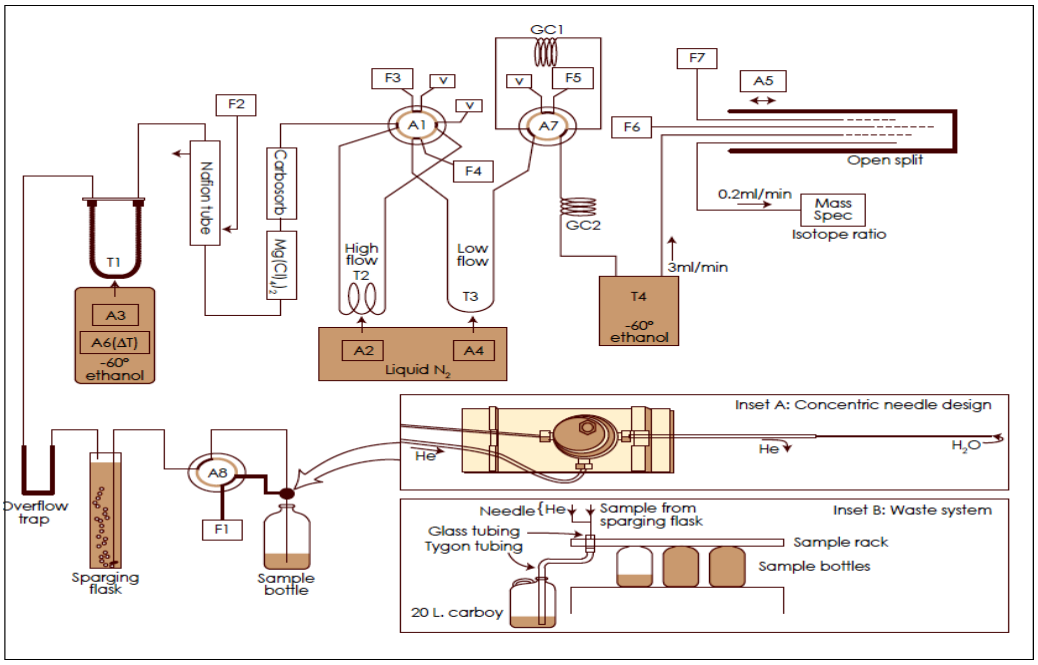

Figure 2.7: Schematic diagram of the automated system (Modified from Mc Ilvin and Casciotti, 2010)

2.5.3.2. The sample analysis cycle

A typical 240 ml seawater sample was determined in the sparger as follows. The explanation is based on the schematic diagram in Figure 2.7 and Table 2.3. The –60 °C trap is automatically lowered into the chilled ethanol (T1) at the start of the run. The N_2O high flow trap is then lowered into liquid nitrogen (T2), and the three multi-port valves (A1, A7, and A8) are set to the black lines in Figure 1.7. At the same time, the autosampler is sent to the sample bottle, and the concentric needle assembly penetrates the septum. Helium (F1) flows through the outer needle into the sample bottle, thus displacing the liquid and forcing it through the inner 18 gauge needle, through the 4-port valve, and into the sparging flask. The 4-port valve is switched to exclude the needle assembly (A8, grey lines) soon after sample transfer is complete (450 s), and the autosampler then moves the needle to the home position inside the waste transfer tube to await backflushing of the sparging column at a later step. The sample is degassed for 2100 s at 60 mL min^{-1} to transfer all dissolved N_2O to the tubing loop immersed in liquid nitrogen (T2). It is important to note that N_2O from the sample is trapped in the immersed tube cryogenically during sample transfer and the sparging period. After sample transfer is complete, at 2070 s, the low flow trap (T3) is immersed in liquid nitrogen to cool the trap. At 2100 s, the 8-port valve switched to the inject position (A1, gray lines) and the –60 °C trap (T1) is removed from the chilled ethanol. , the 4-port valve is set back to inject (A8, black lines), and the high flow trap (T2) is removed from the LN_2. This series of valve switches will initiate He to flow backwards through the sparging column, causing the degassed water sample to be transferred back through the needle into the waste transfer tube, which drains by gravity into the waste container (Figure 1.7, Inset B). The trapped N_2O is simultaneously transferred from T2 to T3 at a He flow rate of 3 mL min^{-1}. Seven seconds after T1 is raised, the trap is heated by passing a current through the convoluted stainless steel tubing (A6). The 6-port valve is then switched to inject mode (A7, grey lines), and the trap is raised to inject the N_2O into the GC column (a 30 m × 0.320 mm i.d. GS-Q GC column, J&W Scientific prod. no. 113-3432). At 2300 s, the low flow trap (T3) is raised, allowing the N_2O to pass through the GC column. After the N_2O peak is detected by the mass spectrometer (less than 2500 s), the 6-port valve is switched to backflush position (A7, black lines). The run is ended at 2600 s, the mass spectrometer was manually tuned prior to each set of measurements, and the sequence restarts with the next sample. Samples in 120 ml serum bottles can be analyzed by adjusting the transfer time, needle position

and sparging time. The measurement of [N_2O] and stable isotopes can be done from the same sample whereas for the current study a second sample is analyzed in the same way for the Site Preference measurements.

Starting its building works from 2011 February the instrument was available for sample analysis in April 2012. The first task was to make the external units (sample rack, sparging and trapping units) as shown in Figure 2.6. Optimization of the instrument was achieved through running a number of the same samples having known [N_2O] prepared in the lab through air equilibration. The same sample was also sent to other labs (NIWA, Wellington and NIAES, Japan) for [N_2O], $\delta^{15}N_{bulk}$-N_2O, $\delta^{18}O$-N_2O and SP_{N2O}. Standardisation was achieved through the following method. Blank water samples were prepared by passing helium through large Cubitainer® (20 L) vessels and were then equilibrated with air and transferred to the 200 ml serum bottles in the same way as samples were collected. These samples were sent to two different labs for concentration, isotope and isotopomer analysis. Similar way standards were prepared using N_2O reference gas by passing through the blank Milli-RO® water which is then transferred to the serum vials using leakage proof techniques and were send to other labs for [N_2O], $\delta^{15}N_{bulk}$-N_2O, $\delta^{18}O$-N_2O and $SP_{N2O.}$

Table 2.3: Analytical event timing for the automated sparging system.

Time (s)	A1 8 - port valve	A7 6 - port valve	A8 4 - port valve	A3 -60 C trap	A2 high - flow trap	A4 low - flow trap	A6 -60 trap heater
0	load	backflush	inject	down	down	up	off
300			bypass				
2090						down	
2100	inject		inject	up	up		
2107							on
2200		inject					
2295							off
2300						up	
2500		backflush					
2600	end run						

The instrument was in perfect condition for one year, and later it developed split double peak structures. All traps were replaced. The 8 port and 6 port Valco® valves were also replaced. A new

GC- Column was also installed. The instrument was in leak-proof condition. This troubleshooting procedure took four months to bring the instrument back to working condition.

2.5.3.3. Measurement of dissolved N_2O concentration

Dissolved [N_2O] was determined using the above described automated purge and trap system. After the analysis major ion peak areas (mass-to-charge ratio [*m*/*z*] = 44) were used to determine the dissolved nitrous oxide concentrations. For calibration m/z = 44 peak areas from N_2O concentration standards of 30.5 nM and 10.5 nM were measured. Triplicates of standards were measured after each set of five samples. The average of the standards measured before and after the sample analysis was used as the correction factor to determine the sample [N_2O]. The actual [N_2O] of the samples were determined as follows.

$$[N_2O] = \text{Calculation factor} \times \text{Peak Area}$$

The equilibrium N_2O concentrations ($[N_2O]_{equilibrium}$) in the seawater samples were measured using solubility equation of N_2O in moist air given by Weiss and Price (1980), using CTD temperature and salinity and N_2O partial pressure.

$$[N_2O]_{equilibrium} = F\ x'\ P$$

$[N_2O]_{equilibrium}$ is the equilibrium concentration of N_2O (mol/L) in seawater in equilibrium with moist air at P = 1 atm. F is the solubility coefficient of N_2O, expressed in mol L^{-1} atm^{-1}, x' stands for the dry mole fraction of atmospheric N_2O, and P stands for the ambient pressure. Atmospheric dry mole fractions for N_2O varies according to regions. For Southwest Pacific Ocean regions these data is extracted from the monthly time series of atmospheric N_2O from the Baring Head and Taiaroa Head monitoring stations of NIWA at Wellington, New Zealand (ftp://ftp.niwa.co.nz/51ropic/n2o/bhd/BHDN2O.dat). G. D. Rao of National Institute of Oceanography, Vishakhapatnam, India (personal communications) for the Indian Ocean waters, provided the overlying atmospheric mean N_2O concentrations

2.5.3.4. N_2O percentage saturations

N_2O % saturation were calculated using the equation $R= C_{measured}/C_{equilibrium}$ and is expressed in %, where $C_{measured}$ is the measured N_2O concentration, and $C_{equilibrium}$ is the equilibrium concentration calculated as a function of depth and temperature.

$$N_2O \text{ \% saturations} = [N_2O]_{measured} / [N_2O]_{equilibrium}$$

2.5.3.5. Apparent N_2O production (ΔN_2O)

ΔN_2O was determined by subtracting equilibrium N_2O concentration ($[N_2O]_{equilibrium}$) from the actual measured concentration ($[N_2O]_{measured}$) as shown below.

$$\Delta N_2O = [N_2O]_{measured/observed} - [N_2O]_{equilibrium}$$

2.5.3.6. N_2O Stable Isotopes and Isotopomers

The two stable isotopic components of N_2O of prime importance are $^{15}N/^{14}N$ of N and $^{18}O/^{16}O$ of O. The stable isotope ratio $^{15}N/^{14}N$ of N_2O is expressed as $\delta^{15}N_{AIR}$ relative to atmospheric N_2 and is expressed as $\delta^{15}N_{bulk}$ ($\delta^{15}N$-N_2O).It is the ratio of the heavy (rare) isotope to the light (abundant) isotope.

$$\delta^{15}N_{AIR} \text{ (sample) [‰]} = (((^{15}N/^{14}N) \text{ sample} / (^{15}N/^{14}N) \text{ standard} - 1) \quad (1)$$

$\delta^{18}O_{VSMOW}$ is the isotope ratio $^{18}O/^{16}O$ of N_2O also expressed in the same way, relative to Vienna Standard Mean Ocean Water (VSMOW). $\delta^{18}O_{ATM}$ relative to O_2 in the atmosphere can be used after the following equation: $^{18}O_{ATM} = -23.0 + {}^{18}O_{VSMOW} / 1.0235$ (Kim and Craig., 1990). $\delta^{18}O_{ATM}$ for nitrous oxide is expressed as $\delta^{18}O$-N_2O.

$$\delta^{18}O_{ATM} \text{ (sample) [‰]} = (^{18}O/^{16}O) \text{ sample} / (^{18}O/^{16}O) \text{ standard} - 1 \quad (2)$$

In IRMS the ion currents at masses 44, 45 and 46 are continuously using Isoprime EA- Masslynx 3.6 *i* software. Mass peaks are integrated over time and are ratioed for 45/44 and 46/44. $\delta^{15}N$ and

$\delta^{18}O$ are calculated relative to 45/45 and 46/44 ratios of a standard using the above equation (1) and 2.

The intramolecular distribution of ^{15}N is often expressed as the site preference (SP= $\delta^{15}N_{\alpha}$ - $\delta^{15}N_{\beta}$, Toyoda and Yoshida., 1999). Quantification of the relative abundances of ^{15}N in the central (α) and terminal (β) positions of the linear N_2O molecule relies on the fragmentation of N_2O^+ to NO^+ within the ion source of a mass spectrometer (Toyoda *et al*., 2005). Molecular (N_2O+) and fragment (NO+) ion measurements at m/z 44, 45, 46, 30 and 31 were made separately on each gas sample using an Isoprime® IRMS for the determination of stable isotopes and isotopomers. 45/44, 46/44 and 31/30 ratios provide $\delta^{15}N_{bulk}$, $\delta^{18}O$ and $\delta^{15}N_{\alpha}$ respectively.

Since $\delta^{15}N_{bulk}$ does not differentiate between the nitrogen isotopomers it is considered as the average of the both isotopomers, $\delta^{15}N_{bulk} = (\delta^{15}N_{\alpha} + \delta^{15}N_{\beta})/2$. So from measuring $\delta^{15}N_{\alpha}$ and $\delta^{15}N_{bulk}$ the value of $\delta^{15}N_{\beta}$ can be deduced, and site preference can be calculated using the equation SP = $\delta^{15}N_{\alpha}$ - $\delta^{15}N_{\beta}$.

In IRMS the difference in ^{15}N abundance between a sample and a certified reference gas calibrated to atmospheric N_2 is measured. A reference gas was used for the normalization of the results and injected through the open split of the IRMS prior to each sample measurement. The reference N_2O gas tank used in this study was calibrated for $\delta^{15}N_{bulk}$, $\delta^{15}N_{\alpha}$ versus AIR N_2, $\delta^{18}O$ versus VSMOW and Site Preference (S.P) by Yoshitaka Uchida at the National Institute for Agro Environmental Sciences (NIAES), Japan. The results of this calibration yielded $\delta^{15}N$ values versus AIR N_2 of +0.05 ± 0.02 ‰ (δ^{15}Nbulk), –2.48 ± 0.05 ‰ ($\delta^{15}N_{\alpha}$), and -5.05 ± 0.08 ‰ (S.P) and a $\delta^{18}O$ value of +39.56 ± 0.09 ‰ versus VSMOW for the Otago-Isotrace lab N_2O reference tank. For the sample measurements, standards were prepared by purging the same reference tank N_2O through helium purged Milli-Q water. These standards were also analyzed for the above parameters at NIAES, Japan.

2.5.4. The isotope labelled incubation experiment

To study the processes prevailing in the Otago Continental Shelf transect labelled isotope incubation experiments were also conducted. The incubation experiments were conducted at the selected stations and depths of Otago continental shelf transect during November 2012 time series

in Polaris II. It was performed at neritic station B and Sub Antarctic station D. For shallow station B incubation was conducted at the surface and for station D at the surface, 100 m and 500 m depths. Total four sets of incubations were stetted up at different depths and stations. For each depths, two sets of samples were collected in the 5 L incubation vessels Cubitainer®. They were treated with labelled isotopes $^{15}NH_4Cl$ and $K^{15}NO_3$ respectively corresponding to the 10 % of the ambient concentration. 99 % ^{15}N labelled ammonium chloride, and potassium nitrate were used for the addition (Cambridge Isotope Laboratories, Inc). Samples for [N_2O], $\delta^{15}N_{bulk\text{-}}$ N_2O, nitrate (NO_3^-) and ammonia (NH_4^+) from the same depths as mentioned earlier were taken as the control samples. $^{15}N_2O$ was not available for the current experiments which will correct the changes due to the variations in purging efficiency during each sample injection, though the natural background level of $^{15}N_2{}^{18}O$ was insignificant. A total of four subsamples were drawn from each Cubitainers at regular intervals of 3 hours during the 12 hours of incubation for the measurement of [N_2O], $\delta^{15}N_{bulk\text{-}}$ N_2O, NO_3^-) and NH_4^+. For the detailed analytical methods see the previous sections.

2.5.5. Apparent oxygen Utilisation (AOU)

Apparent Oxygen Utilization (AOU) is an estimate of the O_2 utilized by biochemical processes primarily respiration. AOU was calculated as the difference between the measured dissolve concentration $[O_2]_{observed}$ and its equilibrium saturation concentration $[O_2]_{equilibrium}$ in water with the same physical and chemical properties.

$$AOU=[O_2]_{equilibrium} - [O_2]_{observed/measured}$$

$[O_2]_{equilibrium}$ was calculated as a function of in situ temperature and salinity, and one atmosphere of total pressure, using the equation of Garcia and Gordon (1992) in µM. $[O_2]_{observed}$ is the calibrated dissolved oxygen concentrations obtained from the CTD data.

2.5.6. Other $\delta^{18}O$ measurements

2.5.6.1. $\delta^{18}O$ of Dissolved Oxygen ($\delta^{18}O$-$O_{2,dissolved}$)

$\delta^{18}O$-$O_{2,dissolved}$ was measured by a modified method described by Barth *et al.* (2004) using a Thermo GasBench attached to a Thermo Delta ^{PLUS} XP IRMS. 10 ml headspace was created in 12.1 ml Exetainer® vials prior to the analysis followed by ultrasonication to bring the dissolved oxygen to the headspace. After equilibrium is re-established, these samples were injected to the IRMS through the Gas Bench. The oxygen standards of known concentrations and isotope values are prepared by mixing various amounts of air with helium. The concentrations of oxygen standards established through additions of air (200, 400 and 800 µL) to the helium flushed vials were 3.0, 5.9 and 11.5 parts per thousand O_2(g) respectively. All dry air standards had an isotopic composition 0 ‰ of AIR (+23.8 ‰ VSMOW) ± 0.3 ‰.

2.5.6.2. Water oxygen ($\delta^{18}O$-H_2O)

$\delta^{18}O$-H_2O isotope ratios were measured using a Picarro 2120 wavelength-scanned cavity ring-down spectrometer (WS-CRDS; Picarro Inc, USA). Eight repeat aliquots of 1.8 µl were injected into a vapouriser unit using an HTC-Pal autosampler (Leap Technologies, USA) and each transferred into the spectrometer cavity under software control. The final five of the eight raw results were filtered by removal of values more than 1 standard deviation from the average. The average was corrected to the international VSMOW-SLAP isotope scale using a three-point calibration provided by three laboratory standards measured before and after every batch of 80 samples (Table 2.4). Also, a control sample was chosen to be similar to the samples being measured and was measured after every 6 samples. Instrumental drift correction, if applied, was calculated from a linear regression of the control sample result against time. Accepted values for the laboratory standards were obtained from 6-year internal laboratory calibration records against primary reference materials, VSMOW, GISP and SLAP, external 6-member interlaboratory comparison exercise and by back-calculation from the ~170 member IAEA inter-laboratory comparison exercise, WICO2012. The laboratory standards and their consensus values are as shown in table 2.4.

Table 2.4: Laboratory standards and their isotopic values for $\delta^{18}O\text{-}H_2O$

"ICE"	**"TAP"**	**"SEA"**
$\delta^{18}O_{VSMOW}$, ‰	$\delta^{18}O_{VSMOW}$, ‰	$\delta^{18}O_{VSMOW}$, ‰
-32.20 ± 0.09	-12.00 ± 0.09	-0.27 ± 0.09

2.5.7. Assessment of the measurements

Table 2.5: The precision and standard deviation of the measurements for the various parameters. For the precision, units are ‰ for all except $[N_2O]$ for which it is µM.

Measured Parameter	**Precision**	**Standard Deviation (%)**
N_2O Concentration	0.3	0.7
$\delta^{15}N\text{-}N_2O$	0.8	0.6
$\delta^{18}O\text{-}N_2O$	0.5	0.4
S.P	1.1	0.6
$\delta^{18}O\text{-}H_2O$	0.4	0.2
$\delta^{18}O\text{-}O_{2,dissolved}$	0.3	0.3

The precision and accuracy of measurements made with the purge and trap system were assessed by the following method. Tropospheric N_2O equilibrated with Milli-RO® was measured at NIAES, Japan and excellent agreement was found with measurements of the present study. A summary of the results obtained by comparison of 15 replicates measured with the instrument for N_2O parameters and other isotopic parameters on different instruments is presented in table 2.5. The same set of tropospheric air equilibrated water samples was used as control samples after every 5 real samples.

2.6. Conclusions

1. A new analytical system to determine the concentration, stable isotopic and isotopomeric characteristics of nitrous oxide was developed with very good accuracy and precision.

Chapter 3

N_2O in the Southwest Pacific (SWP) Ocean

3.1. Introduction

Oceanic N_2O plays a significant role in the atmospheric N_2O budget (Bange. H. W., 2006). Approximately one quarter to one-third of natural N_2O comes from marine systems (Houghton *et al.*, 2001). N_2O is produced in the oxic subsurface and deep ocean during microbial nitrification. Similarly, in anoxic to suboxic parts of the ocean, N_2O can be produced and/or consumed during denitrification (Bange. H. W., 2010). Large parts of the surface ocean are close to equilibrium with the atmosphere.

The Southern Ocean and Southwest Pacific Ocean are poorly sampled, and there is insufficient data available about N_2O distribution (Nevison *et al.*, 1995). Particularly poorly represented are seasonal data and isotopic and isotopomer studies to infer its production and processes in these regions. There are many reasons why the subantarctic and subtropical sectors of the Southwest Pacific (SWP) are crucial to knowledge about N_2O in the ocean, as explained in the previous chapter (Section 2.3.2.1). New Zealand lies in the SWP, and its maritime domain is one of the largest on the planet, which intersects with the Southern Ocean. Three major oceanic frontal zones, STF (subtropical front), SAF (subantarctic front) and PF (polar front), are very close to New Zealand and so the regions around New Zealand may be a source of N_2O due to nearby productive frontal zones. The major changes in oceanic physical, chemical and biological properties occur across the convergence zone (STF), and hence New Zealand is an important place for N_2O oceanographic studies.

3.2. Objectives

The objectives of this chapter are:

1. to quantify and describe the water column N_2O distribution and variations in the Southwest Pacific Ocean and subantarctic sector of the Southern Ocean

2. to interpret the N_2O data in the context of the hydrographic properties and water mass distributions to understand N_2O cycling in the ocean. In particular:

- to establish whether these regions are sources or sinks for atmospheric N_2O by studying the percentage saturation of N_2O
- to understand the variations and relationship between N_2O, DO and nitrate to study the processes responsible for N_2O in these regions

3. to study the seasonal variations of N_2O distribution along the Otago continental shelf transect and identify long-term changes in N_2O in intermediate and deep waters.

3.3. Sampling and locations

As discussed in Chapter 2, samples from the SWP were collected on four different voyages: Geotraces, Mooring, Bloom and Polaris. From Polaris transect samples were collected from different water masses: subantarctic (PD), subtropical front (PC), modified subtropical water (MSTW) (PB) and neritic (PA) during different seasons. The samplings were conducted between June 2011 and November 2012. Details about sampling stations and methodologies are given in Figures 2.1, 2.2, 2.4a, 2.4b and Tables 2.1 and 2.2 respectively. The locations of the sampling stations are given in Figure 3.1

.

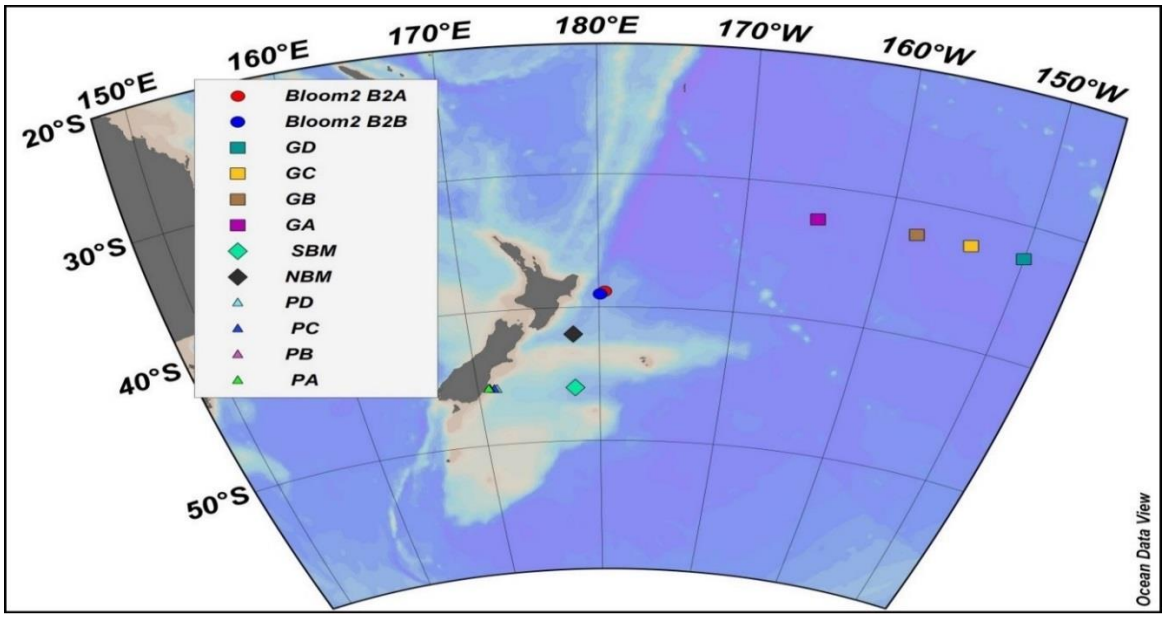

Figure 3.1: Sampling stations

3.4. Characteristic water masses in the study regions

Surface processes in the ocean create water masses with well-defined temperatures and salinity properties. In the polar regions water masses cool, increase in density and sink and then mix slowly with other water masses as they move along the isopycnal surfaces. The water masses can be identified by their characteristic temperature-salinity (T-S) relationship. A T-S diagram devised by Helland-Hansen (1916) was used (Fig. 3.2) to understand the different water masses in the current study regions of the SWP.

The T-S plot for the study regions shows the prevailing major oceanic water masses at each sampling location. Southwest Pacific Ocean waters are characterised by subtropical surface water (STSW) at the surface, followed by Antarctic Intermediate Water (AAIW) in the mid-water column (500-1200 m) and Circumpolar Deep Water (CPDW) at the bottom. Subantarctic sectors of the SWP have all the same characteristic water masses except at the surface, where it is characterised by cooler and fresher subantarctic surface water (SASW).

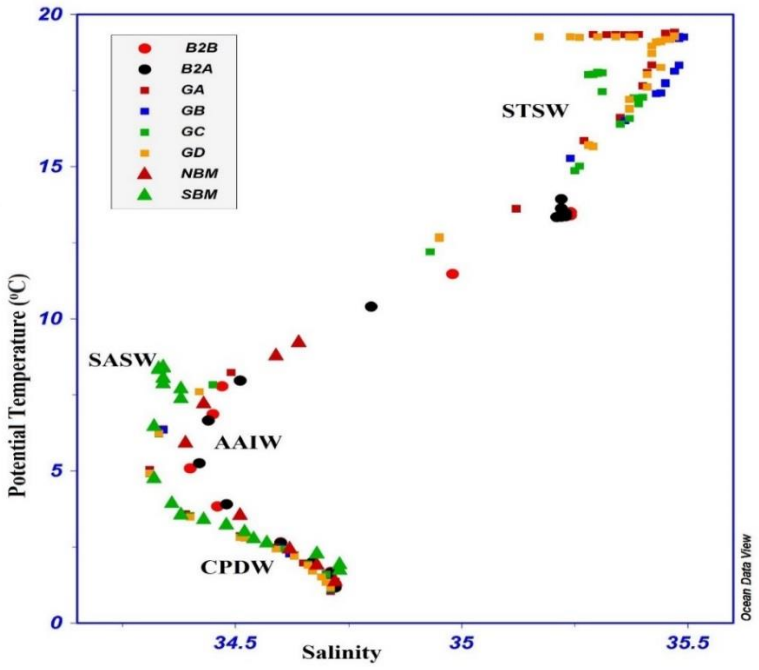

Figure 3.2: T-S diagram for the three transects NZ-Geotraces (GA, GB, GC and GD), Bloom II (B_2A, B_2B) and Biophysical Mooring (NBM and SBM) stations. STSW- Subtropical Surface Water, SASW- Subantarctic Surface Water, AAIW-Antarctic Intermediate Water and CPDW-Circumpolar Deep Water.

Similar characteristic water masses have been identified for these regions in earlier studies (Sverdrup *et al.*, 1942; Jillet. J. B., 1969; Baer Jones. K. N., 2012). The four Geotraces stations (Fig. 3.1) have almost the same T-S curves, indicating consistent water mass structure across the transect. Surface waters (0 - 250 m) corresponded to the warm and saline subtropical surface water (STSW) and had a temperature of 12-20 ^{o}C and salinity of 35.2-35.5. The two Bloom II and Northern Biophysical Mooring (NBM) stations showed identical water mass characteristics with a similar T-S curve (Fig. 3.2), although the surface waters were slightly fresher and cooler than the Geotraces surface waters (for more details, see the study area descriptions in Chapter 2). Salinity ranged between 34.90 - 35.30 for these waters and temperatures between 11 and 14 ^{o}C. The second type of surface water mass present in the study region was in the subantarctic section of the Mooring transect (SBM). T-S properties (Fig. 3.2) shows the characteristic properties of subantarctic surface water (SASW) (Burling. R. W., 1961; Jillet. J. B., 1969). The temperature values ranged between 7.3 and 8.4 ^{o}C and salinity between 34.34 and 34.38, suggesting that these waters are subantarctic surface water (Jillet. J. B., 1969).

To understand the water mass variations in detail, T-S relationships alone are insufficient, particularly in the surface ocean here they undergo property changes in response to atmospheric conditions. Potential density (σ_t) values were also studied to give more indications about the respective water masses as indicated in Figure 3.3 (Table 3.1). From the σ_t values it is evident that the Geotraces STSW and the STSW from the Bloom II and Mooring stations were distinct from one other and SASW.

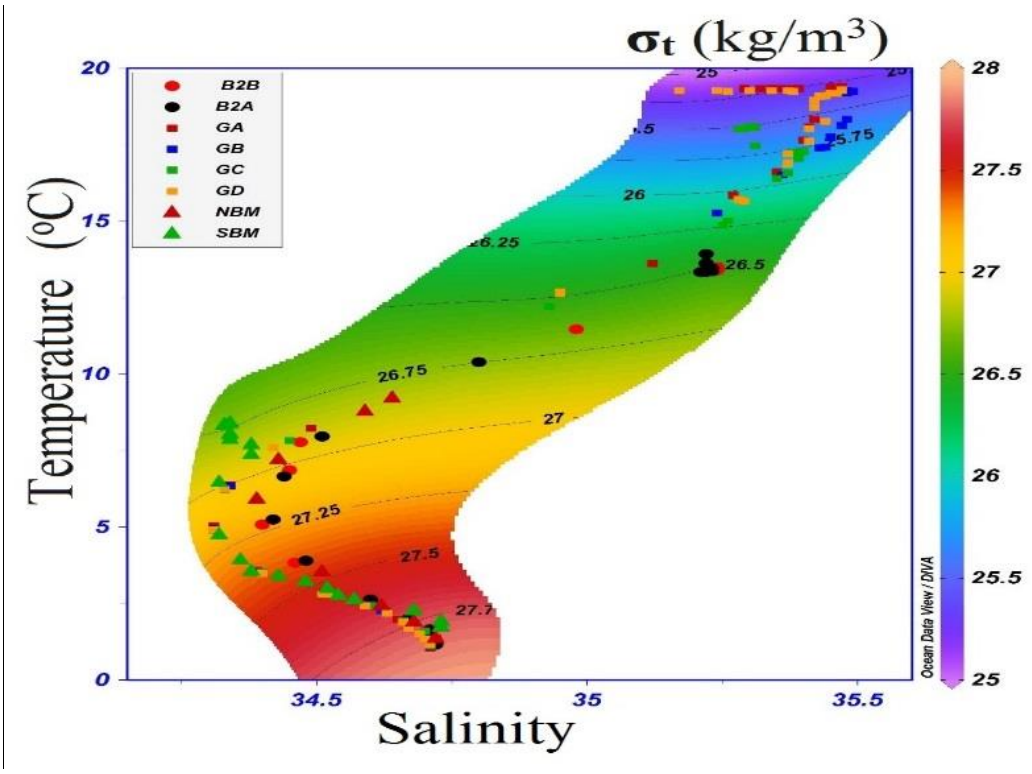

Figure 3.3: Potential density (σ_t) characteristics for different stations as identified in the legend.

Below the 500 m, at all stations and beneath surface central water masses, temperature decreased with increasing depth. The T-S curves obtained for the present study (Fig. 3.2) were comparable with those of earlier water masses studies by Jillet. J. B (1969) for subantarctic regions to the south of New Zealand and more recently by Bostock *et al.* (2013). From these results, it can be inferred that Antarctic Intermediate Water (AAIW) was present below the surface central water masses and had the lowest salinity of all water masses. A comparative evaluation of the present study results with those from above-mentioned earlier observations is given in Table 3.2 and Figure 3.4. Potential density values were used to locate the core AAIW positions as well as T-S values.

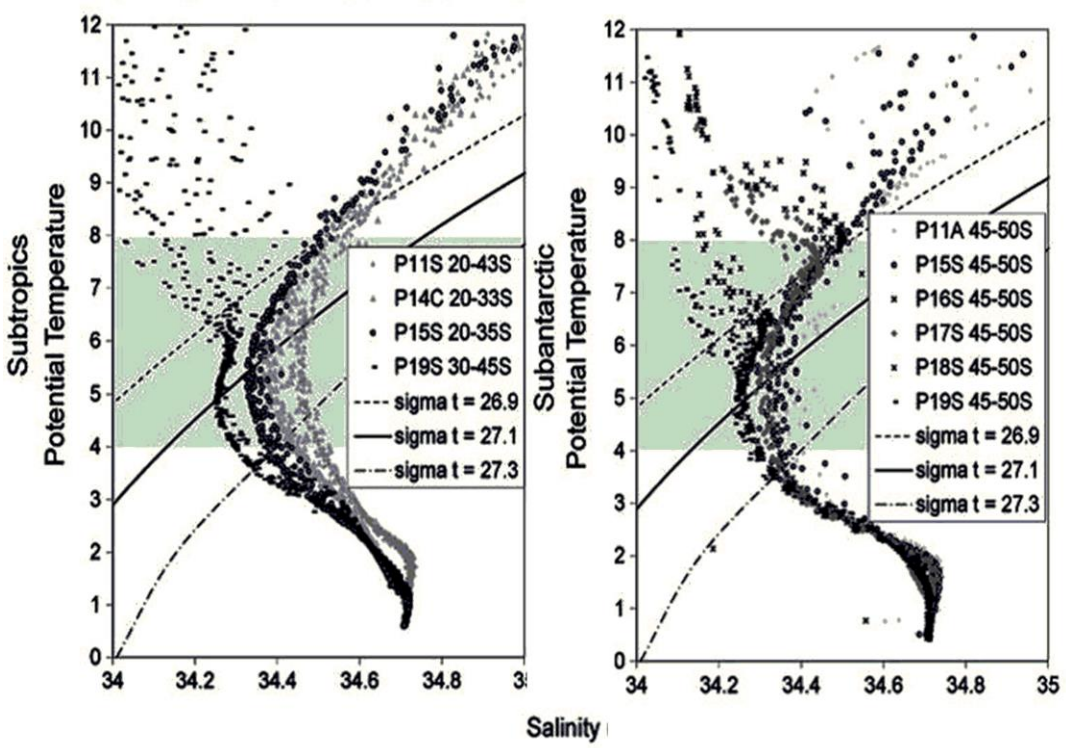

Figure 3.4: T-S diagram for AAIW of subtropical and subantarctic waters shown under the shaded areas (Bostock *et al.*, 2013)

Throughout the study regions, the salinity minimum was at the AAIW, with the salinity increasing to the bottom and remaining constant below a depth of 2500 or 3000 m. The observed temperature and salinity properties were similar to the cold and saline circumpolar deep water (CPDW) (Tomczak *et al.*, 2003) and were found in the deepest regions of all stations, as shown in Figure 3.2. These temperatures ranged between 1 and 2.5 ^{o}C for all deep waters at the different stations. Earlier studies (Sverdrup *et al.*, 1942) also suggest a temperature between 0.5 ^{o}C and slightly over 2 ^{o}C for CPDW. Salinity values were between 34.68 and 34.73 for the stations in the present study, while previous observations ranged from 34.70 to 34.76 for CPDW for different oceanic regions (Sverdrup *et al.*, 1942). A potential density range of 27.50 - 27.83 kg m^{-3} was also observed for present stations, which is in accordance with the previous studies (Sverdrup *et al.*, 1942) is a characteristic property of CPDW.

Table 3.1: Properties of AAIW for Geotraces, Bloom II and Mooring station

Stations	Depth range for AAIW (m)	Temperature (^oC)	Salinity	σ_t (kg/m^3)	Core AAIW Properties (T, S, σ_t)
Geotraces					
GA	500-1200	4.0-8.0	34.3-34.5	26.9-27.3	(5.2,34.3,27.1)
GB	500-1200	4.0-8.0	34.3-34.5	26.9-27.3	(4.9,34.3,27.1)
GC	500-1200	4.0-8.0	34.3-34.5	26.9-27.3	(4.9,34.3,27.1)
GD	500-1200	4.0-8.0	34.3-34.5	26.9-27.3	(5.0,34.3,27.1)
Bloom II					
B_2A	500-1200	5.3-7.9	34.4-34.5	26.91-27.20	(5.25,34.4,27.2)
B_2B	500-1200	5.1-7.8	34.4-34.4	26.95-27.20	(5.08,34.4,27.2)
Mooring					
NBM	500-1000	4.9-7.3	34.3-34.4	26.95-27.15	(4.88,34.3,27.1)
SBM	300-1000	4.8-6.5	34.3	26.98-27.18	(4.76,34.3,27.1)

Table 3.2: Comparison of various conservative properties of different AAIW as classified by Bostock, 2013 with present study results

Physical and geochemical tracers	SE Pac AAIW (30-55ºS,80-105ºW)	SO AAIW (45-55ºS,150ºE-120ºW)	Eq PIW (5-20ºS,110-80ºW)	Tasman AAIW (12-45ºS-145-175ºE)	Present study 30-46ºS,170ºE-149ºW
Salinity	34.2 - 34.4	34.28 - 35.6	34.5 - 35.6	34.45 - 35.6	34.2 - 34.5
Potential temperature	4 - 8	4 - 8	4 - 8	4 - 8	4 - 8
Potential density	27.1	27.1	27.3	27.1	26.9 - 27.3

The surface water mass movements are shown in Figure 3.5. The central subtropical surficial water masses in the study regions are formed through Ekman subduction from the mixed layer waters in the subtropical convergence (STC), now more commonly referred to as the Subtropical Front, which is then advected towards the tropics along isopycnal surfaces (Sprintall and Tomczak., 1993). AAIW is initially formed in the SWP, west of southern Chile (Mc Cartney., 1977); it is a mixture of both Antarctic surface water and subantarctic water and is formed by subduction beneath the surface in the Antarctic convergence zone (Jillet. J. B., 1969), as shown in Figure 3.5. AAIWs then moves northwards into the South Pacific subtropical gyre and mixes with equatorial Pacific intermediate water. Bostock *et al.* (2013) propose a modified pathway for AAIW, according to which the AAIW water mass is advected towards the northwest, bisecting the Geotraces transect in the present study. A second source region of AAIW is north of New Zealand, originating in the Tasman Basin, formed through the mixing of AAIW with thermocline waters of Tasman gyre, advecting along Chatham Rise and present at the Bloom II stations. Conversely, along the South Island and south of New Zealand, AAIW originates directly from the Southern Ocean AAIW and is present at the Mooring stations. It is relatively fresh and colder and more recently ventilated and hence more oxic than AAIW in the other regions, (Bostock *et al.*, 2013). The bottom CPDW water masses are supplied from Antarctic circumpolar water and current flow is relatively slow (Fig. 3.5) (Millero *et al.*, 2006).

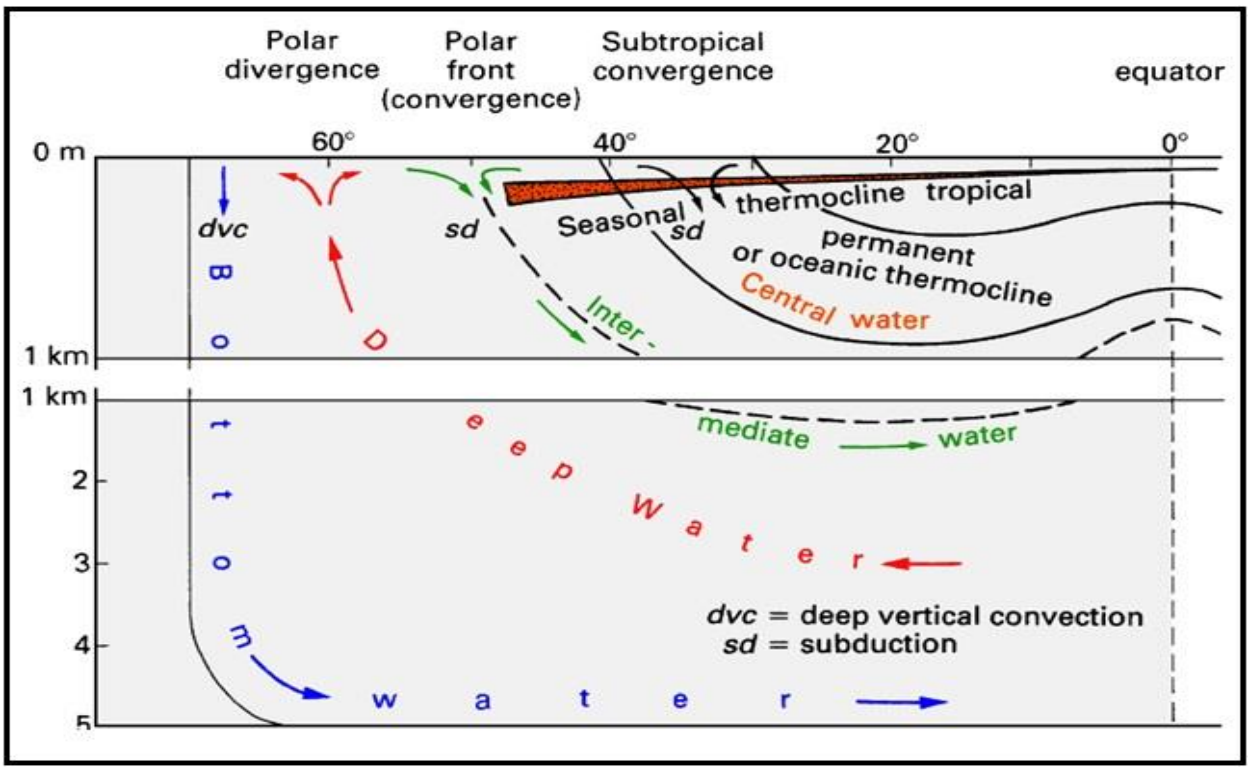

Figure 3.5: Water mass movements in the Southern Hemisphere (Tomczak, 2001)

Insight into the ocean mixed layer, isopycnal and thermocline depths is important for water mass identification in order to understand the various processes and cycling involved. The surface mixed layer is the upper homogeneous layer of hydrographic properties, such as temperature, salinity and density, across which heat and freshwater transfer take place between the atmosphere and the sub-surface ocean (Pickard and Emery., 1990). The surface mixed layer (ML) depth is calculated from the temperature profile at each station (Kara *et al.*, 2000); and is defined as the depth at which the temperature differs from surface temperature by 0.2 ^{o}C. Details of the ML at the different stations are given in Table 3.3, and the CTD temperature and potential density profiles for each station in Figure 3.3. The thermocline is the depth zone of a significant change in vertical temperature below the upper, warmer isothermal ML and deeper, colder water, and varies in gradient and depth with geographic locations (Pickard and Emery., 1990). Details of the thermocline depth for the different stations of present study regions are given in Table 3.3.

Table 3.3: Depth ranges for ML and thermocline for different stations.

Station ID	Surface mixed layer (m)	Thermocline(m)	Station ID	Surface mixed layer (m)	Thermocline(m)
Geotraces			Bloom II and Mooring		
GA	0-160	200-1000	B2A	0-150	300-1200
GB	0-140	200-1200	B2B	0-200	300-1200
GC	0-140	250-1000	NBM	0-150	200-1200
GD	0-140	200-1000	SBM	0-75	100-1000

Table 3.4: Depth ranges for ML at Otago Continental Shelf transect for different stations.

Station ID	Surface mixed layer (m)		
	September 2011	November 2012	May 2012
PA	0-75	0-15	0-75
PB	20-100	20-100	0-100
PC	0-60	0-15	0-100
PD	0-85	0-10	0-70

The Otago continental shelf transect includes coastal, subtropical frontal and subantarctic waters, and so shows significant differences in water mass characteristics between stations. During spring, the two coastal stations (PA and PB) had properties of neritic water with reduced salinity of 34.3-34.5 and a higher temperature at the surface (0-20 m). The bottom waters were modified subtropical water (MSTW) with characteristic salinity of 34.6-34.9 (Garner. D. M., 1961; Houtman. T. H. J., 1966; Jillet. J. B., 1969). Previous studies also identified MSTW as a subsurface feature underlying neritic waters in spring and summer (Jillet. J. B., 1969; Currie and Hunter, 1999; Hopkins *et al.*, 2010; Baer Jones, K. N., 2012). Both these stations showed uniform density from the surface to the bottom during September but were less mixed in late spring in November 2012 (Table 3.4). The neritic waters of inshore regions were formed by land run-off, especially from the Clutha River, which brings fresh waters that mix with water in the Southland Current (Jillet. J. B.,

1969; Currie and Hunter., 1999). T-S plot and variations of density with depth for different sampling periods for the Otago Continental Shelf water masses are shown in Figure 3.6. From the coast to the open ocean, surface water mass characteristics are influenced by the presence of the subtropical front (STF, station C) and then the fresher and colder subantarctic surface water (SASW, station D). However, below 500 m at both PC and PD stations, the T-S properties were similar to those of AAIW (Fig. 3.6). The mixed layer depths corresponding to different sampling periods are given in Table 3.4.

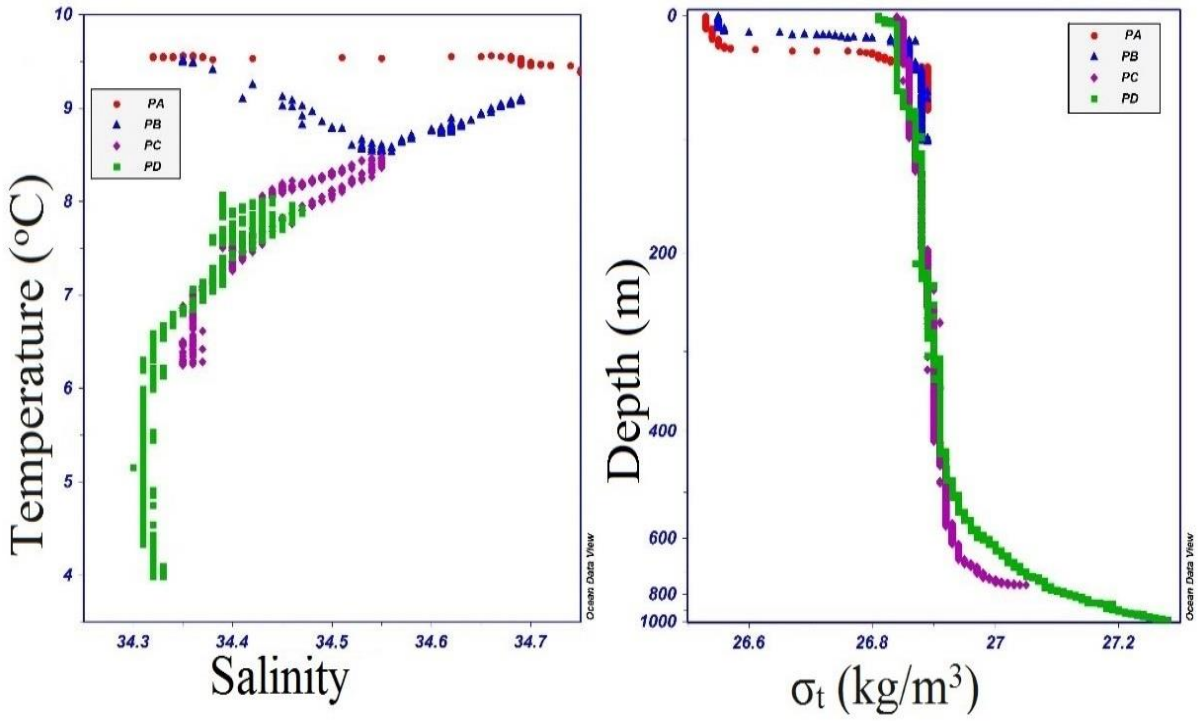

(a)

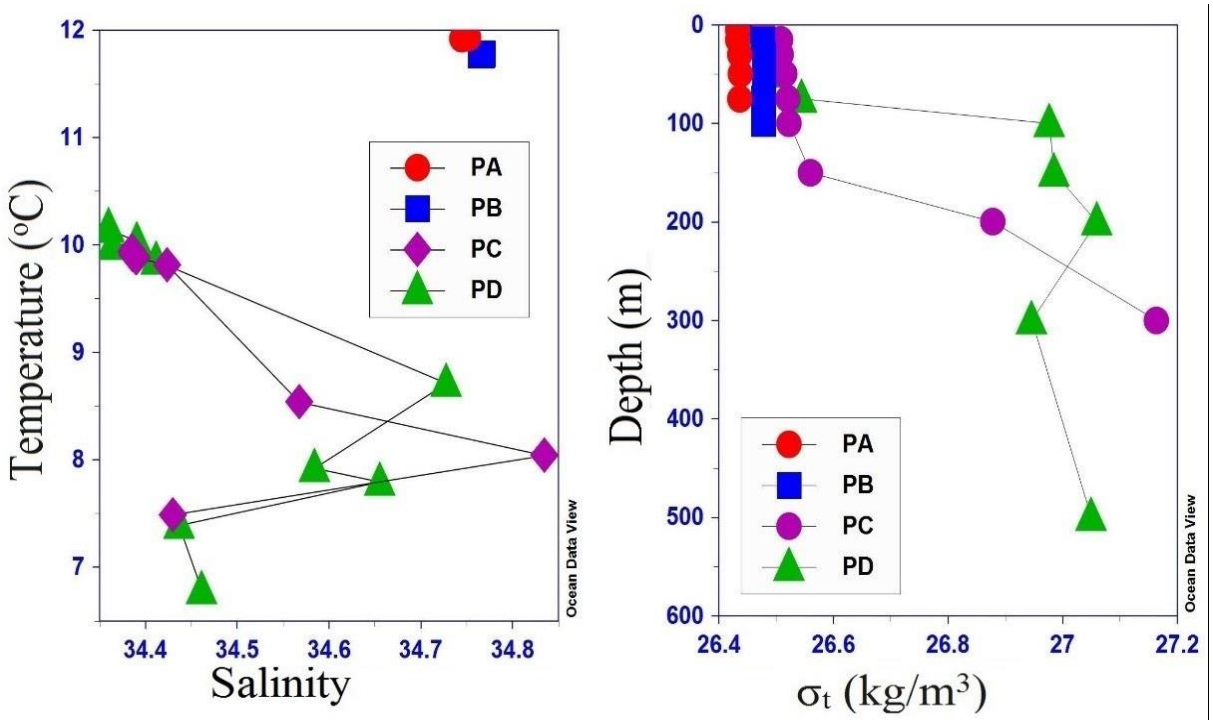

(b)

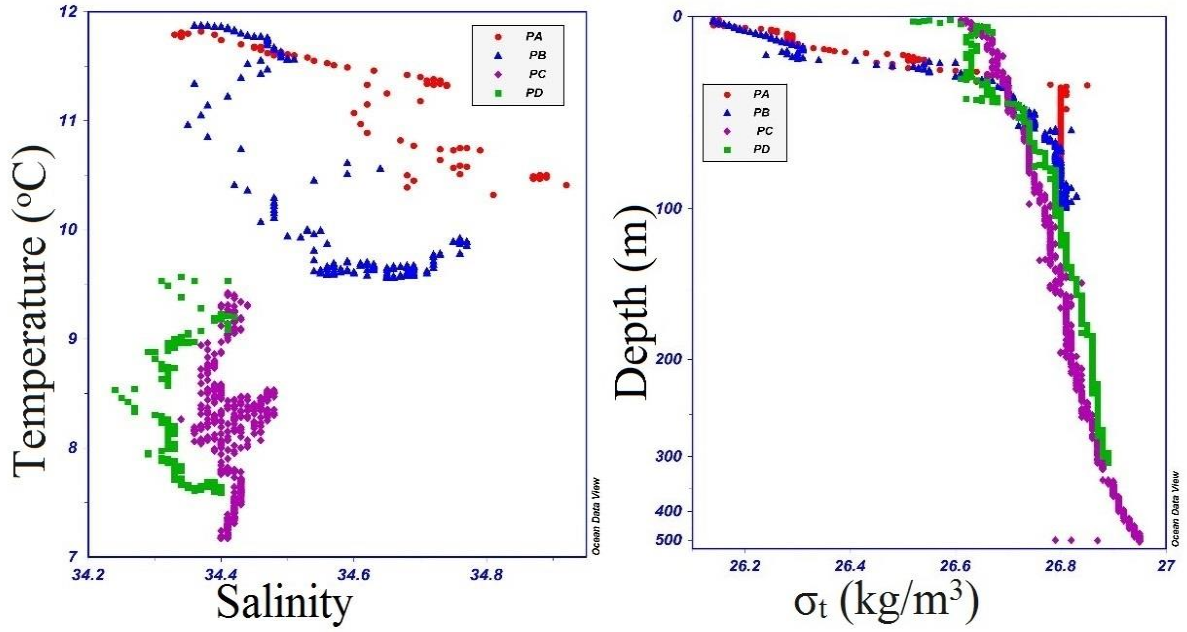

(c)

Figure 3.6: T-S properties and Potential Density (σ_t) characteristics of Otago continental transect a) September 2011 b) May 2012 and c) November 2012.

3.5. N_2O analytical procedures

Discrete samples for N_2O concentration collected from various cruises were measured using a newly constructed purging and trapping system attached to an IRMS (Isoprime), with the analysis conducted at the University of Otago Isotrace Laboratory. The instrumentation and methodologies used, including standard calibrations for N_2O and other basic hydrographic parameters, have been described in detail in Chapter 2. Water samples for N_2O concentration measurement were collected from 12 different stations in triplicate from various depths.

3.6. N_2O in the Southwest Pacific Ocean (SWP)

3.6.1. NZ-Geotraces transect N_2O distributions

The N_2O distribution in the oligotrophic subtropical waters north of New Zealand at stations GA, GB, GC and GD along the NZ Geotraces GP-13 transect are shown in Figure 3.7a and Table 3.5. [N_2O] measurements have not been made previously along this transect. The [N_2O] profiles showed no systematic variations between the four stations of the transect. The minimum [N_2O] was at the surface layer (σ_t = 25.3), and was relatively uniform along the transect, with an average of 7.9 ± 0.5 nM; whereas below the surface mixed layer [N_2O] varied with depth. In the upper thermocline layers (σ_t = 25.8- 26.5), [N_2O] increased to an average of 11.1 ± 0.4 nM, reaching 16.8 ± 0.8 nM at the base of the thermocline in AAIW (σ_t = 26.9- 27.1). The maximum [N_2O] was found at a depth of ~1500 m, with an average of 21.3 ± 0.6 nM. In the CPDW along the isopycnal layers (σ_t =27.5-27.8), [N_2O] were an average of 19.8 ± 0.2 nM. Some general features of N_2O distribution were common to all stations.

Oceanic N_2O formation strongly depends on DO, and a significant inverse relationship between DO and N_2O accumulation is generally reported, except in surface waters and oxygen-deficient regions (see also Chapter 1, section 1.4.4.1), (Yoshinari. T., 1976; Cohen and Gordon, 1978; Nevison *et al.*, 2003). The Geotraces transect [O_2] depth profiles are shown in Figure 3.7b and d. The minimum oxygen concentration ranged from 144 to 145 µM in CPDW at 1500-2000 m, and so did not decline to hypoxic conditions, with the maximum [O_2] of 226-230 µM in AAIW (Fig. 3.7b). Even though an increase in DO were observed at AAIW, the average [N_2O] was higher than

the overlaying less oxygenated water in the upper thermocline. This may be attributed to high N_2O production in AAIW. N_2O distribution appeared to be inversely related to $[O_2]$, clear from comparing Figure 3.7a and 3.7b, and also Figure 3c, with the maximum N_2O concentration in the oxygen minimum regions at all stations. This trend is consistent with studies from other oceanic regions (Cohen and Gordon, 1979; Butler *et al.*, 1989; Walter *et al.*, 2006).

Interestingly a second oxygen minimum zone was present at all stations at a depth of 250-300 m, but there was no associated N_2O maximum. The decrease in dissolved oxygen at the subsurface layer in upper thermocline is due to the existing local remineralization at these layers. A slight decrease in $[N_2O]$ was seen at a depth corresponding to AAIW, where the dissolved oxygen concentration was highest. The variations in nitrate concentration ($[NO_3^-] + [NO_2^-]$) in Table 3.6 and Fig 3.11 show that the nitrate depth profile was similar to that of $[N_2O]$ except in the upper nitrate-depleted waters. The DO and nutrient (nitrate + nitrite) distributions across the transect showed a similar trend from the surface to the bottom water at all stations (Figures 3.7b and 3.11).

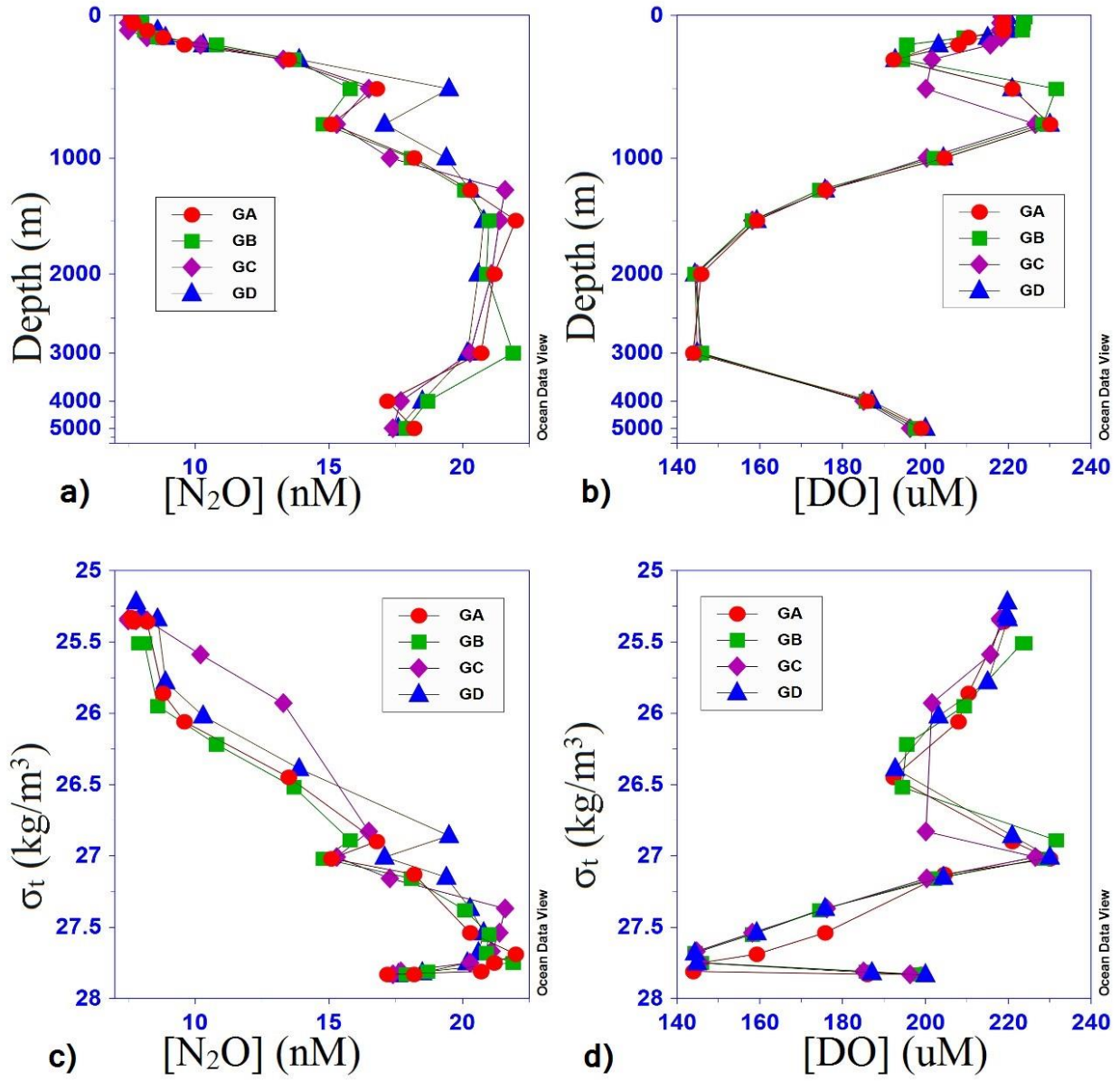

Figure 3.7: a) [N_2O] vs depth, b) [O_2] *vs* depth, c) [N_2O] *vs* σ_t and d) [O_2] *vs* σ_t , for GA, GB, GC and GD during Geotraces GP13.

Figure 3.9 shows the N_2O saturation and apparent oxygen utilisation (AOU) with respect to ambient air. N_2O saturation is an indicator of inferred *in-situ* production of N_2O under ambient conditions. AOU is an inferred estimate of the amount of O_2 consumed during organic matter remineralisation (oxidation) since the water was last at the ocean surface, where it is assumed to be in equilibrium with atmospheric oxygen (Riley and Chester., 1971).

Surface N_2O saturations for the entire region had an average value of 101.9 ± 1.0 % in STSW. This shows the region is in equilibrium with the atmosphere as regards to N_2O saturations with values very close to the global mean of 103.5 % (Nevison *et al.*, 1995; Bange *et al.*, 2008). Saturation values indicate that this region may not be a large net source of N_2O to the atmosphere; however, sea-to-air fluxes will be discussed in the next chapter.

Table 3.5: The geochemical properties of water masses along the Geotraces transect for stations GA, GB, GC and GD. (The values are the means of the measured samples from different depth of the corresponding water masses, the standard deviations are in parenthesis).

Water mass	N_2O[nM]	DO [uM]	Nitrate [µM]	Δ N_2O	N:P	% N_2O Saturation
ML(STSW)	7.9 (0.5)	220.2 (2.1)	0.1 (0.1)	0.2 (0.2)	0.5 (0.6)	101.9 (1.0)
Upper Thermocline (UT)	11.1 (0.4)	203.3 (3.4)	6.2 (2.0)	2.5 (0.4)	12.3 (4.0)	128.8 (9.6)
AAIW	16.8 (0.8)	218.0 (2.9)	25.4 (1.5)	5.0 (0.7)	16.6 (3.3)	138.7 (6.1)
CPDW	19.8 (0.2)	168.3 (1.7)	34.3 (0.6)	5.8 (0.1)	14.0 (1.0)	140.9 (1.8)

Below the surface mixed layer, the percentage saturation values increased to the bottom, which is a strong indication of *in-situ* production in those waters. The bottom water saturation values ranged from 120 - 162 %. The average AAIW saturations were almost 139 %, while those in CPDW were 145 - 155 %. The contributions of N_2O to these water masses through transportation or any other sources will be discussed in the following sections and Chapter 4.

The vertical distribution of N_2O saturation resembled that of AOU (Figure 3.9 a and b), reflecting that the yield of N_2O production increased as O_2 consumption increased, in accordance with earlier studies (Yoshinari. T., 1976). The direct relationship between [N_2O] and AOU can be interpreted as a preliminary evidence of nitrification as the source of N_2O, as inferred in earlier studies

(Yoshida *et al.*, 1989, Nevison *et al.*, 2004). The relationship between [N_2O] and AOU (Figure 3.8) showed a significant positive correlation ($R^2 = 0.93$), with similar N_2O - AOU gradients at for all stations, indicating the absence of any regional variations in N_2O production and oxygen consumption. However, the different water masses had different slopes.

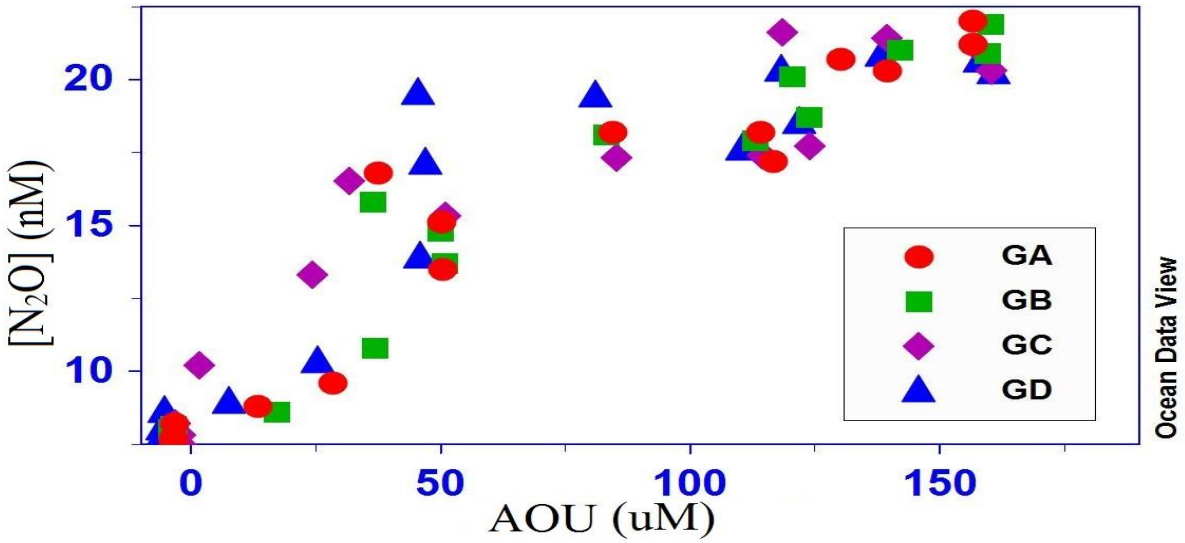

Figure 3.8: The variation of N_2O with AOU.

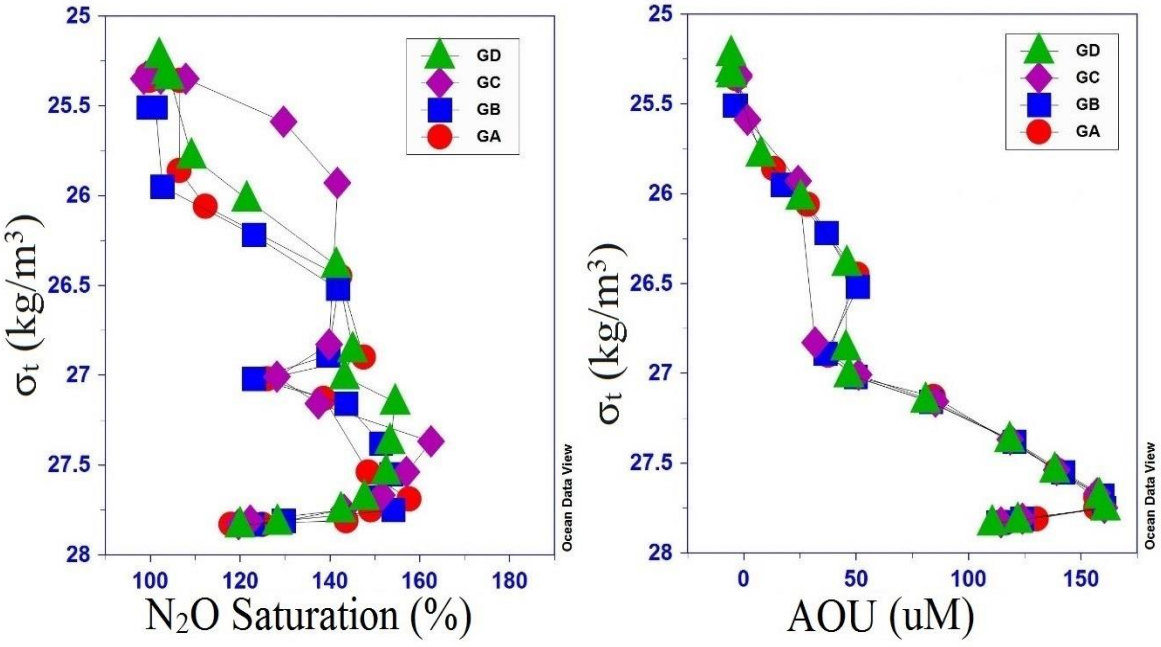

Figure 3.9: Density profiles of a) % N_2O saturation b)AOU for Geotraces transect.

3.6.1.1. ΔN_2O and its relationship with AOU and nutrients

The $[O_2]$ *versus* $[N_2O]$ relationship for the SWP stations was examined further by examining the relationship of ΔN_2O with AOU and $[NO_3^-]$ (Fig. 3.10 b). A positive linear correlation between ΔN_2O and AOU (Table 3.7) is suggestive of nitrification, as the main formation pathway (Yoshinari. T., 1976; Nevison *et al.*, 2004; Walter *et al.*, 2006; Frieng *et al.*, 2009), since nitrification is directly linked to organic matter remineralisation. Previous studies have reported variability (Nevison *et al.*, 2003; Walter *et al.*, 2006; Farias *et al.*, 2007; Frieng *et al.*, 2009; Rees *et al.*, 2011) in the N_2O:AOU relationship with depth. Oceanic $[N_2O]$ has been modelled based on oxygen and nitrate concentrations (Freing *et al.*, 2009). The depth-decreasing feature of ΔN_2O/AOU is clearly visible here (Figure 3.10 a and Table 3.7), as reported in earlier research (Suntharalingam and Sarmiento., 2000), and ranged from 0.10 in the upper ocean to less than 0.05 in the deeper regions, except AAIW. This indicates a much lower ratio of N_2O production to oxygen consumption in the deeper water column.

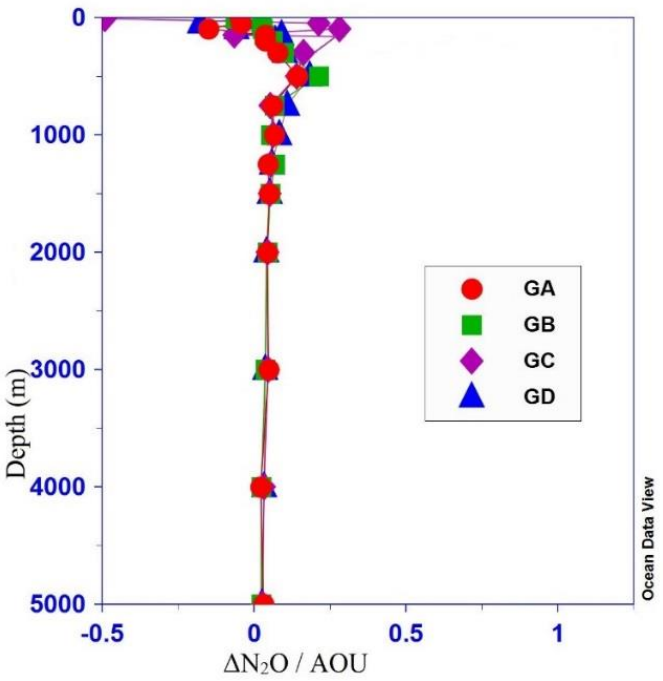

Figure 3.10.a: ΔN_2O/AOU depth profiles for the Geotraces transect

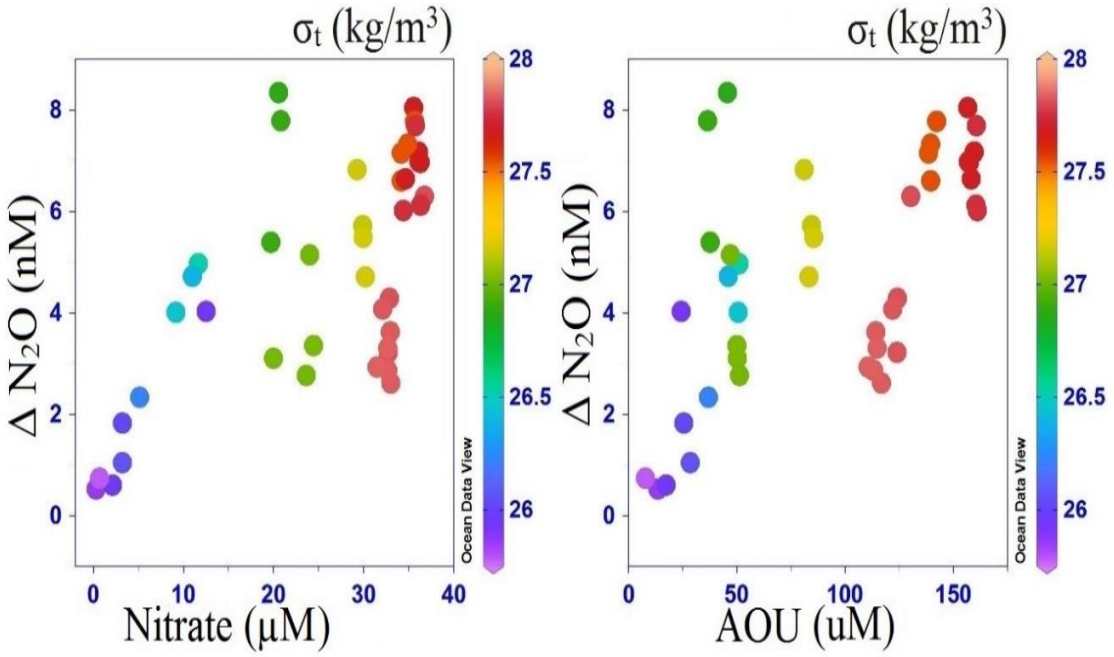

Figure 3.10 b: The relationship between a) ΔN_2O vs nitrate and b) ΔN_2O vs AOU for Geotraces stations below surface mixed layer.

The surface mixed layer values were omitted from Figure 3.10b, as both $[N_2O]$ and O_2 will be influenced by gas exchange with the atmosphere and oxygen production during photosynthesis. Due to the difference in the ratio with depth, the data were split into three subgroups by potential density: - < 26.9 kg m^{-3} (< 500 m or "upper"), 26.9 - 27.1 kg m^{-3} (≤ 1200 m or "AAIW") and > 27.1 kg m^{-3} ("deep"). We applied single regression analysis for the three-isopycnal levels (below the mixed layer such as upper thermocline, AAIW and CPDW) below the mixed layer. ΔN_2O/AOU did not differ significantly from the results of previous studies, which are presented in Table 3.6. The slope obtained for the different stations (Table 3.8) were also in agreement with 0.05-0.10 recorded in earlier studies (Nevison *et al.*, 2003; Walker *et al.*, 2006; Frieng *et al.*, 2009; Rees *et al.*, 2011), as shown in Table 3.6. Although the correlation values were slightly different from one other along the water column in different water masses or density subgroups, a statistically significant positive correlation was observed at each depth within each water masses and providing further evidence of nitrification. The upper thermocline waters had a significant positive correlation ($R^2 = 0.94$). Below this layer in the AAIW due to the increased oxygen concentration and the relative decrease in AOU, the correlation was lower. However the slopes obtained along

the isopycnal layer (σ_t = 26.9 - 27.1) were comparable (slope = 0.05, R^2 = 0.60) to slopes obtained for AAIW in the other studies (Yoshinari *et al*., 1976; Walter *et al*., 2006). In the bottom water below 1500 m along the isopycnal layer (σ_t =27.5 - 27.8, CPDW) a significant positive correlation (slopes = 0.09, R^2 = 0.74) was obtained for the ΔN_2O *vs.* AOU. Overall, the ratio showed little variation, except for the AAIW.

The slope of the ΔN_2O *vs* AOU linear relationship provides an estimate of the N_2O yield per oxygen molecule consumed (Bange *et al.*, 2008; Walker *et al.*, 2010). From the slope, it can be concluded that 0.05-0.10 nmol of N_2O was produced per µmol of O_2 consumed in the shallow and deep water layers. This is consistent with previous observations of 0.004-0.027, 0.14 nmol and 0.09, respectively, for the western North Pacific (Yoshida *et al.*, 1989), Central Pacific (Elkins *et al.*, 1978) and Southeast Pacific.

Table 3.6 : ΔN_2O vs AOU relationship in previous studies

Study Region	Reference	Comments	ΔN_2O= a AOU+ b	
			a	b
NW Atlantic	Yoshinari, 1976	Deep Water	0.09	-2.04
Tropical Pacific	Elkins *et al.*, 1978	Below mixed layer	0.09	-10.5
NW Atlantic	Cohen and Gordon, 1979.	100-2500 m	0.09	-0.43
NE Pacific	Cohen and Gordon, 1979.	100-2500 m	0.22	-46.25
ETNP	Cohen and Gordon, 1979.	700- 3000 m	0.15	-31.33
NW Indian Ocean	Law and Owens,1990	AOU 197 AOU 197	0.03 0.31	+5.55 -49.40

Eastern South Pacific	Farias, *et al*, 2007	Upper Oxycline Lower Oxycline OMZ	0.18 -0.20 -0.72	
North Atlantic	Walter *et al*, 2006	Entire water column	0.09	-3.25
North Atlantic	Freing *et al*, 2009	Sigma 27.5 Sigma 27.5	0.05 0.09	1.08 -5.10
South East Pacific	Charpentier *et al.*, 2007	200-1000 m	0.09	1.21

.

Table 3.7: Comparison of ΔN_2O vs AOU relationship for the Geotraces stations

Study Region	Comments	Average ΔN_2O/AOU	ΔN_2O = a AOU+ b	
			a	b
All	200-500 m	0.07	0.03	2.38
Upper thermocline	500-1000 m	0.10	0.10	-0.45
AAIW	1250-5000 m	0.06	0.05	0.82
Bottom Water		0.04	0.09	-6.20

Significant differences in the N_2O/AOU slope between the two layers of higher and lower oxygen concentrations are apparent in OMZ and upwelling regions (Freing *et al.*, 2009; Rees *et al.*, 2011). A slope change in N_2O/AOU at AOU levels of 50 to 100 µM with a significantly lower slope for AOU levels < 100 µM was reported in the Mauritanian upwelling region. Similar results were reported from other suboxic regions of the world's oceans (The Arabian Sea; Law and Owens., 1990). An increase in ΔN_2O/AOU has also been recognised from increased N_2O yield during nitrification with decreasing oxygen concentrations (Bange and Andreae., 1999). At the SWP stations, a sudden change of ΔN_2O/AOU from 0.03 to 0.1 can be seen at a depth of 200-500 m. This change may indicate a change in N_2O production mechanism and will be further examined via the isotopic composition of N_2O (Ostrom *et al.*, 2000; Popp *et al.*, 2002). Shifts in ΔN_2O/AOU slopes are absent for more oxic waters, such as the Atlantic, Pacific and Indian Oceans (Cohen and

Gordon., 1979; Butler *et al.*, 1989; Outdot *et al.*, 1990, 2002), as in the 200-500m depth range in the present study.

The ΔN_2O/AOU relationship suggests that a single process is the major N_2O formation pathway at the Geotraces stations. However, there is evidence of additional processes at a 200-500 m in the upper thermocline. The slight changes in the ΔN_2O/AOU ratio for different water masses indicate that this process takes place at different rates in different water masses. A positive linear ΔN_2O *vs* nitrate relationship is additional indirect evidence of nitrification (section 1.4.4.1) (Yoshida *et al.*, 1989). Hence, the ΔN_2O *vs* [NO_3] relationship for these regions was also studied, and the statistical values are shown in Table 3.8. Earlier studies from Southeast Pacific had a slope of 0.24 at a depth of 200 – 1000 m (Charpentier *et al.*, 2007). For the subtropical North Pacific the ratio ranged between -1.3 – 0.3 (Walter *et al.*, 2006). The present study results are comparable to these earlier results. The relationship for the entire water column below the mixed layer showed a statistically significant positive correlation (R^2= 0.65), with slope and intercept values as shown in Table 3.8. The $\Delta N_2O/NO_3$ ratios were comparable to results from earlier studies. The correlations were less significant in the case of AAIW (R^2= 0.60). However, these waters showed a positive correlation for $\Delta N_2O/NO_3$ variations. The differences in these ratios between the different water masses are due to the differences in the nutrient remineralization rates and accompanying differences in the rate of N_2O production.

Table 3.8: Comparison of ΔN_2O *vs* Nitrate relationship for the present and previous studies.

Reference	**Study region**	**Comments**	**ΔN_2O= a [NO_3^-]+ b**	
			a	**b**
Walter *et al.*, 2006	ETNA	Cold temperate Subtropical Tropical	0.16 - 0.21 -1.3 - 0.3 0.38- 1.3	-3.2- -0.88 0.02- 0.68 0.20- 0.81
Kock. A, 2011	ETNA	Depth <500 m, Depth >500 m	0.74 1.33	1.43 -31.27
Kock A, 2011	ETSP	[O_2] <50 μM [O2] >50 μM	1.06 2.68	-2.47 -96.3
Charpentier *et al*, 2007	South East Pacific	200-1000 m	0.244	-0.57
Present study				
General UT AAIW Bottom Water	SWP	Below ML 200-500 m 500-1000 m 15000-5000 m	0.12 0.37 0.28 0.99	1.73 0.33 -2.56 -28.39

3.6.1.2. Nutrients and N_2O distribution in the water column

Nitrate (NO_3^-) and phosphate (PO_4^-) concentrations are shown for the Geotraces transect in Figure 3.11. Nitrite concentration ([NO_2^-]) was below 0.1 μM throughout data is not shown here. There was little variability in the nutrient profile between stations, except in the isopycnal layers σ_t = 25.6 – 27, although there was variability in nutrient concentration between water masses. The surface waters (surface mixed layer) were depleted with respect to nitrate (~6 nM) and phosphate (65 nM), with concentration increasing into subsurface waters. Nitrate and phosphate concentrations were higher in AAIW than the upper mixed layer, and increased down the water column, with maximum values in CPDW (see Table 3.4). The vertical distribution of both nutrients resembled that of [N_2O] or N_2O saturation, as shown by comparing Figures 3.7a, 3.9 and 3.11. Maximum [N_2O] was in close spatial association with the depth of the [NO_3^-] and [PO_4^-]

maximum. Within the transect in the upper thermocline layer, the nutrient distributions were different; with an increase towards the western side of the transect (GA to GD). The nutrient increase can be linked to the remineralization process in these layers.

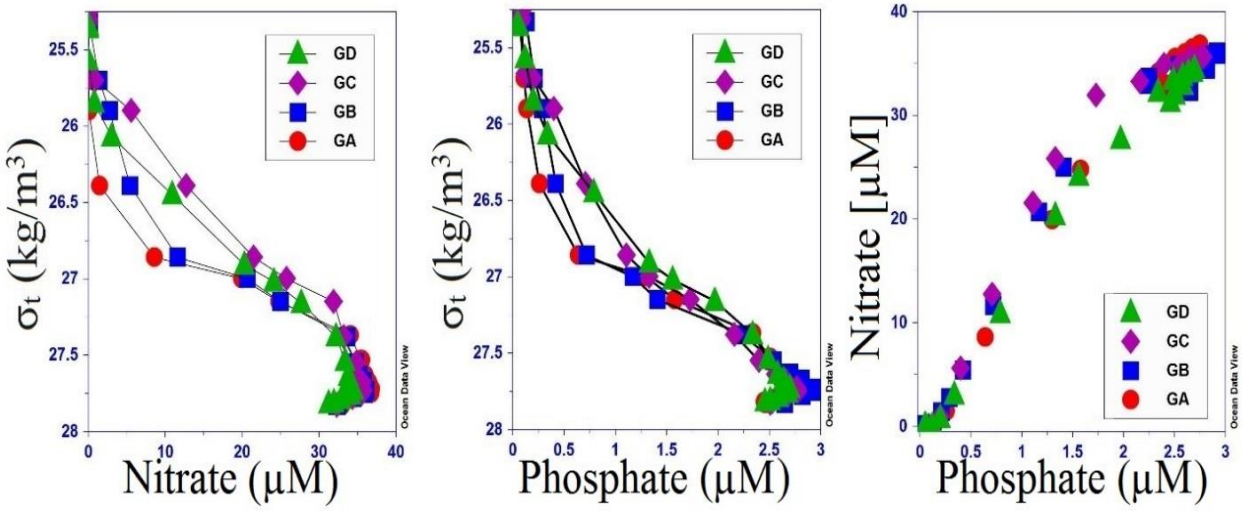

Figure 3.11: The Nitrate (a) and Phosphate (b) variations with σ_t and that of nitrate with phosphate (c) for the Geotraces transect.

The nutrient data reveals that their distribution in surface mixed layer does not show any zonal variability among the stations. Excess P can be seen in the surface water, with an N: P of 0.1 in the mixed layer (Figure 3.11 and 3.13) which is indicative of nitrogen limitation. the excess P may be due to low Fe supply to surface waters which limits N fixation, and so there is P accumulation. The increase in nitrate is more rapid with depth and may be due to the preferential remineralisation of N at these depths. The N:P ratio shows lower values in the upper thermocline along the isopycnal layers of σ_t = 25.8 - 26.5, and highest values at AAIW along isopycnal layer σ_t = 26.9-27.1. In the upper thermocline N: P ratio is lower (see Figure 3.13), which can be an indication of complete remineralization of sinking organic matter at these layers. N: P ratio is comparatively lower in CPDW relative to AAIW; however higher than that in upper layers and closer to the 16:1 (Redfield ratio). Hence the nutrient distribution shows that there exist different remineralization rates for organic phosphorus and nitrogen along the water column (Figure 3.13).

3.6.1.3. Summary of Water Column N_2O in the Geotraces Transect

I. N_2O in the Surface mixed layer (STSW)

In the surface mixed layer of the Geotraces transect, particularly in the euphotic zone, the distribution of N_2O was uniform with depth and were near to atmospheric equilibrium saturation. The surface N_2O productions are comparatively lower than the deep layers due to the high oxygen concentrations and light inhibition of nitrification (Horrigan *et al.*, 1981; Olson *et al.*, 1981). Productivity is low in these oligotrophic waters, with little variability along the transect, as indicated by the chlorophyll fluorescence data which will also indirectly affect the N_2O production (Figure 3.12). Consequently, solubility and mixing are the main drivers of N_2O in the surface layer. The N_2O contribution of nitrification in the surface waters will be looked at in detail (Chapter 4).

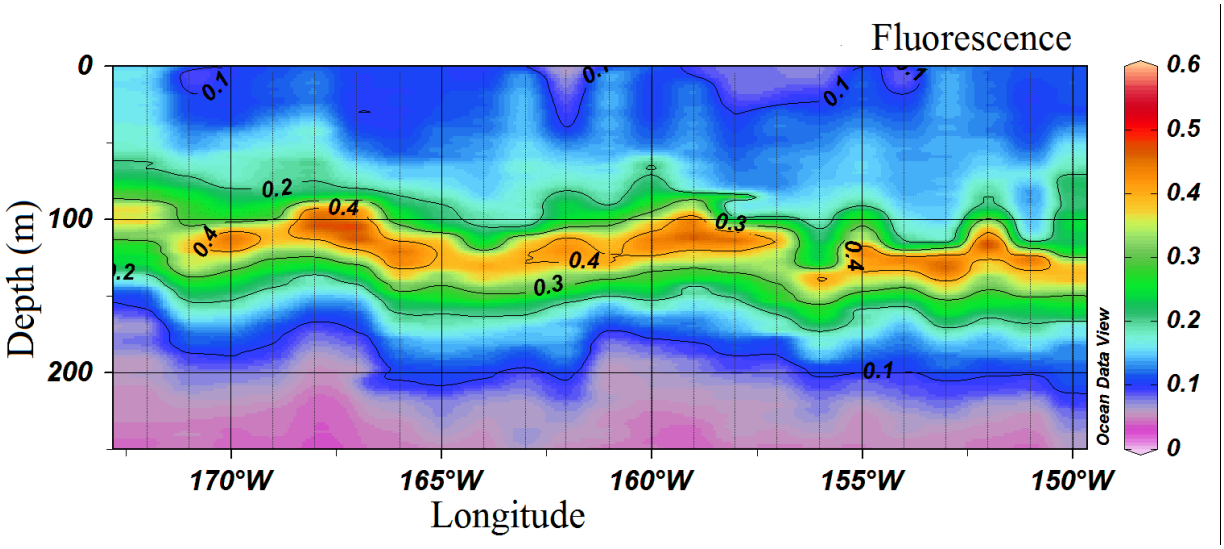

Figure 3.12: Chlorophyll fluorescence value for the upper 250 m in the Geotraces transect.

II. N_2O in the upper thermocline (σ_t = 25.8-26.5)

Both physical and biogeochemical factors influence the water column distribution of [N_2O] below the mixed layer. First, mixing of water masses with different N_2O concentrations may play a role. The yield of N_2O also depends on [DO] (Goreau *et al.*, 1980; Poth and Focht, 1985; Codispoti *et al.*, 1992; Richardson, 2000), with high [DO] preventing the detectable formation of N_2O (Walter *et al.*, 2006). Vertical export of a proportion of productivity results in remineralisation and associated consumption of DO in subsurface waters. As a result, the decomposition of organic

matter supports the production of N_2O. There is a strong positive correlation between ΔN_2O *vs.* AOU and ΔN_2O *vs.* nitrate. N: P indicates the increased uptake or preferential remineralization of nitrate over phosphate as compared to the below or above water masses. Therefore, the results show N_2O produced in these depths from nitrification.

III. N_2O in the Intermediate water (AAIW, σ_t = 26.9-27.1)

The ΔN_2O reflects the rate of N_2O production and mixing as the water moves away from the ocean surface (Nevison *et al.*, 2003). The *in-situ* productions are evident from ΔN_2O, ΔN_2O *vs* AOU and ΔN_2O *vs* nitrate relationships. Even though there is a DO maximum as compared to the other water masses, a corresponding decrease in [N_2O] was absent. This is another indication of increased *in-situ* production at these layers than the overlying oxygenated waters due to the increased remineralization and resulting nitrification. AAIW has higher nutrient and organic matter concentrations when it forms (Bostock *et al.*, 2013), and receives more on sinking as it moves northwards as compared to the surface waters. Therefore it undergoes more nitrification and oxygen utilisation compared to the surface waters. This is primarily evident from AOU and nitrate data (Figure 3.9 and 3.11).

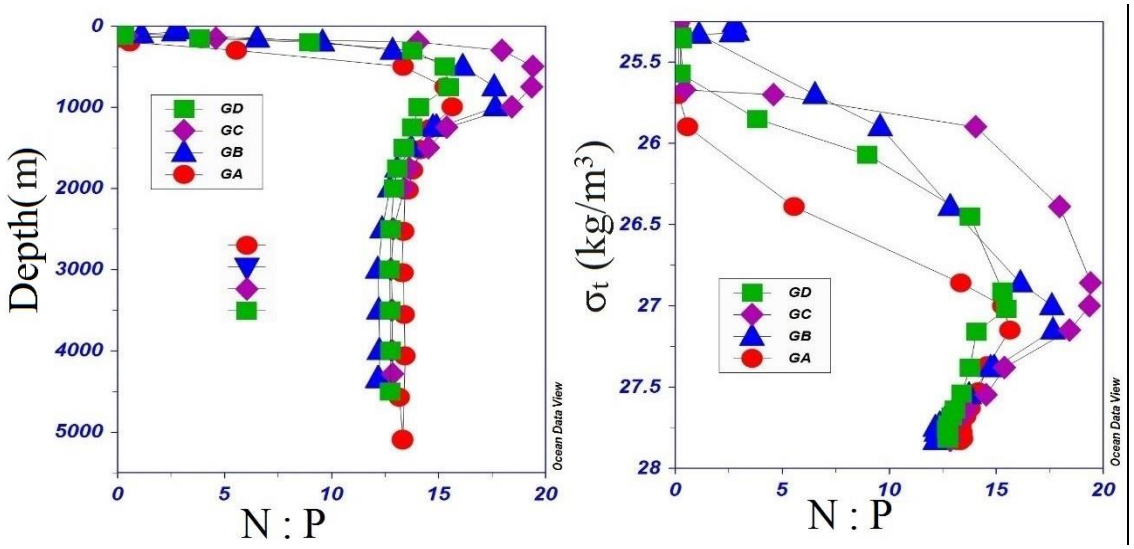

Figure 3.13: The N: P ratio along depth and σ_t for Geotraces transect stations.

In oxic waters, nitrification is a major respiratory process in which organic nitrogen is remineralised to nitrate (Richards, 1965). Generally during nitrification nitrate is correlated with phosphate and dissolved inorganic carbon (DIC), with a slope close to the stoichiometric ratio of photosynthesis and respiration (the Redfield ratio, 106:16:1), implying that biogeochemical processes primarily control the distribution of these constituents. The organic matter remineralisation processes are apparent in Fig. 3.11, with a strong co-variation of [NO_3^-] and [PO_4^-], a slope of 14.47 and a near-zero intercept (intercept, b = -0.010), that reflects the stoichiometry of organic matter synthesis and remineralisation, and a rapid increase in [nitrate] with depth. The N:P is also higher than the Redfield ratio suggesting that N is preferentially remineralised in AAIW (see Figure 3.13).

IV. N_2O in bottom waters (CPDW)

[N_2O] increased in the bottom waters reaching the highest concentrations in the water column. Additional factors may increase [N_2O] in bottom waters such as production in the sediments by denitrification/nitrification and release into the overlying bottom water (Seitzinger, 1990; Usui *et al.,* 1998). *In-situ* production is evident from the increased ΔN_2O, and significant N_2O from denitrification in the water column seems unlikely due to its high [DO]. From ΔN_2O *vs.* AOU and ΔN_2O *vs.* nitrate relationships (Fig. 3.10), it can be assumed that nitrification was mainly responsible for N_2O production in CPDW. [N_2O], [ΔN_2O], [NO_3^-] and [PO^-_3] were higher in CPDW, compared with AAIW, with N: P ratios closer to the Redfield ratio (Figure 3.13).

However, a decrease in [N_2O] was observed below 3500 m, which may be due to a decrease in nitrification. The decrease in [N_2O] may reflect that the sinking organic material has been degraded in the overlying water, and there is little organic matter reaching the deep water available for nitrification. Another possible reason for this N_2O decrease in the bottom water could be consumption by sediment denitrification (Cohen and Gordon, 1978; Bange *et al.*, 2001b; Walker *et al.*, 2010). Both of these possibilities will be discussed in detail in Chapter 5 using stable isotope results.

3.6.1.4. Age of the water mass and N_2O

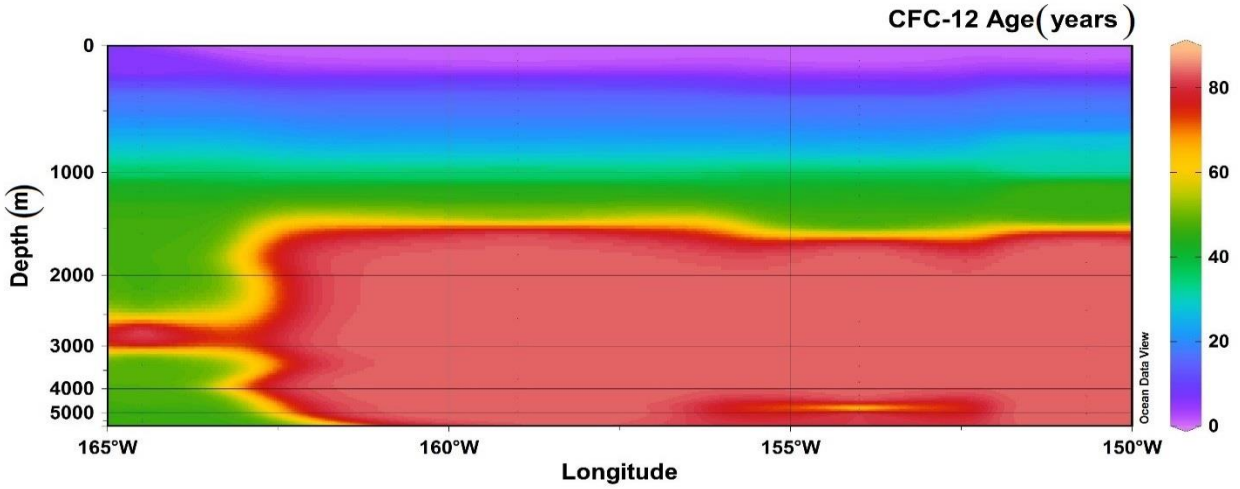

Figure 3.14: The age of the water mass calculated by CFC-12 method along the water column for the Geotraces transect (Key *et al*., 2004).

The age of the water mass will also affect the [N_2O] since N_2O is produced *in situ* as the water mass sinks & advects through the ocean. The age of the water mass is defined as the average time since the water parcel was in contact with the atmosphere (Warner *et al*., 1996, Sonnerup *et al*., 1999). As the age of the water mass increases, the [N_2O] will increase concomitantly with a decrease in DO. The mean age of the water masses at different depths for the Geotraces transect was derived using data obtained from WOCE experiments, together with gridded GLODAP CFC-12 data (Figure 3.14, Key *et al*., 2004).

From the above Figure 3.14, it can be concluded that the oldest water masses were seen in the CPDW at a depth of 2000- 3000 m with an average age of 75 years. AAIW were comparatively youngest as compared to CPDW with an average of 25 years.

3.6.1.5. N_2O production rate and Apparent Oxygen Utilization Rate in the Geotraces transect

The water mass age in the ocean interior is highly variable, but establishing it by the use of transient tracers such as CFC-12 allows estimation of an N_2O Production rate (N_2OPR), further insight into the processes responsible for N_2O production. N_2OPR was calculated as

$$N_2OPR = \Delta N_2O / t$$

where t is the mean CFC-12 age of the water sample. To exclude influence of seasonal variation affecting the near-surface ocean, production rates calculated only for samples with a mean age of at least one year, so excluding mixed layer samples. A mean N_2OPR for a water sample based that has experienced advection and mixing, N_2O production is not necessarily equivalent to a local or instantaneous N_2O production rate. However, scaling by the mean age is a way of averaging the N_2O production over the time period since the water mass was ventilated at the surface and assumed to be in equilibrium with atmospheric N_2O.

The apparent oxygen utilisation rate (AOUR) was estimated in a similar fashion:

$$AOUR = AOU / t$$

The *in-situ* organic carbon remineralization rate (OCRR) was calculated as in Feeley *et al.* (2004), by integrating the estimated AOUR (200 – 1800 m), and using a Redfield ratio of 0.573(C:O) for South Pacific (Anderson and Sarmiento, 1994).

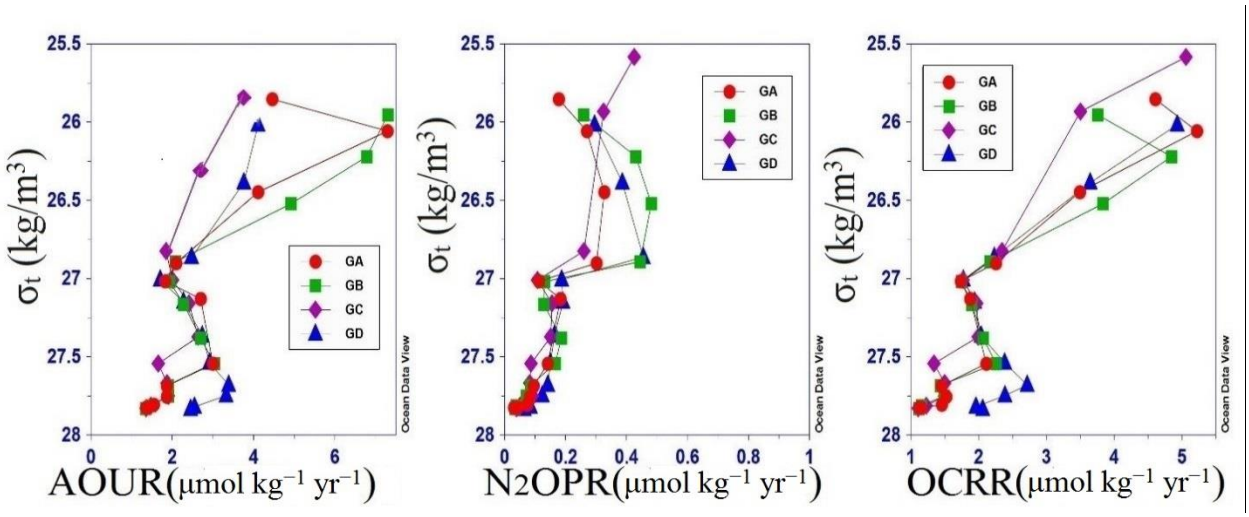

Figure 3.15: AOUR, N_2OPR and OCRR with respect to σ_t along the Geotraces transect. Note that surface mixed layer data are not included

The AOUR estimates (Figure 3.15a) show a maximum in the thermocline waters. The rate varies between 0.2 and 7.3 μmol kg^{-1} yr^{-1} (200-500 m), 1.7- 2.9 μmol kg^{-1} yr^{-1} (500 −1250 m), ~1.0 (below 1500 m), with an overall mean AOUR of 2.9 ± 1.4 μmol kg^{-1} yr^{-1}. These rates show good agreement with prior estimates of AOUR of 0.02 − 10 μmol kg^{-1} yr^{-1} (100−1000 m) and an overall mean of 2.1 μmol kg^{-1} yr^{-1} for the Southwest Pacific (30 °S) based on CFC age (Feely *et al*., 2004). The OCRR follows the same trend as AOUR, with the highest values below the surface mixed layer (2.9 - 3.8 μmol kg^{-1} yr^{-1}) at depths of 200 - 500 m (Figure 3.15c). In the AAIW, the values decreased (1.5 – 1.8 μmol kg^{-1} yr^{-1}) relative to the upper subsurface waters, and OCRR values were lowest (0.9 – 1.2 μmol kg^{-1} yr^{-1}) in the bottom waters. These estimates agree reasonably well with the that of Feeley *et al.* (2004) for South Pacific waters (0.05 - 3.3 μmol kg^{-1} yr^{-1} with an average of 1.4 μmol kg^{-1} yr^{-1}).

From the AOUR and OCRR data, it is evident that in the upper thermocline at a depth of 200 -500 m remineralization rates are five times faster than in deeper waters. Ten times faster rates below the euphotic zone were observed in the Northern Pacific by earlier researchers (Feeley e*t al.*, 2004, Freing *et al.*, 2009). The AOUR estimates given by Feely *et al.* (2004) were approximately 10 μmol kg^{-1} yr^{-1} for upper thermocline and 0.1 μmol kg^{-1} yr^{-1} (below 1200 m). The North Pacific mean AOUR estimates (Freing *et al.*, 2009) were of 4.3 ± 0.7 μmol kg^{-1} yr^{-1} and 0.6 ± < 0.1 μmol kg^{-1} yr^{-1} respectively for subsurface and bottom waters respectively.

The two-fold difference between North and South Pacific OCRR waters were identified as the cause of differences in productivity of oligotrophic southwest Pacific and euphotic North Pacific waters (Feeley *et al*., 2004). Feeley *et al.* determined an amplified organic carbon remineralization rate of 0.3 – 1.3 Pg C yr^{-1} in the highly productive regions to the 0.3- 0.6 Pg C yr^{-1} from the regions of low productivity in the Pacific Ocean. They also suggested that the AOUR estimates are directly related to the productivity and export flux of carbon from the overlying water mass. The above results also indicate that water column remineralization of organic carbon in the upper 1250 m (3 μmol kg^{-1} yr^{-1}) contributes to the most of the organic carbon remineralization in the water column in this region as compared to the bottom waters (< 1 μmol kg^{-1} yr^{-1}).

N_2OPR varies between 0.03 − 0.48 nmol kg^{-1} yr^{-1} with an overall mean N_2OPR of 0.18 ± 0.12 nmol kg^{-1} yr^{-1}. Between 100−500 m N_2OPR varies between 0.18 - 0.48 nmol kg^{-1} yr^{-1}, but it is lower below 500 m, at 0.08 ± 0.03 nmol kg^{-1} yr^{-1}, indicating that the most significant amount of N_2O is produced in the upper thermocline of the water column. Our results are in good agreement with modelled data for global oceans, N_2OPR 0 − 3.3 nmol kg^{-1} yr^{-1} with an overall mean N_2OPR of 0.2 ± 0.04 nmol kg^{-1} yr^{-1} (Freing *et al*., 2009). The N_2OPR for SWP from our studies shows an average of 1.6 ± 0.1 nmol kg^{-1} yr^{-1} at the core of AAIW, and these values are comparable to the results obtained by Freing *et al* modelled data for AAIW in these regions (0 – 0.3 nmol kg^{-1} yr^{-1}). The comparatively higher N_2OPR in the AAIW than the bottom waters can be attributed to the age of the AAIW. Modelling studies in North Pacific revealed that approximately 40 % − 75 % of the net flux of N_2O to the atmosphere is produced between 100 m and 300 m depth (Popp *et al*., 2002). Comparing these results to present estimates, here also N_2OPR also shows its peak values between 100 m and 500 m.

3.6.2. N_2O in the Spring Bloom II and Mooring stations

NZ Geotraces sampling was conducted in winter (July 2011) while all the study regions were sampled in spring when biological activity is elevated (Boyd, P. W., 2002). The Spring Bloom II voyage and sampling took place in an eddy in the SWP east of the New Zealand North Island. The southern mooring station SBM lies in the subantarctic region of the SWP, southeast of New Zealand, and the northern NBM is in subtropical water east of NZ (detailed descriptions of these

two sampling regions are given in Chapter 2, Section 2.3.1, Fig. 2.1 and Table 2.1). The distribution and water column profile of [N_2O] at these stations are shown in the Figure 3.16.

[N_2O] and DO variation along isopycnal surfaces reflect the different water masses at each station, as shown in Table 3.9. The minimum [N_2O] was at the surface layer (σ_t = 26.5), with an average of 9.3 ± 0.1 nM in STSW and was 11.41± 0.5 nM along the isopycnal surfaces (σ_t = 26.7) of SASW. Below the surface mixed layer [N_2O] varied with respect to depth and water masses. In the upper thermocline isopycnal layers (σ_t = 26.8) where a subsurface (200- 500 m) decrease in DO was seen, [N_2O] increased with an average 11.9 ± 0.7 nM, similar to the Geotraces transect. In the SBM, the [N_2O] was close to the surface mixed layer values with an average of 11.6 ± 0.3 in the upper thermocline (200 - 300 m). At the base of the thermocline in AAIW along the isopycnal layers of σ_t = 26.9- 27.1 [N_2O] increased with an average of 16.0 ± 0.7 nM. An increase in DO was observed at these depths except in the SBM; however average [N_2O] was higher than the overlying less-oxygenated water in the upper thermocline. At the SBM station, AAIW was present in the upper thermocline as a subsurface water mass at a depth of 300-750 m. The maximum [N_2O] was found at a depth of ~1500 - 2000 m, with an average of 19.8 ± 0.6 nM in the CPDW. Therefore, the vertical distribution of N_2O showed characteristically similar profile to that of Geotraces, and within the study region with exceptions in the SASW of SBM. Below the Surface Mixed layer at B_2A of Spring Bloom II, a decrease in both [N_2O] was observed concomitant with a decrease in N_2O saturations (will be discussed later); which can be due to analytical errors.

Higher biological activity because of increased productivity may account for the higher [N_2O] in the surface waters (< 2 %) especially from June to September in these four stations compared to the Geotraces stations (Morel *et al.*, 2010). Even though the subantarctic HNLC regions are less productive than the subtropical regions, the lower temperature and corresponding increased solubility of N_2O along with higher wind speed are the factors that control the surface N_2O in these waters.

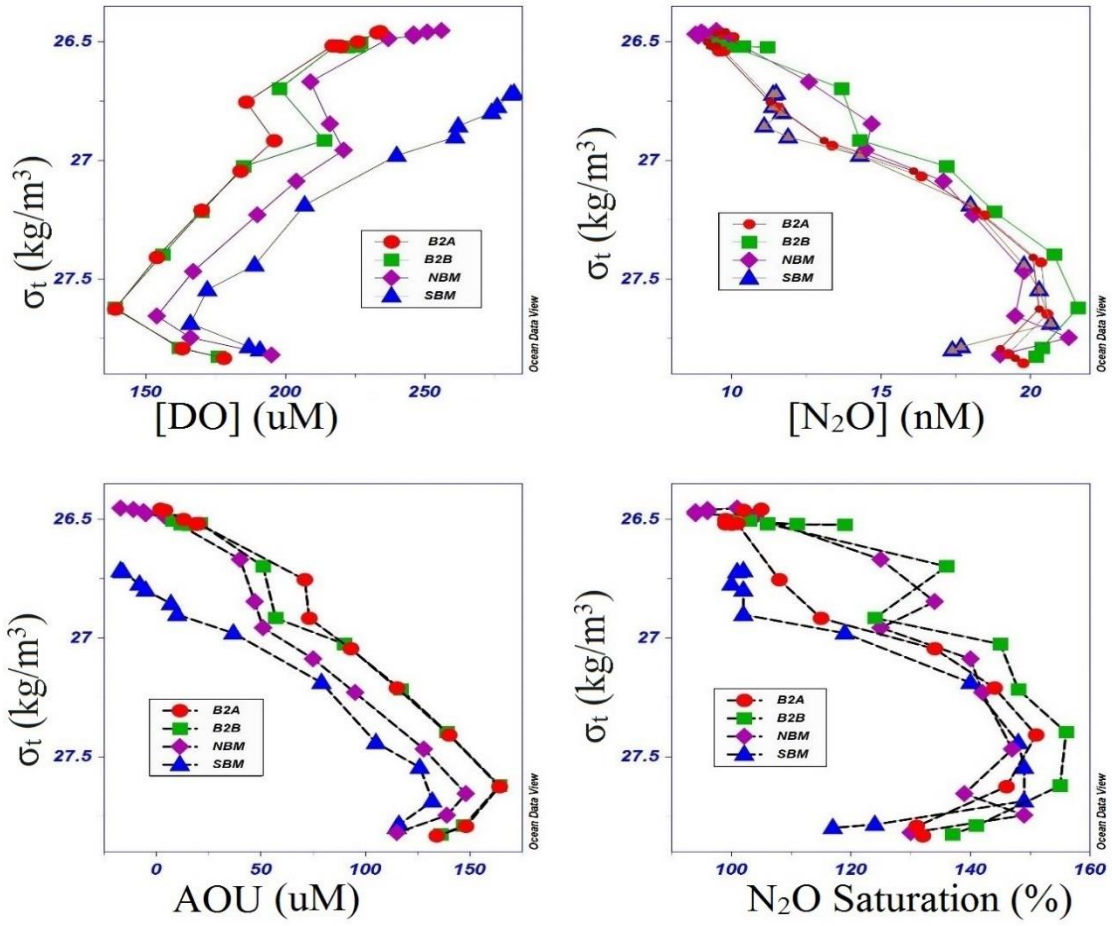

Figure 3.16: Density profiles of N_2O, Percentage N_2O saturation, AOU and Dissolved Oxygen for Biophysical Mooring stations NBM & SBM, and Spring Bloom II transect stations, B_2A and B_2B, respectively in clockwise order.

Table 3.9: The mean water mass properties of Spring Bloom II and Mooring stations

N_2O(nM)	B_2A	B_2B	NBM	SBM
STSW	9.5	10.2	9.7	-
AAIW	15.8	16.8	16.6	14.7
CPDW	19.7	20.8	19.9	19.6
SASW				11.5
DO (µM)				
STSW	228	225	249	
AAIW	183	170	204	242
CPDW	158	158	174	181

SASW	[redacted]			278
Nitrate (µM)				
STSW	4.7	3.4	4.6	
AAIW	NA	NA	30.4	24.9
CPDW	NA	NA	32.9	34.6
SASW	[redacted]			15.3

Table 3.10: ΔN_2O vs AOU properties for the Spring Bloom II and Mooring stations

Average ΔN_2O / AOU ratio								
Upper water	0.004		0.06		0.08		0.07	
AAIW	0.060		0.05		0.05		0.05	
CPDW	0.040		0.05		0.04		0.05	
ΔN_2O vs AOU, [ΔN_2O= a [AOU] ± b								
	a	b	a	b	a	b	a	b
Upper water	0.02	-0.32	0.11	-1.50	0.07	0.03	0.05	0.25
AAIW	0.06	-1.11	0.05	-0.16	0.06	1.15	0.07	-0.29
CPDW	0.06	-3.17	0.08	-5.39	0.06	-1.01	0.24	-24.8

The variation in [O_2] depth profiles for the study area is shown in Figure 3.16 and Table 3.9. The minimum oxygen concentration ranged from 139 to 164 µM in CPDW at 1500-2000 m, and so did not fall to hypoxic conditions in all stations. The maximum [O_2] of 226-230 µM and 256 µM for STSW in subtropical and subantarctic regions respectively. The AAIW had subsurface DO secondary maximum at the Spring Bloom II and NBM stations which was absent in case at the SBM. Notably in all these stations [O_2] did not fall to hypoxic conditions. N_2O distribution was inversely related to [O_2], as shown by comparing Figure 3.16a and 3.16 b, with the maximum N_2O concentration in the oxygen minimum regions for all stations. The variations in nitrate concentration ([NO_3^-] + [NO_2^-]) in Fig. 3.19 show that the nitrate depth profile was similar to that of [N_2O] except in the surface mixed layer. The DO and nutrients (nitrate + nitrite) distribution across the Mooring transect showed a similar trend from the surface to the bottom water for all stations.

Figure 3.16 shows the percentage N_2O saturation and apparent oxygen utilisation (AOU) with respect to ambient air, which indicate that production of N_2O increases as O_2 consumption increases. The relationship between [N_2O] and AOU has a significant positive correlation with a slope of 0.07 ($R^2 = 0.95$). The water column N_2O-AOU slopes were similar for all stations except in the SASW of SBM, as shown in Figure 3.17. This figure indicates the absence of regional variations in the rates of N_2O production and oxygen consumption below the mixed layer.

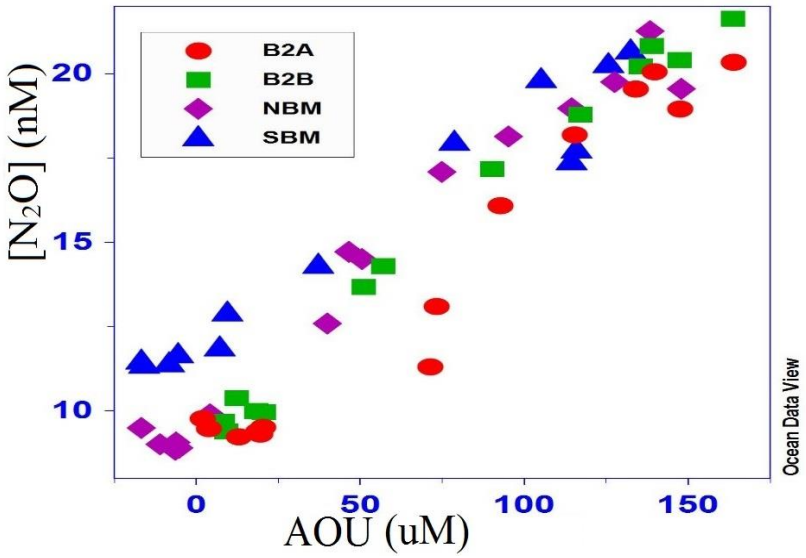

Figure 3.17: [N_2O] vs AOU relationship at Spring Bloom II and Mooring stations

N_2O in subtropical waters had an average saturation of 103 ± 1 %, while that in the subantarctic surface water was 102 ± 1 %. Both the subantarctic and subtropical SWP stations were slightly supersaturated but were within the global surface ocean mean supersaturation (Bange *et al*., 2006). Below the surface mixed layer, the percentage saturation values increased to the bottom as an indication of in-situ production. In the bottom water, percentage saturation values ranged between 108 - 156 % for the three Southwest Pacific stations and 120-156 % for SBM, with a slight decrease in bottom waters. The average AAIW saturations were almost 135-145 %, while those in CPDW were close to 140 - 160 %.

3.6.2.1. Nutrients and N_2O in the water masses

The distribution of the nutrients in the above four stations are shown in Figure 3.18 (except for nitrate and phosphate at the spring Bloom II stations). The water column distributions of nitrate and phosphate concentrations and variations with depth were similar to that observed in the Geotraces transect, except for the SBM. As expected, SBM surface nutrients were higher since it is in the HNLC region.

The N: P ratio was studied to understand the contributions of organic matter remineralisation and nitrification to the nitrous oxide pathway (Figure 3.19). For a detailed explanation, see section 3.6.1.2. Nitrate and phosphate had a strong positive correlation with $R^2 = 0.96$ and a slope close to 16, that points to nitrification during organic matter remineralisation. The N: P distribution was low in the surface waters in STSW, as expected, while it was higher in the highly productive HNLC regions of SASW. However N: P was highest in the phosphate-depleted subtropical AAIW waters at NBM, where the N_2O saturations were also high relative to other regions. It can also be inferred from the overall results that in NBM and the two Spring Bloom II transect stations, nitrification controlled N_2O distribution as the dominant pathway, similar to that in Geotraces.

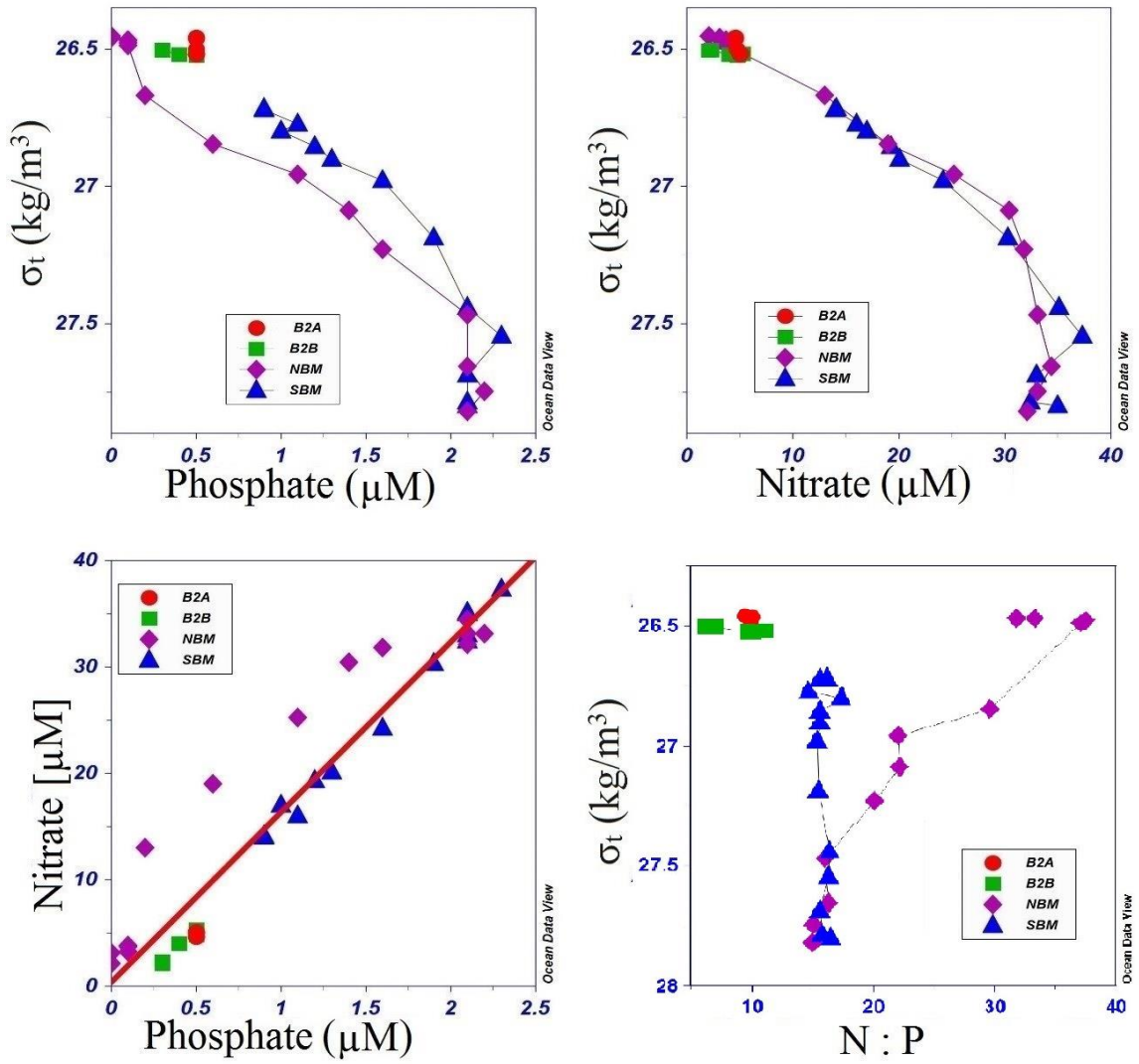

Figure 3.18: Density profiles of Phosphate, Nitrate, and N: P ratio and Nitrate/ Phosphate ratio for NBM & SBM, and Bloom II B2A and B2B, respectively in clockwise order.

3.6.2.2. ΔN_2O and its relationship with AOU and nitrate

The mean concentration anomaly (ΔN_2O) is close to zero (less than one nM) in the surface-mixed layer (Figure 3.18), which may reflect that gas exchange negates any in-situ N2O production to the atmosphere. The correlations between ΔN_2O and AOU for all the stations were analysed (Figure 3.19, Table 3.10), to determine if there were differences in the relationship with depth using the same methodology as for the Geotraces transect. ΔN_2O *vs* AOU and ΔN_2O *vs* [nitrate] variations for the subantarctic and subtropical waters were studied separately. AOU showed a

positive linear relationship (Fig. 3.19 a) with ΔN_2O, with an average slope of 0.040 (0.037- 0.045) and an R^2 of 0.88 in the subtropical stations. However, subantarctic waters had a slope of 0.043 and a correlation of 0.70. These results were within the range of earlier reported values for other regions, and were comparable to the results from Geotraces (0.05 - 0.10), although the R^2 values differed for different water masses (Table 3.7). The ΔN_2O/nitrate was 0.19 and 0.28 for the subtropical and subantarctic surface waters respectively, with a strong positive correlation (R^2 = 0.96 and 0.89) in both regions

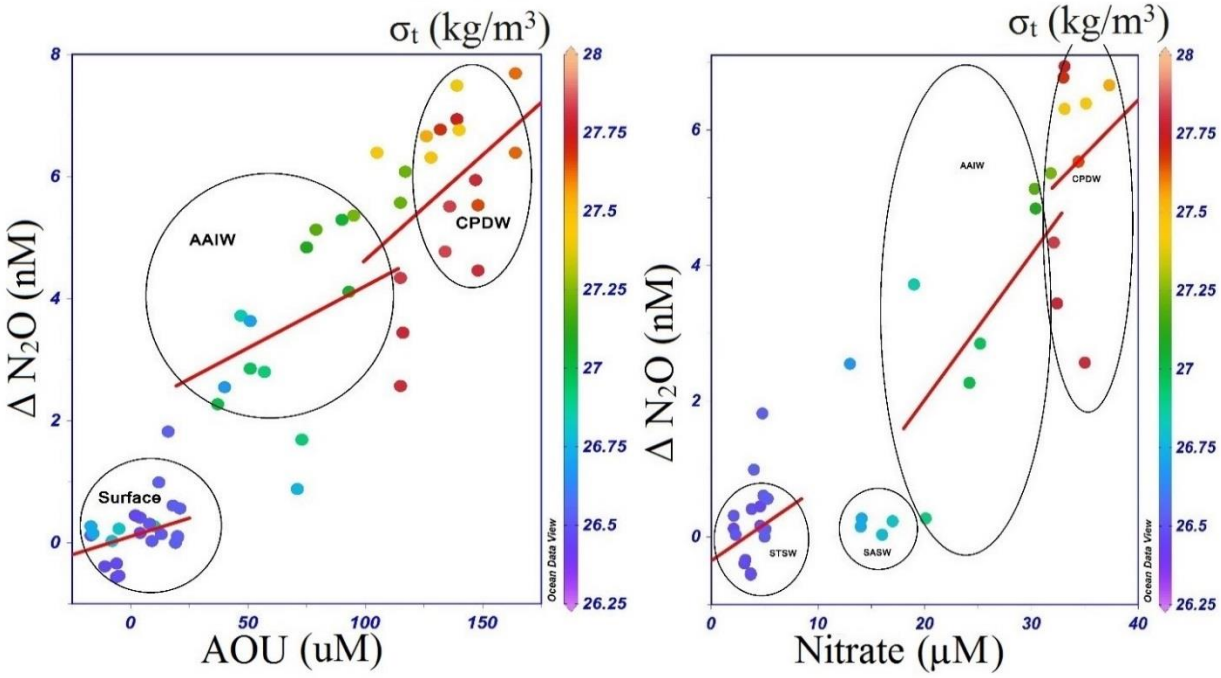

Figure 3.19: Relationship between a) ΔN_2O and AOU for B_2A, B_2B and NBM, b) ΔN_2O and [Nitrate] at the NBM and SBM.

Significant differences were absent in these correlations for deep waters, as also observed in the Geotraces transect (Table 3.7). The significant positive correlation within different water masses is evidence of nitrification at the bottom waters. The upper thermocline waters showed a significant positive correlation (R^2 = 0.94). Below this layer in the AAIW, due to the increased DO and the relative decrease in AOU, the correlations decreased. However the slopes obtained along the isopycnal layers of 26.9- 27.1 were comparable (slope = 0.05, R^2 = 0.60) to slopes obtained for AAIW in the other studies (Yoshinari *et al.*, 1976, Walter *et al.*, 2006). In the bottom water below 1500 m (along the isopycnal layer σ_t = 27.5-27.8, CPDW) a significant positive correlation (slopes = 0.09, R^2 = 0.74) was obtained for the ΔN_2O *vs.* AOU. From the slope, it can be concluded that

0.02 – 0.03 (upper thermocline), 0.05 – 1.15 (AAIW) and 0.06-0.20 (CPDW) nmol N_2O was produced per µmol of O_2 consumed. N_2O yield per µmol of oxygen was 0.004 - 0.027 and 0.14 nmol respectively for the western North Pacific (Yoshida *et al.*, 1989) and Central Pacific (Elkins *et al.*, 1978).

A sudden change of ΔN_2O/AOU from 0.03 to 0.1 can be seen at a depth of 200-500 m (Figure 3.20). A rapid change in ΔN_2O/AOU ratios may indicate a change in the N_2O production mechanism, which can be clarified from the isotopic composition of N_2O (Ostrom *et al.*, 2000; Popp *et al.*, 2002). ΔN_2O/AOU also indicates the change in the rate of N_2O production during nitrification. Such differences in ΔN_2O/AOU slopes are absent for the oxic waters of the world's oceans, as in major parts of the Atlantic, Pacific and Indian Oceans (Cohen and Gordon., 1979; Butler *et al.*, 1989; Outdot *et al.*, 1990, 2002), similar to the present study (except in the 200-500 m depth range). The ΔN_2O/AOU relationship suggests that at these stations there was a single process as the major N_2O formation pathway except at a depth of 200-500 m in the upper thermocline. The slight changes in the ΔN_2O/AOU ratio for different water masses show that the nitrification process takes place at different rates in different water masses. The role of nitrification in the N_2O production process is to be confirmed before reaching a conclusion.

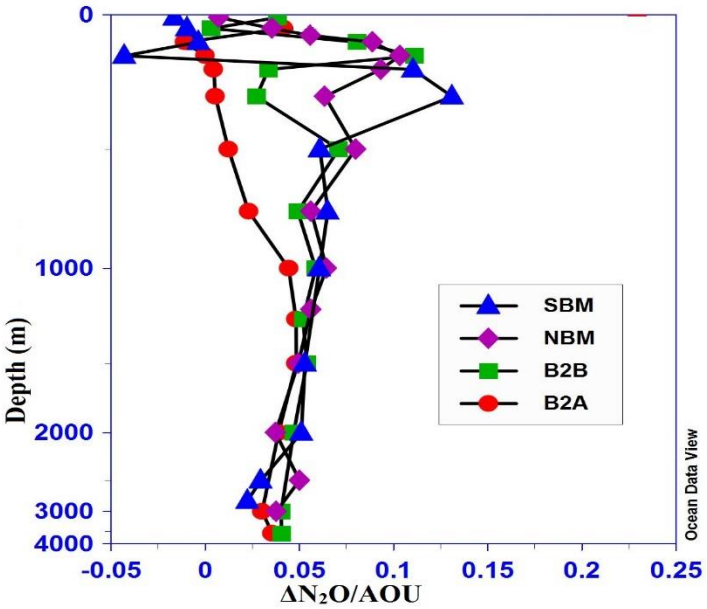

Figure 3.20: ΔN_2O/AOU depth profile for Mooring and Spring Bloom II stations

ΔN_2O *vs* $[NO_3]$ relationship for these regions was also studied, and the statistical values are shown in Figure 3.19. The results show the relationship for the entire water column below the mixed layer, and suggests a significant positive correlation (R^2 = 0.83) with slope (0.17) and intercept values (-0.10) in the NBM and R^2 = 0.70, slope = 0.32 and intercept = -5.8 respectively for SBM. The $\Delta N_2O/NO_3$ ratios were comparable to the earlier reported values (Table 3.6a). The correlations were significant in the case of AAIW (R^2= 0.60) and the CPDW (0.72). However, there was a difference in the ratios between the water masses.

These results indicate the absence of significant differences between each water mass within the stations (Table 3.10). The data are comparable to the previous results from the other regions including the Geotraces transect. However, SBM stations in the subantarctic sector showed an increase in the ratio in CPDW (Table 3.10), which was due to the increase in DO and associated decrease in AOU at SBM. There was a slight decrease in N_2O concentration in the bottommost layers, similar to that observed in Geotraces.

3.6.2.3. Summary of Water Column N_2O in the Spring Bloom II and Mooring stations

1). N_2O in the Surface layer (STSW along σt = 26.5 and SASW along σt = 26. 7)

In the surface mixed layer, the distribution of N_2O was uniform and minimum along the water column. It was in near equilibrium concentrations with the atmosphere. Therefore, it is suggested that solubility and mixing effects most likely drive N_2O distribution in the surface layer. Productivity is low in these oligotrophic SWP (Claustre and Maritorena., 2003); however, the role of nitrification in N_2O production at the surface mixed layer will be discussed later (Chapter 4).

2). N_2O in the upper thermocline (σ_t = 26.8)

In the upper thermocline [DO] concertation show a subsurface minimum (σ_t = 25.8 - 26.5) except in the SBM. There is a strong positive correlation between ΔN_2O *vs* AOU and ΔN_2O *vs* nitrate in these layers. N: P indicates the preferential remineralisation of nitrate over phosphate relative to the bottom water masses. However, there was no variation in N: P at SBM. So the increased $[N_2O]$

at these depths than the surface waters is a result of elevated rates in nitrification. As indicated from ΔN_2O *vs* AOU and ΔN_2O *vs* nitrate relations the role of any other possible mechanisms needs to be analysed in more detail.

3). N_2O in the Intermediate water (AAIW, σ_t = 26.9 - 27.2)

From the above descriptions about the N_2O in AAIW, it can be deduced that N_2O contributions from deep water mixing and resulting diffusion from the deep waters will not be a relevant factor in the AAIW as observed from the T-S diagram. ΔN_2O indicates an amplified *in-situ* production at these waters than the surface mixed layer/ upper thermocline. As evident from AOU and Nitrate data (Figure 3. 16), AAIW is subjected to increased nitrification and oxygen utilisation compared to the overlying water masses. At the AAIW in both the SWP stations increased remineralisation of N contributes to the increase in N_2O.

4). N_2O in bottom waters (CPDW, σ_t = 27.4 - 27.8)

$[N_2O]$ was highest in the bottom waters and were the highest along the water column. The ΔN2O indicated N2O production. Among the different factors that cause an increase in $[N_2O]$ *in-situ* N_2O production appears to be most likely. The ΔN_2O *vs* AOU and ΔN_2O *vs* nitrate relationships suggest nitrification was mainly responsible for N_2O production in CPDW. The variations of $[NO_3^-]$ and $[PO_4^-]$ (Figure 3.19) that reflect the Redfield relationship; suggest the remineralisation of nitrogen-enriched organic material might be responsible for increased N_2O yield. $[N_2O]$, $[\Delta N_2O]$, $[NO_3^-]$ and $[PO^-_3]$ were higher for CPDW compared to AAIW. The N: P ratios were closer to the Redfield ratio and were consistent with depth in CPDW (Figure 3.19).

3.6.2.4.Age of the water masses

As the age of the water mass will also affect the *in situ* production of N_2O the mean age of the water masses at different depths for the Mooring and Spring Bloom II stations were derived using data from the WOCE database with gridded GLODAP CFC-12 data (Figure 3.21, Key *et al*., 2004).

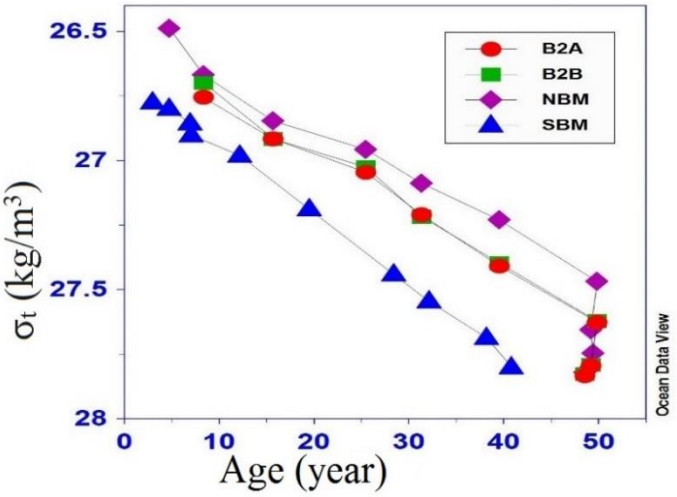

Figure 3.21: Density profile of water column age for Spring Bloom II and the Mooring stations. Note that surface mixed layer data are not included.

From the above figure, it can be concluded that the oldest water masses were the CPDW at a depth of 2000 - 2500 m as indicated by the density surface below 27.1, where dissolved oxygen concentration was the lowest. The age of the CPDW were ~ 50 years in the subtropical SWP, while it was ~ 35 years in the subantarctic SWP. AAIW ($\sigma_t = 27.1$) was younger than CPDW with ~ 30 years old waters in the subtropics and ~ 20 years older waters at the subantarctic. The upper thermocline waters were of ~ 10 years in the subtropics and f ~ 5 years in the subantarctic. Overall SBM (subantarctic) shows younger water column as compared to the subtropical SWP.

3.6.2.5. AOUR, OCRR and N_2OPR

The production rates were estimated for samples with a mean age of at least one year (i.e. excluding mixed layer samples) as detailed in the previous section 3.6.1.4. The AOUR (Figure 3.22) shows a maximum in the thermocline waters at the Spring Bloom II & NBM Stations. It varies between 0 and 8.5 µmol kg^{-1} yr^{-1} (200- 500 m), decreasing to 1.7- 3.3 µmol kg^{-1} yr^{-1} (500 −1250 m), and ~ 2.0 µmol kg^{-1} yr^{-1} (>1500 m) with an overall mean AOUR of 3.4 ± 0.9 µmol kg^{-1} yr^{-1}. Comparatively younger waters were observed in the subantarctic SWP where average water column AOUR estimates below the mixed layer was higher (~1.0 µmol kg^{-1} yr^{-1}) than that in the subtropical SWP (NBM, B_2A and B_2B). At the subtropical SWP, the AOUR maximum was (~3

μmol kg^{-1} yr^{-1}) in the AAIW and in CPDW (~ 2 μmol kg^{-1} yr^{-1}). It is due to the age differences among the waters masses between the two regions. These rates estimates agreed reasonably well with prior estimates (Feely *et al*., 2004) for South Pacific and the Geotraces estimates (section 3.6.1.4) in the subtropical SWP.

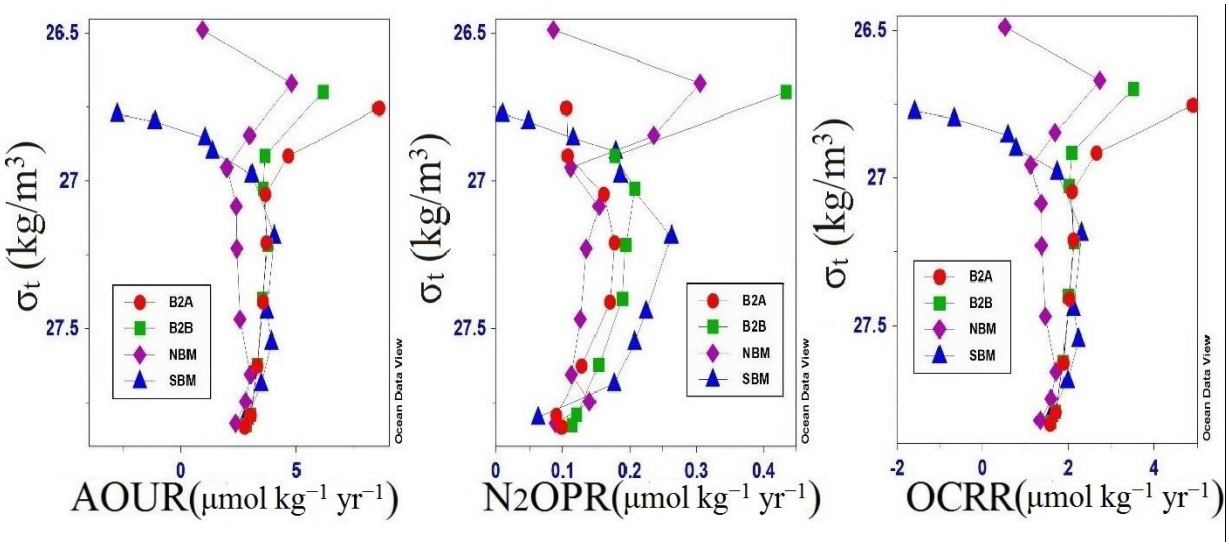

Figure 3.22: Apparent Oxygen Utilization rate, N_2O production rate, Organic Carbon Remineralization rate with respect to σ_t for Spring Bloom II and Mooring stations.

Using the estimated AOUR, the OCRR was also calculated and follows the same trend as AOU with the highest values below the surface mixed layer (2.9 - 3.8 μmol kg^{-1} yr^{-1}) at a depth of 200 - 500 m in the thermocline at the Spring Bloom II & NBM stations (Figure 3.22). However, at the SBM station where AAIW were seen as a shallow water feature, the OCRR values were highest in the AAIW. The OCRR in the subtropical AAIW decreased (1.5 – 1.8 μmol kg^{-1} yr^{-1}) as compared to the upper subsurface waters, and OCRR values were lowest (0.9 – 1.2 μmol kg^{-1} yr^{-1}) in the bottom CPDW waters. This estimate agrees reasonably well with the earlier estimates (Feeley *et al*., 2004) and with the Geotraces estimates.

From AOUR and OCRR estimates, it is evident that in the upper thermocline at a depth of 200-500 m remineralization rates are three to five times faster than the deep water rates. A five times faster rates below the euphotic zone were observed in the Geotraces transect. The above results

also indicate that water column remineralization of organic carbon in the upper 1250 m accounts for most of the organic carbon remineralization in the water column in this region.

In the subtropical SWP N_2OPR (Figure 3.22) varies between 0.04 − 0.40 nmol kg^{-1} yr^{-1} with an overall mean N_2OPR of 0.16 ± 0.07 nmol kg^{-1} yr^{-1} (Figure 3.22). N_2OPR of 0.15 ± 0.07 nmol kg^{-1} yr^{-1} were obtained for the subantarctic SBM estimation. The water column variations of N_2OPR shows maximum with an average of 0.21 nmol kg^{-1} yr^{-1} in the upper thermocline, 0.12 nmol kg^{-1} yr^{-1} in the AAIW and minimum rates of 0.09 nmol kg^{-1} yr^{-1} in the CPDW at the subtropical SWP. At the subantarctic station, maximum production rates were in the AAIW (0.21 nmol kg^{-1} yr^{-1}), followed by CPDW (0.17 nmol kg^{-1} yr^{-1}) and the minimum in Upper thermocline (0.06 nmol kg^{-1} yr^{-1}). However, the AAIW were present as a shallow water feature in the subantarctic. N_2O is primarily produced in the upper thermocline (above 500 m) of the water column. Our results are in good agreement with modelled data for N_2OPR 0 − 3.3 nmol kg^{-1} yr^{-1} with an overall mean N_2OPR of 0.20 ± 0.04 nmol kg^{-1} yr^{-1} (Freing *et al*., 2009) for South Pacific region. The N_2OPR seems to be more in the AAIW/CPDW of the subantarctic region than the subtropical region. It is due to the presence of comparatively younger AAIW with elevated ΔN_2O at the subsurface.

When compared to the subtropical stations of the Geotraces transect the Spring Bloom II and Mooring stations show higher production rates in the bottom waters. These higher rates may be due to comparatively younger waters at these transects, while the ΔN_2O remained more or less similar at all stations. The above estimates indicate that more N_2O is produced in the upper thermocline of the water column. Our results are in good agreement with modelled data for global oceans, N_2OPR 0 − 3.3 nmol kg^{-1} yr^{-1} with an overall mean N_2OPR of 0.2 ± 0.04 nmol kg^{-1} yr^{-1} (Freing *et al*., 2009). The N_2OPR for SWP from our studies shows are comparable to the results obtained by Freing *et al.* modelled data for AAIW in these regions (0 – 0.3 nmol kg^{-1} yr^{-1}). Comparatively higher N_2OPR in the AAIW than the bottom waters can be due to the large differences in the age of the AAIW as compared to the ΔN_2O.

3.6.3. N_2O in the Otago continental shelf transect

3.6.3.1. Distribution of N_2O

There are four sampling stations in the 60 km Polaris transect: neritic (PA), modified subtropical (PB), subtropical front (PC) and subantarctic (PD) (see Chapter 2 and Figure 3.23). Samples were collected in three different seasons. The water column profiles of nitrous oxide from coastal waters to the open ocean are shown in Figure 3.24a, b and c for September 2011, May 2011 and November 2012 respectively.

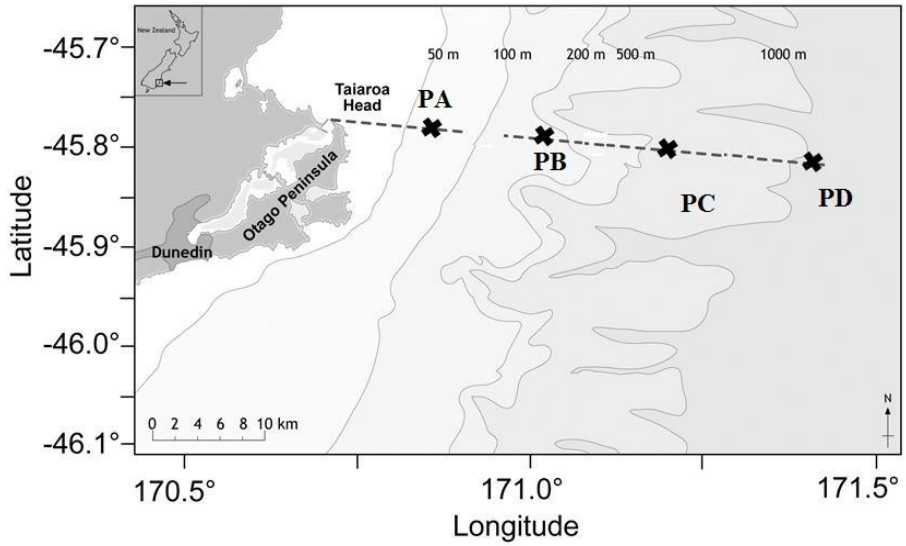

Figure 3.23: Otago Continental Shelf transect stations.

Information on the spatial and temporal variations of N_2O off the coast of Otago is the first seasonal study for this region. The basic hydrographic features and water mass characteristics are explained in section 3.3. The neritic and MSTW had the highest concentrations of surface N_2O, with a decrease in concentration from the coast to SASW in the open ocean during 2011 and 2012 (Figure 3.24.a & c). Neritic and MSTW waters have higher chlorophyll-a concentrations and productivity compared to subtropical and subantarctic waters (Currie and Hunter., 1999; Baer Jones, K. N., 2012) and are influenced by the discharge from the Clutha River, especially during major flood events (Baer Jones, K. N., 2012). The satellite chlorophyll data obtained for the study regions corresponding to the respective sampling period from the NASA website also supported these

findings (Figure 3.25). The data shows that irrespective of the sampling period chlorophyll concentrations were highest in the coastal regions and MSTW and the minimum in the SASW. Globally, coastal regions are one of the dominant marine sources for N_2O, particularly when influenced by freshwater input (Bange *et al.*, 1996; Bange. H. W., 2006, 2008). MSTW showed higher N_2O concentrations than STSW in the Southwest Pacific Ocean, as discussed in the previous sections (3.6.1.1 and 3.6.2.1), and nitrate concentration was high compared to STSW. Modified subtropical waters in these regions also have higher primary productivity than SASW (Bradford, 1980; Bradford-Grieve *et al.*, 1998; Vincent *et al.*, 1991).

N_2O distributions for the different water masses at all four stations during different sampling periods are shown in Table 3.9. During the spring seasons of 2011 and 2012, the N_2O distribution patterns are the same along the transect. During late autumn, in May 2012, an opposite trend for N_2O distribution was observed in the transect, with the highest surface concentration in SASW and the lowest in MSTW, as shown in Figure 3.20 and Table 3.9. This difference in [N_2O] can be due to the temperature and salinity differences and related changes in solubility. It can also be due to the proximity to the coast because of which the increased mineralization rates will increase the N_2O. Lower primary productivity in this transect during autumn and winter as compared to spring and summer can affect the N_2O production indirectly. A reduction in phytoplankton productivity after the peak bloom period has been reported for the same study regions (Baer Jones, 2012). Satellite-derived chlorophyll data for the study regions corresponding to the sampling periods show the same trend. The seasonal N_2O concentration variations were lower in SASW compared to the other waters. Therefore, the productivity-related effects were not seen in the SASW N_2O.

Neritic surficial waters are supersaturated with N_2O, with an average value of 130.1 %. The percentage N_2O saturation values were obtained for three different sampling periods and are shown in Figure 3.20 and Table 3.9. In the SASW average N_2O is in near equilibrium with the atmospheric values. The supersaturations at the warm, fresher, nutrient-depleted Otago coastal waters as compared to the SASW shows the importance of biological process, which will be looked in detail in the following sections and Chapters (Chapter 4 and 5).

The data show that the surface waters were slightly under-saturated in N_2O for samples collected in May 2012. During the same period, the chlorophyll values were also at their minimum (Figure 3.25 b). The under-saturations can be related to both biological and physical factors. Physical factors such as heating/cooling, refreshing or mixing of water masses can result in N_2O under-saturation. Any water mass mixing that will lead to an under-saturation is absent in this regions as described in the previous section on water mass properties. Freshwater intrusion can decrease salinity and hence can affect the solubility; however, a decrease in salinity from 34 to 10 is required to cause this much undersaturation (Farias *et al*., 2015) which is not seen in these regions. A decrease or increase in temperature of more than 3 ºC can also affect the solubility (Farias *et al*., 2015). Such differences were also absent. Moreover, a decrease in temperature will increase solubility and hence that cannot be the reason for the under saturations during autumn or winter seasons. Therefore, the biological processes will be the major reasons for these under saturations during the autumn period.

In the eastern South Pacific (ESP) Ocean, Farias *et al.* (2015) observed N_2O consumption which takes place faster rates than the sea to air exchange and N_2O fixation (as an alternative to N_2 fixation) and has been demonstrated as a responsible mechanism for this. We have to consider the possible analytical errors also associated with the measurements.

The only intermediate water mass found at these stations was AAIW, which is present at the open ocean station. The [N_2O] were 15.6-18 nM at the AAIW at around 300-1000 m depth (σ_t = 26.9-27.2). These values are consistent with results from the SBM station located closer to these regions than the other SPW stations. Moreover, the AAIW at these regions is comparatively young (eg. recently ventilated) compared to the Geotraces stations were average [N_2O] were ~ 18 nM.

Table 3.11: The distribution of [N_2O] in nM and Percentage saturation values along water masses of Otago Continental Shelf transect during different time periods.

Water Mass	PA	PB	PC	PD	PA	PB	PC	PD
	[N_2O]				N_2O Percentage saturation			
Polaris-September 2011								
Neritic	14.3	13.8			133.4	124.3		
MSTW	14	14.4			127.3	149.2		
SASW			12.6	11.8			112.4	104.2
AAIW			15.6	18			134.7	140.5
Polaris-May 2012								
Neritic	9.4				98.3			
MSTW		9.3				97.0		
SASW			10.1	10.0			100.6	99.6
Polaris-November 2012								
Neritic	10.6	11.5			105.8	115.8		
MSTW	11.5	12.5			110.3	116.6		
SASW			11.9	12.2			103.4	107.6

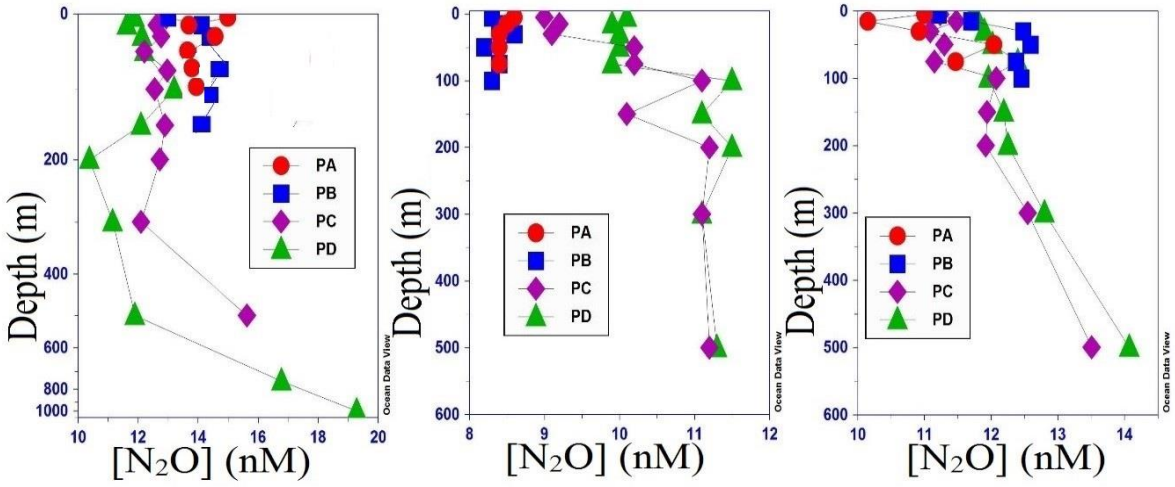

Figure 3.24: The [N_2O] along the transect PA,PB,PC and PD from left to right a) September 2011 b) May 2012 and c) November 2012.

3.6.3.2. The effect of DO, nutrients and productivity on N_2O

The DO profiles for the study region during November 2012 are given in Figure 3.25 (DO profiles are not available for the other two sampling periods). The DO measurements presented in Figure 3.25 shows that the water masses were well oxygenated throughout the transect. The figure also shows the nutrient distribution along the stations during different sampling periods. In November 2012, [N_2O] varied inversely with DO, indicating nitrification as the source in this region.

ΔN_2O *vs* AOU and ΔN_2O *vs* [NO_3^-] analysis during November are shown in Figure 3.26. At the neritic/MSTW shallower stations, the correlations could be affected by water mixing from coastal intrusions. The correlations (excluding the surface mixed layer) were statistically significant and positive for the other two stations (PC and PD). ΔN_2O *vs* AOU and ΔN_2O *vs* [NO_3^-] slopes were within the earlier reported values for different oceanic regions (Table 3.6 and 3.7). The regression equations obtained for the Otago transect are shown in Figure 3.26. During September 2011 nitrate also showed a significant positive correlation with ΔN_2O along PC and PD. The nitrate *vs* phosphate relationship for the Otago continental shelf transect was also studied (Figure 3.26). The nitrate *vs* phosphate variations confirms that a strong nitrification process exists below the surface waters and has a linear relationship with a slope of ~16 and intercept close to zero.

The above results point towards the nitrification processes as N_2O production mechanism in the Otago Continental shelf transect and will be examined in detail (Chapter 4 and 5). It is evident from the above results from Otago Continental shelf transect that in the SWP (at selected stations); higher N_2O is observed during the spring season in the surface waters and diminished from autumn to winter. This seasonal difference in N_2O is less apparent in the subantarctic sector of the Southern Ocean.

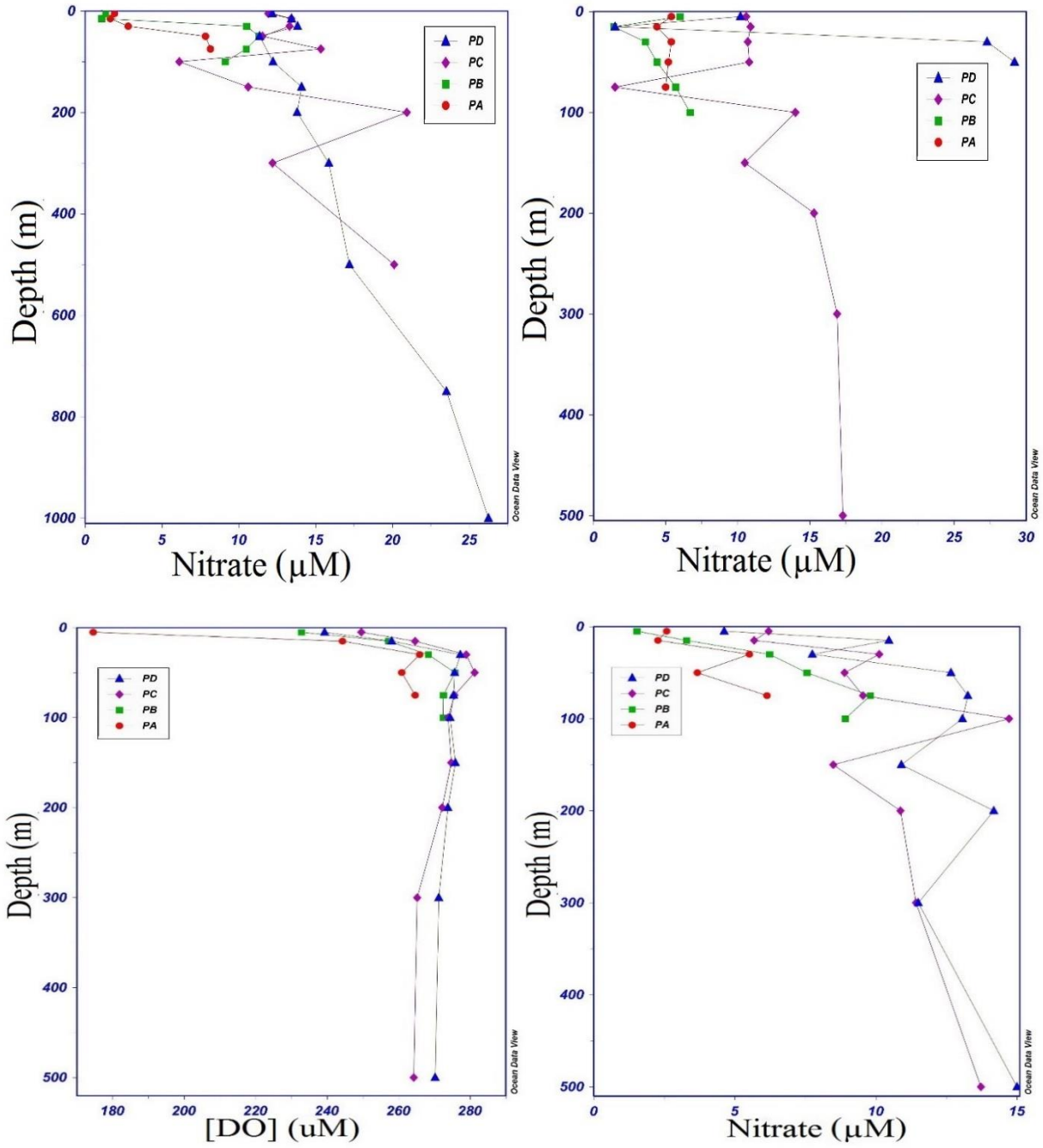

Figure 3.25: The variation of a) DO with depth in November 2012 and [Nitrate+Nitrite] with depth in b) September 2012 c) September 2011 d) May 2012.

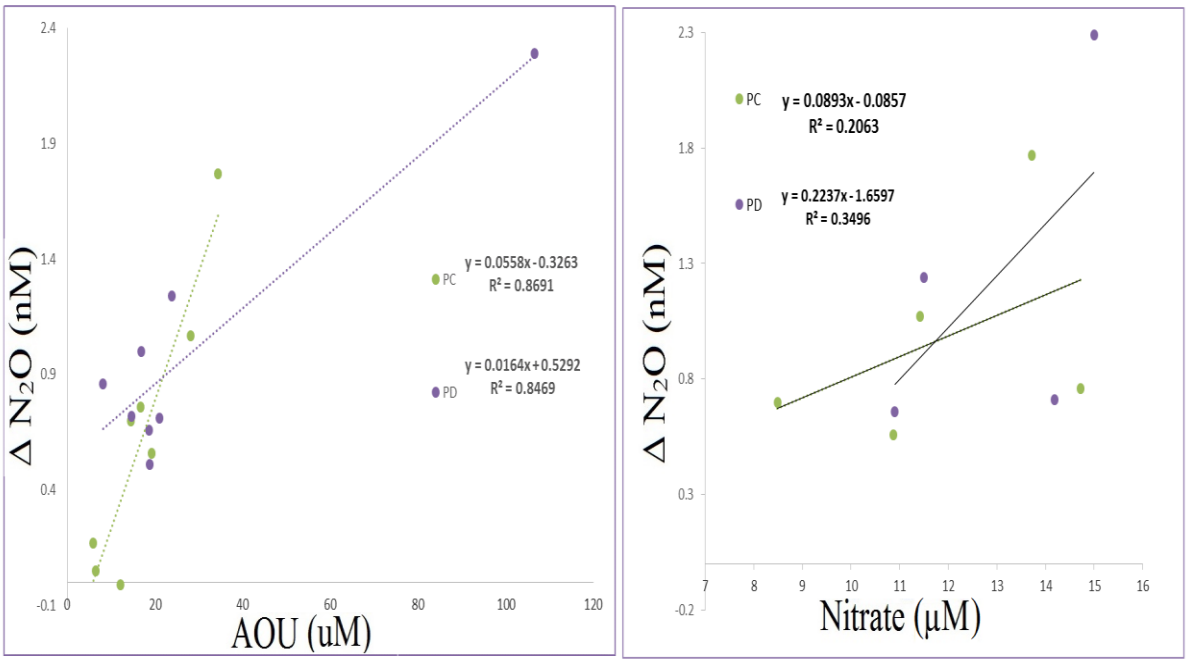

Figure 3.26: The variations of a) ΔN_2O vs AOU and b) ΔN_2O vs $[NO_3^-]$ for the two stations (PC and PD) of the Otago Continental shelf transect during November 2012.

3.8. Conclusions

N_2O measurements provide a substantial new dataset for understanding the distribution and production of this trace gas in the South Pacific waters. The major results from this work can be summarised as follows:

- N_2O distribution at selected stations showed characteristic variations in the horizontal and vertical distributions.
    - At the subtropical SWP stations, the [N_2O] profiles were consistent across the transect. Relatively lowest N_2O were found at the surface (STSW and SASW). [N_2O] increased below the mixed layer as depth increased with an average of 16.8 ± 0.8 nM in AAIW and the maximum of 21.3 ± 0.6 nM in CPDW.
- Surface waters are slightly oversaturated or in near equilibrium with respect to the global atmospheric mean value of N_2O in the SWP (101-105 %) as an indication of the sea to air flux. Otago coastal neritic and MSTW exhibited supersaturations up to 150 %.

- The [N_2O] vs [DO], [Nitrate] along with the positive correlation between ΔN_2O and AOU, and ΔN_2O and nitrate indicates that production of N_2O is mainly through nitrification.

- The CFC based water mass age, AOUR and N_2OPR estimations indicate that in the Southwest Pacific maximum N_2O is found in the upper thermocline (between 200- 500 m) and it is 3 - 5 times higher than that of the upper or lower waters. N_2OPR in the bottom of the ocean is uniform.

Chapter 4

N_2O Emissions from the South West Pacific Ocean

4.1. Introduction

The ocean-atmosphere interface is the site for the transfer of heat, momentum, aerosols and gases between the two phases and is the link between the oceans and atmosphere (Pickard and Emery., 1990). Direct and accurate measurement of the gaseous fluxes across the air-sea interface has been successfully established recently (McGillis *et al*., 2001); before that, it was not made at sea due to technological limitations (Nightingale *et al*., 2000). An accurate quantification of the sea to air flux and exchange processes is necessary to understand the vital role of this interface in marine productivity, atmospheric chemistry, oceanography and climate.

The Southern Ocean and Southwest Pacific Ocean occupy more than 30 % of the global ocean surface area, yet the N_2O estimates for these regions are poorly constrained due to the paucity of the data. Many earlier studies (Weiss *et al*., 1992, Nevison *et al*., 1995, Suntharalingam and Sarmiento., 2000, Foster *et al*., 2007, Charpentier *et al*., 2010, Farias *et al*., 2015) predicted that these regions (especially between 40 - 60º S) are significant sources of N_2O.

It is well known that the oceans act as a global source for N_2O. However the magnitude of this source is not well established (IPCC, 2013). N_2O production occurs mainly in the oxic subsurface ocean and deep ocean during nitrification, whereas in anoxic to suboxic parts of the ocean N_2O can be produced and/or consumed during denitrification. There will be a surface mixed layer (ML) source if the sea-to-air flux of N_2O (F_{s-a}) exceeds the supply of N_2O across the thermocline (F_{c-t}). If this is not the case, the sea-to-air flux of N_2O (F_{s-a}) should be the same as the supply of N_2O across the thermocline (F_{c-t}) to the mixed layer (ML). In steady state, N_2O concentration in the ML will represent the balance between physical processes such as vertical mixing, air-sea gas exchange with the overlying atmosphere, vertical and horizontal advection and biological processes such as nitrification and denitrification. Assuming no horizontal gradients in [N_2O] then the fluxes across the ocean-atmospheric (F_{s-a}) and cross–thermocline (seasonal thermocline at the base of mixed layer) (F_{c-t}) interfaces are the key physical terms in determining the N_2O ML budget and hence the flux.

4.2. Objectives

This chapter focuses on the following topics related to the N_2O flux in the Southwest Pacific and Sub-Antarctic regions.

1. To improve understanding and quantification of the N_2O air-sea flux (F_{s-a}) in the selected regions of Southwest Pacific Ocean (SWP) to permit calculation of regional sea to air N_2O emissions using different parameterizations, and establish the contributions to the global N_2O flux from this regions.
2. To study the cross thermocline N_2O flux (F_{c-t}) in the water column to quantify the in-situ production in the mixed layer and its contributions to the total global sea to air N_2O flux.
3. To compare the N_2O flux estimates of F_{s-a} with F_{c-t} from different stations of Southwest Pacific and Sub-Antarctic regions. In particular, obtain more detailed information on the role of different processes in the N_2O formation and pathways in the respective oceanic regions.

4.3. Methodology

4.3.1. Study Locations

As described in chapter 2, water and air samples were collected from four different transects in the SWP region. Sea to air and cross-thermocline fluxes of nitrous oxide were then calculated for these regions based on the measurements. The four transects are Geotraces, Otago continental shelf, Bloom II and Mooring. The station maps and sampling methodologies are described in chapter two. (Figure 2.2, 2.3 and table 2.1).

F_{s-a} and F_{c-t} were averaged over six geographical boxes (see Table 4.1 and Figure 4.1 for the definition of each box) to provide a comparison between F_{s-a} and F_{c-t}. The geographical boxes A, B and C belong to the Subtropical Pacific regions and are comprised of the same waters masses, as determined by T-S diagram (see Chapter 3, Figure 3.1). However, the samples were obtained in different seasons. Box A represents the campaigns in 2011 June (winter) while C that in October (spring) and B represents the same oceanic region after one year in 2012 spring (October). Box D represents Sub-Antarctic waters of same seasons from different voyages. Boxes E and F represent Subtropical Frontal regions and coastal waters respectively.

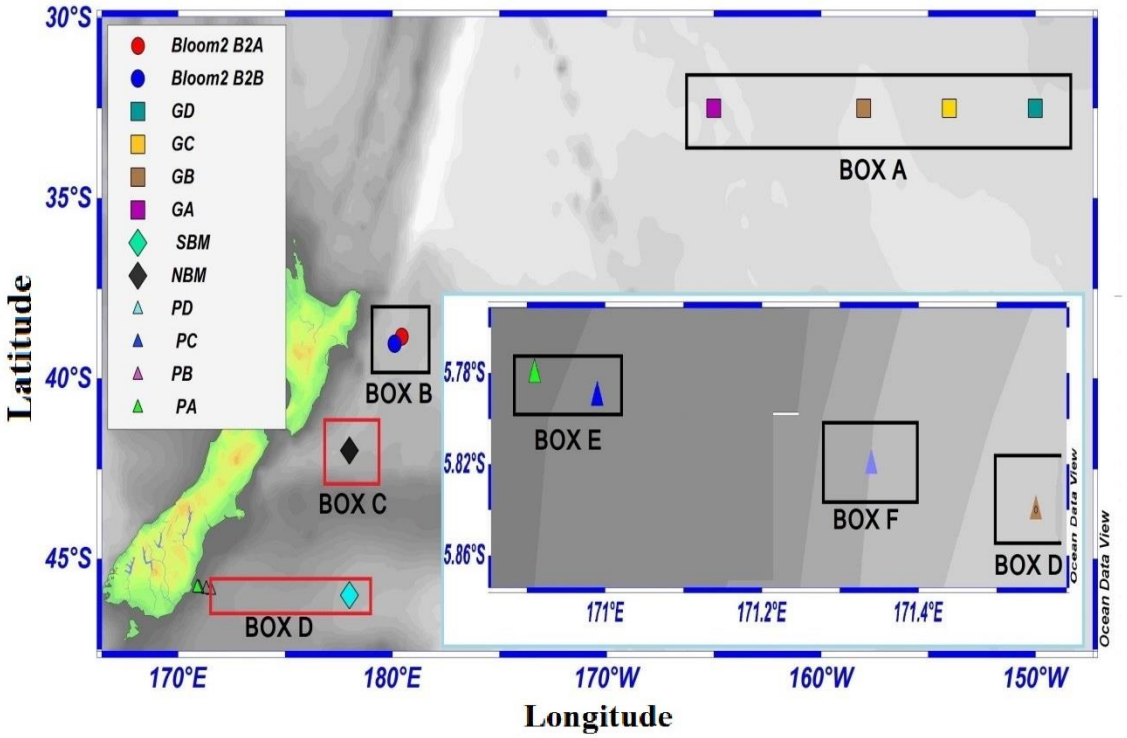

Figure 4.1: The geographical boxes defined based on latitudinal and longitudinal positions. The Otago Continental shelf region (inset shows the magnified view of Polaris transect) plotted separately, Box E and Box F.

Table 4.1: The geographical locations and oceanic regions of the Geographic Boxes

Geo.Box	Latitude	Longitude	Oceanic Region	Sampling season
Box A	32˚.0 S - 33.0˚S	166.0˚W-149.0˚W	Sub-tropical Pacific	Winter 2011
Box B	38.6˚S - 39.1˚S	180.0˚E-180.5˚E	Sub-tropical Pacific	Spring 2012
Box C	41.8˚S - 42.3˚S	178.0˚E-178.5˚E	Sub-tropical Pacific	Spring 2011
Box D	45.8˚S - 46.5˚S	171.5˚E-178.5˚E	Sub-Antarctic	Spring 2011
Box E	45.8˚S - 46.0˚S	171.0˚E-171.5˚E	Sub-tropical Front	Spring 2011
Box F	45.8 ˚S- 46.0˚S	170.8˚E-171.0˚E	Coastal/Neritic	Spring 2011

4.3.2. Nitrous oxide measurements

Water samples for N_2O concentration measurement were collected from 12 stations in triplicates from various depths. 622 samples were analysed for N_2O concentrations measured by purging and trapping system as explained in Chapter 2. Measured N_2O concentrations and their profiles are shown in Figure 4.2 for all the stations.

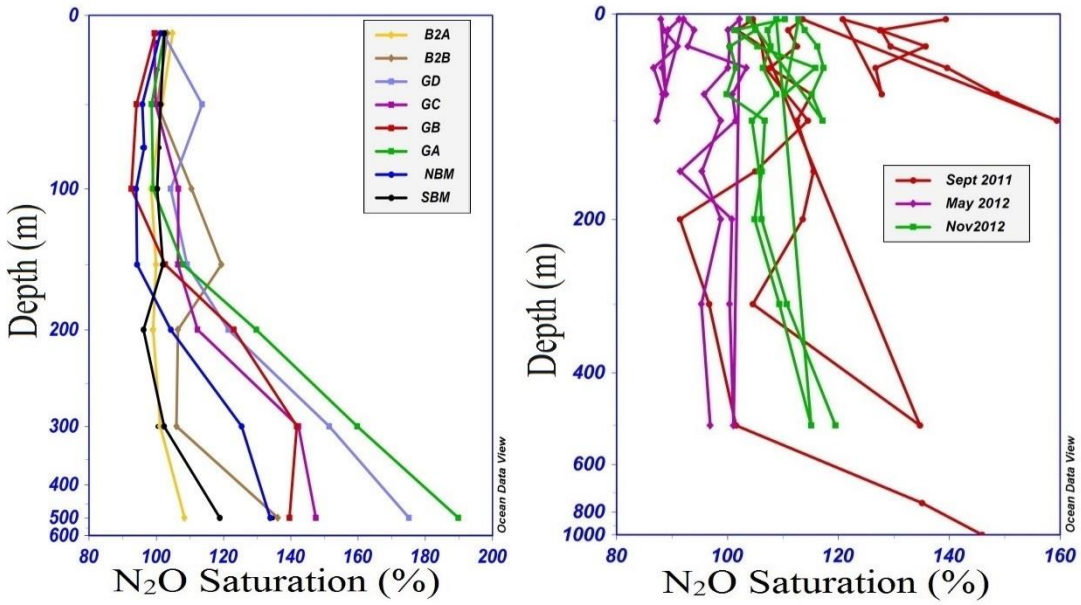

Figure 4.2: N_2O saturation measured during different cruises for (a) Geotraces, Bloom and Mooring stations and (b) Otago Continental Shelf transect stations during the three sampling periods, already discussed in chapter 3, presented to compare the maximum concentrations and corresponding depths.

4.3.3. Sea to air N_2O Flux

Sea to air flux of N_2O (Fs-a) from the ocean is estimated as the product of the difference between the measured partial pressure of N_2O in surface water and the atmospheric equilibrium partial pressure (concentration difference between the two phases that drives the flux) , and the sea to air gas transfer coefficient (Nightingale. P. D., 2009).

The sea to air N_2O flux (Fs-a) can be determined from the gas exchange equation below.

$$Fs\text{-}a = K_w \mathbf{(}[N_2O]_w - [N_2O]_e\mathbf{)} = K_w \Delta N_2O \quad \text{---------- (4.1)}$$

Where F_{s-a} is flux in nmol/m^2/s, K_w is the gas transfer coefficient/velocity in m/s, $[N_2O]_w$ is the N_2O concentration at the shallowest depth measured in the surface mixed layer (5–10 m). $[N_2O]_e$ is the N_2O equilibrium concentration. It is calculated using the mean dry mole fraction of N_2O in air (extracted from the monthly time series of atmospheric N_2O from the Baring Head monitoring station of NIWA at Wellington, New Zealand (ftp://ftp.niwa.co.nz/114ropic/n2o/bhd/BHDN2O.dat) and the solubility equation of Weiss and Price (1980, for more details, see section 2.5.3.3). The temperature and salinity at the corresponding sampling depths were obtained from the CTD data.

Gas exchange between the air-sea phases is mainly controlled by turbulence in the upper millimetres of the ocean and molecular diffusion. Since wind is a major driver of near-surface turbulence and linked to most of the other physical factors such as wave breaking and bubble formation, K_w is often parameterized in terms of wind speed (Liss. P. S., 1983; Wanninkhof. R., 1985; Nightingale. P. D., 2009). Three alternative relationships for K_w based on wind speed, as suggested by Liss and Merlivat (1986) (denoted by LM86), Wanninkhof (1992) (relationship for climatological winds, denoted by W92), and Nightingale, (2000) (denoted by N2000) were used to give lower and upper boundaries for fluxes. A wide range of wind speed is expected with the regular westerlies especially in the "roaring forties" of the subantarctic SWP which is believed to have a larger positive effect on the sea to air flux densities (Pickard and Emery., 1990). Later Ho *et al.* (2006) introduced a new relationship after Southern Ocean experiments which also suggested that the key factors controlling sea to air exchange processes in the Southern Ocean are similar to that in the other regions of the globe. This relationship was also more consistent with the measurement of gas transfer velocities at higher wind speeds. As Ho *et al.* (2006) conducted experiments to the southeast of New Zealand, their parameterizations are also used in the following calculations and are denoted as H2006.

To calculate K_w (in m/s) using the tri-linear relationship of LM86 the following three equations were used:

$$K_w = 4.72 \times 10^{-7} \times u_{10} \; (u_{10} \leq 3.6 \text{ m/s})$$

$$K_w = 7.92 \times 10^{-6} \times u_{10} - 2.68 \times 10^{-5} \; (3.6\text{m/s} \leq u_{10} \leq 13\text{m/s})$$

$$K_w = 1.64 \times 10^{-5} \, u_{10} - 1.40 \times 10^{-4} \; (u_{10} > 13\text{m/s})$$

Where u_{10} is the wind speed in 10 m height from the ocean surface, LM86 is usually applicable for both short-term and long-term wind speed averages.

The quadratic relationship for climatological wind data of Wanninkhof (1992) (W92), is

$$K_w = 1.08 \times 10^{-6} u_{10}{}^2$$

This approach is only valid when using long-term averaged (climatological) wind speeds. The combined linear and quadratic equation from Nightingale *et al.* (2000) (N2000) is as shown below.

$$K_w = 9.25\times 10^{-7} u_{10} + 6.17 \times 10^{-7} u_{10}^2$$

The N2000 relationship shows a dependence on wind speeds intermediate between those of Liss and Merlivat (1986) and Wanninkhof (1992). Moreover, the N2000 relationship is in reasonable agreement with globally averaged wind speeds estimates of K_w (Nightingale. P.D., 2009).

As K_w is provisionally estimated for CO_2, K_w was adjusted for N_2O by multiplying with $(S_c/600)^{-n}$, where n = 2/3 for wind speeds < 3.6ms−1 and n = 1/2 for wind speeds >3.6ms−1 for LM86; $(S_c/660)^{-0.5}$ for W92, and $(S_c/600)^{-0.5}$ for N2000, where S_c is the Schmidt number for N_2O. S_c was calculated using empirical equations for the kinematic viscosity of seawater (Siedler and Peters., 1986) and the N_2O diffusion coefficient in water. The N_2O diffusion coefficient (DN_2O, m^2/s) was calculated using the equation

$$DN_2O = 3.16 \times 10^{-6} \exp(-18370/RT)$$

where T is the water temperature in K and R is the universal gas constant.

Wind speed data were obtained from the ship's underway observations for each respective cruise (Geotraces, Bloom II voyage and Mooring), or from the daily wind speed data from Taiaroa Head (Port Otago) for the Otago transect. These data were used to calculate the gas transfer velocities (M. Smith and S. Nodder of NIWA and A. Sutherland of Port Otago provided the respective data).

Literature values were used for the uncertainty of air-sea gas transfer coefficient (Freing *et al*., 2009, Nightingale *et al*., 2009), and the analytical error for the N_2O measurements was used for the ΔN_2O estimations. Assuming an uncertainty of approximately 20 % for the air-sea transfer coefficient and wind speed and ~8 % uncertainty for ΔN_2O, when used in the gas flux equation 4.1 a root sum of squares uncertainty of ~21.5 % was estimated for the N_2O fluxes. The evaluated analytical error for the measurements was on the same order of magnitude as previous estimations (Bange *et al*., 2001; Charpentier *et al*., 2010).

4.3.4. Cross-Thermocline N_2O Flux

The total flux $F_{c\text{-}t}$ N_2O from the sub-mixed layer into the mixed layer was calculated as

$$F_{C\text{-}T} = K_z \, grad N_2O \qquad (4.2)$$

Where K_z is the diapycnal mixing coefficient (m/s), and $grad N_2O$ is the concentration gradient of N_2O between the lower boundary of the mixed layer and the depth of the subsurface N_2O maximum in mol/m^4, with the flux calculated in nmol/m^2/s. To calculate $grad N_2O$ the depth of the N_2O maximum ($d N_2O$max) was determined for every station from the depth profile. The mixed layer depths (d_{ml}) were calculated from the temperature profile at every station using CTD data using the method of Kara *et al.* (2000) as explained in Chapter 3 (Section 3.4). $[N_2O]_{ml}$ and $[N_2O]_{max}$ were determined using the two points of the profile above and below the calculated mixed layer depth, respectively, for $grad N_2O$ calculations.

The N_2O gradient was calculated as

$$grad N_2O = ([N_2O]_{max} - [N_2O]_{ml}) / (d_{N2Omax} - d_{ml}) \qquad (4.3)$$

Where $[N_2O]_{max}$ is the maximum N_2O concentration and d is depth .

In Equation 4.2 the diapycnal mixing coefficient K_z was estimated according to Watson and Ledwell (2000) as

$$K_z = 0.49 \, bf \qquad (4.4)$$

Here *bf* is a mean buoyancy frequency for the respective station. There are other methods for the K_Z estimation. However, we choose Watson and Ledwell method since they estimated Kz at greater depth in the water column. *bf* was calculated for the depth interval between the N_2O maximum and the base of the mixed layer using temperature and salinity data from the CTD.

$$bf = \sqrt{(-g/\rho_0 \, d\rho_{(z)}/dz)} \qquad (4.5)$$

where g is the acceleration due to gravity, ρ_0 is the reference density which corresponds to the depth of the d_{ml} , and $\rho_{(z)}$ is the mean density profile which corresponds to the density at d_{N2Omax}. The uncertainty for the cross thermocline flux measurement is the root sum of the squares of the uncertainties on Kz and *grad*N_2O. An uncertainty of 10 - 15 % was observed for *grad*N_2O based on the error values in the N_2O measurements, while an uncertainty of 35% was used for K_Z , based on the literature values. Therefore the total uncertainty in $F_{c\text{-}t}$ was between 36 - 38 % for the different stations.

In 2001, Law *et al*. measured K_z for the southern ocean regions and these values were used for the present study regions as an alternative approach to calculating the cross thermocline flux. Law *et al*. reported an average value of (0.1 ± 0.2) cm^2/s for K_Z. $F_{c\text{-}t}$ N_2O were also calculated based on K_Z estimations from other studies and compared with the fluxes from different oceans.

4.4. Results and Discussion

4.4.1. Nitrous oxide Flux: Sea to Air

The surface N_2O distribution for each study region is explained in detail in chapter 3. The N_2O saturation ranged from 100.9 -103.2 % in the sub-tropical water, while it was 102.4 - 104.6 % in Sub-Antarctic regions of SWP (Figure 4.2) (For more details see Chapter 3), and 130.1% in coastal waters. These saturation levels indicate that the coastal waters on the Otago shelf transect were a net source of N_2O to the atmosphere, while most of the open ocean regions close to equilibrium with the atmosphere as they contribute relatively very little to the N_2O flux per unit area.

Average N_2O fluxes for the study regions were calculated as explained in section 4.3.3 based on the in-situ measurements of temperature, salinity, wind speed and the N_2O concentration. The estimated fluxes obtained using the four different parameterizations for different stations are shown below in Table 4.2. The average fluxes, based on the N2000 parameterization can be summarized as follows; in the Southwest Pacific Ocean, a slight increase in flux was observed from north to south, with lowest values in the northern Geotraces stations (Box A) and highest in the SBM (Box D). In the Otago continental shelf transect, the flux estimates showed a decreasing trend from the coastal ocean towards the open ocean. The average flux was 4.00 µmol/m^2/d (0-8.10 µmol/m^2/d) in the frontal regions (Box F) and 1.35 µmol/m^2/d (0-2.70 µmol/m^2/d) in Sub Antarctic waters (Box D). These fluxes are similar to the values observed in the subantarctic SWP mooring transect during the same time. These values were consistent with that of Law *et al.* (2001) who estimated -1.18 to +1.75 µmol/m^2/d for the Southern Ocean. Earlier studies from the South Pacific showed slightly negative fluxes from central South Pacific Gyre (-0.48 ± 0.44), and slightly positive values from its eastern parts (0.41±0.34) (Charpentier *et al*., 2010). Recently Farias *et al.* (2015) reported considerably greater N_2O flux from the Southern Ocean that ranged between -10.5 to 8.65 µmol/m^2/d. Table 4.3 describes the reported fluxes from different ocean regions from earlier studies. Flux estimates from the Arabian sea and some other world oceanic regions are also shown in Chapter 6 (Table 6.9 and 6.11).

Table 4.2: The average nitrous oxide flux calculated for various parameterizations for the six different boxes. Values are in µmol/m^2/d (uncertainties obtained for the measurements are as mentioned in the respective sections).

Geo.Box	$\mathbf{F}_{s\text{-}a}^{LM86}$	$\mathbf{F}_{s\text{-}a}^{W92}$	$\mathbf{F}_{s\text{-}a}^{N2000}$	$\mathbf{F}_{s\text{-}a}^{H2006}$
Box A	0.14	0.26	0.18	0.56
Box B	0.41	0.77	0.66	0.56
Box C	0.20	0.38	0.30	0.28
Box D	0.93	1.82	1.21	1.33
Box E	2.82	5.54	3.69	4.05
Box F	5.91	11.62	7.73	8.50

To account for the large uncertainties in gas exchange velocities, we additionally calculated sea-to-air fluxes using the gas exchange parameterizations by Liss and Merlivat (1986) and Wanninkhof (1992) as lower and upper boundaries (Wanninkhof *et al*., 2009). The values obtained for these parameterizations are shown below in Table 4.2. The flux values based on the Ho *et al* parameterizations were also estimated and are shown in Table 4.2.

The estimated N_2O fluxes based on different parameterizations were used to compare the spatial variations of the N_2O atmospheric flux within the different geographical boxes (for definitions of boxes see Figure 4.3 and Table 4.1). Irrespective of season the SWP between 170º E to 140º W and 32º S to 47.5º S are a source of N_2O to the atmosphere, though the extent of the fluxes varies regionally and seasonally per unit area per time. The sub-tropical Pacific contribution to the atmospheric source is lower in comparison among the present study regions. The highest sea to air fluxes was found close to the coast. Otago continental shelf regions showed higher fluxes which decreased with distance from the shelf to the open ocean throughout the study region. So this study confirms the importance of the coastal regions as the sources of N_2O flux compared to the open ocean. Coastal and shelf waters are expected to be influenced by processes such as terrestrial source input (run off from rivers) and are sites of increased *in situ* biological activities such as primary productivity, nitrification, denitrification and sedimentation compared to the deep waters.

Table 4.3: The Flux estimations from different oceanic regions

Reference	Oceanic region	Remarks	Sea to air Flux (μmol/m^2/d)		
			LM 86	N 2000	W 92
Popp *et al*., 2002	Subtropical Pacific, North Pacific Gyre	ALOHA station	0.4-1.0	NA	1.1±0.7
Dore and Karl.,1996	Subtropical Pacific, North Pacific Gyre	ALOHA station	1.05-4.72	1.83-8.11	1.53-6.06
Morrell *et al*., 2001	Carribean Sea, Tropical Atlantic		0.07-4.90	NA	NA
Oudot *et al*., 1990	Tropical North Atlantic		NA	1.09-1.76	NA
Oudot *et al*., 2002	Tropical South Atlantic		NA	2.52±2.18	NA
Walter *et al*., 2004	Tropical North Atlantic		NA	0.17±0.16	NA
Charpentier *et al*., 2010	South Pacific Gyre		0.36-0.67	NA	NA
	Coastal upwelling - off Chile		44.24	NA	NA
Farias *et al*., 2015	Kergulean Pleateu, Southern Ocean	N-S Transect	-10.5–8.65	-22.9-15.5	NA
	Kergulean Pleateu, Southern Ocean	W-E Transect	-9.65-5.25	-1.52-8.10	NA
	ETSP		-1- 10.7	NA	NA

The oceans are the largest natural sources of N_2O emissions. Even though estuaries and rivers contribute N_2O to the atmosphere, emissions of N_2O from these other aquatic environments are typically classified as anthropogenic since the majority of nitrogen entering these systems is believed to be related to human activities. The Table 4.4 shows the global annual flux estimates from different aquatic environments and their contributions to the global flux.

Table. 4.4: The global aquatic N_2O emission scenario (based on various publications and IPCC fourth assessment report).

	Annual Emissions, (Tg N/yr)	**Percent of Total Emissions** (%)
Open Ocean	3.2	59
Continental shelves	1.5	28
Upwelling zones	0.4	7
Estuaries	0.2	4
Rivers	0.1	2
Total	**5.4**	

Published estimates of open ocean fluxes generally range from 3 to 6 Tg N/yr with (1.4 - 98.5 Tg N/yr for the entire ocean including coastal regions). For example, the IPCC fourth assessment reported an estimate of natural emissions from oceans of 3.8 Tg N/yr, with a range of 1.8 to 5.8 Tg N/yr. Combining different emission estimates with recent models of natural and anthropogenic nitrogen export from rivers and estuaries shows the natural N_2O from the continental shelves (which receive drainage from rivers and estuaries and are impacted by humans) is 1.5 Tg N/yr.

Table 4.5: The total annual N_2O emissions from the present study regions and its contributions to the global flux

Oceanic Region	Tg N_2O/yr	Tg N/yr	% contribution to the Global open ocean Flux (3.2- 3.8 Tg N/yr)	% contribution to the Global Oceanic Flux (5.4 Tg N/yr)
South Pacific	0.11	0.07	2	1
Sub Antarctic	0.59	0.38	10-12	8
Coastal	0.15	0.09	NA	2
Sub tropical convergence	1.00	0.63	17- 20	13
Total	1.85	1.17	29- 34	24

Earlier estimates (Nevison *et al*., 2004) suggested that the oceanic regions from 30 ^{o}S to 90 ^{o}S made the largest contribution to global emissions (45-50 percent of the total). More recent work has reduced this flux estimate, and inverse modelling results suggest that this region may contribute as little as 7 percent to the global total since some of the SWP regions in the subantarctic have been identified as sinks for N_2O. However, this study is supportive of the earlier findings which suggested a strong source of N_2O from this regions.

The biological processes, nitrification and denitrification, which influence N_2O, are discussed Chapter 5, which interpreted the AOU and ΔN_2O relationships as indicating nitrification as the major biological process for N_2O production in this region. Frontal regions also recorded very high net N_2O flux rates, and frontal regions are well known for their higher biological activities (Vincent *et al*., 1991). Nevison *et al.* (1995) and Suntharalingam and Sarimento (2000) identified relevant contributions of frontal regions between 30 - 90˚S to the global N_2O budget as approximately 35 % and 45 % respectively. However the present study identified lower fluxes in the Geotraces stations in Box A relative to the subantarctic sector in Box D, even though both of these regions had similar values for ΔN_2O. The higher wind speeds in the 40°

and 50° latitudes of Southern Ocean, the subantarctic sections, is the key driver for the more positive net flux of N_2O. The high wind-speeds over subantarctic and frontal regions will bring higher emissions as a combined effect with ΔN_2O that are significantly higher than STW.

The extrapolation of the daily values in Figure 4.3 and Table 4.2 to mean annual fluxes assumes that the observed surface N_2O concentrations and wind speeds are representative of mean values throughout the year. The values were 55.6, 340.3, 2158.5, and 282.0 μmol/m^2/y (LM86) for subtropical Pacific, subantarctic, coastal and subtropical Frontal regions respectively. The annual fluxes based on W92 estimations were 103.6, 663.8, 4243.1 and 554.4 μmol/m^2/y respectively in the above order. These values are comparable to that estimated by Nevison *et al.* (1995) values that implied a mean flux of 0-182 μmol/m^2/y for subtropical Pacific and 180-364 μmol/m^2/y for subantarctic and coastal regions. However the mean annual fluxes in the latter regions were slightly lower than that of Nevison's calculations, but all were well in the range of Law *et al.* (2001) estimations.

Table 4.6: a) wind speed in m/s, b) sea surface temperature (ºC), c) ΔN_2O and d) net sea to air flux based on Nightingale, 2000 parameterization for the study area in SWP.

Boxes	Oceanic Region	Sampling season	Wind Speed (m/s)	Flux (μmol/m^2/s)	SST (ºC)	ΔN_2O (nM)
A	Sub-tropical	Winter 2011	7.0	0.18	19.0	0.07
B	Sub-tropical	Spring 2012	6.3 and 5.9	0.66	13.6	0.38
C	Sub-tropical	Spring 2011	5.9	0.30	13.4	0.27
D	Sub-Antarctic	Spring 2011	8.9 and 8.5	1.21	8.2	0.32
E	Sub-tropical Front	Spring 2011	8.9	3.69	8.0	1.55
F	Neritic	Spring 2011	8.9	7.73	9.5	3.24

The role played by seasonal changes in the oceanic N_2O cycle is mainly due to the temperature-related changes that will affect the oceanography physically, chemically and biologically. In order to understand the seasonal changes, the data were sub-divided into four categories: summer (December, January, February), autumn (March, April, May), winter (June, July, and

August), spring (September, October, November) for the Otago samples. Seasonal surveys were not obtained for the other survey regions; however Box A (Geotraces) represents winter samples sub-tropical Pacific, and Box B represents spring in the same oceanic region. Box C (bloom II) is similar to Box B both in season and location, but samples were taken after one year in 2012. The variations of net flux along the study regions with sea surface temperature, wind speed and ΔN_2O are shown in Table 4.6.

The two factors on which the N_2O sea to air flux depends are ΔN_2O and wind speed. In subtropical latitudes, average wind speeds are higher during winter/autumn and comparatively lower during spring/summer (Piccard and Emery., 1990), whereas ΔN_2O values will be influenced by organic matter availability, and so primary productivity, and temperature. Nevertheless, the ΔN_2O may be lower or even negative during winter and autumn due to the decrease in temperature following a decrease in biological activities. Increased mixing will cause degassing as a result of which there may be under-saturation of ΔN_2O if it doesn't mix up with the sub-surface water with higher ΔN_2O.

Fs-a was very low irrespective of the season in different stations of subtropical Pacific (see Table 4.6). The effect of higher wind speed was nullified to a greater extent by accompanying under-saturation or lower ML N_2O concentrations in summer and autumn. The increase in N_2O flux was weakened by the decrease in average wind speed in spring and summer. The average net flux (Fs-a) was higher in spring as compared to the winter in these regions.

4.4.2. Diapycnal N_2O Flux

Based on equations 4.2, 4.3 and 4.4 and measurements of $[N_2O]$ profiles along each transect, the N_2O flux across the base of the ML was estimated (for the mixed layer depth approximations see chapter 3) (Table 4.7). The contributions from cross thermocline flux to the sea to air flux in each box were also calculated (Table 4.8). The average diapycnal flux in Box A was 0.002 μmol/m^2/d with little variability across the transect, whereas geographical boxes B, C, D and E showed a similar N_2O diapycnal flux. Along the Otago continental shelf, $F_{c\text{-}t}$ increased from open ocean to the coast. In the open ocean Box D, a flux of 0.001 μmol/m^2/d was observed while that in the Subtropical Frontal zone was 0.0004 μmol/m^2/d, and the first

coastal station in Box F was extremely well-mixed while the second station showed a flux value of 0.003 µmol/m^2/d.

In an alternative approach, F_{c-t} was estimated using the *grad*N_2O measured for the present study regions and K_z measured by Law *et al.* (2001), and the values compared. The flux values (F_{c-t}) were also calculated by using different Kz values measured for different oceanic regions by earlier researchers in past three decades (Table 4.7). These results indicate that Fc-t values are relatively similar between Boxes, with only slight variations from one another. The major reason for this limited variation is the lack of significant variation in stratification across the base of the mixed layer and also in average N_2O_{max} in the respective Boxes. With the exception of coastal regions (Box F), the highest value of F_{s-a} occur in the Subtropical Frontal region in Box F, whereas this region has the lowest value of F_{c-t}. In the Geotraces transect (Box A) the lowest values for F_{s-a} were obtained while higher values for F_{c-t}. On moving from south to north, an increase in *grad*N_2O was observed similar to the observation of Walter *et al.* in the Atlantic Ocean (2006). Also similar to the Walter *et al.* results the flux density (F_{s-a}) did not exhibit a similar trend to *grad*N_2O. This lack of discernible relationship with flux density is due to the variation in the K_z value used, which reflects differences in stratification at the base of the mixed layer.

In general, the mean fluxes across the base of the ML were lower than the N_2O sea to air flux based on all parameterizations; however, they are within the error range and so are not significantly different (Table 4.2 and 4.3). However, the air-sea flux estimates are based on climatological wind speeds, and there is a large uncertainty in the different estimates of Kw as mentioned earlier. As Kz can vary significantly over short time periods, the Kz estimated in different conditions and regions were used to provide a range (Table 4.7).

4.4.3. The N_2O production in the surface mixed layer

From the above estimations of the N_2O fluxes, and consideration of the uncertainty in these estimates, it may be inferred that the N_2O production in the upper mixed layer may contribute to the sea to air flux. When the above-estimated air-sea and diapycnal flux values were used to close the mixed layer N_2O budget, this suggests that there is a biological source in the mixed layer (Table 4.8). This result is in accordance with that of Dore and Karl (1996), who found an average 2-9 % contribution from vertical diffusion to the total flux (F_{s-a}) in the sub-tropical North Pacific.

The influence of biology (i.e. microbial processes and primary productivity) of the oceanic mixed layer especially on its role in N_2O chemistry is still a major topic of debate. A few studies suggest that the upper ocean [N_2O] is mainly controlled by gas exchange, sea surface temperature variations and diapycnal N_2O exchange (Bange. H. W., 2004). Earlier studies suggested photoinhibition of nitrification processes in the euphotic zone (Horrigran *et al*., 1981) which in fact may minimise N_2O production as a result of decreased nitrification. However, modelling studies (Yool *et al*., 2007) and in-situ measurements in the various parts of the ocean, such as the N Pacific (Dore and Karl., 1996; Dore *et al*., 1998), and Atlantic Ocean (Morell *et al*., 2001; Clark *et al*., 2008) suggested nitrification as the dominant N_2O production process in the upper mixed layer.

Table 4.7: The cross thermocline flux for the study regions, all values in µmol/m^2/d, calculated using K_z values estimated using Buoyancy Frequency values, and directly measured K_z estimates from the ocean during last three decades. The K_z values are shown in parenthesis.

Regions	Present Study	Law *et al*, 2003 (0.3)	Howard *et al* , 2004 (0.1)	Morrell *et al*, 2001 (1.5)	Yuan, 1984 (1.7)	Yuan, 1984 (1.6)	Charpentier *et al*, 2007 (0.1)	Polzin *et al*, 1997 (1)	Lie *et al*, 1984 (1.6)
Box A	0.002	0.005	0.002	0.023	0.026	0.024	0.002	0.015	0.024
BOX B	0.001	0.004	0.001	0.019	0.021	0.020	0.001	0.012	0.020
BOX C	0.001	0.004	0.001	0.018	0.021	0.020	0.001	0.012	0.020
BOX D	0.001	0.003	0.001	0.013	0.014	0.013	0.001	0.008	0.013
BOX E	0.0004	0.002	0.001	0.010	0.012	0.011	0.001	0.007	0.011

The nitrification rate for the study regions is calculated and shown in Table 4.8 on the assumption that uniform production will take place with depth and time in the mixed layer. The estimations were based on an average yield of 0.25 % N_2O from nitrification based on Goreau *et al*., 1980. However recent studies suggest that the N_2O yield from nitrification may range between 0.004 to 0.4 % (Elkins *et al*., 1978; Yoshida *et al*., 1989; De Wide and De bie., 2000; Punshon and Moore., 2004). The calculated subtropical Pacific nitrification rate was smaller than that of the subantarctic and coastal waters (see Table 4.8). The calculated nitrification rates were consistent with rates in the Southern Ocean measured during SOIREE (0-0.7 mmol/m^2/d; Law *et al*., 2003). Earlier studies reported nitrification rates of 0.42-0.63 mmol/m^2/d for the upper 100 m at 52º S (Binachi *et al*., 1997) and 0.04-0.08 mmol/m^2/d in the Scotia Sea (Olson.R. J., 1981). On the Otago Continental Shelf transect much of the mixed layer N_2O production arises from the horizontal transport from riverine input to the coastal waters and resulting lateral mixing with MSTW (Baer Jones. K. N., 2012); consequently, the high N_2O production rates and inferred nitrification rates in these waters are regarded as overestimates. However, it is assumed that horizontal gradients at the open ocean stations are negligible, compared to the coastal regions.

Table 4.8: Sea to air and cross-thermocline flux of N_2O, and their relative contributions to the total N_2O flux. Flux values and nitrification rates are in µmol/m^2/d.

Geo.Box	F_{N2000}	F_{c-t}	In-Situ N_2O production	% Fct/Fs-a	Inferred Nitrification	
					Goreau, 1980	De wilde, 2000
Box A	0.018	0.002	0.180	53.7	0.0004	0.001
Box B	0.098	0.001	0.978	4.5	0.0024	0.004
Box C	0.020	0.001	1.212	18.5	0.0030	0.005
Box D	0.121	0.001	7.732	3.6	0.0193	0.031
Box E	0.369	0.0004	3.687	0.6	0.0092	0.015
Box F	0.773	0.003	0.197	3.9	0.0005	0.001

4.5. Conclusions

- The present study results indicate that the Southwest Pacific Ocean regions act as sources of atmospheric N_2O.
- The N_2O flux density values indicate lower N_2O emissions from Subtropical waters than from Subantarctic Waters.
- Coastal regions were identified as the largest source of N_2O to the atmosphere per unit area in the region.
- The N_2O flux (F_{c-t}) values illustrate the importance of surface mixed layer N_2O production. The discrepancy between the diapycnal N_2O flux and air-sea flux suggests in situ biological production, most likely by nitrification, in the surface mixed layer.
- Wind speed, temperature and biology (mainly nitrification) are the main factors, which control the N_2O flux density.

Chapter 5

Isotopes, Isotopomers and Incubation studies to unravel the N_2O Cycling in Southwest Pacific Ocean

5.1. Introduction

The greenhouse gas N_2O is increasing globally in the atmosphere at an average rate of 0.25 % annually (IPCC., 2007). Present studies on N_2O in SWP waters as explained in Chapter 3 and 4 clearly suggest that most of these regions are significant to the global budget both in the open ocean and coastal waters. In the ocean, N_2O is formed as a by-product of nitrification (Yoshida and Alexander., 1970; Goreau *et al*., 1980) and intermediate of denitrification (Smith and Zimmerman., 1981; Knowles. R., 1982; Firestone and Davidson., 1989) processes. Consumption of N_2O in suboxic and anoxic regions through denitrification is also reported (Cohen and Gordon., 1978; Elkins *et al*., 1978; Hattori. A., 1983). However, it is not known completely which mechanism is important for production in the ocean. According to most researchers, it is produced mainly through nitrification in the open ocean (Yoshinari, 1976; Elkins *et al*., 1978; Cohen and Gordon., 1979; Butler *et al*., 1989; Outdot *et al*., 1990). Preliminary results from ΔN_2O, AOU, and $[NO_3^-]$ also suggest that the SWP derives most of its N_2O from nitrification processes (see Chapter 3 and 4). The available results based on the DO/nitrate and N_2O relationships are not conclusive about the prevailing mechanism in the respective regions.

Since the nitrification and denitrification processes follow different pathways, the direction and magnitude of isotopic discrimination for each of the processes will likely be distinct. Hence the stable isotopic data will be a good tool to provide insight into the sources and predominant biochemical mechanisms of production and consumption of N_2O (Yoshida and Matsuo, 1983, Ostrom *et al*., 2000; Rahn and Wahlen., 2000). The oxygen isotopic signal in N_2O produced during nitrification is introduced by the $\delta^{18}O$ of both dissolved O_2 and H_2O depending on the formations pathway (Ostrom *et al*., 2000). The changes in dual isotopic signatures of N_2O resulting from sea to air exchange is small compared to the biological processes, and therefore biological N_2O formation should yield a clear isotopic signature in oceanic N_2O (Kroopnick and Craig., 1976; Bange. H. W., 2010).

In order to understand the N_2O production mechanism in detail the following stable isotopic signatures were measured: double/dual isotopes of N_2O- $\delta^{15}N_{bulk}$-N_2O and $\delta^{18}O$-N_2O, $\delta^{18}O$-$O_{2,\ dissolved}$ and $\delta^{18}O$-H_2O. N_2O is an asymmetrical molecule and analyses of the intramolecular distribution of isotopic isomers or isotopomers of N_2O were also performed. The intramolecular distribution of nitrogen isotopes in N_2O is expressed as the site preference, SP = $\delta^{15}N_\alpha$ - $\delta^{15}N_\beta$. This analysis offers additional information to more tightly constrain sources and sinks of this greenhouse gas (Toyoda and Yoshida., 1999). Further insight into the processes was achieved by conducting controlled incubation experiments. This chapter deals with all the above-mentioned data and discussions based on these results. Key concepts on N_2O dual isotopes are presented below. Further description on isotopes is given in Chapter 1 (Section 1.5 and 1.6).

The isotope compositions of N_2O are mainly controlled by kinetic isotopic effect during nitrification and denitrification processes. During which the ^{14}N or ^{16}O are preferred over the heavier isotopes ^{15}N and ^{18}O by microbes and will be transferred to the end products of the reaction. As a result, the remaining molecules with heavier isotopes will react slowly during the biological processes and substrates will become isotopically enriched and the products depleted (Kroopnick and Craig., 1976). N_2O is a product of both nitrification and denitrification marked depletions were expected in $\delta^{15}N_{bulk}$-N_2O with respect to that of substrate NH^+_4 and NO^-_3 (Ostrom *et al*., 2000). Denitrification also results in consumption of nitrous oxide which will leave residual N_2O having enriched ^{15}N and ^{18}O (Yoshinari. T., 1976; Yamazaki *et al*., 1987; Barford *et al*., 1999). Depletion is generally indicative of production by nitrification or nitrifier- denitrification and enrichment attributed to consumption by denitrification. During formation of N_2O regardless of the starting material, the heavier ^{15}N isotope will be concentrated at the central alpha position. The precursor molecule contains only one nitrogen atom and hence the distribution of the ^{15}N will largely depend on the formation process and not on the $\delta^{15}N$ (Toyoda *et al*., 2002). The stable isotope signatures of N_2O in these waters can be used to trace the N_2O production process more reliably since the debate is over nitrification or denitrification and whether the contributions from the latter cannot be completely ruled out.

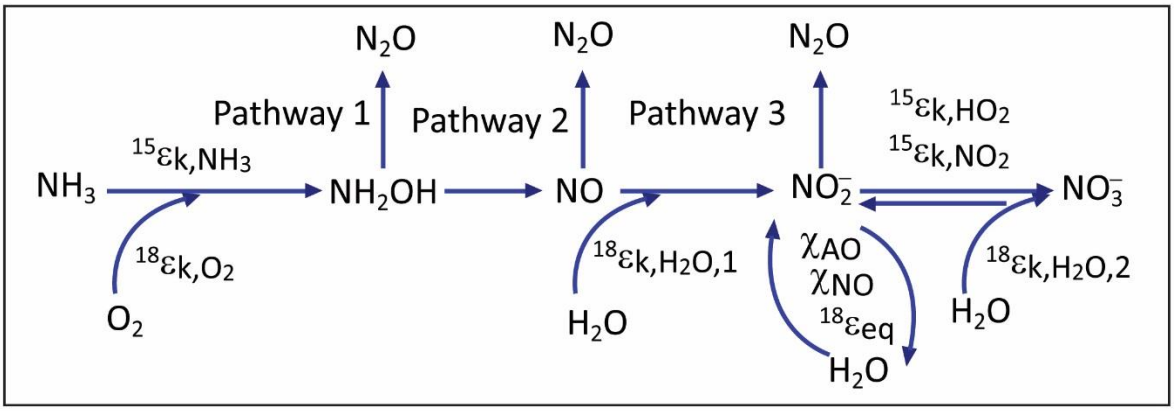

Figure 5.1: The isotopic fractionation and exchange of N and O during nitrification. Nitrogen fractionation occurs at ammonia monooxygenase and oxygen isotopic fractionation occurs when O_2 and H_2O are incorporated and exchanged. During nitrite oxidation N and O isotopic fractionation occurs at nitrite oxidoreductase and O isotopic fractionation during H_2O incorporation and exchange. (Picture adopted and modified from Ostrom *et al*., 2000).

The isotopic fractionation and exchange during nitrification processes are shown above in Figure 5.1. Ammonium (NH_4^+) is the major nitrogen source for N_2O in the oxic environments whereas nitrate $(NO_3)^-$ in the suboxic conditions. During N_2O formation through nitrification regenerated ammonium from the fixed nitrogen is the nitrogenous substrate and hence the N-N_2O will be isotopically lighter than that of the NH_4^+ and similar or lower than that of sinking particulate nitrogen (Yoshinari *et al*., 1997). Hence the N_2O in the surface waters which are isotopically similar or depleted with respect to the $\delta^{15}N_{bulk}$ of atmospheric N_2O is evidence for production through nitrification (Dore *et al*., 1998; Naqvi *et al*., 1998; Ostrom *et al*., 2000). Since denitrification causes both production and consumption of N_2O, the differences are reflected in the isotopic signatures of N_2O. If N_2O is produced through denitrification, then N_2O will be isotopically depleted (production) or enriched (consumption). However, production of N_2O via denitrification happens in suboxic conditions only. When N_2O is consumed during denitrification, the residual N_2O will be considerably isotopically enriched. An increase in $\delta^{15}N_{bulk}$ of N_2O up to 27 ‰ to 39 ‰ is also expected in the regions where denitrification consumes N_2O (Yoshida *et al*., 1984).

The formation of N_2O through nitrification is uncertain and as explained in Chapter 1 (Section 1.4.1), is through multi-pathway (Figure 5.1). During nitrification, N_2O is either released from nitrification of NH_2OH (pathway 1), or is an intermediate between hydroxylamine and nitrite-NO (pathway 2) which is the processes taking place at most of the depths and at some particular depths (100-500 m) it is also formed from reduction of $(NO_2)^-$, nitrifier denitrification

(pathway 3) (Ritchie and Nicholas., 1972; Groffman., 1991; Ostrom *et al*., 2000). Understanding the sources of O in the N_2O will enable to unravel the respective mechanisms responsible for its production through various biochemical pathways of nitrification (Ostrom *et al*., 2000). Due to the differences in the magnitude and isotopic fractionation direction between different pathways (Figure 5.1), oxygen isotope signatures can be applied as an important tool to explore these processes (Ostrom *et al*., 2000). These can be achieved through measurement of $\delta^{18}O$ of N_2O, DO ($O_{2,\ aqueous}$) and H_2O. During nitrification the first oxygen atom added is derived from DO while the second one is added from the water, Figure 5.1 (Dua *et al*., 1979; Hollocher *et al*., 1981). $\delta^{18}O$ of water and dissolved oxygen in the ocean differ by more than 20 ‰ (Kroopnick and Craig., 1976). So the measurement of $\delta^{18}O$ of N_2O, DO ($O_{2,\ aqueous}$) and H_2O will provide significant information about the source of oxygen in N_2O and hence about the pathways from which it is formed (Ostrom *et al*., 2000).

Most of the previous extensive studies using stable isotopes and isotopomers of N_2O were on less oxygenated waters of the Black Sea, Sub Arctic, North Pacific, Arabian Sea and Upwelling Oceanic regions. The present work offers the first detailed isotopic and isotopomeric study for the subtropical and subantarctic SWP.

5.2. Aims and Objectives

The overall aim of the work presented in this chapter is to identify the formation pathways of N_2O and the major process responsible for its production in the SWP. This is achieved by fulfilling the following specific objectives.

1. Measure the dual isotopic signatures of N_2O to make available the first such data for these regions.

2. Use the oxygen isotope variations of DO and oceanic water with that of N_2O in order to differentiate between N_2O production mechanisms.

3. Determine the intramolecular distribution of N_2O to confirm the N_2O production pathways in these waters.

4. Use isotope and isotopomeric signatures for understanding the role of the study regions in the global budget of N_2O.

5. Apply incubations experiments to elucidate the mechanisms of N_2O production at selected stations and hence to confirm the inferred results from isotopes.

5.3. Analytical Methods

To study the processes in detail the N_2O isotopes and isotopomers were analysed. $\delta^{15}N_{bulk}$-N_2O, $\delta^{18}O$-N_2O, $\delta^{15}N_{\alpha}$, $\delta^{15}N_{\beta}$, SP, $\delta^{18}O$-$O_{2,\ aqueous}$ and $\delta^{18}O_{H2O}$ were measured. More details on the study area, sampling and analytical methods are provided in sections 2.3, 2.4 and 2.5 respectively.

5.4. Results and Discussions

5.4.1. The Dual Isotopic Signatures of N_2O- $\delta^{15}N$-N_2O and $\delta^{18}O$-N_2O

For a better understanding of the discussions in this chapter, the water column properties of this regions are given below in Figure 5.2 and 3. More detailed information about the study regions of the Geotraces Bloom II and Mooring stations see Chapter 2, Section 2.3.1. Detailed water column properties are presented in Chapter 2 Section 2.3.1.

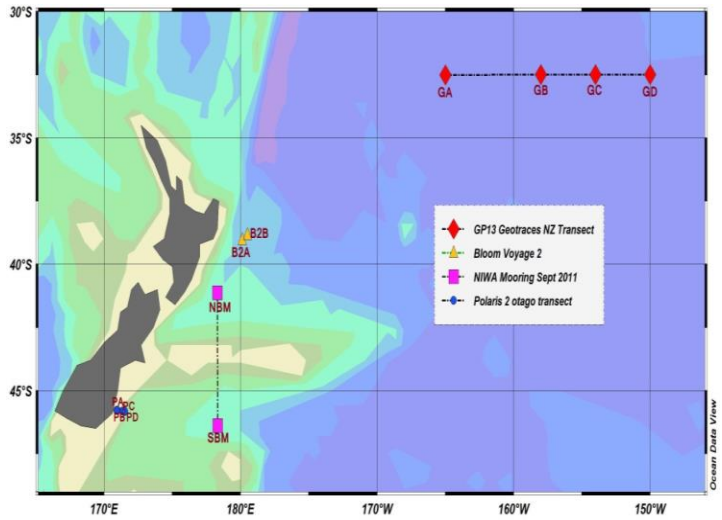

Figure 5.2: The sampling stations for the present study in SWP.

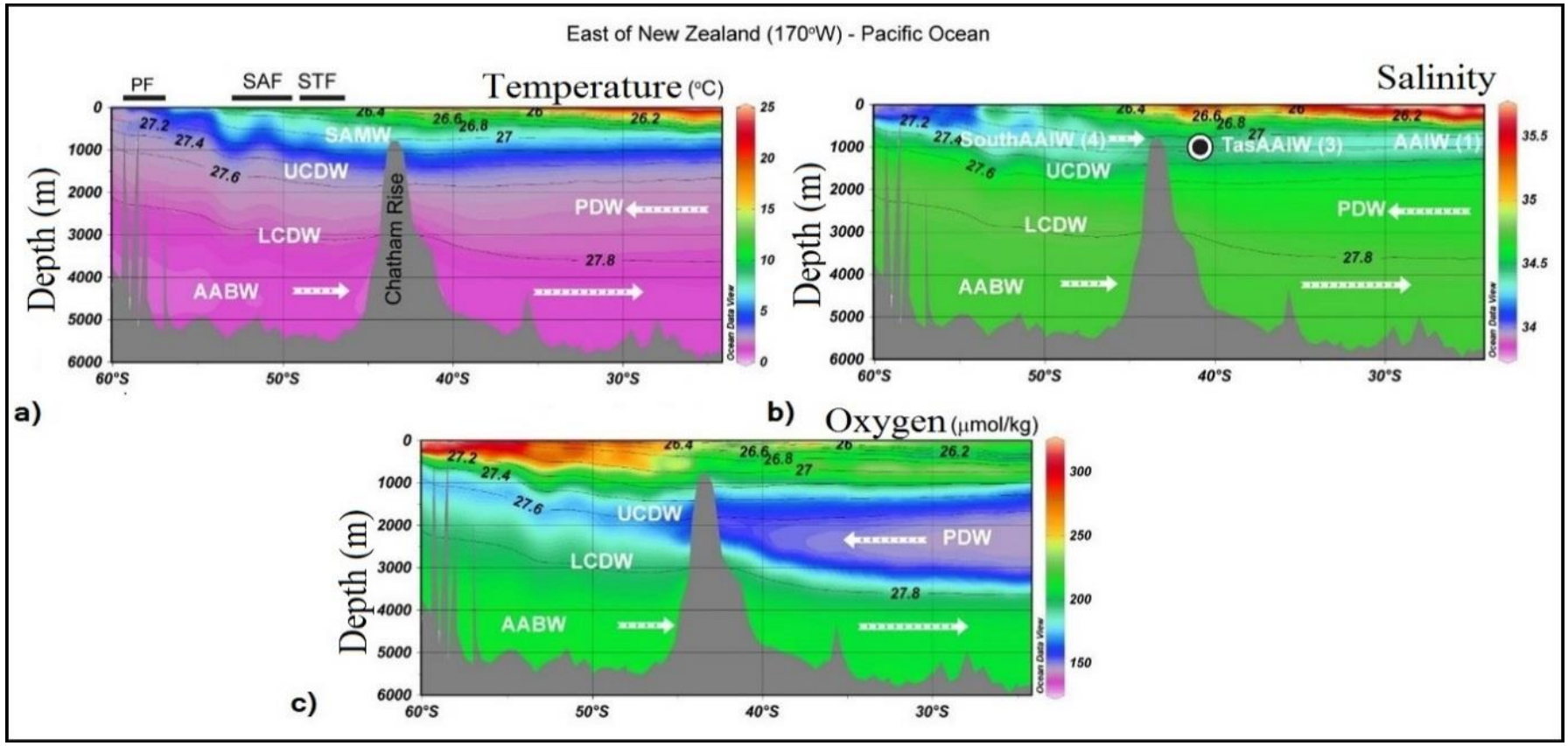

Figure 5.3: a) Temperature, b) Salinity and c) Dissolved oxygen characteristics for different water masses for the entire regions East of New Zealand, adopted from WOCE survey data.

5.4.1.1 Geotraces Transect:

The dual isotopes of N_2O measured for the Geotraces transect are shown in Figure 5.4 a and b. Table 5.2 summarises the stable isotopes of N_2O-$\delta^{15}N_{bulk}$ and $\delta^{18}O$ for different water masses of the entire Geotraces transect, and Table 5.3 shows that for each station. These figures show that both $\delta^{15}N_{bulk}$ and $\delta^{18}O$ of N_2O follow similar trends with density. $\delta^{15}N_{bulk}$ and $\delta^{18}O$ values are lower in the upper 500 m layer with the minimum at 300-500 m depth; while higher values were observed at a depth below 500 m with the highest values at a depth of 2500-3000 m. These results were comparable to the very first results for South Pacific Ocean at 23º44' S and 153º 37' W as shown in Table 5.1 (Kim and Craig., 1990). Kim and Craig's results are the only available data for comparison closer to the present study regions. Even though these results show same variations down the water column to the Kim and Craig results, the values were lower than their results at each depth. However, these variations in the isotope values were seen in their own results at different locations. Moreover, Yoshida *et al.* observed a range of $\delta^{15}N_{bulk}$ values from 3.7 to 8.6 ‰ in the in the surface waters of North Pacific Ocean in 1988.

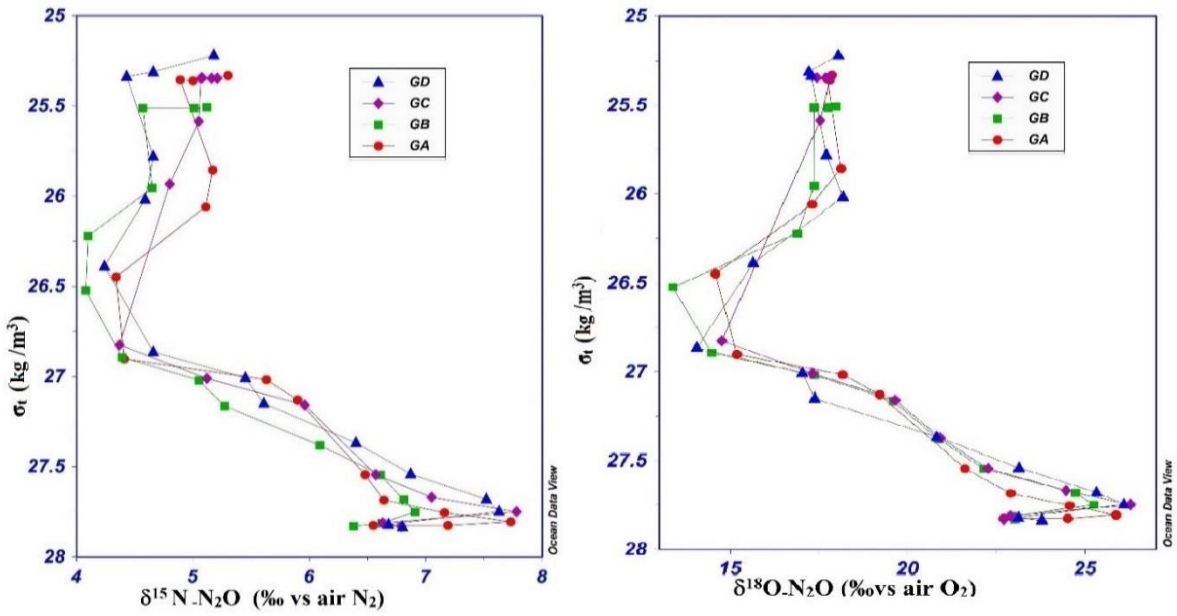

Figure 5.4: Water column variations of a) N_2O- $\delta^{15}N_{bulk}$ and b) N_2O- $\delta^{18}O$ of Geotraces stations GA, GB, GC and GD.

Table 5.1: Variations of $\delta^{15}N_{bulk}$ and $\delta^{18}O$- N_2O (Kim and Craig., 1990, in South Pacific).

$\delta^{15}N_{bulk}$(‰ *vs* air N_2)	$\delta^{18}O$(‰ *vs* air O_2)	Depth (m)
6.7	18	300
6.4	17.9	400
6.4	18.2	575
7.6	21.9	800
8.9	26.5	2400
8.7	25.2	3750
8.4	24.2	4900

The average $\delta^{15}N_{bulk}$ values in the surface mixed layer were 5.2 ± 0.1 ‰, which increased up to a maximum of 7.5 ± 0.4 ‰ at a depth of 2500-3000 m. However, the water column changes in $\delta^{15}N_{bulk}$ values with depth were much less and uniform for all stations. Mean atmospheric $\delta^{15}N_{bulk}$ and $\delta^{18}O$ of N_2O in the clean tropospheric air are 6.72 ± 0.12 ‰ and 20.60 ± 0.21 ‰ respectively (Kaiser *et al*., 2003). The $\delta^{15}N_{bulk}$ values depleted in the surface, while enriched below the upper thermocline waters with respect to atmospheric mean values. Similar observations of isotope depletion in highly oxygenated shallow waters and enrichment for deeper, less oxygenated waters were reported previously (Yoshida *et al*., 1984; Kim and Craig., 1990). The observed depletions in the surface shallow waters were pronounced at a depth of 300-500 m with an average of 4.3 ± 0.1 ‰. Average $\delta^{18}O$ of N_2O in the surface waters was 17.9 ± 0.2 ‰ and increased with depth up to a maximum of 25.9 ± 0.5 ‰ at 2500-3000 m. The changes in $\delta^{18}O$ values with depth from that of the surface were more pronounced than for $\delta^{15}N_{bulk}$ and were uniform for all stations. The results indicate that the $\delta^{18}O$ values are depleted in the surface with respect to the atmospheric values and were moderately enriched at the deeper oceanic regions. The depletions in $\delta^{18}O$ with respect to the atmospheric equilibrium values were higher at a depth of 300-500 m with an average value of 14.6 ± 0.9 ‰.

$\delta^{18}O$ - N_2O shows similar characteristics and trends to that of $\delta^{15}N_{bulk}$ of N_2O in the upper 500 m, but the magnitude of the enrichments are quite high (5 - 9 ‰) as compared to latter in the bottom waters. Usually, enrichments are associated with isotopic fractionations from denitrification as stated earlier. Nevertheless, some studies (Kim and Craig., 1990; Kim and Craig., 1993; Dore *et al*., 1998) also reported an increase in $\delta^{18}O$ with depth to higher values in oxygenated oceanic regions where denitrification was not so important. It is also reported that the larger increase in $\delta^{18}O$ with depth to greater than 15 ‰ is an indication of

denitrification, but N_2O depleted in ^{15}N with regards to atmospheric values are not expected in this case (Ostrom *et al*., 2000).

Table 5.2: The mean $\delta^{15}N_{bulk}$- N_2O and $\delta^{18}O$-N_2O and isotopomer values for all stations of the Geotraces transect

Water Masses	$\delta^{15}N_{bulk}$ -N_2O (‰ *vs* air N_2)	$\delta^{18}O$-N_2O (‰-*vs* air O_2)	$\delta^{15}N\alpha$ (‰)	$\delta^{15}N_{ß}$ (‰)	SP (‰)	σt (kg/m^3)
Surface ML	5.2	17.7	14.2	-4.2	13.3	25.5
Upper thermocline	4.4	16.0	11.9	-2.8	9.7	26.1
AAIW	5.5	18.2	13.3	-3.1	11.3	27.0
CPDW	7.0	23.9	17.4	-3.5	15.9	27.7

Table 5.3: The mean $\delta^{15}N_{bulk}$- N_2O and $\delta^{18}O$-N_2O and isotopomer values for the different water masses obtained for the Geotraces stations GA,GB, GC and GD.

Station	Water Mass	$\delta^{15}N_{bulk}$ -N_2O (‰ *vs* air N_2)	$\delta^{18}O$-N_2O (‰-*vs* air O_2)	$\delta^{15}N\alpha$ (‰)	$\delta^{15}N_{ß}$ (‰)	SP (‰)	σt (kg/m^3)
GA	Surface Mixed Layer	5.3	17.9	13.3	-3.1	11.4	25.5
	Below mixed layer	4.3	15.9	12.4	-3.0	10.3	26.3
	AAIW	5.8	18.7	14.8	-4.1	13.9	27.0
	CPDW	7.1	24.1	16.9	-2.8	14.7	27.8
G B	Surface Mixed Layer	4.7	17.6	14.8	-5.0	14.7	25.6
	Below mixed layer	4.1	15.1	11.6	-3.4	9.8	26.4
	AAIW	5.2	18.5	12.2	-2.7	9.8	27.0
	CPDW	6.7	23.6	17.7	-4.4	17.0	27.7
GC	Surface Mixed Layer	5.1	17.7	15.1	-4.8	14.9	25.3
	Below mixed layer	4.9	15.9	11.6	-1.8	8.4	25.8
	AAIW	5.5	18.5	13.2	-2.9	11.0	26.8
	CPDW	7.0	23.7	17.2	-3.3	15.4	27.7
GD	Surface Mixed Layer	4.7	17.6	13.5	-4.0	12.4	25.4
	Below mixed layer	4.4	16.9	12.0	-3.2	10.2	26.2
	AAIW	5.5	17.2	13.1	-2.6	10.7	27.0
	CPDW	7.1	24.3	17.9	-3.6	16.4	27.7

N_2O dual isotope ratios are also presented for each water mass in Table 5.3 (mean values for the whole transect) and Table 5.4 (for each station). Similar to the variations in [N_2O] (Chapter 3), the isotope ratios also showed an increase in values from the surface to bottom water masses. The lowest values were seen in the surface waters, STSW. However, the values increased below the surface mixed layer as a reflection of the complex mechanisms that produced N_2O. At the bottom CPDW, more [N_2O] were present and highest $\delta^{15}N_{bulk}$ signatures were also seen. The more the [N_2O], $\delta^{15}N_{bulk}$ and $\delta^{18}O$- N_2O also increased. AAIW showed values of dual isotopes in between that of surface waters and CPDW.

5.4.1.2. Bloom and Mooring Transects

The water column profiles of $\delta^{15}N_{bulk}$-N_2O and $\delta^{18}O$-N_2O for Bloom II voyage and Mooring stations are shown in Figure 5.5 a and b. These figures indicate that the N_2O dual isotopes from this SWP waters closely resembles that of Geotraces transect (Figure 5.4, Table 5.2 and 5.3). $\delta^{15}N_{bulk}$-N_2O and $\delta^{18}O$-N_2O showed similar variations down the water column. Here also both the $\delta^{15}N_{bulk}$ and $\delta^{18}O$ of N_2O values were lowest in the surface waters down to 500 m, with the minimum at 300-500 m depth. The higher values of the isotope pairs were observed below 500 m with the highest at 2500-3000 m for both the transects.

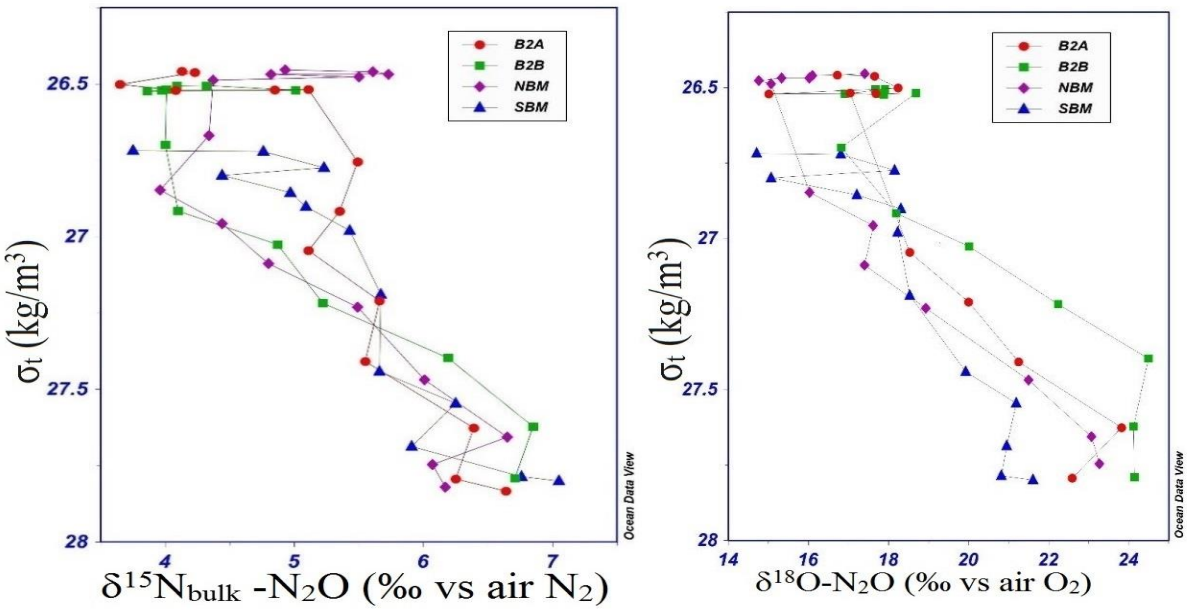

Figure 5.5 : Water column variations of a) N_2O- $\delta^{15}N_{bulk}$ and b) N_2O- $\delta^{18}O$ of Bloom II stations B_2A, B_2B and Mooring stations NBM, SBM.

The average values measured for N_2O dual isotopes at different stations are summarised below in Table 5.4. The average surface $\delta^{15}N_{bulk}$-N_2O values were 4.4 ± 0.1 ‰, followed by an increase in the bottom waters with a maximum of 6.6 ± 0.3 ‰ at a depth of 2500-3000 m for the subtropical waters of Bloom II and Mooring. $\delta^{15}N_{bulk}$-N_2O ranged from 4.5 ‰ at the surface and 7.1 ‰ at the bottom for subantarctic waters of Mooring transect (SBM). The variations of $\delta^{15}N_{bulk}$-N_2O from the surface to the bottom waters were much less and uniform for all stations. $\delta^{15}N_{bulk}$ values are depleted in the surface, while slightly enriched at the bottom waters with that of the atmospheric imprints. The $\delta^{15}N_{bulk}$ was depleted in the surface with respect to the atmospheric equilibrium values, and maximum depletions were seen at a depth of 150-500 m with an average of 4.0 ± 0.1‰. Average $\delta^{18}O$ - N_2O in the surface were 17.3 ± 0.5‰ which increased with depth up to a maximum of 23.9 ± 0.6 ‰ between 1500-3000 m in the Subtropical waters. In the s

ubantarctic waters the surface $\delta^{18}O$ - N_2O was 16.6 ‰ followed by an enrichment to the bottom with a maximum of 21.6 ‰. However, the changes in $\delta^{18}O$ values with depth from that of the surface values were more pronounced than that of $\delta^{15}N_{bulk}$-N_2O and were uniform for all stations. It is evident from the above N_2O dual isotopes that, there exists an isotopic minimum layer at a depth of 150-500 m.

N_2O dual isotope ratios for each water mass are also presented (Table 5.4). The variations in [N_2O] (Chapter 3) and that of the isotopes were similar and showed an increase in values from the surface to bottom water masses. The lowest values were seen in the surface waters, STSW. However, the values increased below the surface layer which will give an idea of the complex N_2O production mechanism. At the bottom CPDW, with higher [N_2O], $\delta^{15}N_{bulk}$ and $\delta^{18}O$- N_2O values were also highest. AAIW dual isotope signatures were in between that of surface waters and CPDW.

Table 5.4: The mean $\delta^{15}N_{bulk}$- N_2O and $\delta^{18}O$-N_2O and isotopomer values for the different water masses obtained for the NBM,SBM, B_2A and B_2B stations.

Station	Water Mass	$\delta^{15}N_{bulk}$ -N_2O (‰ vs air N_2)	$\delta^{18}O$-N_2O (‰-vs air O_2)	$\delta^{15}N\alpha$ (‰)	$\delta^{15}N$ ß (‰)	SP (‰)	σt (Kg/m^3)
NBM	Surface Mixed Layer	5.0	16.9	16.5	-6.4	17.8	26.47
	Below mixed layer	4.4	14.9	13.9	-5.2	14.0	26.58
	AAIW	5.1	17.8	14.2	-4.6	13.8	27.02
	CPDW	6.1	20.8	17.6	-5.2	17.7	27.58
SBM	Surface Mixed Layer	4.5	16.6	15.5	-6.9	17.4	26.75
	Below mixed layer	5.0	16.9	15.0	-6.1	16.0	26.80
	AAIW	5.4	17.9	16.9	-6.1	17.9	27.02
	CPDW	6.3	20.3	19.3	-6.4	20.6	27.65
B_2A	Surface Mixed Layer	4.2	17.8	14.3	-6.3	15.5	26.49
	Below mixed layer	5.5	17.0	19.9	-8.9	23.8	26.76
	AAIW	5.4	18.5	18.8	-8.1	21.9	27.06
	CPDW	6.2	21.9	20.5	-7.8	23.2	27.67
B_2B	Surface Mixed Layer	4.3	17.6	16.6	-8.1	19.6	26.52
	Below mixed layer	4.0	18.2	17.6	-9.6	22.1	26.61
	AAIW	5.1	18.7	15.0	-4.8	14.8	27.12
	CPDW	6.6	23.7	20.6	-7.2	22.5	27.66

5.4.1.3. Otago Continental Shelf transect

Table 5.5: The mean $\delta^{15}N_{bulk}$- N_2O and $\delta^{18}O$-N_2O values for the Otago continental shelf transect obtained for the three different sampling periods.

Water Mass	PA	PB	PC	PD	PA	PB	PC	PD
	$\delta^{15}N_{bulk}$- N_2O (‰ vs air N_2)				$\delta^{18}O$-N_2O (‰ vs air O_2)			
Polaris-September 2011								
Neritic	5.5				18.2			
MSTW		5.6				17.9		
SASW			5.2				17.6	
AAIW			5.5	5.7				17.4
Polaris-May 2012								
Neritic								
MSTW	5.2	4.8			19	17.7		
SASW			5.5	5.6			18.2	19.5
Polaris-November 2012								
Neritic	5.9	5.4			19.7	19.2		
MSTW			6.4				19.8	
SASW				5.2				18.2

The dual isotopic signatures of N_2O for Otago Continental shelf transect (For sampling stations and locations refer Chapter 2, Section 2.3.1. Detailed water column properties are presented in Chapter 2 Section 2.3.1) were measured during three different periods September 2011, May 2012 and November 2012 respectively. The average water mass values of N_2O dual isotopes for each station during different periods are shown in Table 5.5. These results show that both $\delta^{15}N_{bulk}$ and $\delta^{18}O$-N_2O values followed similar trends along the water column irrespective of the seasons and did not show much variation either with depth or locations. The isotope signatures varied much less from time to time and surface to the bottom (Table 5.5).

5.4.1.4. The dual isotopes and the N_2O production pathways in SWP

Results from T-S and potential density analysis showed that there is little potential for mixing between the water masses (Chapter 3, section 3.6). To understand the effect of mixing on N_2O production /exchange in these water masses mixing diagrams (a plot of isotope ratios versus the reciprocal N_2O concentration (1/ [N_2O])) were constructed (Pataki *et al*., 2003; Toyoda *et al*., 2002; Popp *et al*., 2002; Yamagishi *et al*., 2007). Mixing diagrams for the study regions are shown in Figure 5.6 for both $\delta^{15}N_{bulk}$ -N_2O and $\delta^{18}O$-N_2O.

From the Figure 5.6, it is notable that both the $\delta^{15}N_{bulk}$ and $\delta^{18}O$ follow a similar trend and they separate into two groups, which do not follow a linear relationship. The upper mixed layer and lower isotopically enriched regions in the graph can be seen as two separate groups and within the group, it showed more or less constant isotopic ratios. These results support our findings that mixing-related fractionations are insignificant.

Otago continental shelf transect figures 5.6 (e and f) shows a notable difference from the other stations. The graph for each species is plotted taking results for the whole seasons. At all stations irrespective of the seasons especially in the neritic mixing regions both the isotopes had a similar trend. Instead of separating into two groups as observed in previous transects here they mostly stayed in one group. While from the two figures (Fig 5.6 e and f) it is also notable that the isotopes separated into two groups which do not follow a linear relationship for subantarctic water masses represented by PC and PD (September 2011). For PC and PD, the upper mixed layer and lower isotopically enriched regions can be seen from the graph as two separate groups, and within the group, it showed more or less constant isotopic ratios.

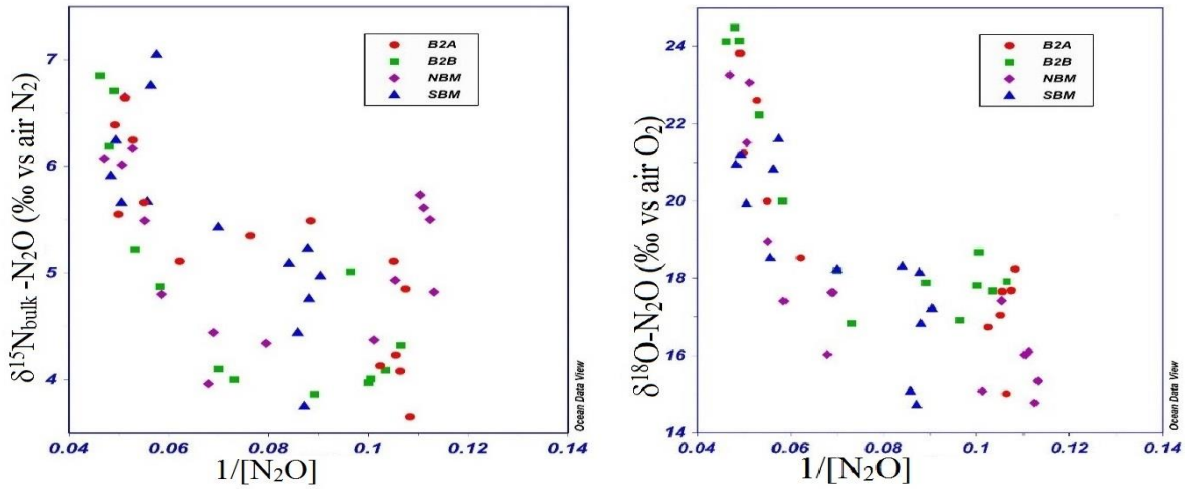

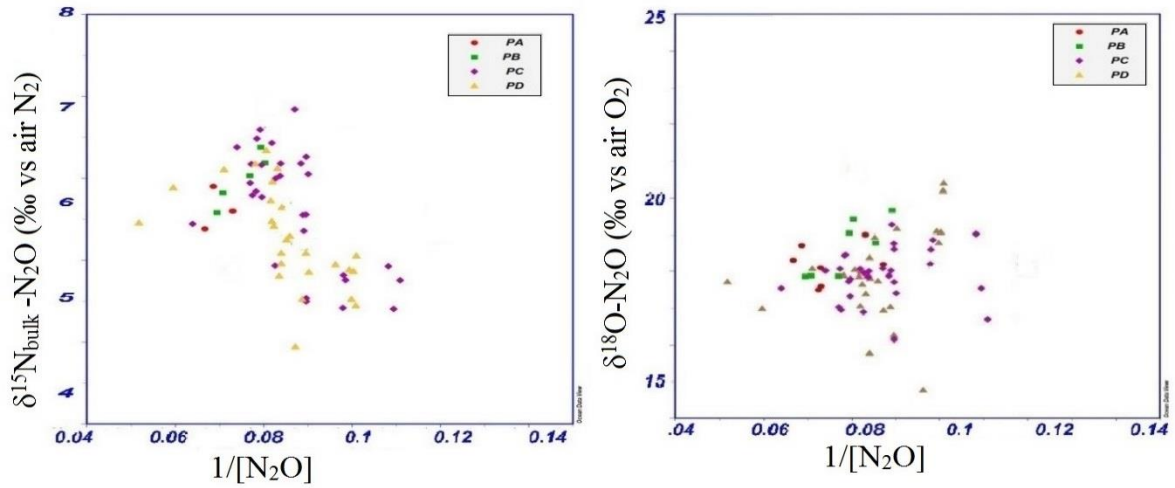

Figure 5.6: $\delta^{15}N_{bulk}$ (left) and $\delta^{18}O$-N_2O (right) variations with 1/[N_2O] for Geotraces stations (a and b-top). Bloom II stations (B_2A, B_2B) and Mooring stations (NBM, SBM) (c and d- middle) and for Otago Continental Shelf transect (e and f- bottom).

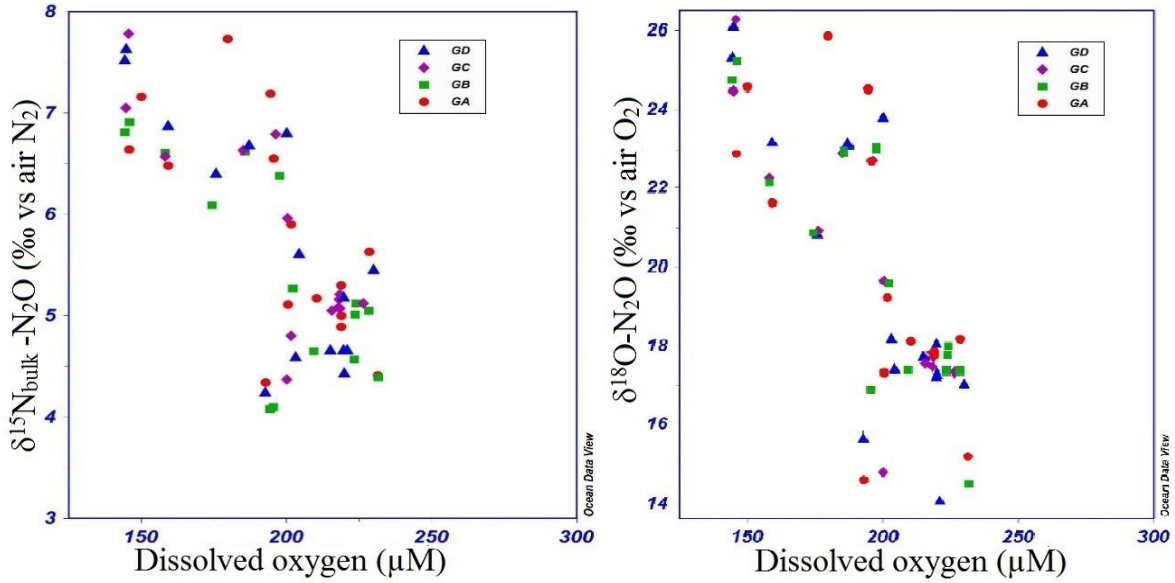

Figure 5.7: (a) $\delta^{15}N_{bulk}$ and (b) $\delta^{18}O$-N_2O variations with dissolved oxygen for Geotraces stations GA, GB, GC and GD with depth.

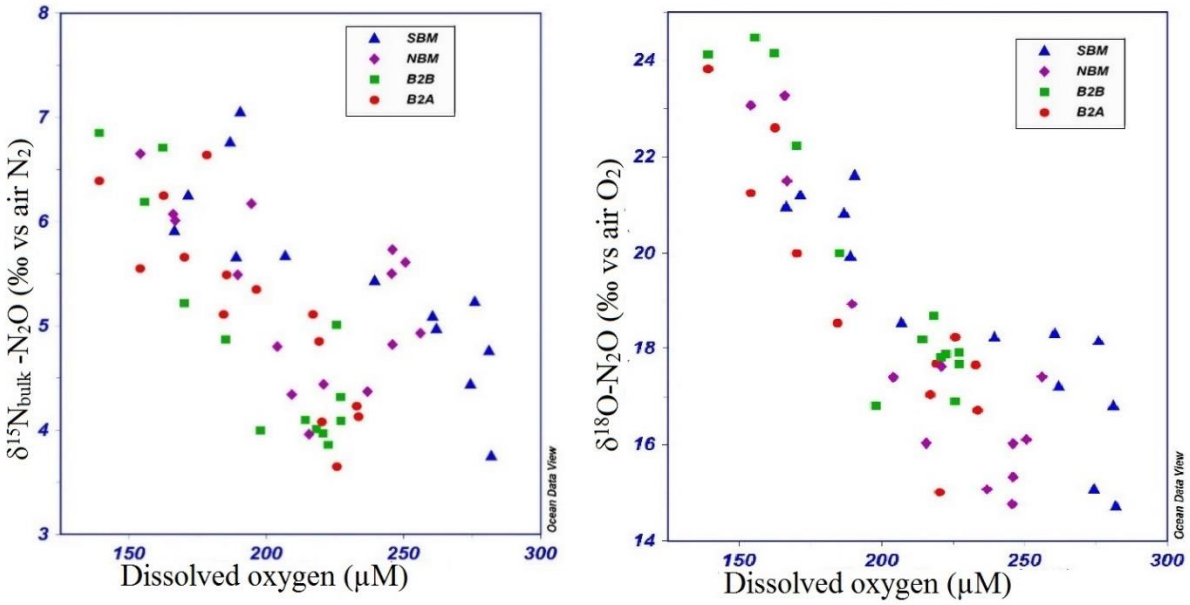

Figure 5.8: (a) $\delta^{15}N_{bulk}$ and (b) $\delta^{18}O$-N_2O variations with dissolved oxygen for Bloom II stations B_2A, B_2B and Mooring stations NBM, SBM.

$\delta^{15}N_{Bulk}$-N_2O and $\delta^{18}O$-N_2O variations with DO were plotted (Figure 5.7 and 5.8). These figures show the isotope ratios vary with DO variations. Therefore it can be concluded that the existing redox conditions would be the reason for the prevalence of two different isotope groups in these water masses. On the basis of similar observations in 1997, Yoshinari *et al.* suggested the existence of these isotope groups are due to the different redox conditions. Nevertheless, the redox conditions for the present study regions are not as far apart (from anoxic to oxic) as that observed by Yoshinari. The figures also indicate that the isotopically enriched N_2O is present in the oxygen-poor waters. The absence of a wide range of N_2O dual isotopic signatures suggests the absence of multiple processes in those regions as a production mechanism (Yoshinari *et al*., 1997). Therefore the above figures suggest that the processes responsible for N_2O production should be the same. Both the isotopes of N_2O varied considerably less down the water column below and above the isotopic minimum which again strengthens the concept of single process as the responsible mechanism for the production.

The $\delta^{15}N_{Bulk}$-N_2O and $\delta^{18}O$-N_2O variations with DO were plotted (Figure 5.9) for the Otago Continental Shelf transect. DO data were not available for the two sampling periods for which these parameters were studied with regards to [nitrate]. A similar trend to that of the mixing diagrams was obtained without much variation in neritic stations while that varied the deep

stations of PC and PD. In some cases, the sampling was not conducted for the entire water column, and the variations were absent in PC and PD.

Moreover, from all other parameterizations from previous chapters, it is found that denitrification is an unlikely factor in these oxygenated waters. Even though an increase of $\delta^{15}N_{bulk}$ is reported as an indication of denitrification, here the small increase in $\delta^{15}N_{bulk}$ and larger increase of $\delta^{18}O$ with depth is still less than that expected for denitrification.

So having established that denitrification is not a significant source of N_2O, next is to investigate more closely the nitrification processes taking place in these water columns. From the Figure 5.12 and Chapter 1 Section 1.4.1) it is clear that nitrification produces N_2O mainly through intermediate compounds NH_2OH or NO or coupled nitrification-denitrification (Kim and Craig., 1990; Naqvi and Noronha., 1991; Naqvi *et al*., 1998). From understanding the sources of O in the N_2O it is possible to derive the respective mechanisms responsible for its production through various biochemical pathways of nitrification (Ostrom *et al*., 2000).

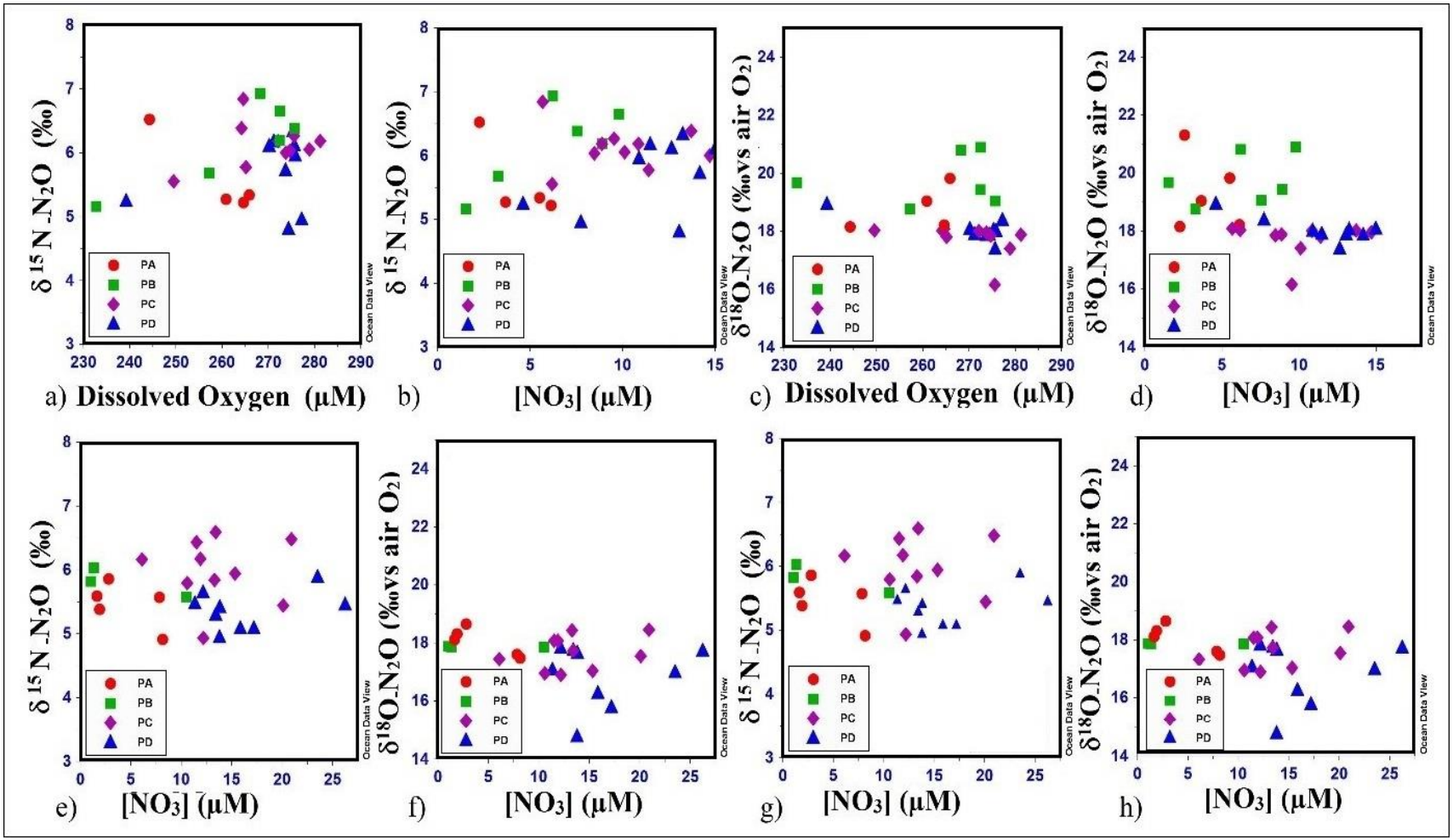

Figure 5.9: The variations of dual isotopes a), b), e), g) $\delta^{15}N_{bulk}$ and c), d), f), h) $\delta^{18}O$ with nutrient concentrations and dissolved oxygen for the four Otago stations during three seasons. (Top four figures for November 2012. In the bottom row e and f for September 2011; g) and h) for May 2012).

5.4.2. $\delta^{18}O$ of Dissolved Oxygen ($\delta^{18}O$-$O_{2,\ aqueous}$ and Water oxygen ($\delta^{18}O$-H_2O)

5.4.2.1. $\delta^{18}O$ - Geotraces , Mooring and Bloom stations

$\delta^{18}O$ of DO ($O_{2,\ aqueous}$) and H_2O was measured for all four stations of the Geotraces transect, for the two stations of Mooring transect and all four stations of Otago Continental shelf transect sampled during September 2011. The measurements were not made for the Bloom II transect and the other two samplings of Otago continental shelf transect (May and November 2012). Bloom II transect had similar characteristics to other SWP stations having similar water mass properties with respect to N_2O distributions, variations, flux and its dual isotope signatures.

The measured $\delta^{18}O$- $O_{2,\ aqueous}$ and $\delta^{18}O$-H_2O for the four stations of the Geotraces transect are shown in Figure 5.10 a and b respectively. These results are comparable to the previous studies done by Kroopnick and Craig (1976), Kim and Craig (1990).

The average water column oxygen isotope ($\delta^{18}O$ of N_2O ,$\delta^{18}O$- $O_{2,\ aqueous}$, $\delta^{18}O$-H_2O and $\Delta^{18}O$) values for different water masses are summarised in Table 5.6. The $\delta^{18}O$- $O_{2,\ aqueous}$ were minimum at the surface with an average of 23.6 ± 0.3 ‰. $\delta^{18}O$ increased down the water column with a mean value of 30.2 ± 0.6 ‰. For all stations, $\delta^{18}O$ of O_2 varied between 23.3 ‰ and 30.8 ‰. The surface isotope values reflect atmospheric equilibrium values ($\delta^{18}O_{vsmow}$ = 23.5 ‰) after accounting for the isotope fractionation during the sea-to-air exchange (Kroopnick and Craig., 1972; Benson and Krause., 1980; Barth *et al*., 2004). The isotopically depleted waters with regards to $\delta^{18}O$ of O_2 (Figure 5.13 a) at the chlorophyll maximum (Chapter 3) are due to the presence of isotopically depleted oxygen released during photosynthesis (Kroopnick and Craig., 1976; Bender and Grande., 1987; Kim and Craig., 1990; Quay *et al*., 1993). At the same time, $\delta^{18}O$ of O_2 increased to the bottom from a depth where productivity is supposed to be limited, and respiration will be the major biological process. This is due to the fact that respiratory dissolved oxygen consumption will result in heavy isotope enrichment (Bender. M. L., 1990; Quay *et al*., 1993). The $\delta^{18}O$ of H_2O in the Geotraces transect is shown in Figure 5.13 b, and all stations exhibited a similar trend in the water column. Here the values were ranged between -0.9 ‰ to 0.8 ‰ along the water column. The maximum values were

observed in the surface with an average of 0.6 ± 0.2 ‰ while that in the bottom waters were minimum with an average of -0.2 ± 0.3 ‰. The results obtained are closer to the results obtained for previously measured values for North and Equatorial Pacific waters (Ostrom *et al*., 2000).

Table 5.6: The average water column oxygen isotope values ($\delta^{18}O$ of N_2O ,$\delta^{18}O$- $O_{2,\ aqueous}$, $\delta^{18}O$-H_2O and $\Delta^{18}O$) for different water masses for the different study regions

Stations	Water masses	$\delta^{18}O$-N_2O, (‰ vsmow)	$\delta^{18}O$-$O_{2,\ aqueous}$ (‰ vsmow)	$\delta^{18}O$-H_2O (‰ vsmow)	$\Delta^{18}O$ (‰)
Geotraces	ML	40.6	23.6	0.6	18.0
	Below ML	38.9	26.4	0.5	12.1
	AAIW	41.5	27.9	0.0	15.2
	CPDW	46.9	29.6	-0.1	18.9
NBM	ML	39.9	24.3	0.6	15.7
	Below ML	39.1	26.6	0.8	12.5
	AAIW	40.6	29.7	0.5	15.0
	CPDW	45.8	30.0	0.1	17.5
SBM	ML	40.3	24.2	0.2	15.6
	Below ML	12.4	26.8	0.2	11.4
	AAIW	42.5	28.2	0.5	14.9
	CPDW	45.0	30.3	0.3	16.9

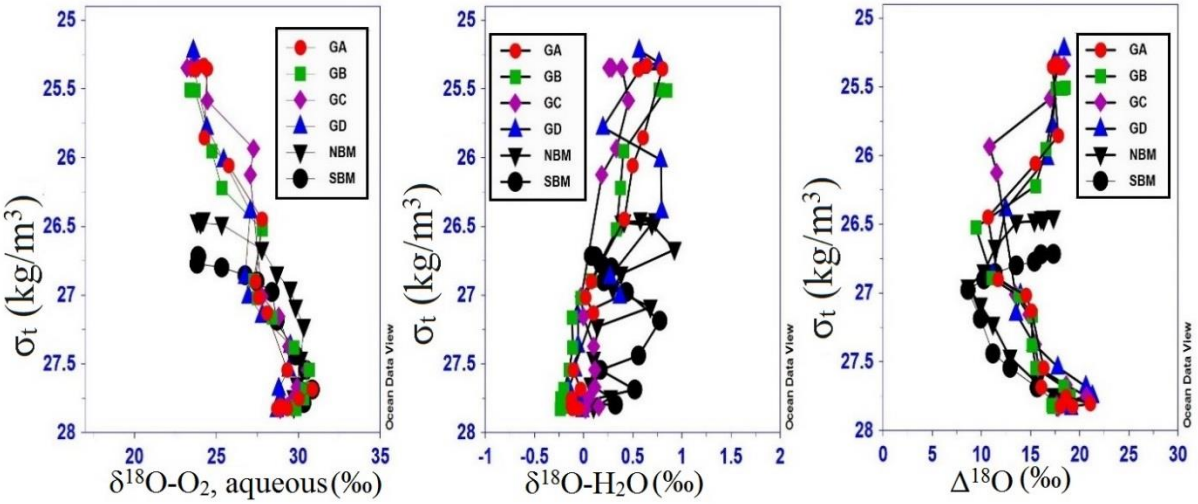

Figure 5.10: $\delta^{18}O$-O_2, aqueous and b) $\delta^{18}O$-H_2O for Geotraces stations and the two Mooring stations NBM and SBM. All $\delta^{18}O$ values are in VSMOW.

A similar set of results for $\delta^{18}O$ of $O_{2,\ aqueous}$ and H_2O of two mooring stations (NBM and SBM) are given in Figure 5.10 and Table 5.6 respectively. The observed values can be read as more or less similar to that obtained for the Geotraces transect and follow a similar trend. The $\delta^{18}O$ of $O_{2,\ aqueous}$ values observed in minimum at the surface and maximum at the bottom oxygen minimum layers for the two stations NBM and SBM. The average values are 24.2 ± 0.1 ‰, 30.2 ± 0.1 ‰ and 23.9 ± 0.01 ‰, 30.6 ± 0.3 ‰ for NBM and SBM in the surface and bottom layers. Here also the $\delta^{18}O$ of $O_{2,\ aqueous}$ were slightly depleted in the surface productive regions and enriched in the bottom layers. $\delta^{18}O$ of H_2O was similar to that of Geotraces for the NBM while it was slightly lower in the SBM in surface SASW as compared to the STSW of NBM. This differences mainly arise due to the enrichment in the NBM as compared to the SBM due to the surface evaporation as a result of higher sea surface temperature in this regions. Similar to the Geotraces results, Mooring transect showed $\delta^{18}O$ values very close 0 ‰ and varied by less than 1 ‰ for the entire water column for H_2O.

Based on the above results on $\delta^{18}O$ of $O_{2,\ aqueous}$ and H_2O and $\delta^{18}O$ of N_2O (section 5.4.1, Table 5.6) more detailed conclusion on the nitrification can be derived as follows. Understanding the source of O in the N_2O is the key to the question since the first O atom added to NH_4^+ during the nitrification process comes from the dissolved oxygen ($\delta^{18}O$ of $O_{2,\ aqueous}$). Both NH_2OH and NO (pathway 1 and 2) are formed during this step, followed by addition of another O atom from water ($\delta^{18}O$ of H_2O) which results in the formation of NO_2^- (Figure 5.1). So during pathway 3 of nitrification (nitrifier denitrification) isotopically depleted N_2O is formed. However this pathway 3 is an unlikely mechanism for production in oxygenated waters. So in the bottom waters of this transect having enrichments in the dual isotopic signatures either pathway 1 or 2 of nitrification is the only possible mechanism for N_2O production.

In all these study regions an enrichment in both the $\delta^{18}O$ isotopes was seen below 500 m and down the water column to the bottom. The enrichment in $\delta^{15}N$ of N_2O was not so pronounced, however, that in $\delta^{18}O$ were significant. Water $\delta^{18}O$ values were close to zero throughout the study regions and did not vary much either with depth or location. The $\delta^{18}O$-H_2O trend (Figure 5.10) does not show any significant correlations with dual isotope signatures of N_2O. The observed enrichment and associated positive shifts in the $\delta^{18}O$ signatures for both the species with depth shows that the source of oxygen in the N_2O is dissolved oxygen and not water (except at 200- 500 m).

So it can be inferred that the production of N_2O at these depths is mainly from NH_2OH/NO. The enrichment in $\delta^{18}O$ of N_2O can be justified as follows. During nitrification when the first two intermediates NH_2OH and NO formed from pathway 1 and 2 respectively, they will be oxidized to NO_2^-. So the residual NH_2OH/NO will be highly enriched, and these isotopic signals will be transferred to the N_2O if it is produced from either of these two compounds. Or it can also be explained that the formation of NH_2OH through pathway 1 of nitrification proceeds through three steps

$$NH_3 + O_2 + H^+ + 2e \rightarrow NH_2OH + H_2O \qquad \textbf{(a)}$$

$$NH_2OH + O_2 \rightarrow HNO_2 + H_2O \qquad \textbf{(b)}$$

$$2NH_2OH + O_2 \rightarrow N_2O + 3H_2O \qquad \text{©}$$

After the oxidation of NH_4^+ to NH_2OH by dissolved oxygen, it is carried further through two steps. One is the formation of N_2O as a by-product through the oxidation of hydroxyl ami©(c); while the second pathway is the oxidation of the NH_2OH which will lead to the formation of nitrite from which N_2O will be formed during nitrification (b). The second step (b) is the dominant production process. N_2O with the enriched isotopes in the bottom waters can be due to two reasons. One is microbial denitrification as a consequence of reduction processes taking place in the sinking organic particulates. The second is the more plausible mechanism in oxic waters and is the NH_2OH oxidation of nitrification (step b). Fractionation occurs during this microbial process which will leave the pool of NH_2OH enriched with heavy isotopes. So when deep water N_2O is derived from this NH_2OH that will produce isotope enrichment to some extent in the resulting product (Kim and Craig., 1990; Ostrom *et al*., 2000).

This mechanism of NH_2OH oxidation (step b) can be used to justify the difference between enrichment of $\delta^{18}O$ of N_2O and $\delta^{18}O$ of O_2, since it is more pronounced in the former because of the same enrichments happening for NH_2OH/NO during the NO_2^- formation (step c). So it can be stated that throughout the study regions below the 200-500 m layer N_2O is formed from NH_2OH/NO (pathway 1 or 2) of nitrification while in the upper euphotic layer up to 200-500 m pathway 3 (nitrifier denitrification) can also be a possible process of formation of N_2O. This mechanistic explanation for nitrification can be further supported using $\Delta^{18}O$ data which is a measure of $\delta^{18}O$ of N_2O - $\delta^{18}O$ of O_2 (Figure 5.10). $\Delta^{18}O$ is more useful to distinguish between different processes since the $\delta^{18}O$ of N_2O formed from NH_2OH/NO will have contributions

from dissolved oxygen alone, and that formed from NO_2^- will have contributions from both $\delta^{18}O$ of O_2 and H_2O.

Even though there exists a close relationship between the two isotopic signatures $\delta^{18}O$ of N_2O - $\delta^{18}O$ of O_2 (Figure 5.10. c), there were some significant variations in $\Delta^{18}O$ values which are not consistent with the depth for all Southwest Pacific stations of Geotraces transect and Moorings. $\delta^{18}O$ varied between 18.6 ‰ and 21.3 ‰ with depth. At 200-500 m for Geotraces, NBM and SBM station, it was found that $\Delta^{18}O$ values were very low. From top to bottom along the water column, $\Delta^{18}O$ values varied with more than 9 ‰ difference to the minimum values observed at these depths. These differences were 8.6, 10.4, 9.6, 9.9, 10.2 respectively for NBM and the four Geotraces stations in the order. The similar kinds of results were obtained for oligotrophic waters of North Pacific gyre ALOHA station between depths 350-500 (Ostrom *et al*., 2000). Lower $\Delta^{18}O$ values between 300 and 500 m compared to the upper and lower layers shows that the source of oxygen in N_2O is different at this depths (Ostrom *et al*., 2000). The decrease in $\Delta^{18}O$ can be interpreted as a contribution to the N_2O oxygen from water as result of nitrifier denitrification (Popp *et al*., 2002).

All the above results suggests that around these particular depths of 200- 500 m at Geotraces transect and NBM, N_2O is not solely formed from NH_2OH/NO but at least a considerable portion of it will be derived from the reduction of NO_2^- through nitrifier denitrification (Poth and Focht., 1985; Popp *et al*., 2002; Ostrom *et al*., 2000). The reducing conditions that will readily favour these processes at any of these stations are not apparent from dissolved oxygen concentrations. Nevertheless, at these depths, a secondary oxygen minimum was observed as shown in Chapter 3 (section 3.4.1). Also, ΔN_2O /AOU ratios were highest at this small depth ranges below the surface mixed layer and above the AAIW. Since this process is an unlikely mechanism for oxic waters, possible chances for this mechanism to takes place will be the low oxygen or anoxic microsites in the sinking particles (Alldredge and Cohen., 1987; Paerl and Prufert., 1987; Karl *et al*., 1988,). Preferential remineralization of nitrate takes places at these depths in Geotraces stations (Chapter 3, section 3.4.1.2); which in effect will serve as a rich source of NH_4^+ to facilitate nitrification along with increased microbial activity and oxygen depletion (Ostrom *et al*., 2000). It can be concluded that throughout the Southwest Pacific ocean there exist a second process at a depth of 200-500 m which is responsible for N_2O production and is consistent with the nitrifier denitrification. So this study is partly in

agreement with the previous findings by Ostrom *et al.* (2000) who suggested this third pathway in this depth interval likely to be a ubiquitous phenomenon throughout the Pacific and possibly other oceans as well after incorporating with the results from Kroopnick and Craig, 1976 and Kim and Craig, 1990.

Nevertheless from top to bottom along the water column for the subantarctic SBM Mooring station these variations were less pronounced and did not show low values below 10 ‰. However, the minimum values were seen at a depth of 200-500 m. So at this waters throughout the water column N_2O is derived from NH_2OH/NO with a minor contribution from the nitrifier denitrification as that in the other stations.

5.4.2.2. $\delta^{18}O$ of Otago Continental Shelf Transect

Complete $\delta^{18}O$ characteristics ($\delta^{18}O$ of N_2O, $O_{2,\ aqueous}$ and H_2O) for this transect is available only for the month of September. From section 5.4.1.3, it is evident that the dual isotope variations with seasons are not pronounced in the transect. The measured $\delta^{18}O$- $O_{2,\ aqueous}$ and H_2O signatures for the four stations of Otago Continental Shelf transect are shown in the Figure 5.11 a and b respectively. Here also the isotope O_2 values are in VSMOW. The $\delta^{18}O$ of O_2 for the first two neritic stations does not show much variation from each other or with depth. The observed average values were 23.2 ± 0.2 ‰ and 23.2 ± 0.1 ‰ respectively for PA and PB. For PC and PD significant enrichments were observed from top to bottom. For PC the average surface $\delta^{18}O$ values were 23.5 ± 0.4 ‰ while the bottom waters had an average of 28.2 ± 1.3 ‰. Similarly $\delta^{18}O$-O_2,aq was 23.8 ± 0.4 ‰ and 27.4 ± 0.1 ‰ in the same order for PD. The surface isotopic values reflect atmospheric equilibrium (23.5 ‰) values. The $\delta^{18}O$ of H_2O values were close to 0 ‰ and varied slightly from top to bottom along the water column. The average $\delta^{18}O$ of H_2O for the four stations PA, PB, PC and PD were 0.20 ± 0.10 ‰, 0.10 ± 0.10 ‰, -0.05 ± 0.08 ‰ and -0.08 ± 0.09 ‰ respectively.

The enrichment in $\delta^{18}O$ of N_2O and its variations with depth for these transect were compared with $\delta^{18}O$ of $O_{2,\ aqueous}$ and H_2O. Neritic regions affected by strong vertical mixing, $\delta^{18}O$-N_2O and $\delta^{18}O$-O_2 do not have any discernible relationship with each other. For the other two stations (PC and PD) both N_2O and O_2 oxygen isotopes show shifts and enrichments at similar depths, while $\delta^{18}O$ of H_2O does not show any correlations.

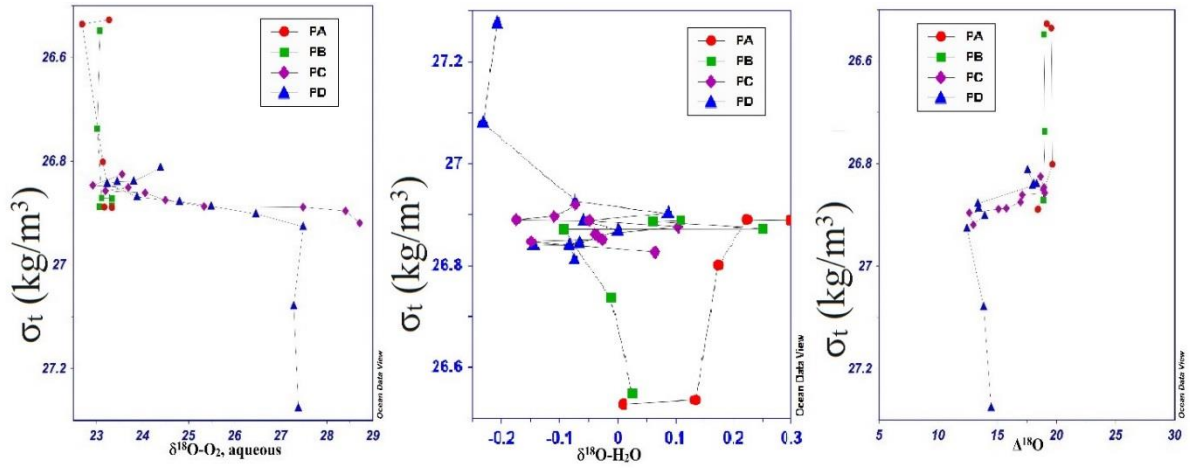

Figure 5.11: The variations of (a) $\delta^{18}O$ of $O_{2,\ aqueous}$ (b) $\delta^{18}O$ of H_2O and (c) $\Delta^{18}O$ with density for the Otago Continental Shelf transect during September 2011. All $\delta^{18}O$ values are in VSMOW

The $\Delta^{18}O$ measurements (Figure 5.11 c) shows that both neritic and subantarctic waters showed consistent values for $\Delta^{18}O$ values without much larger variations along water column. In the two neritic stations, $\Delta^{18}O$ was very much constant throughout the water column and is due to the absence of multiple nitrification pathways. $\Delta^{18}O$ is close to 20 ‰, and $\delta^{18}O$ of N_2O is enriched from that of $O_{2,\ aqueous}$, and is due to the absence of any possible contributions from water oxygen. Henceforth it is evident that the N_2O is derived in these shallow coastal waters only from NH_2OH/NO during nitrification process. Moreover, in the subantarctic sector of the transect, a similar trend in $\Delta^{18}O$ was seen as that of SBM. Enrichment in $\delta^{18}O$ of N_2O and $O_{2,\ aqueous}$ with depth along with a positive correlation between the two parameters is observed. The variations in $\delta^{18}O$ of H_2O are very small compared to those in $\delta^{18}O$ of N_2O and $O_{2,\ aqueous}$ and does not show any correlations with the other two parameters. It is also evident from the $\Delta^{18}O$ results that the variations between different depths are less than 6 ‰ which again strengthens the concept of a major contribution from a single mechanism similar to that in SBM.

5.4.3. Isotopomers of N_2O

Measurement of N_2O isotopomers (i.e. the intramolecular distribution of $\delta^{15}N$ within the linear NNO molecule) can provide insight into N_2O production processes since site preference (SP) is dependent on the production process and is independent of the $\delta^{15}N$ of precursor molecules (Toyoda and Yoshida., 1999; Toyoda *et al*., 2002; Popp *et al*., 2002).

5.4.3.1. Isotopomer distributions in the Geotraces , Bloom-II and Mooring stations

The $\delta^{15}N_{\alpha}$, $\delta^{15}N_{\beta}$ and site preference (SP) of N_2O for the Geotraces transect showed similar trends along depth (Figure 5.12 a, b and c respectively). The same ratios obtained for the Bloom II transect and Mooring stations are plotted below (Figure 5.13 a, b and c respectively). Nevertheless, these four stations did not show similar trends with respect to the two isotopomer species. However, at all depths, $\delta^{15}N_{\alpha}$ values were enriched with respect to $\delta^{15}N_{\beta}$, yielding a positive ^{15}N SP for all the above stations. $\delta^{15}N_{\alpha}$ in surface waters were nearly in equilibrium with N_2O in the troposphere (16.2 ‰) while $\delta^{15}N_{\beta}$ and SP values were slightly depleted with respect to tropospheric values of -1.2 ‰ and 18.7 ± 2.2 ‰ respectively. An isotopic minimum was observed for $\delta^{15}N_{\alpha}$ of N_2O between 200-500 m which were more pronounced near to 300 m except at SBM Mooring station. $\delta^{15}N_{\beta}$ profiles were mirror images of the $\delta^{15}N_{\alpha}$ profile with a maximum at depths where $\delta^{15}N_{\alpha}$ were minimum producing a minimum SP at same depths. SP profiles for N_2O were similar to that of $\delta^{15}N_{\alpha}$ down the water column. These results were similar to the trends observed by Popp *et al.* for ALOHA stations (2002) and also to the results obtained for KNOT stations (Toyoda *et al*., 2002). Though values obtained for these South Pacific waters were slightly lower than those of the North Pacific ALOHA stations results. Law and Popp in 2003 measured intramolecular distributions and SP for the November 2003 Mooring Voyage (TAN0311), these stations are closer to the present Mooring stations. The present results are comparable to the results obtained for 2003 Mooring results (Popp and Law., 2003, personal communications).

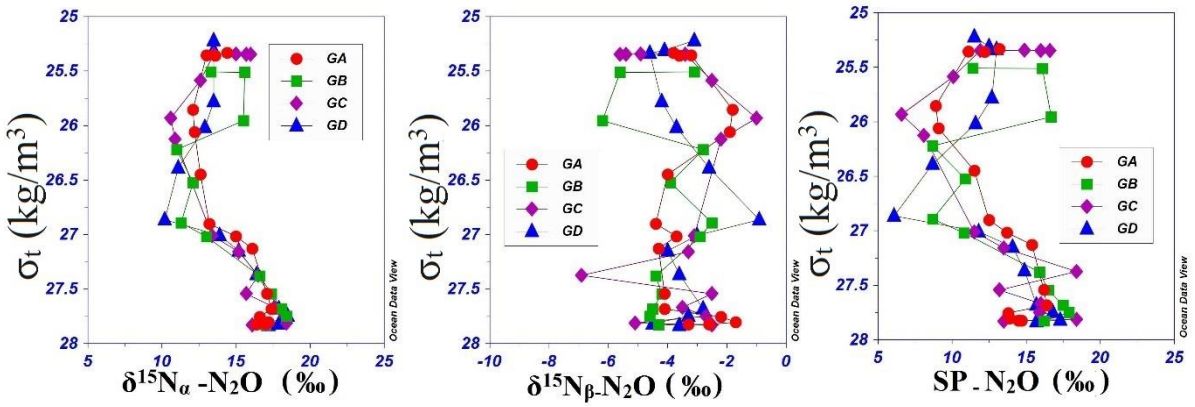

Figure 5.12: The variations of isotopomers a) $\delta^{15}N\alpha$ b) $\delta^{15}N_{\beta}$ and c) SP for four Geotraces stations.

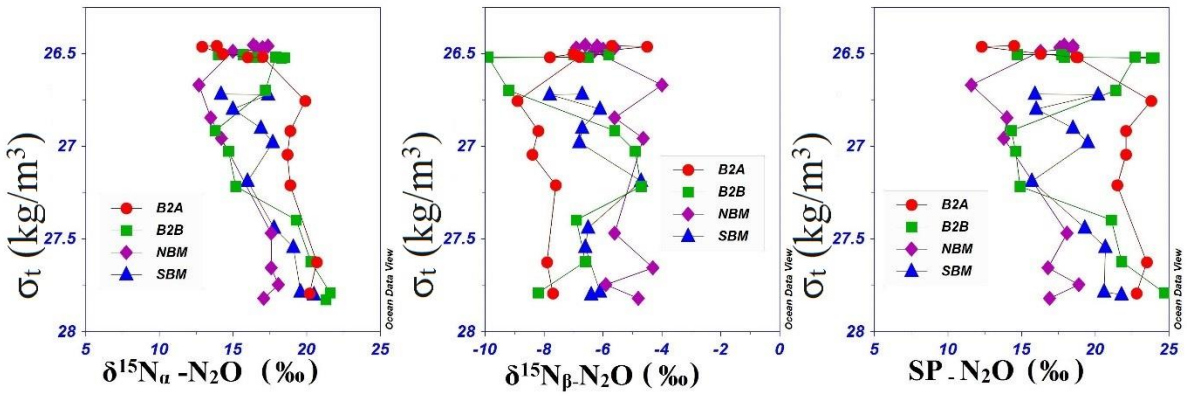

Figure 5.13: The variations of isotopomers a) $\delta^{15}N\alpha$ b) $\delta^{15}N\beta$ and c) SP for two Bloom II and two Mooring stations.

As compared to the $\delta^{15}N_{bulk}$ values isotopomer results are more variable with depth. The minimum values for $\delta^{15}N_{\alpha}$ and SP and the contrasting results for $\delta^{15}N_{\beta}$, with an opposite trend up to a particular depth down the water column from the surface, followed by a gradual increase in the values below these depths were seen. It can be inferred as the result of the in-situ production of N_2O at these depths. $\delta^{18}O$ and SP and $\delta^{18}O$ and $\delta^{15}N_{\alpha}$ varied in a similar way to that of $\delta^{18}O$-N_2O and $\delta^{15}N_{Bulk}$-N_2O (Section 5.4.1.1). This similarity in the water profiles between these independent parameters shows the existence of a single N_2O formation process except at the isotopomeric minimum. Low SP values were observed by previous studies (Toyoda *et al*., 2002; Popp *et al*., 2002; Westley *et al*., 2006) associated with nitrifier denitrification. The N_2O SP values produced from denitrification and nitrifier denitrification (pathway 3 of nitrification) are approximately 34 ‰ lower than nitrification (pathway 1 and 2) (Toyoda *et al*., 2005; Sutka *et al*., 2003, 2004, 2006). However, the distributional variations in isotopomers at this isotopic minimum are again concordant with the findings from the oxygen isotope studies (section 5.4.2.1) in which it is concluded that a partial contribution occurs from nitrifier-denitrification as a productive mechanism of N_2O during nitrification at these depths. At ALOHA stations Popp *et al.* also observed a similar decrease in SP and $\delta^{15}N_{\alpha}$ which are lower than the below and above layers with isotopic signatures that do not match the tropospheric values and were ≤ 0 ‰ and ≥ 8 ‰.

Lower SP values ranging between 10 - 40 ‰ are indicators of N_2O formation via nitrification (Yoshida and Toyoda., 2000; Toyoda *et al*., 2002; Popp *et al*., 2002). Isotopomeric results are in accordance with the previous findings that N_2O is formed in these waters from nitrification alone (except at subantarctic SBM). Nitrifier- denitrification process in the subsurface waters

of depth range 200-500 is mainly concentrated near 300 m which in fact reduces the subsurface isotopomer values from the expected nitrification values by contributions from its depleted site preference values. It is supported by the findings of Sutka *et al.* (2003) which concluded that SP of N_2O produced from NH_2OH oxidation is higher than that of nitrifier denitrification. Sutka *et al.* (2006) concluded from bacterial culture studies that there is no major difference between the SP values of N_2O produced from the pathway 1 and 2 of nitrification.

In order to look further into the SP results to unravel the mechanisms responsible for N_2O production kinetic isotopic effects and equilibrium, isotopic effects should be examined in detail. Young and Miller (1997) calculated and found the ground state zero-point vibrational energy (ZPE) of N-O bond for prominent isotopomers of N_2O as follows, $^{14}N^{14}N^{16}O > {}^{15}N^{14}N^{18}O > {}^{14}N^{14}N^{18}O > {}^{14}N^{15}N^{16}O$. I.e., the relative bond strength within the isotopomers of N_2O is inversely proportional to their ZPE's. So the ZPE for $^{14}N^{15}N^{16}O$ is less than that for $^{15}N^{14}N^{18}O$. Their calculations also indicated that there exists an exchange of ^{15}N between the alpha and beta positions of N_2O as a result of which the energy level of the molecule will be lowered. So during the formation of N_2O under equilibrium conditions, $^{15}N_2O$ will be favoured over $^{14}N_2O$ or SP will be positive. It can also be inferred that when N_2O is formed from two N atoms having similar ^{15}N values, because of equilibrium isotope effect greater enrichment at the alpha position than in the beta position and a positive SP value will be observed (Popp *et al*., 2002). Similarly, during consumption of N_2O (only observed during denitrification) preferential consumption of $^{14}N^{14}N^{16}O$ over the other isotopologues of N_2O will result in a residual pool enriched with ^{18}O and ^{15}N of N_2O regardless of the starting material. Therefore during N_2O consumption process, SP of N_2O will be increased (Westley *et al*., 2006) along with a decrease in the concentration of the N_2O. Kinetic fractionation during nitrification is due to the following reaction steps: $NH^+_4 \rightarrow NH_2OH \rightarrow NOH \rightarrow NO \rightarrow N_2O$ and $NH^+_4 \rightarrow NO^-_2 \rightarrow NO \rightarrow N_2O$. Oxidation of NOH is not supposed to affect SP since it is not subjected to any primary kinetic isotope effect. In the second step, reduction of $^{16}O^{14}N^{16}O$ to $^{14}N^{16}O$ is favoured over the reduction of $^{16}O^{15}N^{16}O$ to $^{15}N^{16}O$. However this process is not supposed to affect SP, and later N_2O will be formed from NO producing positive SP (Toyoda *et al*., 2002; Popp *et al*., 2002; Toyoda *et al*., 2005). It can be inferred that both the equilibrium and kinetic isotope effects during the formation through nitrification pathways causes the $\delta^{15}N$ enrichment at the alpha nitrogen atom when N_2O is formed directly from its precursors. It can also be assumed that at the isotopic minimum, isotope ratio of N_2O formed from a two-component mixing

between the isotopically depleted N_2O produced in situ at these depths and isotopically enriched N_2O coming through diffusion across the thermocline (also see section 4.3.2) (Popp *et al*., 2002). Now $\Delta^{18}O$ values (section 5.4.2.1) can be compared with SP, and both have similar trends with a minimum at the subsurface layer (200-500 m) and enriched values in the least oxic deeper regions of the ocean. Reported SP values are ≤ 0 for nitrifier denitrification as stated earlier. However, our findings of SP values strongly suggest the later mechanism since it is also evident from the other isotopic and nutrient results. However, the SP results are inadequate to differentiate between pathway 1 (NH_2OH) and pathway 2 (NO) of the N_2O formation.

To conclude it can be stated that the isotopomeric values strongly support the previous results that N_2O is solely formed from the single process of nitrification through NH_2OH/NO at all stations and depths except the isotopic and isotopomeric minimum layers.

5.4.3.2. Isotopomers in the Otago Continental Shelf Transect

The vertical profiles of the intramolecular distribution of nitrogen isotopes of N_2O- $\delta^{15}N_\alpha$, $\delta^{15}N_\beta$ and Site Preference (SP) observed at the four stations PA, PB, PC and PD of Otago Continental Shelf transect for three different time periods are shown below (Figure 5.14. a, b, c, d, e and f). $\delta^{15}N_\alpha$, $\delta^{15}N_\beta$ and SP varied very little with depth and seasons especially in the first two neritic stations in the shallow well-mixed waters. At the four stations, similar trends were seen with depth for $\delta^{15}N_\alpha$ and SP while $\delta^{15}N_\beta$ varied in the opposite trend. Subantarctic waters showed less variation as a result of a single major process as the responsible mechanism of N_2O formation in these waters. Thorough mixing (Chapter 3), wind and tidal effects along with the predicted single microbial production mechanism could be the reason for uniform and homogenous distribution of isotopomers and dual isotopes of N_2O in shallow neritic regions.

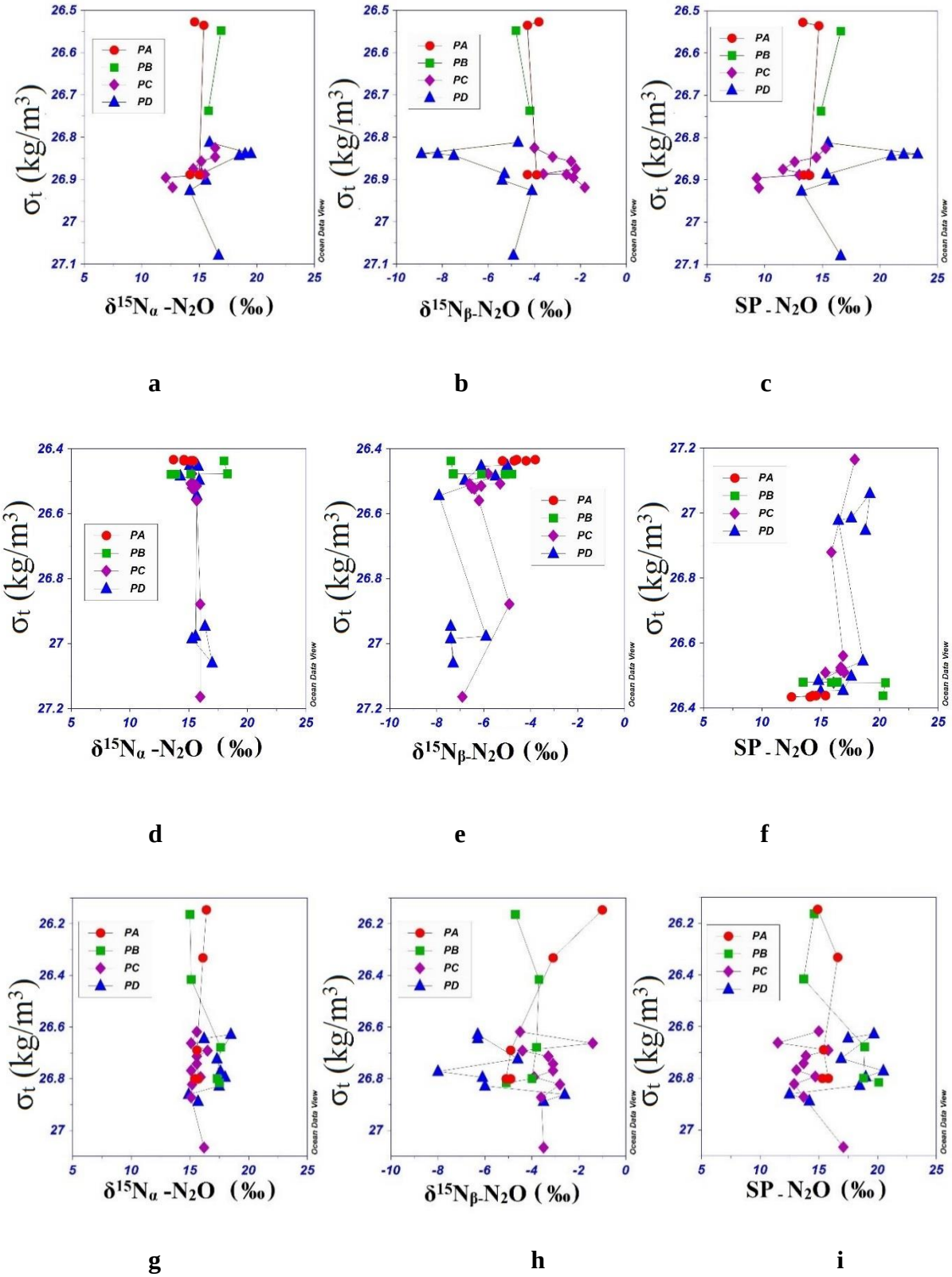

Figure 5.14: The variations of isotopomers a), d), g) $\delta^{15}N\alpha$ b), e), h) $\delta^{15}N_{\beta}$ and c), f), i) SP for four Otago stations during three periods Septemebr 2011, May 2012 and Novemebr 2012 from top to bottom in order.

At all depths $\delta^{15}N_{\alpha}$ values were enriched with respect to the $\delta^{15}N_{\beta}$, yielding a positive ^{15}N site preference. The surface $\delta^{15}N_{\alpha}$ signatures were in equilibrium with N_2O in the troposphere values while $\delta^{15}N_{\beta}$ and SP values were depleted with respect to the tropospheric values. Similar to the $\delta^{18}O$ and $\delta^{15}N_{Bulk}$ of N_2O variations, similar kind of variations were observed at all depths between $\delta^{18}O$ and SP and $\delta^{15}N_{\alpha}$. This variation between all these independent parameters are the evidence for the existence of a single process of formation for N_2O. Now $\Delta^{18}O$ values in the previous section (5.4.2) can be compared with that of SP, and it shows both have similar trends. So the intramolecular distributions show that the formation of N_2O is through a single process and in favour of previous findings that N_2O is formed in these waters from nitrification through NH_2OH/NO.

5.4.4. Isotopes, Isotopomers and Water Masses

The above results and discussions give a detailed overview of the processes occurring at different stations and study regions. It is inferred that in surface waters [N_2O] is slightly supersaturated in N_2O with respect to the atmospheric values except in the coastal regions. Adding to these results the dual isotope and isotopomer values suggest an atmospheric equilibrium in the surface waters with respect to N_2O and the possible production through nitrification. Below the surface mixed layer two processes operate which are nitrification and nitrifier denitrification, of which the latter produces isotopically depleted N_2O. There is a small contribution from the isopycnal diffusion of N_2O from the bottom layers of the mixed layer to the surface mixed N_2O, Chapter 4 (Section 4.4.2). These contributions from the bottom layers of the surface mixed layer (200-500 m) where maximum isotopic depletions were seen could be the reason for the decrease in surface mixed N_2O isotopes from that of atmospheric values. It will be due to the result of mixing between the two end members such as atmospheric N_2O and biologically produced N_2O. Below these layers where AAIW and CPDW were seen, [N_2O] was higher and an increase in the isotope and isotopomer signatures were also observed. The isotope results also suggest the production of N_2O in these waters are solely through nitrification and through pathway 1. Highest [N_2O] was observed in bottom waters as result of increased nitrification where the stable isotopes also exhibited an enrichment in the values.

5.4.5. Global Budget of N_2O and Oceanic Source

In spite of the importance of N_2O in global biogeochemical cycles, many uncertainties exist with regards to its global budget due to the various mechanisms causing both formation and

consumption, low concentration of N_2O and relatively lower rate of increase in concentration, longer residence time in the atmosphere and large number of natural and anthropogenic sources (Houghton *et al*., 1990). Isotopic characterization is a potential tool to resolve and reduce these uncertainties of the N_2O global cycle (Yoshida and Matsuo., 1983; Kim and Craig., 1993; Yoshida and Toyoda., 2000; Toyoda *et al*., 2002). In 1993 Kim and Craig suggested that the dual isotopic signatures of tropospheric N_2O are derived from three main end members. They are isotopically depleted terrestrial soil emissions, a highly enriched back – mixing flux of stratospheric N_2O which is formed as a result of photolysis and a third undocumented and hypothesized near-surface oceanic source. Using a global isotopic mass balance analysis using ^{15}N-^{18}O relationship they assumed this oceanic source would have an approximate isotopic composition of 5 ‰ and 15 ‰ for $\delta^{15}N_{Bulk}$ and $\delta^{18}O$ respectively. In 1997 Rahn and Wahlen suggested Kim and Craig over-estimated the stratospheric end member. Dore *et al.* (1998) also provided direct evidence from North Pacific waters for the hypothesized oceanic source by Kim and Craig. In 2002 Popp *et al.* predicted approximate isotopic composition for the shallow oceanic source as 3.5 - 5.5 ‰ and 11.7 - 17.5 ‰ for $\delta^{15}N$ and $\delta^{18}O$ of N_2O respectively.

A property-property plot of oxygen and nitrogen isotope composition of N_2O measured for various oceanic regions including the three end-member assumptions of Kim and Craig (1993) and Dore *et al.* (1998) measurements at North Pacific are shown in Figure 5.15. For the present study regions (Geotraces, Bloom II, Mooring and Polaris) it is concluded that the major process responsible for nitrous oxide formation is nitrification. In subsurface waters of Southwest Pacific, a partial contribution from nitrifier denitrification is also suggested. Since nitrification is considered as one of the largest contributors of the sea to air N_2O flux, the isotopic data obtained for these regions can be used in the same way as Dore *et al.* (1998) to constrain the global flux of N_2O to the atmosphere. It is obvious that the shallow surface flux is very significant in all these regions after considering all other parameters such as diffusion along the thermocline or mixing. There are studies, which showed that shallower N_2O plays a major role in balancing the tropospheric N_2O in the Arabian Sea, eastern tropical North Pacific and central North Pacific (Figure 5.15, Dore *et al*., 1998; Naqvi *et al*., 1998).

In order to understand the role of the present study regions on global budget of N_2O, ^{15}N-^{18}O relationship in the surficial waters of the upper oceanic layer were studied in a similar way. For this purpose, the average values of the measured dual isotopic signatures in the upper mixed layer have been used. The results are shown below in Figure 5.16. These results were then

plotted along with the three end-member values measured by Kim and Craig (1993) as shown in Figure 5.16. It is evident from the figure that the fluxes from all our study regions are very much close to the hypothesized oceanic end member of Kim and Craig. Dual isotope ratios were in the range of the suggested values by Popp *et al.* (2002) as well. Therefore, it can be inferred that the SWP region is a big contributor to the tropospheric N_2O, in support of the findings from Chapter 3 and 4. Based on the above results it can be also concluded that, the SWP waters will help to balance the troposphere against the enriched isotopic composition of the stratospheric return flux and the depleted tropical terrestrial emissions (Yoshida *et al*., 1984; Yoshinari *et al*., 1997; Dore *et al*., 1998; Naqvi *et al*., 1998).

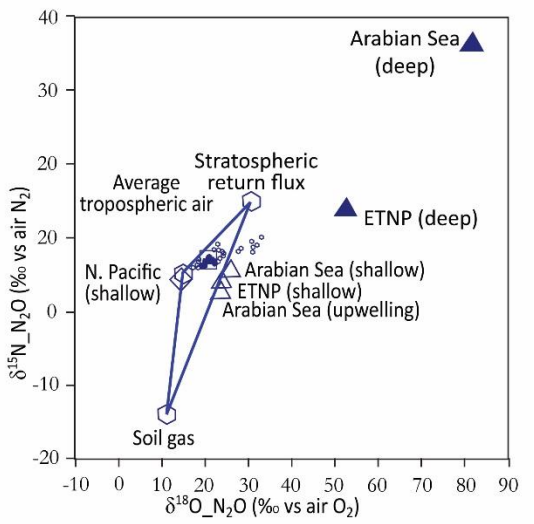

Figure 5.15: $\delta^{15}N$ - $\delta^{18}O$ variations of N_2O for different sources, (Dore *et al*., 1998).

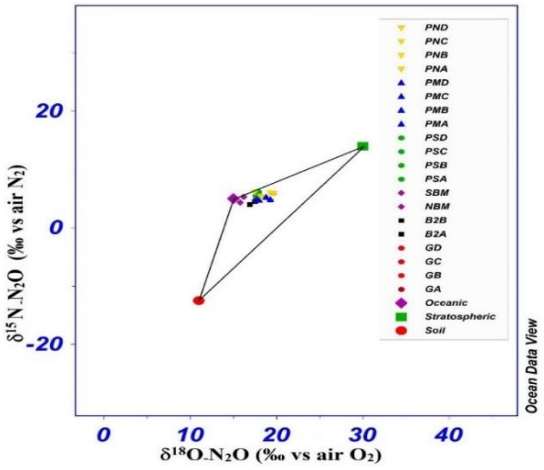

Figure 5.16: $\delta^{15}N$ - $\delta^{18}O$ of present study plotted with the Kim and Craig values, 1993.

Intramolecular distribution of N_2O and hence the SP of N_2O varies vertically throughout the atmosphere (Toyoda and Yoshida., 1999). Yoshida and Toyoda measured isotopomer abundance in the troposphere, stratosphere, terrestrial and oceanic N_2O and constructed an atmospheric mass balance for N_2O. They concluded that isotopomeric signatures are more effective tools to identify and quantify the sources and sinks of N_2O. By applying mass balance modelling Toyoda and Yoshida suggested that the tropospheric N_2O SP (18.7 ‰) is the sum of back injection of enriched SP of the stratosphere (21.3 ‰) which is formed as a result of isotopomer fractionation during photolysis and oxidation and emissions from low-SP oceanic and terrestrial sources. Unless balanced by the enriched stratospheric flux they calculated the 'original' SP would be 11.3‰ (ranging between -0.5 ‰ and 15.1 ‰) in accordance with average production and consumption processes for N_2O in the terrestrial and oceanic environments.

SP - the $\delta^{15}N_{\beta}$ relationship was also studied and compared with the few available previous studies (Yoshida and Toyoda., 2000; Toyoda *et al*., 2002; Popp *et al*., 2002) to understand and resolve the global budget of N_2O (Figure 5.17 a and b). SP *vs* $\delta^{15}N_{\beta}$ relationship gives us information about the oceanic contribution to the atmosphere independent of oxygen isotope ratios (Figure 5.17, Toyoda *et al*., 2002). The results obtained from the present study are shown in Figure 5.17 b. Since the values were very close to each other, the water column average values of each transect were taken for Geotraces and Bloom II. It is evident from the figure that these values are in agreement with the calculated values for oceanic flux by Yoshida and Toyoda through mass balance. The trend observed here for the present study are similar to the previous trend observed (Figure 5.17 a). Based on the isotopomer results it can be confirmed that these SWP waters will help to balance the troposphere against the enriched isotopomeric composition of the stratospheric return flux by contributing to the terrestrial flux.

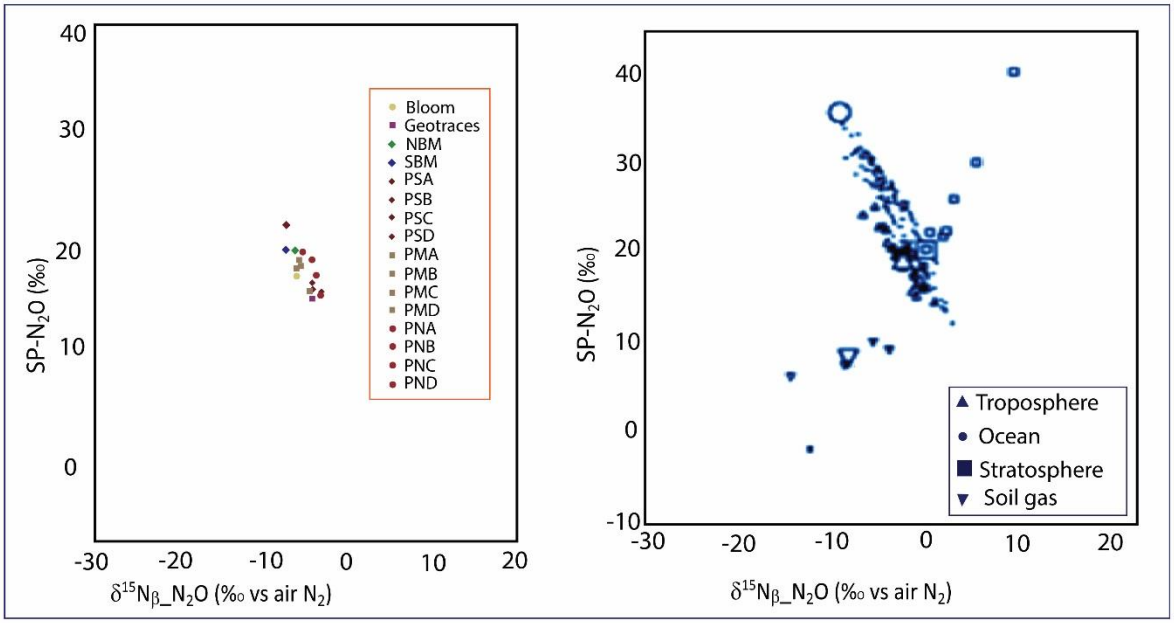

Figure 5.17: a) Site preference *vs* $\delta^{15}N_{\beta}$ for the present study. The stations are shown in the figure b) Site preference *vs* $\delta^{15}N_{\beta}$ obtained for Toyoda *et al*., 2002.

5.4.6. Isotopic Incubation experiments in Otago Continental Shelf Water

Incubation experiments with isotopically labelled substrates of N_2O formation are used to discriminate between nitrification and denitrification in differing aquatic environments (Barnes and Owens., 1998). The methods and materials used for the incubation experiments using ^{15}N isotope labelled $^{15}NH_4Cl$ and $K^{15}NO_3$ are explained in Chapter 2. Experiments were conducted with water samples collected from four selected depths of two stations, one in neritic and the three in Sub Antarctic waters of Otago Continental Shelf transect (Station B- Surface, Station D-surface, 100 m and 500 m).

Table 5.7: Nitrogen parameters obtained for the control samples for each incubation.

Polaris November Stations	N_2O (nM)	Nitrate (µM)	Ammonia (µM)	δ^5N_{bulk}-N_2O (‰ vs air N_2)
Station B-Surface	11.2	1.5	1.0	5.2
Station D-Surface	11.7	4.6	1.2	5.2
Station D-100m	12.0	13.1	1.3	4.8
Station D-500m	14.1	15.0	1.1	6.1

Table 5.8: The results of incubations studies for the two stations of Otago Continental Shelf transect at four depths. The results for four subsamples collected at a regular interval during the 12 hours incubations.

Stations	Added labelled isotope	Incubation Time (Hour)	Ammonia (µM)	Nitrate (µM)	N_2O (nM)	$\delta^{15}N_{bulk}$-N_2O (‰ vs air N_2)
Station B	$^{15}NH_4Cl$	0	6.2	1.6	9.4	5.7
		4	9.5	1.8	10.1	5.7
		8	8.6	1.3	10.1	8.0
		12	6.2	1.0	10.4	9.5
	$K^{15}NO_3$	0	7.7	12.1	9.9	4.1
		4	9.1	13.0	9.9	4.3
		8	5.8	9.5	10.0	6.3
		12	4.0	9.8	10.4	5.9
Station D-Surface	$^{15}NH_4Cl$	0	17.3	9.7	11.0	5.7
		4	19.0	10.3	11.0	10.5
		8	17.4	9.9	12.5	9.8
		12	16.7	8.6	10.7	26.6
	$K^{15}NO_3$	0	11.1	18.9	11.2	7.1

		4	0.0	23.2	11.1	6.9
		8	1.9	25.3	12.6	9.3
		12	2.5	20.9	10.8	8.9
Station D-100 m	$^{15}NH_4Cl$	0	3.6	1.0	10.5	7.0
		4	6.3	1.9	10.7	10.7
		8	1.7	1.6	11.9	14.1
		12	2.0	2.4	10.6	15.0
	$K^{15}NO_3$	0	1.6	8.6	10.7	6.1
		4	7.5	9.9	10.7	5.2
		8	1.5	7.4	11.6	10.7
		12	0.7	7.2	9.8	9.6
Station D-500 m	$^{5}NH_4Cl$ [1]	0	4.9	10.7	11.5	6.9
		4	1.7	12.1	11.4	7.8
		8	2.0	12.1	12.9	11.2
		12	12.6	19.7	10.3	31.6
	$K^{15}NO_3$	0	3.3	14.5	11.5	7.3
		4	7.5	2.0	11.2	6.8
		8	2.7	2.0	12.6	6.5
		12	4.9	3.2	9.4	9.6

The results obtained for each depth are shown below in Table 5.8. The results obtained after three hours interval from the time of spiking until the end of 12 hours of incubation (total four subsamples from each incubation vessels) for each depth are shown in the table in chronological order for $^{15}NH_4Cl$ and $K^{15}NO_3$ additions. The results for ammonia (µM), nitrate (µM), N_2O (nM) and $\delta\,^{15}N_{bulk}$-N_2O (‰) for the corresponding control samples are shown in Table 5.7. The changes in N_2O concentrations with time measured for the treatment samples were more or less close to the control samples. Similar observations were reported by Westley *et al.* in 2006 for Black sea incubation experiments. The variations in nutrient concentrations were indicative of the processes throughout the experiment. They increased with respective substrate additions with time in most of the cases followed by a decrease in concentrations.

However, these changes in nutrient concentrations were not consistent for all incubation depths. It may due to the changes in different incubation bottles raised due to the small differences in each experimental set up which will then result in either enhancement or decrease in the microbial growths (Punshon and Moore., 2004). Nevertheless, $\delta^{15}N_{bulk}$-N_2O gives a clear indication of the processes. The uptake of ^{15}N ammonium into N_2O is evident from added $^{15}NH_4Cl$ to the incubation containers. For each depth, a significant increase in $\delta\,^{15}N_{bulk}$-N_2O was observed with time with these additions as compared to those signatures in the control samples. Contrasting results were obtained for $K^{15}NO_3$ additions without a significant increase in isotope signatures with time. It indicates that the intake of ^{15}N of $K^{15}NO_3$ into the N_2O formed is much less. The above isotope incubation results are also in agreement with the earlier evidence from different measurements that suggested a nitrification source for N_2O that is formed through NH_2OH through ammonia oxidations in the Otago Continental Shelf waters.

5.5. Conclusions

- The dual isotopes of N_2O from the SWP showed characteristic depletions at the surface followed by an isotope minimum (except at subantarctic SWP) at the subsurface and a slight enrichment at the bottom compared to the tropospheric mean values and is a strong indication of nitrification throughout the water column except at the 200-500 m.
- $\delta^{15}N_{bulk}$ *vs* $\delta^{18}O$ relationship and positive correlations between these two independent parameters suggested a single process as a responsible mechanism for N_2O formation except at the minimum isotopic layers.
- The $\delta^{18}O$ of $O_{2,\,aqueous}$ had a similar trend as the dual isotopes of N_2O while $\delta^{18}O$ of H_2O did not exhibit significant difference in different water masses along water column. $\Delta^{18}O$ was determined and showed a minimum (9 ‰ lower than the above and below depths) at dual isotopic minimum layers in SWP suggesting that the major nitrification process is NH_2OH oxidation followed by the NO oxidation. An exceptional contribution to the N_2O source was from the nitrifier denitrification which was observed at the minimum isotope layers of 200-500 m in the subtropical SWP.
- S.P values confirm the existence of nitrification processes as the major pathway of N_2O formation at all depths except at the 200-500 m. At 200-500 m S.P values also proved the co-existence of the nitrifier-denitrification process.

- The present study results based on conventional N_2O- $\delta^{15}N_{bulk}$ and $\delta^{18}O$ relationship and recent site preference - $\delta^{15}N_{\beta}$ suggest that these SWP could be a source of isotopically heavy N_2O to the atmosphere.
- ^{15}N isotope labelled incubation experiments using $^{15}NH_4Cl$ and $K^{15}NO_3$ for the selected stations of Otago Continental Shelf transect also proves the existence of nitrification through ammonium oxidation.

Chapter 6

N_2O Distribution and its Isotopes in the Northeast Arabian Sea (NEAS)

6.1. Introduction

The Arabian Sea contains diverse biogeochemical features such as eutrophic, oligotrophic, and low-oxygen environments. The thickest oxygen minimum zone (OMZ) found in the world's oceans is present in the Arabian Sea (Bange *et al*., 2001). The Arabian Sea plays a major role in global biogeochemistry and climatology due to its landlocked boundaries and existence of suboxic regions at mid-depths which lead to denitrifying conditions (among three such oceanic regions in the world) (Naqvi *et al*., 1994; Codispoti *et al*., 1992).

The Arabian Sea is the most intensely studied region with respect to N_2O among the world's oceans (Bange *et al*., 2001; Bange *et al*., 2008). Though the Arabian Sea occupies only 0.43 % of world oceans, it is estimated to contribute 20-35 % of the global N_2O flux (Law *et al*., 1990; Naqvi and Noronha, 1991; Naqvi *et al*., 2000; Bange *et al*., 2001). This region exhibits very high seasonal variability due to the extremes in atmospheric forcing. Due to the extremities such as strong wind stress and different coexisting types of upwelling (coastal and open ocean) as well as seasonal downwelling conditions, this part of the ocean proved to be a strong source of atmospheric N_2O (Naqvi *et al*., 2010).

Modeling studies suggest that the previous N_2O flux estimates are compromised by significant temporal and spatial biases (Bange *et al*., 2001). In particular, Bange *et al*. claim that the flux from the Arabian Sea appears to be under-estimated mainly due to the relatively low spatial resolution of the applied models and/or missing data from this region. While the discrepancy in the estimates of the ocean-atmosphere flux of N_2O might have been considerably reduced during the last two decades of extensive N_2O studies in these regions, there still exist large uncertainties concerning the internal cycling of N_2O and associated processes in the ocean.

The stable isotopic and isotopomeric techniques offer tools to provide insight into the oceanic N_2O cycle. Stable isotope measurements provide an integrated signal of many processes and

hence are particularly useful in a system with large-scale and short-term variability. The Arabian Sea has been intensively studied with respect to N_2O, but there are a very limited number of studies on N_2O dual isotopic signatures. There is no study that provides combined isotopic outlook from different $\delta^{18}O$ signatures of water, dissolved oxygen and N_2O.

6.2. Objectives

1. To provide more N_2O concentration and stable isotope data from the Arabian Sea upwelling regions during southwest monsoon seasons. Southwest Indian Continental shelf regions are supposed to derive more N_2O to the atmosphere though numbers of available studies are very limited. Therefore, the present study will examine the atmospheric fluxes from this region, which is expected to be higher during SW Monsoon.

2. To measure the dual isotopes of N_2O ($\delta^{15}N_{Bulk}$ and $\delta^{18}O$ of N_2O) to understand the mechanisms of formation and removal of N_2O in the geochemically and physically diverse Arabian Sea waters.

3. To measure the isotopomers ($\delta^{15}N\alpha$, $\delta^{15}N_{\beta)}$ and site preferences (SP) of N_2O to look into the production mechanism for the first time in the Indian Continental Shelf waters.

6.3. Sampling and Analysis

Detailed descriptions of the Northeastern Arabian Sea (NEAS) and sampling locations are given in sections 2.1 and 2.2 respectively. Water sampling methods adopted are explained under section 2.3, and the analytical techniques are described in section 2.4. Also, see Figure 6.1 and Table 6.1 shown below for more details about the stations. Samples were collected from three selected locations (SU, SC and SK, Figure 6.1 and Table 6.1) from the NEAS continental shelf during the Southwest Monsoon (SWM) season from 10-20 June 2012.

Table 6.1: The geographic locations and depths of Indian Ocean stations

Station ID	Depth (m)	Longitude (^{0}E)	Latitude (^{0}N)
SU	25	8.000	77.660
SC	1000	7.380	77.530
SK	1000	9.930	75.480

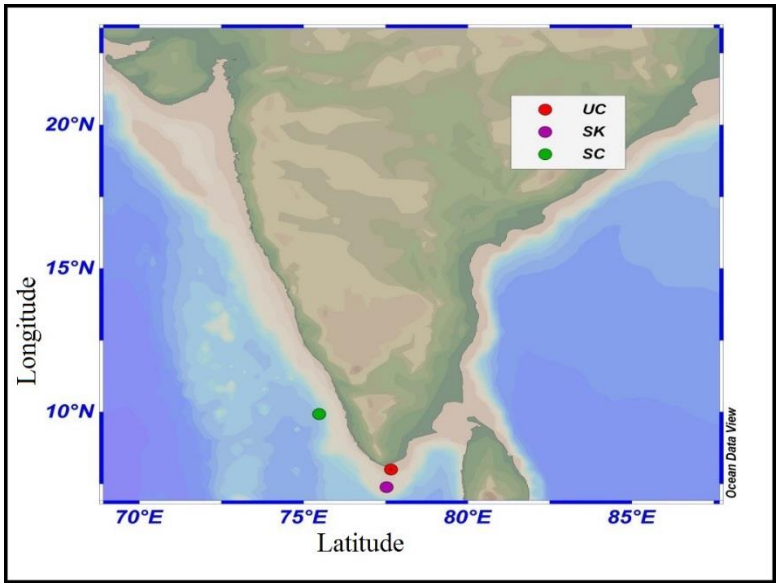

Figure 6.1: The Indian Ocean sampling stations and their location

6.4. Water Mass Properties

The Indian Ocean is the smallest of all oceans. The Arabian Sea water has very limited exchange of water with other world ocean basins. As a result, this small water body has different hydrodynamics that separates it from the remainder of the world oceans. Oceanic circulations in these waters are mainly controlled by thermohaline processes, while that in the other oceans are mainly through wind-driven currents (Piccard and Emery., 1990; Tomczack and Godfrey., 2003). As explained in Chapter 3 (section 3.4) T-S diagrams are used for describing the water mass properties in the oceans as T and S are conservative tracers. Together T and S determine the density of the water and hence water movement as water moves along density gradients.

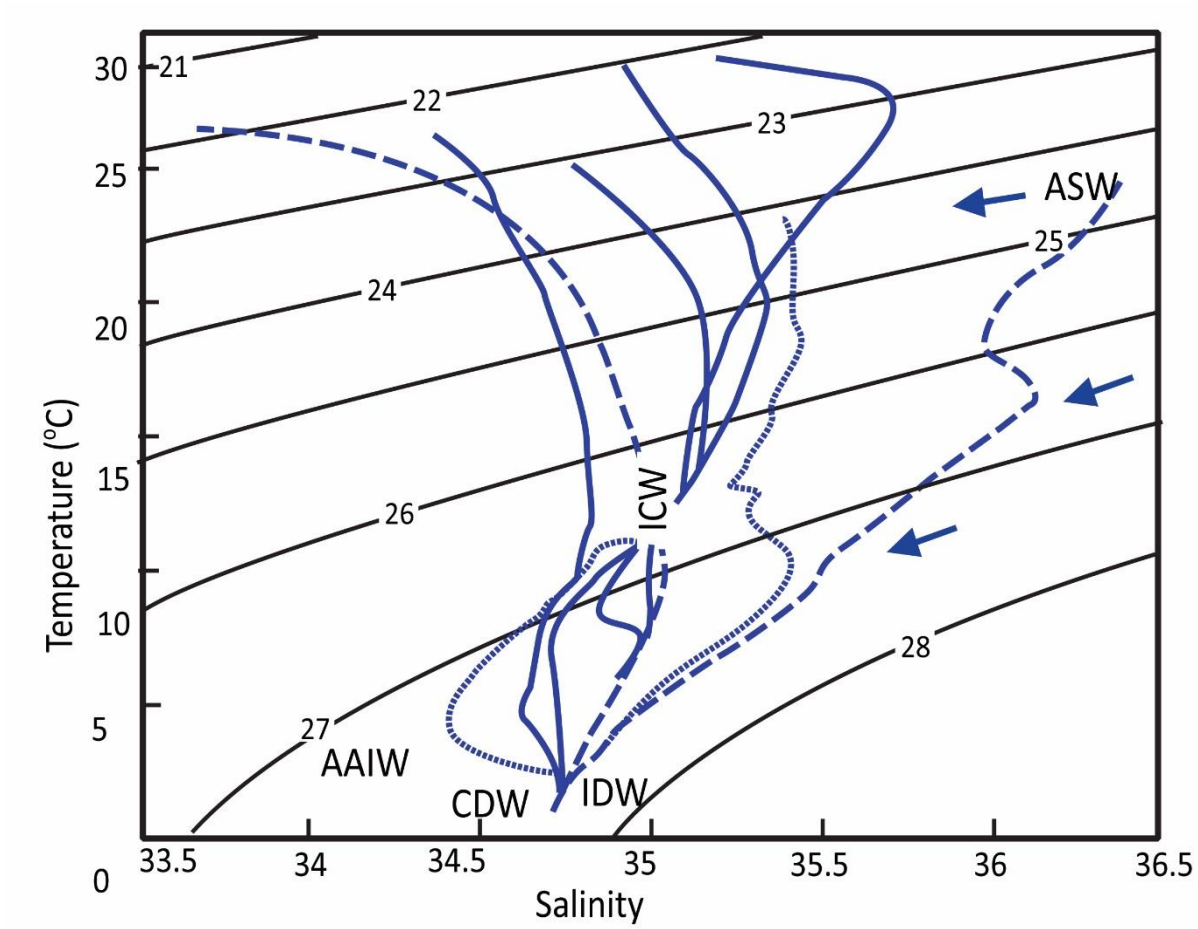

Figure 6.2: T-S diagrams for the water masses of the Arabian Sea. Lines of equal potential density are overlaid. (Tomczak and Godfrey., 2003).

The detailed T-S plot for the Eastern Arabian Sea (Figure 6.2) shows the major water masses and their formation processes in the Arabian Sea (Kumar and Prasad., 1999; Beal *et al*., 2000; Prasad and Ilkeda., 2002a, 2002b; Stramma *et al*., 2002; Tomczak and Godfrey., 2003). Based on their results the Indian Ocean waters masses are divided into three; surface, intermediate and abyssal water masses.

The surface water properties of the Indian Ocean and the Arabian Sea vary strongly with seasons. The major surface water masses are Arabian Sea Water (ASW) and Equatorial Water (EQW). Of the two major surface waters observed in the Arabian Sea, Arabian Sea (AS) surface waters have high salinity of 36.5 due to evaporation. The second water mass is Equatorial Water which is formed in the Intertropical Convergence Zone (ICZ) and carried westward to the Northern Arabian Sea on the South Equatorial Current during the Southwest

Monsoon period (Pickard and Emery., 1990). Due to heavy rainfall, at the region of formation, its salinity is comparatively low. Therefore, for the present study regions from the T and S relationship (Figure 6.3 and Table 6.3), the surface waters are of Indian Equatorial waters.

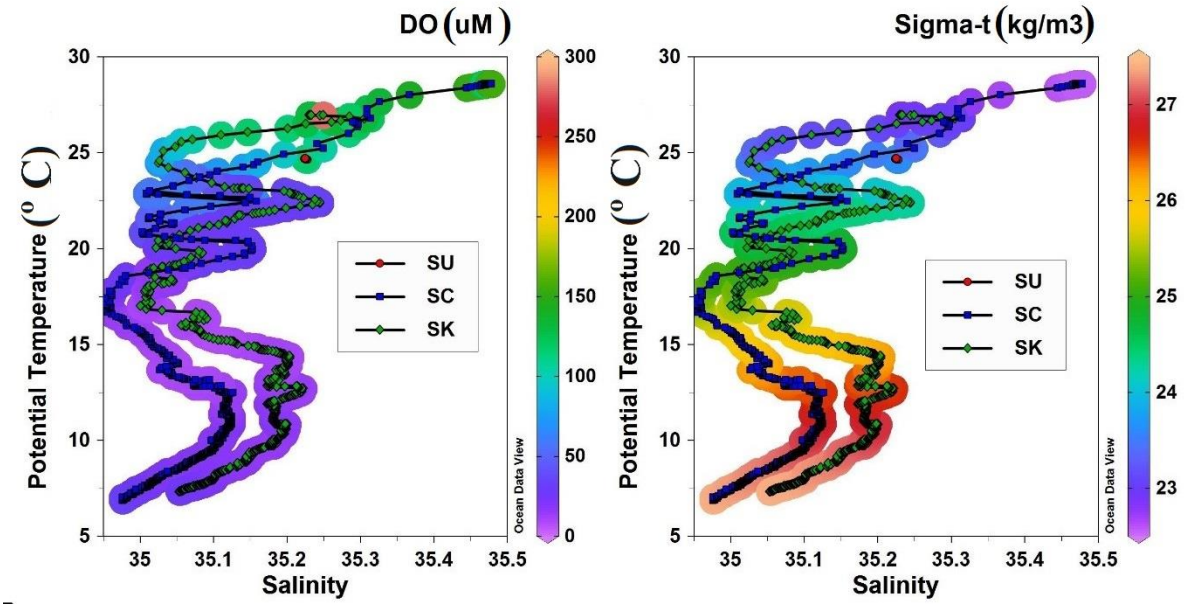

Figure 6.3: T-S diagram with a) DO and b) σ t for UC, SC and SK.

Three Mediterranean seas namely Persian Gulf, the Red Sea and the Australasian Mediterranean Sea influence the hydrographic properties of Indian Ocean water masses at the intermediate depths that are mainly observable from the salinity values. The first two water masses have higher salinities with a minimum of 36 while the latter is mainly found in the near-equatorial regions with low salinities (34.5 or below). All these properties were absent (Figure 6.3 and Table 6.3) below the mixed layer at the two open ocean stations along the intermediate depths. Instead, characteristic properties of another water mass called Indian Central Water (ICW) were observed. The characteristic T and S values for ICW are 5 - 17 ºC and 34.8 - 35.5 along the water column and is in accordance with the earlier studies. In a previous study of ICW along the density surfaces σ_t = 25.7 and σ_t = 26.7, specific characteristics for annual mean temperature, salinity and oxygen were observed (Carton *et al*., 2012). At 25.7, temperature was 16.0 - 16.5 ºC, salinity near to 35.1 and oxygen 0.5 - 1 ml/l. The respective values at 26.7 were 13 ºC, 35.1 - 35.2 and 1 ml/l respectively (Tomczak and Godfrey., 2003). ICW is a subtropical water mass formed in south of the Indian Ocean, which originates at the north of Subtropical Convergence (STC). It has almost a linear T-S relationship and enters the northern hemisphere via a western boundary current off the East African coast (Swallow *et al*., 1988).

The northern Indian Ocean ICW is characterized by very low oxygen concentration due to rapid ageing during its transition to the northern hemisphere. Transfer between the hemispheres is restricted to Southwest Monsoon season which makes the annual net transfer rate very small and thereby the circulation slow (Piccard and Emery., 1990; Tomczak and Godfrey., 2003). The final fate of ICW in the Northern Indian Ocean is yet to be explored. However, in the thermocline region, some water will leave leaving space for new supply. For this, the only possibility is through upward diffusion into the surface layers (Tomczak and Godfrey., 2003). The swift changes in the conservative properties in upper thermocline between 75 and 200 m at SC and between 50-150 m at SK indicate some mixing across those regions (Figure 6.3). Chemical and physical parameters obtained for the respective water masses are given in table 6.3. From σ_t values (Table 6.3 and Figure 6.3) it is obvious that at all stations similar water masses follows similar water currents and are distinct from each other with exceptions at the mixing zone.

From the T-S curve, it is obvious that there exists a third water mass at the bottom depth at both SC and SK. At SC below 600 m and at SK below 750 m there exist AAIW. The temperature and salinity characteristics of AAIW is already explained in Chapter 3.The temperature, salinity, σ_t, nutrients and DO for the AAIW is presented in Table 6.3 for the two stations. Along with the decrease in salinity and increase in DO which is a characteristic feature of AAIW, these water masses show a decrease in $\delta^{18}O_{H2O}$ (Figure 6.16). This decrease in $\delta^{18}O_{H2O}$ is another indication of the presence of AAIW at the bottom. The ML and thermocline depths for the different stations of present study regions are given below in table 6.2. From the T-S diagram obtained for the present three study stations, following conclusions can be made on the water masses and its behaviour. At the very shallow station, SU near the Southern Indian cape very well mixed water mass was observed without much variation in T and S. At station SC, a surface mixed layer was observed with slightly more saline and warmer waters than SU.

Table 6.2: ML depths of three stations from the surface to the bottom.

Station	Surface Mixed Layer (m)
SU	0-25
SC	0-59
SK	0-25

6.4.1.Upwelling

There are two important upwelling processes in the ocean. The first one is the slow upwelling of cold abyssal water, occurring over large areas of the ocean to compensate the sinking of the surface water in limited Polar Regions. The second one is the upwelling of subsurface waters into the euphotic zone to balance for the horizontal divergence occurring in the surface, usually caused by winds. Coastal upwelling systems are highly dynamic and exhibit wide variations in the hydrographic, nutrient and phytoplankton characteristics controlled by local meteorology on short time scales and remote forcing on longer timescales. Deep waters are rich in nutrients, such as nitrate, phosphate and silicate, due to the decomposition of sinking organic matter and lack biological uptake. Upwelling regions are, therefore, significant for very high levels of primary production in comparison to other areas of the ocean (Piccard and Emery., 1990). Coastal upwelling regions are characterized by thermal fronts parallel to the coast with colder and nutrient-rich waters. The coastal side of the front will have lower salinity due to the small freshwater inputs, and the open ocean side will have warmer nutrient-depleted waters with comparatively more saline waters (Morrison. J. M., 1997; Naqvi and Unnikrishnan., 2009).

Table 6.3: Water mass characteristics and hydrochemical properties at stations SU, SC and SK.

Station	Water mass	NO_2 (µM)	PO_4 (µM)	NO_3 (µM)	Salinity	Temp (^{o} C)	σ_t (kg/m^3)	DO (µM)
UC	EQW	0.42	6.62	8.96	35.2	24.7	23.6	112 ± 5
SC	EQW	0.01	0.01	0.07	35.5	28.5	22.6	145 ± 13
	ICW	0.00	46.4	29.55	35.1	12.0	26.6	20 ± 14
	AAIW	0.00	3.5±0.2	31±2	35.0	7.5	27.3	28 ± 3
SK	EQW	0.13	5.8	15.5	35.2	23.1	24.0	41 ± 17
	ICW	0.00	24.4	22.02	35.2	12.0	26.6	16 ± 4
	AAIW	0.00	3.8±0.4	32.0±3.5	35.1	7.6	27.3	25 ± 2

In the northern hemisphere, the Coriolis force deflects wind-driven currents to the right. As a result, a net movement of surface waters takes place at right angles to the direction of the wind (45° at surface to total shift of 90° for the water column); which is known as the Ekman

transport (Ekman. V. W., 1905; Sverdrup *et al*., 1942). When Ekman transport occurs along the coast, nutrient-rich deep, cold, and denser waters, causing coastal upwelling, replace the surface waters. Though upwelling signals are observed in sea level from February (Shenoy *et al*., 2005) onwards, the chemical and biological indications of upwelling in the surface-subsurface waters are observed only in association with the commencement of the SWM(June) (Maheswaran *et al*., 1999).

NEAS regions along the southwest coast of India are reported as significant coastal upwelling regions during the SWM (Johannessen *et al*., 1987; Shetye *et al*., 1990, 95; Shankar *et al*., 2005). Upwelling off the SEAS, as indicated by the rapid upward movement of isotherms and surface cooling occurs during the SWM months from May to September. Earlier studies also showed that fronts occur quite near to the coast (not more than 110 km from the shore with a strong temperature gradient. (Sanil Kumar *et al*., 2004).

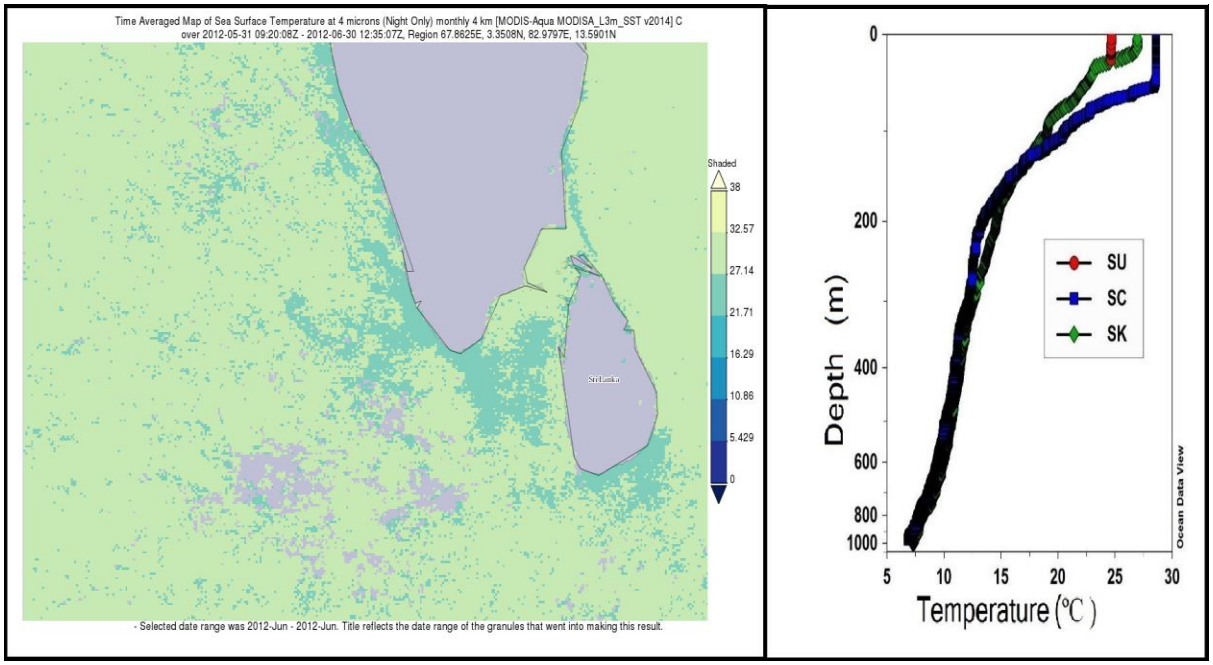

Figure 6.4: a) Sea surface temperature data obtained from Satellite data along the study region (Southwest Indian Continental Shelf) b) Water column potential temperature profile for the Indian stations.

Sea Surface Temperature (monthly average of SST during June 2012, derived from MODIS AQUA at 4 microns with the Giovanni online data system, developed and maintained by the NASA GES DISC) and the vertical structure of temperature profiles obtained from CTD was used to examine the upwelling (Figure 6.4 b). SST (Figure 6.4 a) shows a decrease in surface

temperature in the Southwest Indian coast where the sampling stations are located. The average Arabian Sea surface temperature is 29 ºC (Pickard and Emery., 1990). At SU the surface temperature was low (24.7 º C) while at SC it was 28.6 ºC. At a range of similar coastal upwelling stations (from Kanyakumari cape to the Goa along the Southwest Indian coast) during 1992-96 period Naqvi *et al.* observed a sea surface temperature as low as 22.8º C (Naqvi *et al*., 1998).

At the open ocean station SK, a thin (approximately 20 m) water layer, formed because of intense rainfall over the coastal zone was observed above the cold upwelled waters. This freshwater layer was considerably more buoyant than the underlying water (sigma t = 22.5), and so caps the water column preventing the upwelled water from coming to the surface (Naqvi *et al*., 2010). The temperature below this layer was reduced (23.9 °C). In the open ocean, the wind-induced surface water divergence will cause upwelling of the waters. As a result, the convergence of the waters adjacent to this region will cause downwelling and these are the characteristics of the open ocean upwelling systems. A similar kind of open ocean upwelling system in the central Arabian Sea during Southwest Monsoon was identified by Prasannakumar *et al*., 2001 and Madhuprathap *et al*., 2003. From Figure 6.4, it can also be noted that the thermocline depth was deeper at SC where cold and dense water masses were also absent at the surface, while the thermocline moved further up in the open ocean stations SK. So the above findings are indications of coastal upwelling at SU and an open ocean upwelling at SK, while the absence of any upwelling systems at SC.

Salinity values also show significant differences in the surface of the three stations. At SU and SK the salinity values were the lowest, and at SC it was the highest. Based on water mass studies Stramma *et al.* (1996) had indicated that during upwelling; water at the shelf edge was a mixture of low salinity water advected out of the Bay of Bengal around Srilanka and higher salinity Arabian Sea water. So a decrease in salinity is evident in the upwelled waters while it was absent in the Arabian Sea Surface waters of station SC where upwelling was absent. Studies conducted along the NEAS (McCreary *et al*., 1993; Shankar *et al*., 1997) to address the dynamics of the process of upwelling found that the alongshore wind stress as the most important local forcing responsible for the upwelling through Ekman dynamics during the SWM. To examine the Wind stress along the study region, we used a monthly average of wind speed data (Figure 6.5) 10 m above the sea surface during June 2012, derived from MERRA

MODEL with the Giovanni online data system, developed and maintained by the NASA GES DISC. The data shows a monthly average of more than 6 m/s along the Indian coast which is the characteristic phenomenon observed during SWM upwelling. It is reported that a unique wind-forcing pattern occurs over the Indian Ocean during the southwest monsoon. It forms the Findlater jet over the Arabian Sea with maximum speeds of about 16 m/s with an average of 6 m/s or more.

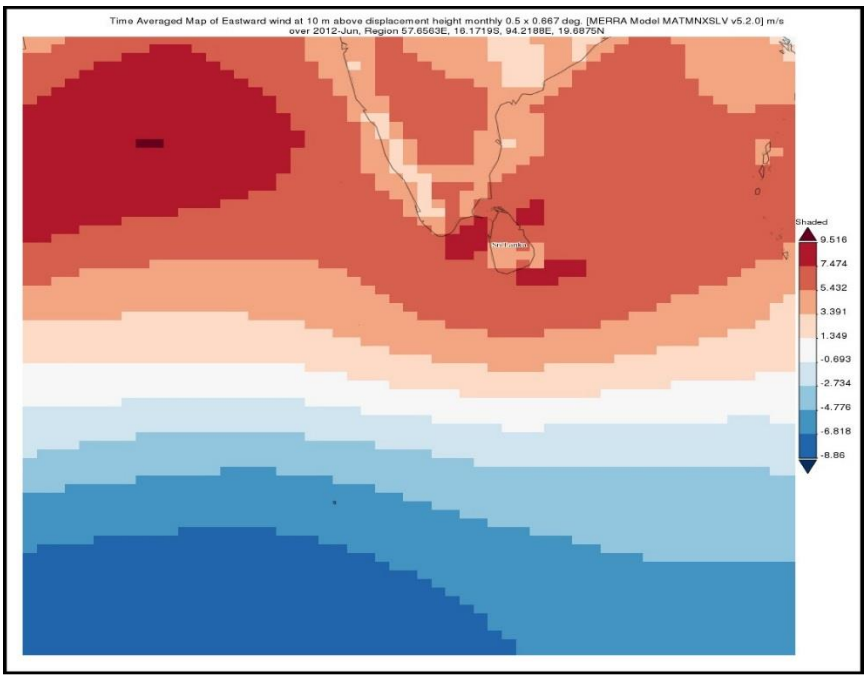

Figure 6.5: Monthly averaged Westward Wind speed over the Indian Ocean during June 2012

In order to study the upwelling behaviour we investigated the characteristics of these waters such as productivity (using Satellite Chlorophyll data), in-situ DO and nutrients. NEAS is biologically one of the most productive regions of the world oceans during SWM due to the well-known upwelling process (Madhupratap *et al*., 2003). An occurrence of hypoxic and nutrient-rich bottom waters at the surface is another significant feature of the upwelled waters (Naqvi *et al*., 1990; Naqvi and Jayakumar, 2000; Naqvi *et al*., 2010). Daily averaged composite maps of Chlorophyll a (mg/m^3) for June 2012, derived from NOBM Model at 0.667 *1.25-degree spatial resolution (from the Giovanni online data system, developed and maintained by the NASA GES DISC) are used to describe the surface productivity patterns in the area. The Figure 6.6 shows that the increased chlorophyll and the existence of a large amount of

phytoplankton along the study region during the sampling period and is an indication of the existence of upwelled waters along the coast.

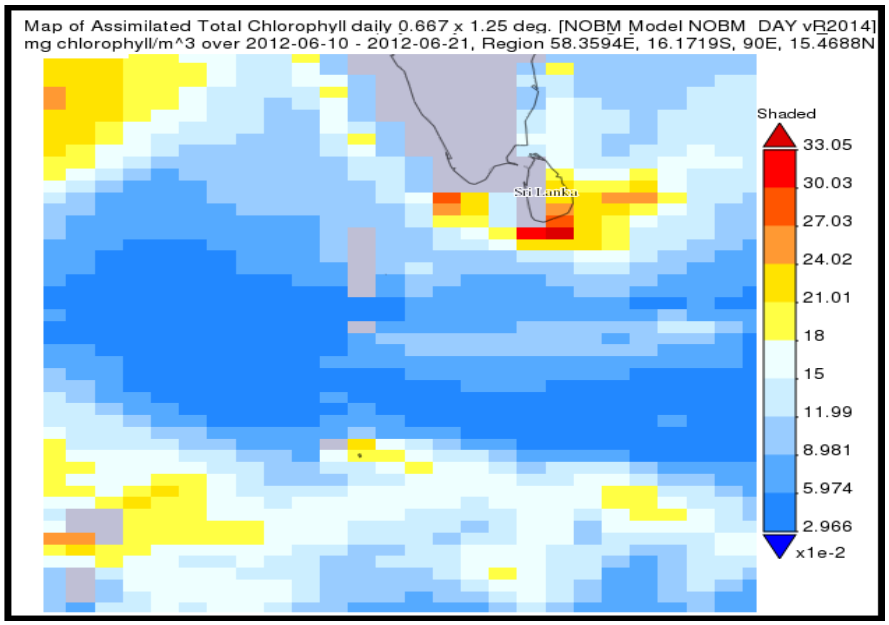

Figure 6.6: Daily averaged composite maps of Chlorophyll a (mg/m3) for June 2012, derived from NOBM Model at 0.667* 1.25-degree spatial resolution from GIOVANNI-NASA.

Table 6.4: Oceanic regions according to dissolved oxygen concentrations (Naqvi *et al*., 2010)

State of the water	Oxygen concentration	Nutrients and concentrations
Oxic	Greater than 1.4 ml/l	Nutrients may or may not be present according to the oceanic conditions
Hypoxic	$0.1 < O_2 \leq 1.4$ ml/l	$NO_3^- > 0$ µM, $NO_2^- = 0$ µM
Suboxic	$0.1 \leq O_2 < 0$ ml/l	NO_3^- , $NO_2^- > 0$ µM; $H_2S = 0$ µM
Anoxic	$O_2 = 0$ ml/l	NO_3^- , $NO_2^- = 0$ µM; $H_2S > 0$ µM
Note: for oxygen, 1 ml/l = 1.43 mg/l = 44.64 µM		

Arabian Sea water OMZ have dissolved oxygen concentrations below 22.5 µM (Morrison *et al*., 1999; Naqvi *et al*., 2010). Based on oxygen concentration water masses can be divided into oxic, hypoxic, suboxic and anoxic waters with characteristic properties as shown in Table 6.4,

adapted from Naqvi *et al*., 2010. The DO and nutrient distributions along the water column for the three stations are given in Table 6.3 and Figure 6.7.b, d and 6.13.

The decreased oxygen content of the surface water masses at SK (41 ± 17 µM), and SU (112 ± 5 µM) provide strong evidence for upwelling. At SK and SU, the nutrients were also high at the surface (NO^-_3 = 15.5 µM and 9 µM respectively). At SC where upwelling was absent, DO increase and nitrate decreased (DO = 145 ± 13 µM, nitrate = 0.07 µM). The results are in accordance with values obtained by earlier studies in the same regions who confirmed the existence of a strong coastal upwelling in the Eastern Arabian Sea during Southwest Monsoon (Sharma *et al*., 1966; Stramma *et al*., 1996).

In NEAS, suboxic conditions accompanied by secondary nitrite maxima and intense denitrification are observed (Naqvi., 1991; Naqvi *et al*., 1994; Morrison *et al*., 1999 a). This OMZ are characterized several biogeochemical changes as compared to oxygenated waters. When the availability of oxygen reduces (between 2-10 µM), facultative organisms will switch over to use available nitrate to oxidize organic matter (Richards, 1965). Free nitrogen will be formed with nitrite being an intermediate (Naqvi. S. W. A., 1991; Naqvi. S. W. A., 1994). These processes will be intense in suboxic conditions and are not usually observed in hypoxic conditions. So the present study is not in the active subsurface denitrification zone as inferred from the studies by Naqvi *et al.* (1994) who proposed that it is mostly spread over the open central Arabian Sea. Nutrient and dissolved oxygen concentrations also show that the present study area is away from the active denitrification zone. However, Codispoti *et al.* (2001) proposed that even though these regions are away from the active denitrification zone and a secondary nitrite maximum is absent, a small amount of denitrification might occur in the Southwest Indian continental shelf regions, depending on climatic conditions. So the hydrographic features point towards complex N_2O chemistry in these regions which are discussed in detail in the coming sections.

6.5. Nitrous oxide distribution

6.5.1. N_2O Concentration in the water column

The water column [N_2O] distributions in the NEAS stations are presented in Figure 6.7.a and Table 6.5. [N_2O] profiles were not uniform in all stations. The shallow well mixed and

upwelled waters of station SU had homogenous [N_2O] throughout the depth along the isopycnal layer (σ_t = 23.6). [N_2O] profiles showed no systematic variations along depth with an average concentration of 17.3 ± 1.0 nM. The DO concentrations were low, and nitrate concentrations were high at this station.

Upwelling properties were absent at station SC, and the [N_2O] along the isopycnal surface layer (σt = 22.56) was lower than the other two stations with an average of 8.7 ± 0.7 nM N_2O. In thermocline layers (across the isopycnal layers of σ_t = 23.9 - 26.5) where a decrease in DO (below 100 µM) were seen, [N_2O] increased with an average 52.0 ± 8.0 nM. The highest [N_2O] values (61.1 nM) were observed at the base of the thermocline where the oxygen was the minimum. Parallel to N_2O profile DO (Figure 6.7.b) decreased, and nitrate concentration increased towards the bottom. A slight decrease in [N_2O] was seen (40.8 ± 2.4 nM) at the bottom of the OMZ where AAIW water was observed (σ_t = 27.91) below 600 m.

At the open ocean upwelling station SK, the N_2O distribution pattern was similar to that of SC with the exception of having higher concentrations in the upwelled nutrient-rich surface layers as expected. The average surface concentrations were 20.5 ± 2.0 nM. The average concentrations in the OMZ were 48 ± 6.7 nM with the highest concentration 55.2 nM at a depth of 150 m. The minimum [N_2O] is present in the surface water masses and maximum at the core of the OMZ along the thermocline waters of ICW. Below the ICW at the bottom of the sea, AAIW was observed and had an average [N_2O] of 40.6 ± 1.0. The variations of nutrients were as similar to that of [N_2O] for respective water masses as both increased from the surface to bottom. So the vertical distribution of N_2O showed characteristically similar profile along the stations with exceptions at the surface. Some general features of N_2O distribution were common to all stations. These were:

1. Relatively low concentration surface layer.

2. High concentration in the thermocline (20.9 ± 0.5 nM) at a depth of 75-200 m.

3. Upwelling induced higher surface [N_2O], while in the absence of upwelling surface [N_2O] was decreased.

4. [N_2O] increased from the surface to bottom accompanied by a decrease in DO and increase in nitrate concentrations.

5. [N_2O] values were higher than [N_2O]$_{Equilibrium}$ throughout the water column and lower values than [N_2O]$_{Equilibrium}$ were absent in contrast to the denitrification zones of the Northern Arabian Sea suboxic waters.

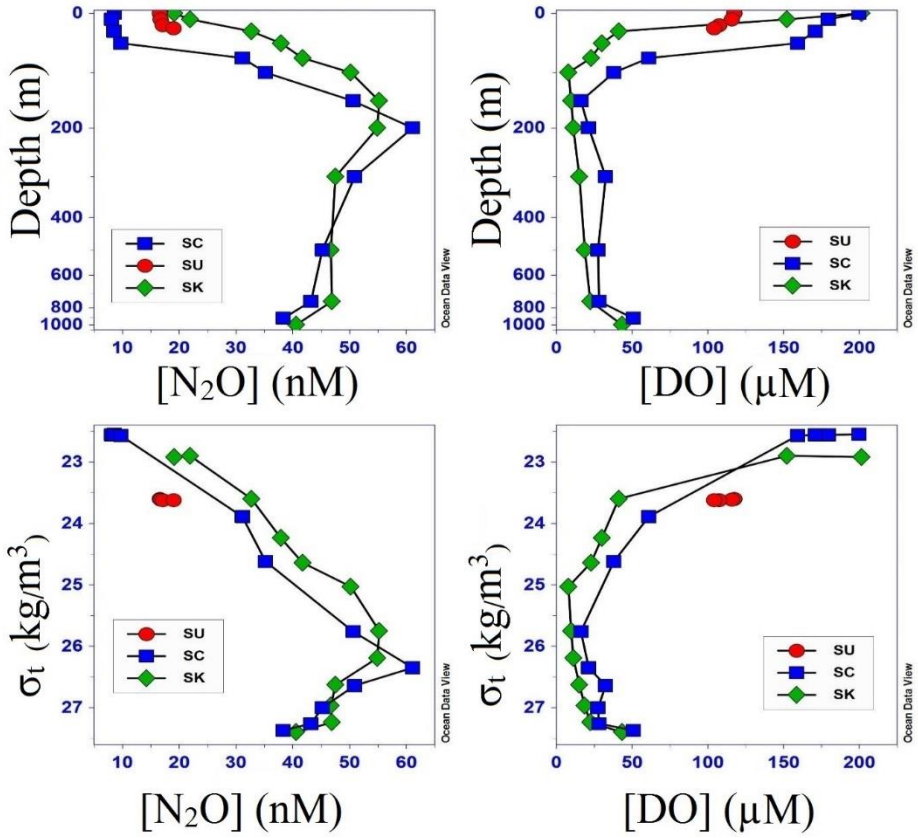

Figure 6.7: [N_2O] (a and c) and [DO] (b and d) concentrations with depth for stations SU, SC and SK in the clockwise order.

With regards to higher [N_2O] in surface and oxygen minimum zones, the present study results are comparable to the results from the earlier studies in the Arabian Sea and in other upwelling regions such as Cline *et al.* (1987) and Elkins *et al.* (1978). The shape of the [N_2O] peak is in agreement with the previously reported N_2O profiles for upwelling regions outside suboxic and denitrification zones in the Arabian Sea. Earlier studies reported double peak curve for [N_2O] in the suboxic regions with an N_2O minimum where denitrification was higher. This double peak was absent in the current study region. Instead a single peak curve was obtained with one broad maximum at the subsurface oxygen minimum depth. The reason for having single peak structure is due to an increased production of N_2O at low [DO] as long as the latter does not fall below the value for denitrification to occur (Codispoti and Christensen., 1985). Similar to previous studies there was a consistent and substantial decrease in [N_2O] below the maximal concentration toward the bottom and is due to the occurrence of AAIW at the bottom

layers. Maximal N_2O concentration for the present study was 55.1 and 61.1 nM for stations SC and SK respectively whereas Naqvi, and Noronha (1991) and Patra *et al.* (1999) observed concentrations up to 80 nM for their stations in suboxic regions and concentrations up to 60 nM for regions outside suboxia. Law and Owens (1990) reported maximum [N_2O] along with their transect in the Northwest Arabian Sea as 59 nM where they observed suboxia and double peak structure for the N_2O distribution. Surface concentrations in the present study were also in the range of earlier values reported for Arabian Sea regions (Bange *et al*., 2005).

The variation in dissolved oxygen for the study area is shown in Figure 6.7. The DO distribution is already discussed in the earlier sections (Section 6.4). N_2O distribution seemed to be inversely related to [O_2], as shown by comparing Figure 6.16a and 3.16 b, with the maximum N_2O concentration in the minimum oxygen regions for all stations, similar to that in SWP (Chapter 3). The present study regions in the NEAS has different oxic conditions where [N_2O] appears to be negatively related to [O_2] as shown in Figure 6.7 (Slope = -3.6 and R^2 = -0.91). Oxygen decreased from near saturation in the surface layers to about 20 µM at SC and 10 µM at SK in the core of the OMZ (100 - 200 m), and then slightly increased with depth. Whereas [N_2O] increased with depth from the surface along the OMZ, and then decreased with increasing depth. The variations in nitrate concentration ([NO_3^-] + [NO_2^-]) in Table 6.3 and Fig. 6.13 show that the nitrate depth profile was similar to that of [N_2O].

The relationship between [N_2O] and AOU showed a significant positive correlation (R^2 = 0.93 and slope = 0.18). The water column N_2O - AOU slopes were different for three stations, as shown in Figure 6.8. This figure indicates the occurrence of regional variations in the rates of N_2O production and oxygen consumption. It can also be seen from this figure that, as expected, different water masses had different slopes and the same water masses had similar slopes for the N_2O/AOU relationship.

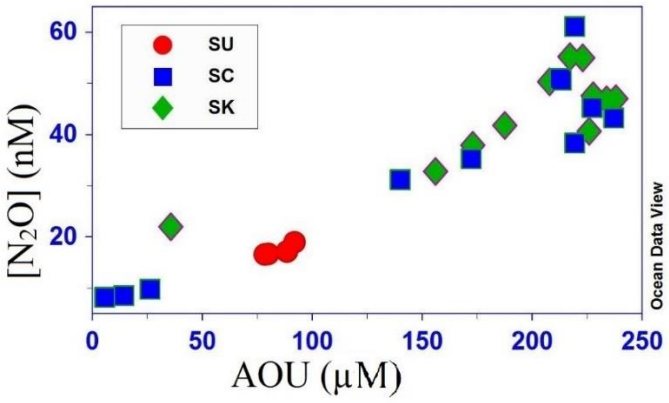

Figure 6.8: The variation of N_2O with AOU

6.5.2. N_2O Percentage Saturation in the water column

All three stations are supersaturated with respect to N_2O at the surface with comparatively higher N_2O saturation than that in equilibrium with the atmosphere. N_2O saturation along the water column is shown in Figure 6.9; the respective water mass distributions can be read from Table 6.5. The surface saturations are very high compared to the global mean surface saturation values. The saturation values at the surface mixed layer were 266, 150, 386 percentage respectively at SU, SC and SK. The N_2O percentage saturations increased with depth to a maximum of ~ 600 % at the base of the thermocline (100-200 m) corresponding to the core of the OMZ in ICW. From these maxima, in the ICW the saturation decreased uniformly with depth to the bottom at the AAIW (369 ± 11).

High surface saturations such as observed here in these regions are typical of upwelling regimes. Elkins *et al.* (1978) observed average saturations 170 % and 140 % in the equatorial Pacific. Pierotti and Rasmussen (1980) reported saturations ranging between 224 % and 264 % for intense upwelling off Peru and Butler et al. (1989) reported saturations up to 137 % from an upwelling zone in the eastern equatorial Indian Ocean. Surface N_2O saturations in the present study and those reported in other studies in the NEAS are shown in Table 6.6. It shows that the present results are in agreement with the previous studies and it confirms that the upwelling regions of the southwest Indian continental shelf are a significant source of N_2O to the atmosphere. However, sea-to-air fluxes will be discussed in the next sections (Section 6.7). At SC where upwelling features were absent, the surface saturations were still above the global mean surface saturation. The possible reasons for this increase such as diffusion and advection from deeper waters and contributions from increased productivity are examined in the

following sections. There may be another contribution from the increased aerosol deposition of NH_4^+ and NO_3^- as result of anthropogenic activities in the Arabian Sea (Naik and Naqvi., 2002).

Vertical distribution of N_2O saturation in the present study (Figure 6.9, Table 6.5) is 418.1 ± 105.4 and 530.5 ± 97.8 respectively at SC and SK, and these values are comparable to the previously reported measurements from both the Arabian Sea and other OMZ. However, the accumulation of N_2O in "low-oxygen" (not suboxic or denitrifying) waters is still a subject of debate for which detailed examinations are required. From Figure 6.9 vertical distribution of N_2O saturation seems to be closely resembled that of AOU, reflecting that the yield of N_2O during O_2 consumption increased as oxygen consumption increased. In more oxygenated AAIW a decrease in N_2O saturation was observed.

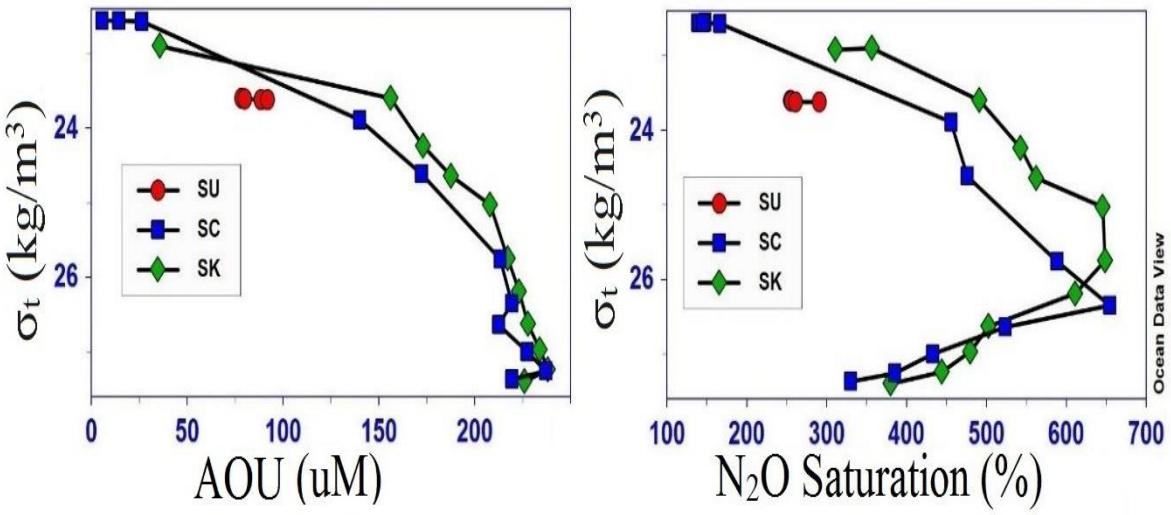

Figure 6.9: N_2O saturation and AOU with respect to sigma t for stations UC, SC and SK of the Arabian Sea.

Table 6.5: The average water column values of DO and N_2O properties for the water masses found at stations UC, SC and SK.

	N_2O[nM]	DO[µm]	N_2OSaturation[%]	ΔN_2O[nM]	AOU[µm]
UC	17.3 ± 1.0	164 ± 21	265± 15	10.8± 1.0	31.8± 21
SC-ML	8.7 ± 0.6	177 ± 15	150± 10	2.9± 0.6	16± 8
SC-ICW	52.0 ± 8.5	35 ± 11	418± 105	33.7± 8.3	224.2± 18.9
AAIW	40.8 ± 2.4	40 ± 11	358± 28	29.3± 2.6	228.3± 8.8
SK-ML	24.5 ± 5.9	177 ± 25	386± 77	18.2± 5.6	95.9± 60.2
SK-ICW	50.2 ± 4.7	18 ± 11	531± 98	40.4± 4.6	225.0± 9.4
AAIW	40.6 ±1	43 ±5	381±10	32.5±2	226.0±10

Table 6.6: Surface N_2O saturation from present and earlier studies.

Region/season	Saturation (%)	Reference
Central and Western A.S		
Late SW Monsoon, 1986	167 ± 46	Law and Owens, 1990
Spring Intermonsoon, 1995	99 ± 2- 103 ± 1.5	Bange *et al*., 1996
SWM, 1995	103 ± 1- 230 ± 46	Bange *et al*., 1996
Late SWM, 1994	97 ±4- 204 ± 16	Upstill- Goddard *et al*., 1999
Fall Intermonsoon, 1994	94 ± 9- 154 ± 1	Upstill Goddard *et al*., 1999
Somali Basin, SWM, 1992	112-330	de Wilde and Helder, 1997
Central and Eastern A.S		
Early NEM, 1988	128-258	Naqvi and Noronha, 1991
Spring Intermonsoon, 1994	105 ± 8	Lal and Patra, 1998
NEM, 1995	132 ± 5	Lal and Patra, 1998
SWM, 1995	133 ± 15	Lal and Patra, 1998
SWM, 1996	130 ± 3	Lal and Patra, 1998
Indian Continental Shelf		
SWM, 1995	193-953	Naqvi *et al*., 2005
Upwelling period (1997-2002)	84-8250	
Indian Continental Shelf- SWM		
Upwelling (coastal, SU)	255-290	
Upwelling (open ocean, SK)	310-330	Present study,
Open ocean (upwelling absent, SC)	139-166	NEAS

6.5.3. ΔN_2O and its variations with AOU

ΔN_2O values were positive at all depths throughout the stations. As shown in Figure 6.10 and Table 6.5, the positive ΔN_2O in the surface-mixed layer is an indication of a positive net loss *via* gas exchange to the atmosphere. Positive values at the bottom waters are interpreted as evidence of *in situ* production all along the water column in the Arabian Sea (Yoshinari. T., 1976).

ΔN_2O versus AOU relationship reported for different regions of Arabian Sea from earlier studies are shown in and Table 6.7 along with results for the present studies. Linear positive trends between ΔN_2O and AOU were observed when the values measured for the whole depths were examined with a significant positive correlation as shown in Figure 6.11. [DO] above suboxic conditions between 0-1000 m were included in the correlation. The ΔN_2O/AOU ratio systematically increases from (0.18 to 0.23 at SC and 0.16 to 0.21 at SK)) in the surface to the bottom of the thermocline. The observed increase in ΔN_2O/AOU to the core of the OMZ is in accordance with the earlier findings that the N_2O production rate increases at low concentrations of oxygen (Carlucci and McNally., 1969; Goreau *et al*., 1980).

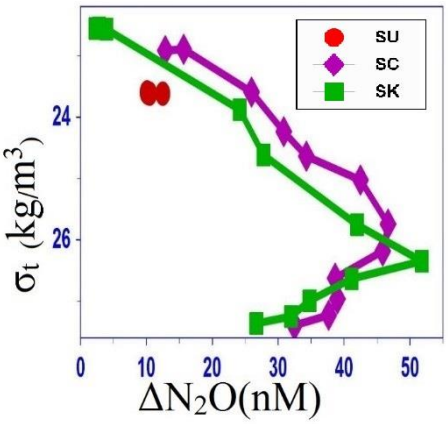

Figure 6.10: ΔN_2O variations with σ_t for the three stations in the NEAS.

While another approach was used evaluate the ΔN_2O/AOU by differentiating depths with a concentration above 197 µM and below 197 µM into two correlations as done by earlier researchers a different result was obtained as shown in Figure 6.11. b and c respectively. A more significant correlation as shown in Table 6.7 was obtained for the upper oxic waters, at the same time, it was much less significant (R^2 decreased from 0.8 to 0.52) for the bottom OMZ

layer. The surface mixed layer values were omitted as these depths will be influenced by gas exchange with the atmosphere and dissolved oxygen productions. The central waters (ICW) had a positive correlation ($R^2 = 0.52$) with a slope of 0.26 while AAIW had a slope of 0.18 ($R^2 = 0.52$). The values reported here for Arabian Sea AAIW is higher than that obtained for Southwest Pacific (slope = 0.05) in Chapter 3. This is because of increased N_2O and decreased DO in these regions of NEAS carrying comparatively aged AAIW.

From the N_2O *vs* AOU correlations obtained for different approaches, it is seen that the slopes of the regression lines are all in agreement with previously obtained results (Table 6.7). For example, within the depth range 0-1000 m, the molar ΔN_2O *vs* AOU obtained for other OMZ's of world oceans are as follows. Elkins *et al* (1978) in the subtropical Pacific- (0.170×10^{-3}), Cohen and Gordon (1978) in the ETNP ($0.140\text{-}0.150 \times 10^{-3}$) and Oudot *et al* (1990) in the eastern tropical Atlantic ($0.129\text{-}0.219 \times 10^{-3}$). For Arabian sea regions Naqvi and Noronha obtained (0.170×10^{-3}) in 1991 for 0-1000 m and for the deep waters it was (0.260×10^{-3}), the similar set of highest values were obtained for Law and Owens (1990) in the Northern Arabian Sea with a slope of 0.31×10^{-3} when AOU was higher than 197 µM.

Due to the presence of highest values found in the literature, Naqvi and Noronha (1991) found the highest [N_2O] concentrations reported in the literature which they attributed to a higher production than average rate of N_2O production. Results from the present study for the upper regions and bottom OMZ were in accordance with Naqvi and Noronha, which suggested that the Arabian Sea has an above average N_2O production zone among the world oceans. The possible major reasons for the different behaviours in the ΔN_2O/AOU are due to the dependence of N_2O on temperature (Yoshida and Alexander, 1970) and hydrochemical discontinuity in the vertical structure (Naqvi *et al*., 1990). Elkins *et al*., (1978) also suggested that the production rate of N_2O depended on both AOU and temperature and suggested a relationship whereby ΔN_2O can be calculated as follows.

$$\Delta N_2O \text{ (nM)} = 3.20 + (0.1066 + 0.00455\ t)\ \text{AOU}, \quad \text{..... (6.1)}$$

where t is the temperature in °C and AOU in µM.

The values calculated from equation 6.1 are plotted in the Figure 6.7.a in brown squares, the actual values are plotted as blue diamonds. The ΔN_2O observed at low [DO] (N_2O maximum) and also at high [DO] is similar to those given by Elkins relationship. While at the mixing zone,

equation 6.1 overestimates ΔN_2O by ~ 6 nM. The reason for the poorer agreement in the OMZ is not known, it may be related to the near-surface variations in the ΔN_2O/AOU ratio or unusual biological and oceanographic conditions that prevailed during the sampling period (Cline *et al*., 1987; Naqvi and Noronha., 1991).

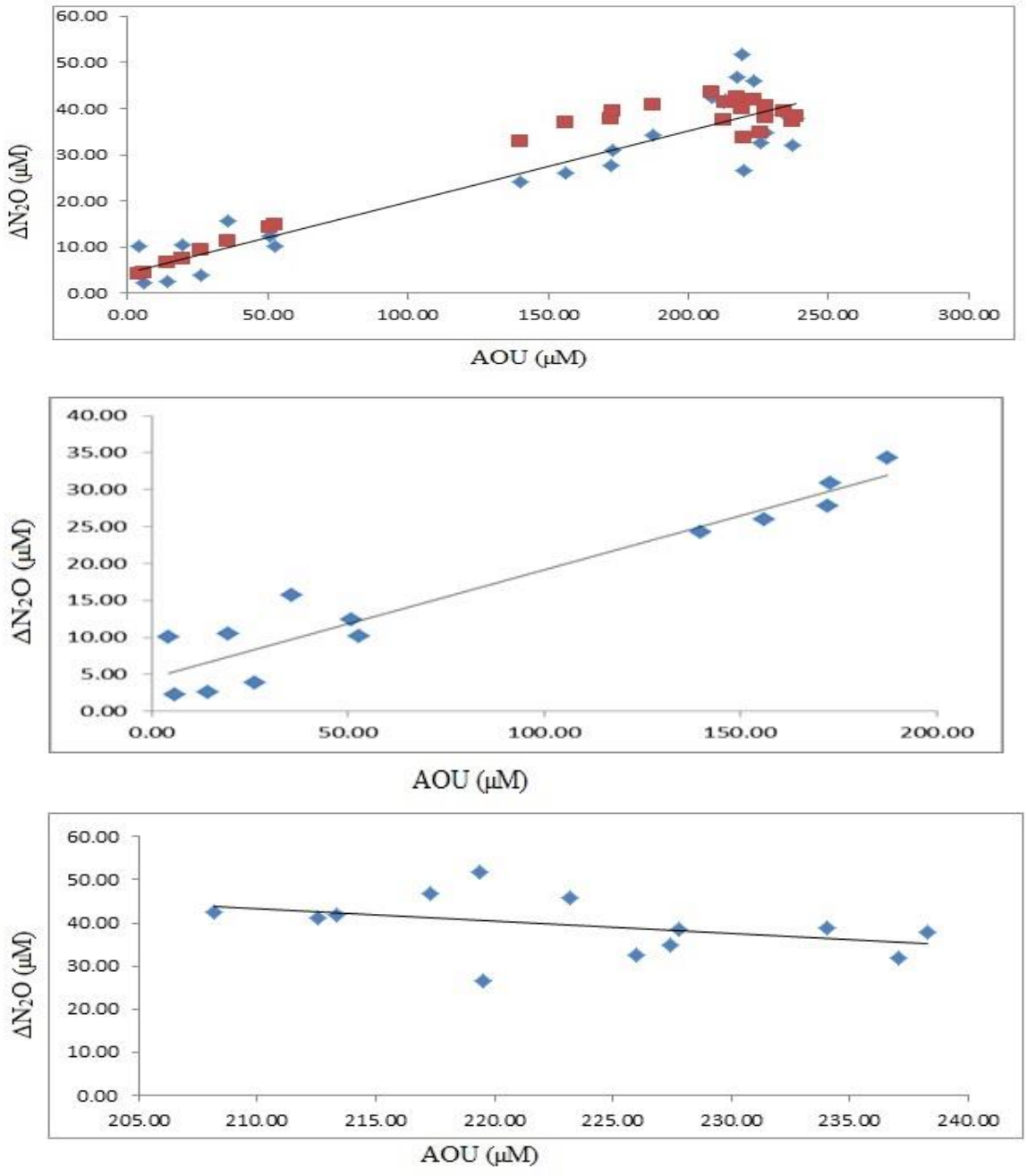

Figure 6.11: The variations and relationship between ΔN_2O vs AOU for a) entire water column b) waters having AOU < 197 µM and c) waters having AOU > 197 µM. The brown squares in figure a show ΔN_2O calculated according to Elkin's relationship (equation 6.1).

So as to conclude the ΔN_2O and AOU linear relationship points towards the existence of a nitrification dominated pathway of formation of N_2O in the NEAS regions as previously reported (Bange *et al*., 2001). However, the existence of more than one pathway cannot be completely ruled out since there are caveats against the straightforward interpretation of this relationship. The positive correlations may not be occurring simply because of nitrification, and there may be some other process active. Moreover, a completely convincing statistical relationship was not obtained for deep OMZ layers in favour a nitrification alone. If N_2O produced by nitrification is reduced subsequently by denitrification as reported (Kim and Craig., 1990; Bange *et al*., 2005) N_2O formed will obscure the ΔN_2O–AOU relationships. A concomitant existence of both the processes of nitrification pathways like ammonium oxidation and nitrifier denitrification also can be possible. At the same time both consumption and production from denitrification can also be expected to small extent at least in the OMZ (Law and Owens., 1990; Naqvi *et al*., 1990; Naqvi. S. W. A., 1991, Naqvi and Noronha., 1991, Patra *et al*., 1998, Bange *et al*., 1999, 2001). So to more clearly understand formation pathways of N_2O in these regions more detailed examination is required.

6.5.4. ΔN_2O and its relationships with nutrients

To explore the N_2O formation pathways, the ΔN_2O–$[NO^-_3]$ variations were examined. The $[NO_3^-]$ varied with similar trend among all the stations with depth and water masses (Figure 6.12). A positive $[NO_3^-]$ – ΔN_2O correlation was present as shown in figure 6.12, (slope = 1.23 and $R^2 = 0.85$). This strong positive correlation suggests the formation of N_2O below the mixed layer from organic matter remineralization associated with nitrification.The $\Delta N_2O/NO_3$ ratios were comparable to the earlier studies reported. The correlations were significant in the case of AAIW ($R^2 = 0.70$, slope = 1.4) and ICW ($R^2 = 0.45$, slope = 0.68). Here also, the ratios were more for AAIW as compared to that obtained for the AAIW in SWP reported in Chapter 3.

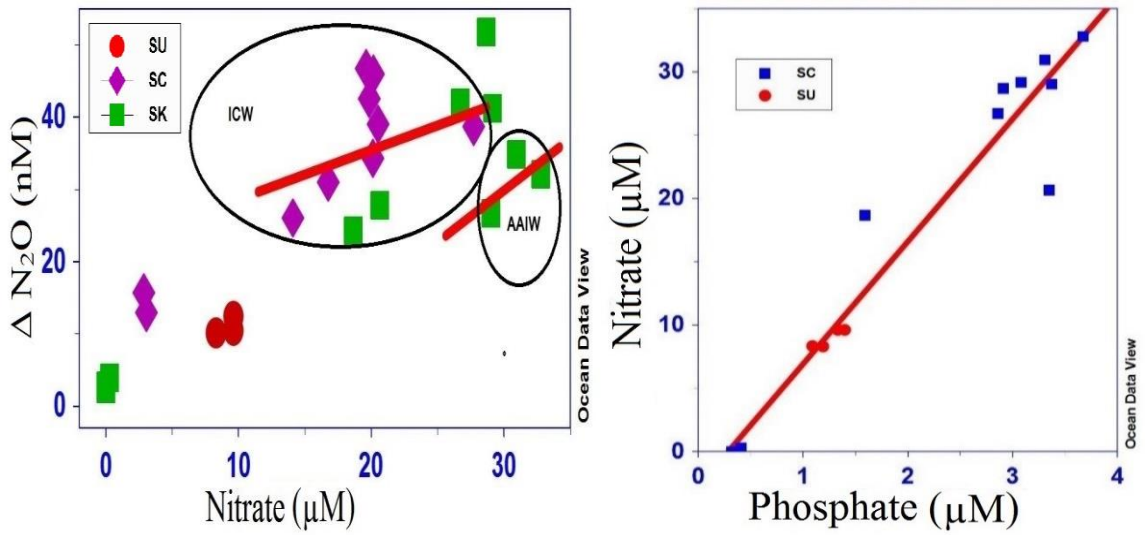

Figure 6.12: a) ΔN_2O – [NO^-_3] and b) [NO^-_3] – [PO^-_4] for SU, SC and SK.

From the Figure 6.13 it is obvious that in the 200 m- bottom depth range there is a rapid increase in nitrate concentration with depth accompanied by decrease in oxygen (increasing consumption of oxygen) and it is due to the preferential remineralization of N compared to P. It can be read from the low N: P ratios of these waters which are shown in Figure 6.13.

In order to understand the contributions of organic matter remineralization and nitrification to the nitrous oxide pathway, the nitrate to phosphate ratio was studied and is shown in Figure 6.12. For a detailed explanation, see section 3.6.1.2. Nitrate and phosphate had a strong positive correlation with $R^2 = 0.97$ and a slope close to 10. This decrease in slope from 16 to 10 can be due to the decrease in the rate of nitrification during organic matter remineralization. It can also be due to the nitrifier denitrification.

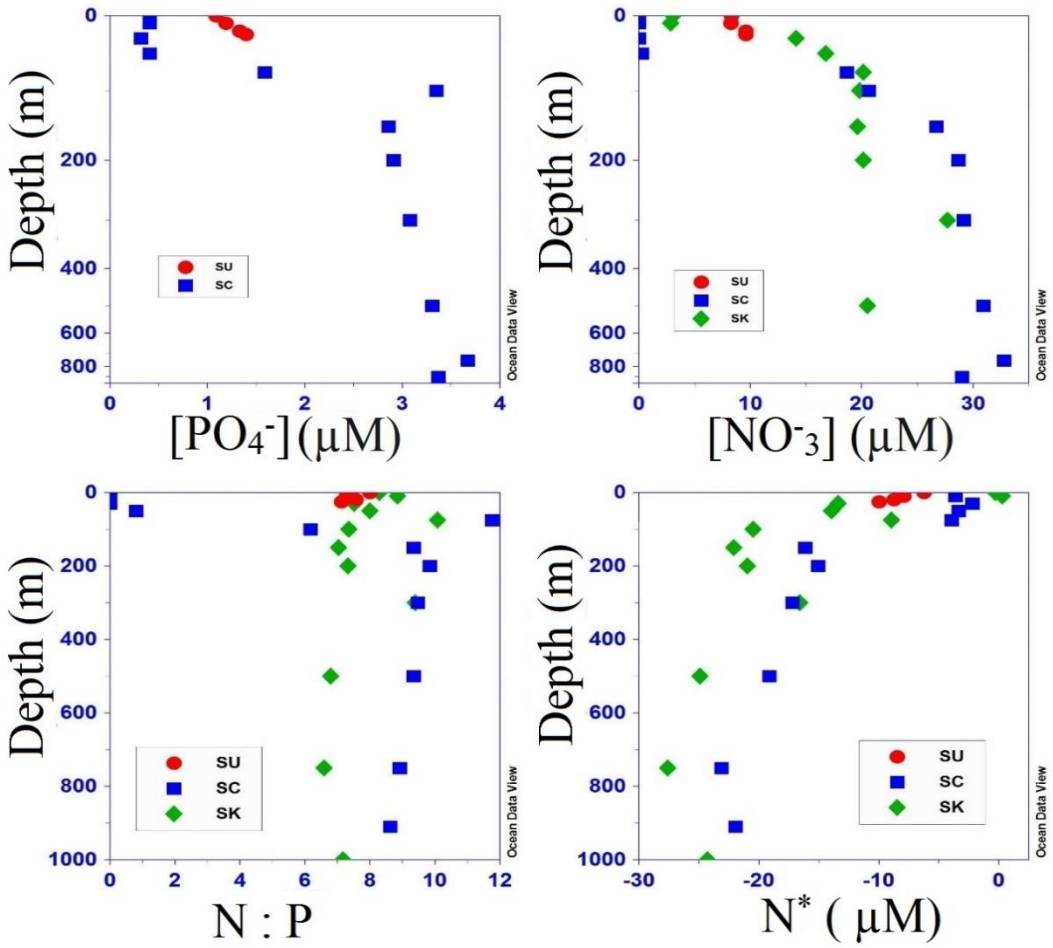

Figure 6.13: The variations of a) $[PO_4^-]$ b) $[NO_3^-]$ c) N: P ratio and d) N* along the depth for the three stations UC, SC and SK.

In 2003 Nevison speculated that remineralization would lead to an increased N_2O yield through nitrogen-rich organic materials since the mineralization of organic matter from sinking particles will supply NH^+_4 to support nitrification and as a result of which microbial activities will be increased (Ostrem *et al*., 2000). However a slight decrease in $[N_2O]$ was observed at the bottom AAIW which may be due to a decrease in nitrification at depth since the export of organic matter might have been so rapid that the nitrifying bacteria could not adapt quickly enough (Walter *et al*., 2005). In support of the former suggestion, it is also found that in OMZ zones of Arabian Sea particles sinks very rapidly due to the absence of certain biological features (Morrison *et al*., 1999). Another possible reason for the decrease in $[N_2O]$ is consumption of N_2O from sedimentary denitrification processes (Cohen and Gordon., 1978; Bange *et al*., 2001; Walker *et al*., 2010). However, the contributions of sedimentary

denitrification were found to be having a minor role in the Arabian Sea nitrogen cycle (Naik and Naqvi. S. W. A., 2002; Bange *et al*., 2005).

The possible contribution from water column denitrification also needs to be examined. Though the argument for the nitrification dominated process as a responsible pathway for N_2O formation leads from all the above results, Figure 6.9 b gives a completely different feedback. In Figure 6.13 d the N^* is an indicator of nitrate deficit ($N^* = [NO_3^-] - 16\,[PO_4^{-3}] + 2.90$ µM (Deutsch *et al*., 2001). The Figure 6.13 d shows a clear negative N^* values for both the open ocean stations in the ICW and AAIW. When a negative N^* observed with very low oxygen conditions a contribution from denitrification can be expected (Yamagishi, H., 2007). It can also be due to the existence of nitrifier denitrification. However, the role of denitrification is examined using stable isotopes and isotopomers.

Table 6.7: ΔN_2O *vs.* AOU relationship reported for various regions of Arabian Sea including the present study

Arbian Sea Region	a,b	c	r^2, no of samples	Remarks	References
Central/east	0 033, 0	5 5	(both significant at the 1% level)	AOU <197	Law and Owens, 1990
	0.310, 0	–49.4		AOU >197	Naqvi and Noronha, 1991
Somali Basin/Gulf od Aden	(0.1066 + 0.00455 *t*), 0	3.2	not given	O_2 > 0.25 mL L^{-1}, *t* is temperature in °C	De Wilde and Helder, 1997
Central/east	0.172, 0	–1.26	0 92 / 51	intermediate waters <2000 m	Patra et al, 1999
	0.1482, 0	1 03	0.71 / 31	water depths <1000 m and 0<AOU<200	
Central/west	0.1553, 0	3 05	0.65 / 59		
	0.1464, 0	1 17	0.90 / 30	water depth <500 m	
	0.049 , 0.0004	0.83	not given	water depth >500 m	Upstill- Goddard et al, 1999
Central/west	–1 58, 0.0043	151.3		only valid above OMZ	
	0.007 , 0.0006	0.25		water depth <150 m	
	0.1256, 0	1.31	0.81 / 16		Bange et al, 2001
	0.0935, 0	2.12	0 73 / 41		
Central/west	0.0799, 0	2.71	0.66 / 33		
	0.1056, 0	1.84	0.86 / 45	water depth <2000 m and O_2>0.25 mL L^{-1}	
	0.0952, 0	2 00	0.70 / 46		
	0.0609, 0	1.61	0 48 / 39		Bange et al, 2001
	0.0700, 0	2.55	0.63 / 63		
Central/west	0.0865, 0	3.27	0.70 / 51	water depth >2000 m	
	0.0910, 0	–15.0	0.14 / 46		Bange et al, 2001
	0.0672, 0	–11.0	0.25 / 15		
	0.3363, 0	–68.4	0.55 / 5		
Indian continental shelf/ northeast Arabian Sea	0.148,0	5.8	0.85/28	O_2 > 0.25 ml/l Depth- 0-1000m	Present Study
	0.146,0	4.6	0.91/14	AOU < 197	
	0.299,0	37.79	0.16/14	AOU >197	

Here ΔN_2O and AOU in µM and r stands for correlations coefficient

6.5.5: Summary of N_2O in different water masses

6.5.5.1. N_2O in the Surface mixed layer (EQW)

In the surface mixed layer, the distribution of [N_2O] varied with stations and was supersaturated with respect to the atmospheric equilibrium values. The surface waters can be divided further as upwelled and non-upwelled waters. In the non-upwelled waters of SC, the surface saturation was well above the equilibrium values. In the surface waters of SU and SK, the increase in [N_2O] is due to the presence of upwelled nutrient-rich waters. Nitrification processes are limited in the presence of light and denitrification is unlikely due to the oxygen concentrations exhibited. Therefore, it is suggested that N_2O distribution in the surface layer is most likely driven by upwelling, solubility and mixing effects. However, the role of nitrification in the surface waters are explained in the following sections.

6.5.5.2. N_2O in the Thermocline-ICW (σ_t = 24.)

Below the mixed layer mixing of water masses with different N_2O concentrations may play a role. The yield of N_2O also depends on [DO] (Goreau *et al.*, 1980; Poth and Focht., 1985; Codispoti *et al.*, 1992; Richardson. D. J., 2000), with high oxygen concentrations preventing the detectable formation of N_2O (Walter *et al.*, 2006). In the thermocline, [DO] decreased with an OMZ (σ_t 25.8-26.5) and increased nutrients to the bottom of the thermocline. Enhanced productivity and consequently lowered O_2 concentrations due to the decomposition of organic matter support the production of N_2O in waters below the productive surface waters (Antia *et al.*, 2001). There is a positive correlation between ΔN_2O *vs* AOU and ΔN_2O *vs* nitrate, and it indicates the significance of nitrification in the N_2O formation in these layers.

6.5.5.3. N_2O in the Intermediate water (AAIW, σ_t = 27.1-27.3)

The *in-situ* productions are evident from ΔN_2O, ΔN_2O *vs* AOU and ΔN_2O *vs* nitrate relationships. Age of the water mass plays a major role in the [N_2O] since N_2O could be produced *in situ* in the water column. We were unable to calculate the mean age of the water masses in the Arabian Sea. However, the literature data (Dutta *et al.*, 2001) shows that the shallow Northern Arabian Sea Intermediate waters have an average age of 163 ± 30 yr based on conventional ^{14}C methods. According to Matsumoto (2007), AAIW in the Arabian Sea region is aged than the Southwest

Pacific AAIW. AAIW of Arabian Sea had lower dissolved oxygen concentration than Southwest Pacific. Therefore, as compared to the Southwest Pacific AAIW, in the Arabian Sea [N_2O] increased.

6.6. N_2O Flux from the Northeast Arabian Sea

A detailed description of the N_2O flux estimations is given in Chapter 4. Here for F_{s-a} calculation, the overlying atmospheric mean [N_2O] was taken as 324 ppbv. G. D. Rao of National Institute of Oceanography, Vishakhapatnam, India (personal communications), provided these values. For flux calculations, monthly average wind speed data measured onboard were obtained from ORV-Sagar Sampada AWS data.

The results obtained for various parameterizations according to Liss and Merlivat (1986-LM86), Wanninkhof (1992- W92 and Nightingale (2000-N2000) are summarised and shown below in Table 6.8. Since the sampling was conducted during the rough Southwest Monsoon period sea to air flux estimate should not be as conservative as the calm seasons (Naqvi and Noronha., 1991). In order to get a more robust estimate of N_2O fluxes, these were calculated using maximum, minimum and monthly average wind speed data Table 6.8 and 6.10. The N_2O Sea to air fluxes computed in the present study compares very well with the published data from various other upwelling regions and hypoxic systems of the world oceans as mentioned in Table 6.9. Upwelling regions are found to have an average flux of more than 5 µmoles/$m^{2/}$day according to (Naqvi *et al*., 2010). The results are also in favourable agreement with the previous results reported from the different Arabian Sea regions as shown Table 6.11. Most of the earlier studies suggested the Arabian Sea as an area of higher surface saturation and increased fluxes to the atmosphere with regards to N_2O.

The integrated N_2O flux to the atmosphere from NEAS (area 2×10^5 km^2) based on the present study was calculated to 0.0009-0.49 Tg N_2O per year. These estimates are in accordance with the earlier estimates of the annually integrated N_2O-flux from the Arabian Sea which ranges between 0.16 and 1.5 Tg N_2O per year (Law and Owens., 1990; Naqvi and Noronha., 1991; Bange *et al*., 1996; Lal and Patra., 1998; Upstill-Goddard *et al*., 1999; Bange *et al*., 2001)**.** These results are

shown below in Table 6.10. Upwelling regions show higher fluxes than non-upwelling regions as expected. All stations in the present study had saturation levels and fluxes that were higher than the reported average open ocean estimates. The N_2O fluxes calculated here support earlier studies that predict much higher fluxes from the inner shelf of the Indian west coast partly due to the intensification of coastal hypoxia from anthropogenic activities (Naqvi *et al*., 2000). Moreover, Naqvi *et al.* in 2005 stated that the sea-to-air flux of N_2O from this region is under-estimated.

Table 6.8: N_2O flux calculated using different parameterization equations of Liss and Merlivat (1986) (LM86) and Wanninkhof (1992- W92) and Nightingale (2000-N2000) for the three stations.

Station ID	$\mathbf{F}_{s\text{-}a}^{LM86}$ (µmoles/$m^{2/}$day)	$\mathbf{F}_{s\text{-}a}^{W92}$ (µmoles/$m^{2/}$day)	$\mathbf{F}_{s\text{-}a}^{N2000}$ (µmoles/$m^{2/}$day)	$\mathbf{F}_{c\text{-}t}$ (µmoles/$m^{2/}$day)
Values obtained for lowest highest and average wind speeds taken three days before and after the sampling				
SU	0.3-47.7 (22.5)	0.5-101.2 (41.7)	0.8-65.8 (29.0)	Nil
SC	0.1-13.2 (6.2)	0.1-28.1(11.6)	0.2-18.6 (8.1)	1.7
SK	0.5-139.6 (15.8)	0.7-324.1(37.1)	1.4-204.7 (28.0)	1.2
Values obtained for monthly average wind speed				
SU	1.3	9.9	8.2	Nil
SC	6.2	11.6	8.1	1.7
SK	2.5	18.6	15.4	1.2

Table 6.9: Sea to air fluxes reported for various regions of world oceans (Adopted from Naqvi *et al.* 2005 and Bange *et al.* 2001).

Region	Sea to air flux (μmol/m2/day)	References
Normoxic Open Ocean	mean value , <1	Butler *et al*.,(1989), Nevison *et al*., (1995), Rhee *et al*. (2009)
Natural suboxic/ hypoxic systems		
Eastern Tropical North Pacific	-5.6-15.9	Cohen and Gordon (1978), Pierotti and Rasmussen (1980), Yamagishi *et al*.,(2005)
Eastern Tropical South Pacific	-1.1-30.7	Pierotti and Rasmussen (1980), Farias *et al*., (2009)
	-1.4-331	Cornejo *et al*., (2006)
Western Bay of Bengal	-0.1-10.7	Naqvi *et al*., (1994)
Anthropogeniccoastal hypoxic systems		
Tokyo Bay	1.51-153	Hashimoto *et al*., (1999)
Changjiang (Yangtze River)	0.7-97.5	Zhang *et al*. (2008)

Table 6.10: N_2O Flux estimates for Southwest Indian coastal side Continental shelf sector calculated according to the air-sea exchange approaches, LM86, W92 and N2000.

Station ID	$\mathbf{F}_{\text{s-a}}^{LM86}$ (T gN_2O/year)	$\mathbf{F}_{\text{s-a}}^{W92}$ (T gN_2O/year)	$\mathbf{F}_{\text{s-a}}^{N2000}$ (T gN_2O/year)	$\mathbf{F}_{\text{s-a}}^{N2000}$ (T gN/year)
SU	0.0009- 0.15	0.0010- 0.33	0.0026 - 0.21	0.0017-0.1330
SC	0.0003 - 0.04	0.0004 - 0.09	0.0007 - 0.06	0.00045- 0.03818
SK	0.0016 - 0.45	0.0020 - 1.04	0.0044 - 0.66	0.0028- 0.42

It is essential to examine the contributions from deeper thermocline layer through eddy diffusion of N_2O (Cline *et al.*, 1987; Oudot *et al.*, 1990) where highest average concentrations were observed. So as to measure this flux through diffusion across the thermocline interface as explained in detail in Chapter 4, $F_{c\text{-}t}$ was determined assuming negligible production and consumption of N_2O within the surface waters. So a steady state will be attained in which the diffusion to the surface layer will be balanced by the flux across the air-sea interface (Table 6.12).

Table 6.11: Sea to air flux of N_2O already reported from various studies in the Arabian Sea. (Adopted from Naqvi *et al*., 2005 and Naqvi *et al*., 2010).

Regions	Seat to air flux (µmol/m^2/day)	References
Central and western Arabian Sea		
Late SW Monsoon , 1986	8.64 ± 4.32–15.51 ± 7.66	Law and Owens (1990)
Spring Intermonsoon , 1995	1.70–2.77	Bange et al. (1996)
SW Monsoon, 1995	4.73–619.4	Bange et al. (1996)
Late SW Monsoon, 1994	4.7 ± 4.8–33.5 ± 20.6	Upstill-Goddard et al. (1999)
Fall Intermonsoon, 1994	–4.4 ± 3.8	Upstill-Goddard et al. (1999)
Somali Basin, SW Monsoon, 1992	260–500	de Wilde and Helder (1997)
Central and eastern Arabian Sea		
Early NE Monsoon, 1988	1.19–9.26 (4.46 ± 2.6)	Naqvi and Noronha (1991)
Sping Intermonsoon, 1994	0.06 ± 0.79	Lal and Patra (1998)
NE Monsoon, 1995	5.11 ± 4.12	Lal and Patra (1998)
SW Monsoon, 1995	10.01 ± 6.68	Lal and Patra (1998)
SW Monsoon, 1996	15.32 ± 7.66	Lal and Patra (1998)
Indian continental shelf		
SW Monsoon, 1995	3.6–271.6 (40.7 ± 53.2)	Unpublished, Naqvi et al. (2005)
Upwelling period (1997–2002)	52–351	Unpublished, Naqvi et al.(2005)
Indian shelf	−1.2–3243	Naqvi et al. (2006b)

Table 6.12: Sea to air, cross thermocline fluxes, Inferred nitrification and in situ production values for the Arabian Sea regions.

Station ID	$\mathbf{F}_{\mathbf{s\text{-}a}}^{N2000}$ (µmol/m$^{2/}$day)	Fc-t (µmol/m$^{2/}$day)	In-Situ N_2O production (µmol/m$^{2/}$day)	Fc-t/Fs-a (%)	Inferred Nitrification (mmol/m^2/d)
SC	9.1	1.7	7.4	18.6	2.9
SK	26.5	1.2	25.4	4.3	10.1

The vertical flux of N_2O was estimated at 1.7 µmol/m$^{2/}$day for the non-upwelling station SC and 1.2 µmol/m^2/day for upwelling station SK. Hence it appears that the N_2O contributions to the upwelled waters are low compared to the other station from diffusion to the mixed layer N_2O budget. The above results are in accordance with findings from the other upwelling regions (Cline *et al*., 1987) and the contributions from the thermocline to the overlying mixed layer through diffusion seems to be lower than the active denitrification zone (Naqvi *et al*., 1991). Much lower contributions of N_2O from thermocline diffusion in the upwelling regions were observed in the present study.

The two factors on which the sea to air flux depends are ΔN_2O and wind speed. Sampling occurred during the Southwest Monsoon period so the effect of wind speed will be large. The second factor is ΔN_2O; this was very high compared to global values in all these waters of Arabian Sea. In the current study, the ΔN_2O *vs* AOU and ΔN_2O *vs* $[NO_3]^-$ relationships (section 6.5) indicate the possibility of a significant contribution from nitrification, especially in the upper mixed layer. Applying estimated values to close the mixed layer N_2O budget implies the major contributions are from biological sources. Vertical diffusion along the thermocline gradient is a minor contribution. The difference between in the N_2O flux to the atmosphere and oceanic vertical diffusion were taken as the *in-situ* production. Therefore, to close the overall budget, this *in-situ* production is assumed to be due to nitrification. The nitrification rate for this study regions is calculated and shown in Table 4.5 on the assumption that uniform production will take place with depth and time in the mixed layer. The estimations were based on an average yield of 0.25 % N_2O from nitrification based on Goreau *et al*., 1980. However recent studies in the Atlantic (Kock *et al*., 2011) showed that biological activity alone couldnot close the discrepancy in Fs-a and Fc-t by acting as a source in ML. However, the role of

advection in the upwelling regions will be the significant driver of N_2O to the surface and is not estimated for the present study. This will be the reason for the high-inferred nitrification at the surface in the upwelling zone.

6.7. N_2O stable isotopic properties in the NEAS

The dual isotopic signatures of $\delta^{15}N_{Bulk}$-N_2O and $\delta^{18}O$-N_2O, the $\delta^{18}O$ variations of dissolved oxygen $\delta^{18}O$-O_2 and water $\delta^{18}O$-H_2O and SP were measured for all the stations in the Arabian Sea. The significance of all these isotopes and isotopomers are described in Chapter 5 in detail. However, the important property of stable isotopes pertinent to the study of N_2O processes is that kinetic isotopic effects mainly control the isotopic composition of N_2O, and thereby measurements of the isotopic composition of N_2O provide information on the processes involved in its formation. (Yoshida *et al*., 1984 and references therein). There are few published studies on the stable isotopic properties of N_2O in the Arabian Sea (Bange *et al*., 2008) and the available data are from denitrification zones where [DO] falls to suboxic conditions. There is a lack of detailed isotopomer datasets of N_2O for this region. Present studies dealt with all the above-explained isotopic parameters at selected stations of Arabian Sea regions and are explained below.

6.7.1. Dual isotopic signatures of N_2O

From chapter 5 descriptions under various sections of isotopes, it is obvious that N_2O-$\delta^{15}N_{Bulk}$ depletions may be due to either production through hydroxylamine or nitric oxide oxidation or associated production of N_2O through nitrification or consumption of N_2O through denitrification. However, it is also observed that the enrichments in $\delta^{15}N_{Bulk}$-N_2O during denitrification and associated consumption are very high (up to 30-40 per mil). Depletions in $\delta^{15}N_{Bulk}$ -N_2O are the signals of either nitrification or nitrifier denitrification. Earlier studies in the Pacific Ocean reported the occurrence of depletions in $\delta^{15}N_{Bulk}$ and enrichment in $\delta^{18}O$ is due to the production of N_2O through the nitrifier denitrification processes (Ostrom *et al*., 2000).

Figure 6.14 a and b illustrate the variations of the dual isotopic signatures of $\delta^{15}N_{Bulk}$-N_2O and $\delta^{18}O$-N_2O respectively for the three stations of Arabian Sea. Both $\delta^{15}N_{Bulk}$ and $\delta^{18}O$ is lower in the shallow waters up to 100 m, while higher values for both the isotope systems were observed at a depth below 100 m in the OMZ. At the 25 m shallow coastal upwelling station SU these trends were absent where almost a homogenous distribution of the isotopes was seen. The results obtained and their trends with depth are comparable to the results from same regions of Arabian Sea (Naqvi *et al*., 1998) and the suboxic regions of Eastern Tropical North Pacific (Kim and Craig., 1990; Ostrem *et al*., 2000) at the surface.

At the same time as observed in the case of [N_2O] profile (a clear double peak structure was absent), isotope distributions do not show the characteristics profiles of the denitrification zones of Arabian Sea. At this regions, large enrichments of both $\delta^{15}N_{Bulk\ N2O}$ (35.1 to 37.5 ‰) and $\delta^{18}O_{N2O}$ (79 to 85 ‰) within the OMZ (denitrifying oxygen minimum zone) as compared to the atmospheric N_2O (Naqvi *et al*., 1998a, 1998b; Yoshinari *et al*., 1997) were observed. According to this studies, N_2O in the OMZ was formed by denitrification, reduction of N_2O to N_2 should result in enriched N_2O, and depleted N_2O found above the OMZ is a product of coupled nitrification-denitrification (Naqvi *et al*., 1998; Yoshinari *et al*., 1997). Figure 6.14 a and b shows that $\delta^{15}N_{Bulk\ N2O}$ and $\delta^{18}O_{N2O}$ follows the increasing trend with depth from upper oxic waters to the bottom oxygen minimal waters. The average $\delta^{15}N_{Bulk\ N2O}$ and $\delta^{18}O_{N2O}$ values obtained for the homogeneously mixed waters of SU, surface mixed layer and bottom OMZ waters of SC and SK are shown below in Table 6.13.

$\delta^{15}N_{Bulk}$ values at the surface were depleted with regard to the atmospheric values at the upwelling regions of SU. Only smaller depletions were observed at SC stations where upwelling was absent, and it can be due to the air-sea exchange. At the open ocean upwelling station SK where a 20 m thick buoyant water layer capped the water column , so the depletions in $\delta^{15}N_{Bulk}$ values was less than that at SU. Similarly, the $\delta^{18}O$ values show a slight enrichment throughout the depth with higher values below the surface mixed layer except for the non-upwelling station SC. $\delta^{18}O$ values were close to the mean tropospheric values at the surface for SC. So the surface waters in the upwelling stations showed a characteristic feature of N_2O which is formed from either nitrification alone or through an additional contribution from the nitrifier denitrification. The non-upwelled SC shows dual isotopic characteristics closer to the mean tropospheric values which is an indication of the surface mixing and interactions with the overlying atmosphere.

Below the mixed layer, a different trend was observed in the $\delta^{15}N_{Bulk}$. The values decreased to the intermediate waters (ICW) with a minimum at the core of the OMZ, then increased to the bottom. The $\delta^{15}N_{Bulk}$ values were higher than the tropospheric mean values below the core of the OMZ. The increase was more pronounced at the less oxic waters of SK. A concomitant decrease in N_2O was seen especially in the layers of minimum [DO] in SK as compared to more oxygenated waters of SC. It is also observed that this increase in values at the bottom of the OMZ was comparatively smaller (0.5 ‰ at SC and 3 ‰ at SK) than that observed for the OMZ denitrification regions of ETNP or Arabian Sea (the enrichment were 30 ‰ and 20 ‰ respectively for the Arabian Sea and ETNP).

Similarly when the $\delta^{18}O$ values were studied an enrichment (from the surface to bottom an increase from 46 ‰ to 52 ‰) was observed throughout the depth. The minimum values were observed at the surface and maximum at the bottom below the OMZ. However, these enrichments were not as strong as that in the OMZ regions having suboxic conditions (the enrichment was 30 ‰ to 40 ‰ for the Arabian Sea and ETNP for various studies reported). So the dual isotopic signals suggest a major role of nitrification in the OMZ. Nonetheless, at SK, which is very close to the denitrification zone a considerable enrichment in isotopic values followed by a decrease in N_2O concentration can be due to the nitrifier - denitrification. These mechanisms will be teased apart further in the coming sections.

Table 6.13: The water column averages of different isotope values obtained for the various depth ranges of UC, SC and SK.

Station ID	$\delta^{15}N_{Bulk}N_2O$ (‰ vs AIR)	$\delta^{18}O$-N_2O (‰ vs VSMOW)	$\delta^{18}O$-H_2O (‰vs VSMOW)	$\delta^{18}O$-O_2 (‰vs VSMOW)	SP (‰)
UC	3.1 ± 0.6	45.0 ± 0.7	0.8 ± 0.08	23.4 ± 0.6	22.5 ± 2.2
SC-ML	5.6 ± 1.1	44.0 ± 0.1	0.5 ± 0.07	26.7 ± 3.1	17.3 ± 0.9
SC-OMZ	6.4 ± 1.4	49.9 ± 2.7	0.6 ± 0.13	33.6 ± 1.7	16.7 ± 2.9
SK-ML	5.2 ± 0.2	45.2 ± 1.7	0.6 ± 0.09	25.3 ± 1.8	15.8 ± 3.6
SK-OMZ	8.3 ± 1.6	49.6 ± 2.2	0.6 ± 0.06	33.6 ± 1.1	22.7 ± 3.4

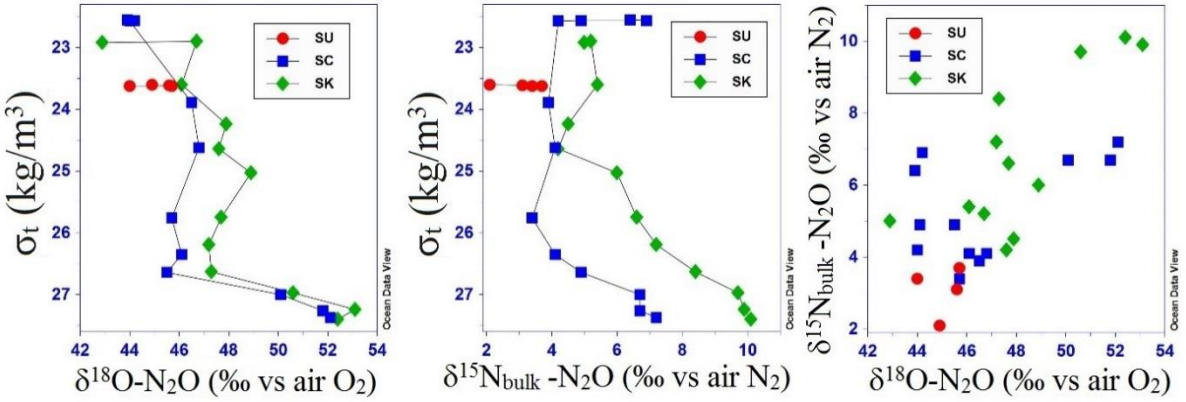

Figure: 6.14: The variations of a) $\delta^{18}O$ and b) $\delta^{15}N_{bulk}$ with density and c) $\delta^{15}N$-N_2O versus $\delta^{18}O$-N_2O relationship for the stations UC, SC and SK.

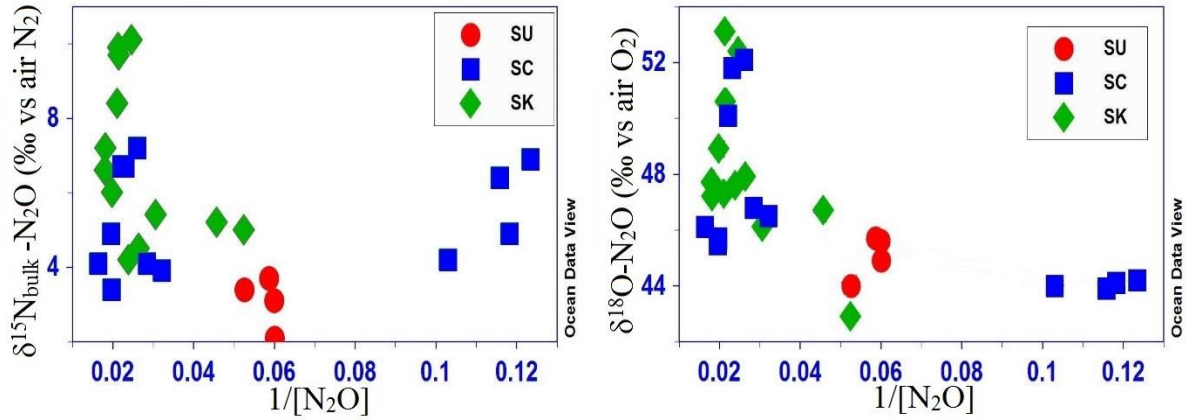

Figure 6.15: a) $\delta^{15}N$-N_2O and b) $\delta^{18}O$-N_2O variations with 1/ [N_2O] for Arabian Sea stations UC, SC and SK.

The results so far can be collectively used and interpreted further using the approach developed in Chapter 3 and 4 for the Pacific sector. ΔN_2O vs AOU and ΔN_2O vs $[NO_3]^-$ correlations are suggestive of either nitrification or more than one pathway with a significant role for nitrification. The T-S diagram and potential density measurements show mixing between the water masses to a small extent at the subsurface. Section 6.7 explains the extent of cross thermocline flux and its contributions along the isopycnal gradient. It is also clear from the same studies that there exist a significant *in-situ* production in the surface mixed layer which is assumed to be from nitrification.

The relationship between the dual isotopic signatures of N_2O was studied as shown in Figure 6.14.c and a weak positive linear relationship was obtained (R^2= 0.69 and slope of 0.51). The data from the present study compares well with previous studies in other oceanic regions were nitrification a prominent mechanism of N_2O formation. However, the extent of correlation was low compared to other studies. The positive correlation between the two independent parameters indicates that either a strong mixing process between two different pools of N_2O or a potential biological reaction that will cause isotopic fractionation exist in these waters (Yamagishi, H., 2007).

To understand further the mixing diagram was drawn for the present study (Figure 6.15 a, b) for both $\delta^{15}N_{Bulk}$-N_2O and $\delta^{18}O$-N_2O. From the two figures, it is notable that both the isotope systems follow a similar trend. This points toward mixing related fractionations or similar pathway of formation. Alternatively contributions from the isopycnal diffusion could be another reason. The absence of a wide range of dual isotopic values of N_2O along depth in a particular oceanic region suggests the absence of multiple processes in those regions as a production mechanism (Yoshinari *et al*., 1997). Both isotope systems of N_2O varied considerably with depth especially at SK followed by SC. At the shallow station UC where mixing was observed throughout the sampled depths, the clusters of $\delta^{15}N_{Bulk}$ -N_2O and $\delta^{18}O$-N_2O are all in the same phase it also suggests that N_2O at these depths may have been formed by similar mechanisms (Yoshinari *et al*., 1997). Nevertheless, at SC, the clusters of $\delta^{15}N$-N_2O and $\delta^{18}O$-N_2O are showing a moderate distribution, and all are not in the same phase (surface waters show different distribution cluster) and is suggestive of more than one pathway at this station. However, at SK the cluster distribution pattern is clearer and are not in the same phase.

6.7.2. Significance of $\delta^{18}O$ signatures

Recapping Chapter 5, the basic concepts required to understand these pathways with regard to $\delta^{18}O$ are as follows. During nitrification, the first oxygen atom added is derived from dissolved oxygen while the second one is added from water (Dua *et al*., 1979; Hollocher *et al*., 1981; Kumar *et al*., 1983). $\delta^{18}O$ of water and dissolved oxygen in the ocean differ by more than 20 ‰ (Kroopnick and Craig., 1976). The $\delta^{18}O$ of N_2O, H_2O and DO (O_2) are shown above in Table 6.13 and also in Figure 6.14. b, 6.16 a and b respectively. Though we have a large number of studies with regard to N_2O in the Arabian Sea there is a paucity of comparable data for $\delta^{18}O$ of H_2O and DO (O_2). As stated earlier this study is first of such kind which incorporates all these isotopes together for the same set of samples. Nevertheless, these results are comparable to the previous studies done by Kroopnick and Craig (1976), Kim and Craig (1990) which is detailed in Chapter 5. The $\delta^{18}O$ of O_2 at the two open ocean stations SC and SK were near to the atmospheric equilibrium values (23.5 ‰) at the surface accounting for the isotopic fractionation during the air-sea exchange (Kroopnick and Craig., 1972; Benson and Krause., 1980; Barth *et al*., 2004) and increased to the bottom with depth. The subsurface isotopically depleted waters are due to the presence of isotopically depleted oxygen released during photosynthesis (Kroopnick and Craig., 1976; Bender and Grande., 1987; Kim and Craig., 1990; Quay *et al*., 1993). At the same time, $\delta^{18}O$ of O_2 values increased to the bottom from a depth where photosynthesis will be replaced by respiration. This is due to the fact that respiratory DO consumption processes will result in heavy isotope enrichment (Quay *et al*., 1993). The $\delta^{18}O$ of H_2O in the Arabian Sea show a similar trend down the water column. In the present study, the values were ranged between 0.4 ‰ to 0.9 ‰. The results are similar to the previously reported values for different oceanic waters (Craig. H., 1961; Craig and Weiss., 1970) with $\delta^{18}O$ values very close 0 ‰ and varied by less than 0.5 ‰ for the entire water column for H_2O.

From the results on $\delta^{18}O$ of DO (O_2) and H_2O and $\delta^{18}O$ of N_2O discussed in section 6.8.1 more detailed conclusions on the nitrification can be derived as follows. Water $\delta^{18}O$ is close to zero throughout the study regions and does not vary much either with depth or location. The $\delta^{18}O$-H_2O does not show any significant correlations with dual isotope signatures of N_2O as well. In contrast to that the depth profiles of $\delta^{18}O$ of O_2 and dual isotopes of N_2O show similar variations. The observed enrichment and associated positive shifts in the $\delta^{18}O$ signatures for

both the DO and N_2O with depth shows that the source of oxygen in the N_2O is dissolved oxygen and not water (Hollocher and Nicholas., 1981; Ostrom *et al*., 2000). So it can be inferred that the production of N_2O at these depths is mainly from NH_2OH/NO (Kim and Craig., 1990; Naqvi. S. W. A., 1991). For details regarding the enrichment in $\delta^{18}O$ of N_2O see section 5.4.2. It can be further supported using $\Delta^{18}O$ which is a measure of the difference between the $\delta^{18}O$ of N_2O and $\delta^{18}O$ of O_2 (Figure 6.16. c). $\Delta^{18}O$ is more useful to distinguish the role of different nitrification processes since the $\delta^{18}O$ of N_2O formed from NH_2OH/NO will have contributions from dissolved oxygen alone, and that formed from NO_2^- will have contributions from both $\delta^{18}O$ of O_2 and H_2O. Here the bottom waters at SK have higher $\delta^{18}O$ of O_2 but the co-existing N_2O has lower $\Delta^{18}O$. In the subsurface waters, a reduced $\Delta^{18}O$ is seen to favour of nitrifier denitrification. To conclude, nitrification is the major pathway of N_2O production in these water masses. At all stations in the surface mixed layer, it is mainly through nitrification and a possible contribution from advected or diffused waters from bottom layers. A combined process through nitrification NH_2OH/NO and nitrifier denitrification prevail throughout the water column except at the surface.

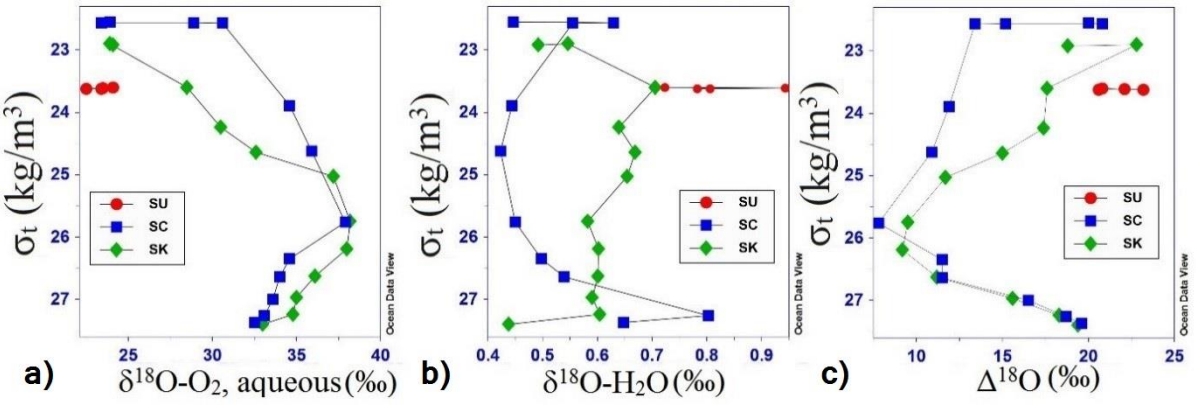

Figure 6.16: The variations of a) $\delta^{18}O$ of DO b) $\delta^{18}O$ of H_2O and c) $\Delta^{18}O$ with depth for the three stations of Arabian Sea SU, SK and SC.

6.7.3. Isotopomers and Site Preference (SP)

The principles of N_2O isotopomers (i.e. the intramolecular distribution of $\delta^{15}N$ within the linear NNO molecule) and its site preference (SP) in explaining the N_2O production processes are detailed in Section 5.4.3. This study presents the first measurements of the intramolecular distribution of $\delta^{15}N$ continental shelf regions of Indian Coast (Northeast Arabian Sea). The only existing water column depth profile of SP of central Arabian Sea is that reported by McIlvin and Casciotti in 2010. They have measured at two selected stations in the denitrifying zones of Arabian Sea.

The ratios $\delta^{15}N_\alpha$, $\delta^{15}N_\beta$ and site preference (SP) of N_2O for the three Arabian Sea stations are shown in Figure 6.17 a, b and c respectively. Average water mass distributions of the isotopomers measured for the three stations are given in Table 6.13. These results are different to the results obtained for the Central Arabian Sea stations (McIlvin and Casciotti., 2010) though we do not have results for similar regions. The trends with depth were different for three different stations for the three different parameters. As compared to the $\delta^{15}N_{bulk}$ of N_2O values isotopomer results were more variable with depth. Here also as observed in the Pacific stations at all depths $\delta^{15}N_\alpha$ was enriched with respect to $\delta^{15}N_\beta$, yielding a positive SP. $\delta^{15}N_\alpha$ in surface waters were depleted with regards to the N_2O in the troposphere (16.2 ‰) at all stations.

$\delta^{15}N_\alpha$ increased below the mixed layer to the bottom. SP values were nearly in equilibrium with respect to atmospheric values (18.7 ± 2.2 ‰) at SU and were slightly depleted at the surface with regards to that of the atmosphere at SC and SK. With a few exceptions, $\delta^{15}N_\beta$ values were depleted throughout the depth at all stations. $\delta^{15}N_\beta$ profiles were mirror images of the SP. The minimum values for the two isotopomer signatures ($\delta^{15}N_\alpha$ and SP) and the contrasting results for $\delta^{15}N_\beta$ in the mixed layer and a gradual increase in values below this depths can be inferred as the result of in-situ production of N_2O at these layers (Toyoda *et al*., 2002; Popp *et al*., 2002; Westley *et al*., 2006). The SP of N_2O derived through denitrification and nitrifier denitrification (pathway 3 of nitrification) is approximately 34 ‰ lower than nitrification (Toyoda *et al*., 2005; Sutka *et al*., 2003, 2004, 2006), and that of N_2O consumed through denitrification will similar or higher depending on the extent of consumption (McIlvin and Casciotti, 2010). It is reported that lower SP values are indicators of N_2O formation via nitrification (Yoshida and Toyoda., 2000; Toyoda *et al*., 2002; Popp *et al*., 2002). It can also be inferred that when N_2O is formed

from nitrogen having similar $\delta^{15}N$ values (through oxidation of NH_2OH/NO), a positive SP value will be observed (Popp *et al*., 2002). During consumption of N_2O (only observed during denitrification) regardless of the starting substrate material SP of N_2O will be enhanced (Westley *et al*., 2006) along with a decrease in the concentration of the N_2O. Popp *et al.* observed very depleted isotopic signatures of SP $\leq$ 0 ‰ and $\Delta^{18}O \leq 8$ ‰ for N_2O formed through nitrifier denitrification at North Pacific ALOHA stations in 2002. Now $\Delta^{18}O$ values in the previous section 6.8.3 and in Figure 6.16.c when compared with the SP values some significant points can be read. In the mixed layer, $\Delta^{18}O$ and SP do not show any signs of denitrification or nitrifier denitrification. However, SP showed a similar decreasing trend as $\Delta^{18}O$ from mixed layer up to the depth of 500-600 m (ICW) followed by an increase in the bottom layers. At the OMZ (75-500 m) SP and $\Delta^{18}O$ values indicate a combined N_2O source from both nitrification and nitrifier denitrification. This increase in $\Delta^{18}O$ and SP in OMZ was more at SK than at SC and is consistent with a decrease in DO. As a result of the rate of nitrifier-denitrification will increase.

In summary, the isotopomer data support the conclusion of others that nitrification is the primary source of N_2O in the NEAS regions located away from denitrification zone. From the results, it can be read that nitrifier-denitrification contributes to the formation pathway below the surface mixed layers at these stations.

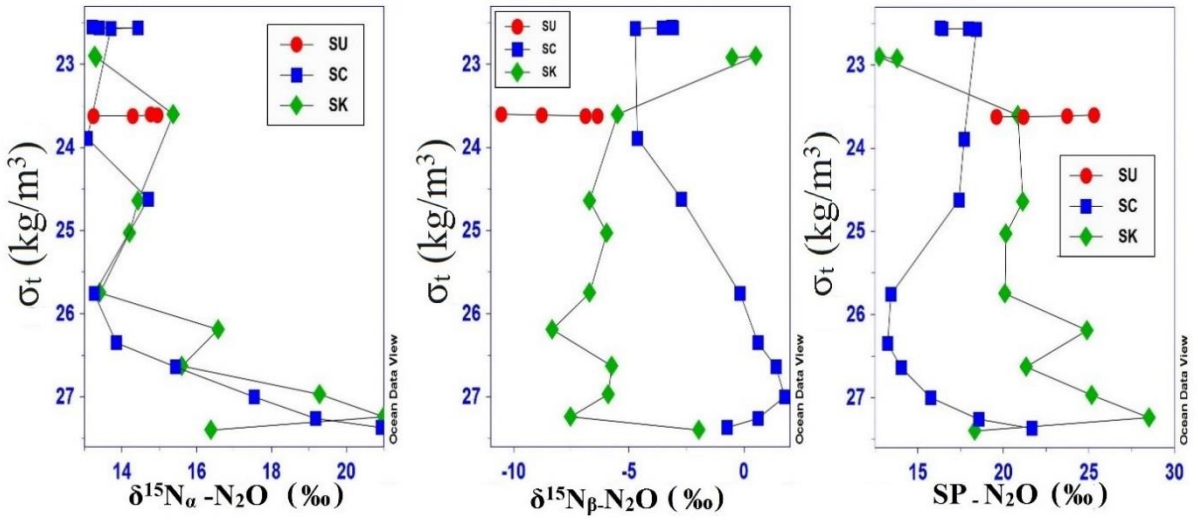

Figure 6.17: The variations of isotopomers a) $\delta^{15}N\alpha$ b) $\delta^{15}N\beta$ and c) SP for three Arabian Sea stations.

6.8. Global Budget and N_2O in the NEAS

The present study results support previous findings that the Arabian Sea is one of the world's largest contributors to the tropospheric N_2O flux (see section 6.7). An isotopic mass balance analysis of $\delta^{15}N$- $\delta^{18}O$ relationship for the present Arabian Sea study regions are given below in Figure 6.18. These results are comparable to the earlier study results of the Arabian Sea and are more realistic to close the tropospheric budget as compared to the previous results (Figure 5.22). There are studies which showed that shallower N_2O plays a major role in balancing the tropospheric N_2O in the Arabian Sea (Figure 5.22, Yoshinari *et al*., 1997; Naqvi *et al*., 1998). However, Naqvi *et al.* (1998) suggested that there may be more unknown sources or sinks of N_2O playing vital role tropospheric isotopic balance. Isotopomeric signatures are more effective tools to identify and quantify the sources and sinks of N_2O using the SP-$\delta^{15}N_\beta$ (Figure 6.18) relationship. These results are comparable to the earlier studies done by Toyoda *et al.* in 2002 (Figure 5.25) for world oceans. It is evident from the figure that these isotopomeric values are in agreement with the calculated values for oceanic flux by Yoshida and Toyoda through mass balance. Both isotopic and isotopomeric results suggest that Northeast Arabian Sea continental shelf regions along the Southwest Indian Coast will contribute to balancing the troposphere against the enriched isotopomeric composition of the stratospheric return flux by adding to the terrestrial flux.

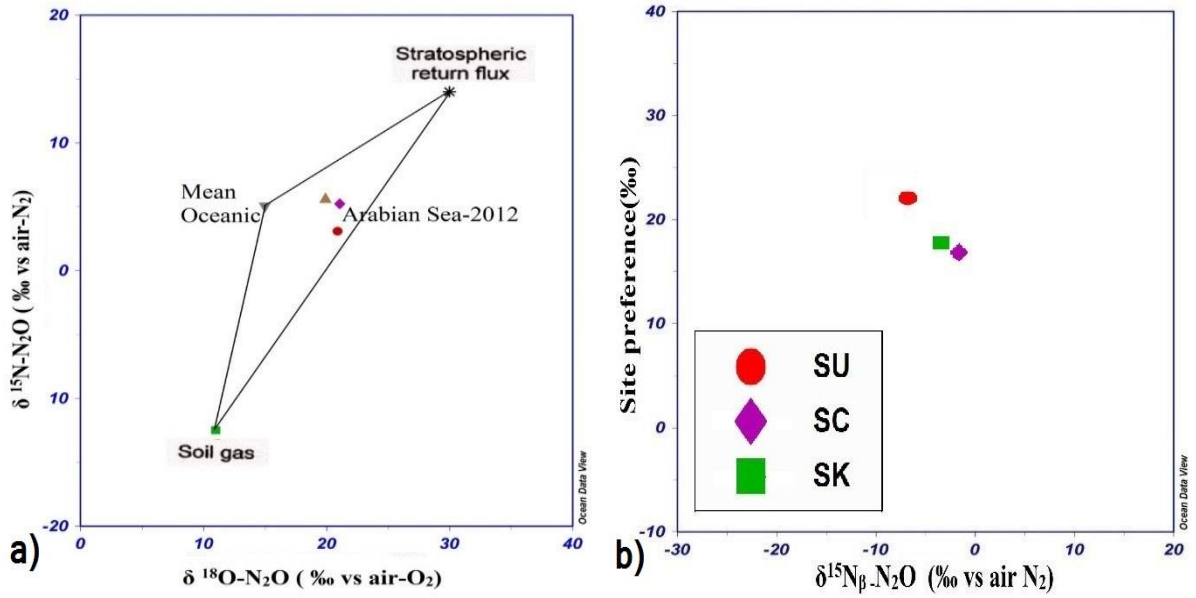

Figure 6.18: a) δ^{15}N-δ^{18}O isotope variations of three Arabian Sea stations plotted with the three end members of Kim and Craig, 1993 and b) Site preference vs $\delta^{15}N_{\beta}$ for three Arabian Sea stations

6.9. Conclusions

Even though Arabian Sea is widely studied oceanic sector with respect to N_2O present work is the first of such kind of studies which incorporates the measurements of N_2O water column distribution, sea to air and cross thermocline fluxes and water column distributions of various isotopes and isotopomers. The key findings are explained below.

- The surface saturations were higher than mean oceanic saturations indicating a strong oceanic flux to the atmosphere.
- The positive correlations between ΔN_2O and AOU and ΔN_2O and nitrate are indirect evidence for N_2O formation mainly through nitrification; however, the relationship showed the possibility of existence for more than one pathway.
- The sea to air flux calculations confirm that findings from earlier studies that the Arabian Sea as a whole appears to be a net source of N_2O. The study also in favour of suggestions from the previous studies that the gross production of oceanic N_2O has been underestimated with an annual estimate of 0.0009-0.49 Tg N_2O per year for the Indian continental shelf regions of the NEAS.
- The dual isotopic signatures of $\delta^{15}N_{bulk}$-N_2O and $\delta^{18}O$ and their relationship proved that there exists more than one mechanism responsible for N_2O production with a nitrification dominated pathway.
- The $\delta^{18}O$ of O_2 had similar trends with depth as that of $\delta^{18}O$-N_2O while $\delta^{18}O_{H2O}$ does not. This confirms that mostly N_2O is derived through nitrification process through the oxidation of NH_2OH/NO. The $\Delta^{18}O$ signatures and its variations along the depth suggest that the nitrifier denitrification exists along the OMZ.
- The SP values confirm the existence of nitrification at the surface and a combined process in the OMZ along the water column.
- The results from conventional N_2O- $\delta^{15}N_{bulk}$ and $\delta^{18}O$ and site preference - $\delta^{15}N_{\beta}$ relationship suggests that the Indian continental shelf upwelling regions of Northeast Arabian Sea as a significant source of N_2O to the atmosphere.

Chapter 7

Summary, Conclusions and Future Work

7.1. Summary and Conclusions

The greenhouse gas N_2O has a significant role in the ocean nitrogen cycle. There is a lack of N_2O data for many oceanic regions, and hence the global budget of N_2O is not fully closed. In addition, the N_2O formation pathways are still unclear. The N_2O and its production mechanisms in the selected regions of Southwest Pacific (SWP) and Northeastern Arabian Sea (NEAS) were studied in this thesis, with water samples collected from Northeast Arabian Sea (NEAS) (three sites), subtropical (9) and subantarctic sectors (3) of Southwest Pacific (SWP) Ocean (for more information see Table 2.1, Figures 2.1, 2.2 and 2.3). The Arabian Sea region is well-studied with regards to N_2O, whereas N_2O measurements are limited or unavailable at the SWP locations. In addition to measurements of N_2O concentration and ancillary parameters, N_2O formation pathways were also studied using stable isotope and isotopomer techniques. As the preliminary requirement of the project, a new analytical system to measure the concentration, stable isotopes and isotopomers of N_2O was achieved with very good accuracy and precision. The following chapter examines the variability and relationship between the measured variables, to identify the N_2O production processes in both regions.

7.1.1. N_2O in the Subtropical and Subantarctic waters in the SWP

7.1.1.1. Spatial and temporal N_2O distributions

The vertical distribution of water masses in the Geotraces, Bloom-II and Mooring stations in the SWP were similar, with STSW at the surface, AAIW below this and CPDW at the bottom. The surface waters at the SBM (Subantarctic) station was SASW. SWP water masses were oxic with DO ranging between 150-250 µM,

whereas DO was higher in the subantarctic waters at 175-280 µM. Surface waters in the subantarctic (HNLC regions) had higher nutrient concentrations than in the subtropical regions. Nutrient profiles exhibited an increase in concentrations with depth, with maximum values below 1500 m. The [N_2O] measurements in the SWP in this thesis are the first spatial and temporal measurements and provide a substantial new data set for understanding the distribution and cycling of N_2O in this region.

7.1.1.1.1.Surface water N_2O and flux

The Otago Continental Shelf N_2O water mass distributions during different sampling periods are shown in Table 3.9 (Chapter 3). During the spring 2011 and 2012 the N_2O distribution was similar in coastal waters; [N_2O] and saturations varied with MSTW > Neritic > SASW. In late autumn (May 2012), an inverse trend in the distribution of N_2O was observed, with the highest surface concentration in SASW and the lowest in MSTW. At the surface, Neritic and MSTW are supersaturated with N_2O, with an average value of 130 % in spring 2011. The saturation values decreased during late spring in 2012. However, surface waters remained supersaturated (saturation < 110 %). During May 2012 the saturation decreased and were below 100 %. The seasonal variations were less in SASW compared to the coastal waters (106 %). The results indicate that the Otago coastal regions are a source of atmospheric N_2O, similar to other coastal regions (110-190 %, Bange *et al*., 1996; Bange. H. W., 2006a, 2008).

At the open ocean stations, the minimum [N_2O] was always found in the surface layer, with an average of 7.9 ± 0.5 and 9.3 ± 0.1 nM, respectively, in the STSW of Geotraces and Bloom 2 - Mooring transects, and 11.4 ± 0.5 nM in the SASW. The surface N_2O saturation values at the SWP stations, of 101 ± 1 % (winter), and 103 ± 1 % (spring) in the STSW, and 102.5 ± 0.5 % in the SASW are similar to the global oceanic mean values (103.5%), derived by Bange *et al.* (2008), close to equilibrium with atmospheric N_2O. Calculated N_2O sea to air (F_{s-a}) fluxes (Chapter 4) indicates that irrespective of season, the Southwest Pacific Ocean between 170º

E to 140º W and 32º S to 47.5º S is a source of N_2O to the atmosphere, though the extent of the fluxes varies regionally and seasonally. The average sea to air flux values estimated for different regions is as follows. Subtropical Pacific - 0.3 - 0.7 µmol/m^2/d during spring and 0.2 µmol/m^2/d during winter, subantarctic – 1.2 µmol/m^2/d, STF - 3.7 µmol/m^2/d and coastal regions- 7.8 µmol/m^2/d. These flux density values are in accordance with the earlier reported values for open ocean and coastal waters from different oceanic regions (South Pacific - 0.4 - 6.06 µmol/m^2/d - Dore and Karl., 1996; Popp *et al*., 2002, Southern Ocean - -9.7 – 15.5 µmol/m^2/d - Farias *et al*., 2015).

The dual isotopic signatures of N_2O - N_2O-$\delta^{15}N_{bulk}$ and $\delta^{18}O$, oxygen isotopes ($\delta^{18}O$) of DO ($O_{2,aq}$) and H_2O (oceanic water), and intramolecular distribution of N_2O ($^{\alpha}N$, $^{\beta}N$ and SP) were also measured in surface waters. The dual isotopic signatures were slightly lower than atmospheric values (atmospheric N_2O-$\delta^{15}N_{bulk}$, 6.72 ± 0.12‰ and $\delta^{18}O$, 20.60 ± 0.21‰), Kaiser *et al*., 2003) at 4.2 – 5.3 ‰, 16.9 - 17.9 ‰ and 4.8 – 5.7 ‰, 17.8 - 19.7 ‰, respectively for the SWP and Otago Continental Shelf transect waters. These results are comparable to previous results in the Pacific, although with a smaller range ($\delta^{15}N_{bulk}$ values 3.7- 8.6 ‰ in North Pacific, Yoshida et al., 1988; Kim and Craig from the SWP, 1990).

$\delta^{18}O$ signatures of DO ($O_{2,aq}$) were 23.2 ‰ – 24.3 ‰, and for H_2O it was -0.05 - 0.6 ‰ from different water masses. The $\delta^{18}O_{(O2)}$ variations did not show significant differences, whereas $\delta^{18}O$ H_2O were lower for fresher coastal and SASW. The values are within the range of reported data from the Pacific (Kroopnick and Craig., 1976; Kim and Craig., 1990). The shallow well mixed neritic waters were well-mixed and showed no variation with depth with respect to $\delta^{18}O$ of DO ($O_{2,aq}$) and H_2O. The intramolecular distribution of isotopomers of ^{15}N in N_2O, S.P, was slightly depleted in the surface with respect to tropospheric values (18.7 ± 2.2 ‰). These results were comparable to reported values from South Pacific (Popp et al., 2002; Toyoda et al., 2002) and study regions (Popp et al., 2003, personal communications).

7.1.1.1.2. Subsurface N_2O

In SWP, below the surface mixed layer [N_2O] varied with respect to depths and these variations were more or less uniform in all stations except in the SBM. In the upper thermocline [DO] decreased below that of the surface (190 – 210 µM) whereas [N_2O] increased (10.7 – 12.6 nM). In the SBM the subsurface [N_2O] was close to the surface mixed layer values with an average of 11.6 ± 0.3. Generally at the SWP stations, beneath the upper thermocline [N_2O] in the AAIW increased to 16.0 - 17.5 nM. This increase is coincident with an increase in [DO] to 215-230 µM. However, at the SBM, AAIW was present in the upper thermocline at a depth of 300-750 m. The maximum [N_2O] was found in the CPDW (19.5 - 20.0 nM) where DO was the minimum (144 to 145 µM). The average AAIW saturation was 135 - 145 %, and in CPDW it was 140 - 160 %. The only intermediate water mass found at Otago transect (AAIW) had similar properties of AAIW was from other stations.

The vertical distribution of isotope ratios also showed characteristic variations with depth and water mass. The $\delta^{15}N_{bulk}$ values are depleted at the surface and enriched in the bottom waters except at the upper thermocline (Table 7.1). Similar observations of isotope depletion (up to 2 ‰) in oxic shallow waters and enrichment in less oxic bottom waters (up to 8.5 ‰) were reported for the SWP (Yoshida et al., 1984; Kim and Craig., 1990). The isotope depletions in the surface shallow waters were pronounced at a depth of 300-500 m. The changes in $\delta^{18}O$-N_2O with depth from that of the surface were more pronounced than for $\delta^{15}N_{bulk}$ and were uniform for all stations. Average isotope values for the Geotrace stations are shown below in Table 7.1. Bloom II and Mooring Stations also exhibited similar distribution pattern for the N_2O dual isotopes. The dual isotope vertical profiles at the subantarctic stations were similar to that of the subtropical stations except in the absence of the upper thermocline isotopic minimum.

The vertical profile of $\delta^{18}O$ and S.P of N_2O for the Geotraces transect are shown in Table 7.1. The results show differences among water masses, as in previous studies (Kroopnick and Craig., 1976; Kim and Craig., 1990; Popp et al., 2002). At the sub-surface oxygen minimum, an isotopic minimum was observed (except $\delta^{18}O$ of H_2O) followed by an increase in isotopic values to the bottom, with maximum isotopic enrichments coincident with the oxygen minimum. The water column distribution of $\delta^{18}O$ of H_2O at all stations was uniform and varied little with depth and locations. The Subantarctic and SWP stations had a similar trend for $\delta^{18}O$ of DO while the $\delta^{18}O$ of H_2O was slightly lower in the fresh SASW.

Table 7.1: The average of different isotopic signatures for Geotraces transect

Water Mass	DO [uM]	N_2O % Saturation	$\delta^{15}N_{bulk}$ (‰)	$\delta^{18}O$-(‰- vs air O_2)	SP (‰)	$\delta^{18}O$-O_2,(vsmow)	$\delta^{18}O$-H_2O(‰ vsmow)
UT	203.3 ± 3.4	128.8 ± 9.6	4.4	16.0	9.7	26.4	0.5
AAIW	218.0 ± 2.9	138.7 ± 6.1	5.5	18.2	11.3	27.9	0.0
CPDW	168.3 ± 1.7	140.9 ± 1.8	7.0	23.9	15.9	29.6	-0.1

7.1.1.2. N_2O production processes

SWP waters are a net source of N_2O to the atmosphere, with the major contribution from MSTW and coastal waters. The results from the present work based on conventional N_2O-$^{15}N_{bulk}$ vs $\delta^{18}O$ relationship and S.P vs $\delta^{15}N_\beta$ suggests that these oceanic regions of SWP and Sub Antarctic water masses could be a source of N_2O to the atmosphere (Chapter 5). ^{14}C and CFC-based AOU rate and N_2O production rate estimations (Chapter 3) show that in the SWP maximum N_2O is produced in

the upper thermocline (between 200-500 m). The N_2O cross thermocline flux (Fc-t) estimates indicate the contribution of N_2O diffusion from subsurface waters to the surface layer, with the discrepancy between the diapycnal N_2O flux and air-sea flux suggesting *in-situ* production in the surface mixed layer.

An inverse relationship between dissolved oxygen and N_2O is observed in the SWP. The concentration of N_2O increased down the water column as DO decreased, in agreement with previous studies (Cohen and Gordon., 1978). This inverse relationship is evidence for nitrification as the major formation pathway for N_2O. This concept was further verified and strengthened by a positive correlation between ΔN_2O and AOU. Positive correlations between ΔN_2O and nitrate (NO_3^-) observed in all study regions provides further evidence for the nitrification process as a source. The depletions in $\delta\ ^{15}N_{bulk}$ and $\delta^{18}O$ in the surface mixed layer, minima in the subsurface, and enrichment at the bottom, suggest nitrification, except in the subsurface 200-500 m (Kim and Craig., 1990). The $^{15}N_{bulk}$ vs $\delta^{18}O$ positive correlation suggests that a single process is responsible for N_2O production except in the upper thermocline. $^{15}N_{bulk}$ vs $1/[N_2O]$ and $\delta^{18}O$ vs $1/[N_2O]$ suggests that this single process is a biological process. At the depths of 200-500 m, the isotopic minimum suggests more than one mechanism responsible for N_2O production.

For further insight into the formation processes $\Delta^{18}O$ values were determined (Figure 7.1, $\delta^{18}O_{N2O}$- $\delta^{18}O$ of DO). $\Delta^{18}O$ was almost constant at all depths for subantarctic waters, while it showed a minimum (roughly 9 ‰ lower than waters above and below) at 200-500 m in SWP waters. $\Delta^{18}O$ gives information about the source of O in the N_2O, since the first O atom added to the NH_4^+ during the nitrification process is derived from $O_{2(aq)}$ followed by addition of a second O atom from water that results in the formation of NO_3^- during the second step of nitrification (Ostrom *et al.*, 2000). The isotope results suggest that the nitrification processes of hydroxylamine (NH_2OH) oxidation followed by nitric oxide (NO) oxidation are occurring. An additional contribution to the N_2O source may be from nitrifier denitrification at 200-300m in the SWP, except in the subantarctic stations

where the upper thermocline regions had oxic AAIW. ^{15}N isotope labelled incubation experiments using $^{15}NH_4Cl$ and $K^{15}NO_3$ for the selected stations of Otago Continental Shelf transect also indicated that ammonium oxidation is the major process responsible for the production of N_2O.

The S.P values are a novel addition to interpreting N_2O production processes (Popp *et al.*, 2002). The S.P of N_2O formed through denitrification, and nitrifier-denitrification (pathway 3 of nitrification) is approximately 34 ‰ lower than that formed through nitrification (Toyoda *et al.*, 2005; Sutka *et al.*, 2003, 2004, 2006). Lower SP values are indicators of N_2O formation via nitrification (Yoshida and Toyoda., 2000; Toyoda *et al.*, 2002; Popp *et al.*, 2002). It is also reported that when N_2O is formed from nitrogen having similar $\delta^{15}N$ values (through oxidation of NH_2OH/NO), a positive SP value will be observed (Popp *et al.*, 2002). Regardless of the starting substrate, the SP of N_2O will be enhanced during consumption of N_2O during denitrification (Westley *et al.*, 2006). Popp *et al.* (2002) observed highly depleted isotopic signatures of SP $\leq$ 0 ‰ and $\Delta^{18}O \leq 8$ ‰ for N_2O formed via nitrification-denitrification in the North Pacific. At all depths, a positive S.P value was observed, with an isotopomeric minimum between 200-500 m. SP values do not show considerable variations with depth in neritic and subantarctic waters. Consequently, the observed S.P values indicate nitrification, as they are not enriched above 45 ‰. However, at 200-500 m, the S.P of ~8 ‰, and above 0 ‰ at dual isotopic minimum layers, are indications of N_2O formed from denitrification.

7.1.2. N_2O in NEAS regions of Indian Ocean

Water samples were collected from the upwelling (SC and SU) and non-upwelling (SC) regions along the Southwest coast of Indian continental in the NEAS. The Arabian Sea is the most studied oceanic region with respect to N_2O, and hence the present study provides a good comparison between oxic and hypoxic waters masses. This thesis contains the first study to combine measurements of N_2O water column distribution, sea to air and cross thermocline fluxes and water column

distributions of isotopes and isotopomers in the Arabian Sea. The comparable results of N_2O with previous observations from this well-studied region, confirms the validity of the methods used in this study.

The shallow upwelling station SU was well-mixed EQW, and the other two stations (SC and SK) had EQW at the surface, ICW in the middle and AAIW at the bottom. The surface mixed layers were poorly oxygenated (20 – 120 µM) relative to the SWP, with a strong oxygen minimum zone (OMZ) present below the mixed layer (25-1000 m). The DO at the surface water masses were 41 ± 17 µM for SK and 112 ± 5 µM for SU. Nutrients were high at SK and SU at the surface (NO_3^- 15.5 µM and 9 µM respectively). In the SC, DO increased and nitrate decreased (DO = 145 ± 13 µM, nitrate = 0.07 µM) at the surface. DO decrease from the surface layers to about 20 µM at SC and to 10 µM at SK in the core of the OMZ (150-200 m).

The N_2O water column distribution showed a single peak structure, as observed in this region by earlier researchers (Cline *et al.*, 1987; Elkins *et al.*, 1978), with only one broad maximum at mid-depths. [N_2O] at the upwelling stations was 16.3 – 30.4 nM compared to 8.7 ± 0.6 nM at the non-upwelling station. The N_2O saturations in the upwelling (250 - 460 %) and non-upwelling stations (140 ± 10 %) confirms that the Arabian sea waters have greater surface supersaturation than in the SWP, even in the absence of upwelling. The N_2O supersaturation at the surface is strong evidence of a significant oceanic flux to the atmosphere. The sea to air flux calculations (F s-a) confirmed the NEAS as a net source of N_2O, with annual flux from upwelling and non-upwelling regions of 0.0017 - 0.42 and 0.00045 - 0.03818 (Tg N/year) respectively.

The N_2O-$\delta^{15}N_{bulk}$ and $\delta^{18}O$ for the three stations were comparable to previous results from Arabian Sea (Naqvi *et al.*, 1998), and also to the suboxic regions of Eastern Tropical North Pacific (Kim and Craig., 1990). Surface $\delta^{15}N_{bulk}$ and $\delta^{18}O$ values were slightly depleted with regards to the atmospheric values at 3.1 - 5.2 ‰, 20.2 – 21.8 and 4.5 - 6.7 ‰, 19.7 - 19.8 ‰, respectively, for upwelling and

non-upwelling stations. $\delta^{15}N_{bulk}$ was more depleted in the Arabian Sea surface waters compared to the South Pacific surface waters. The $\delta^{18}O$ of O_2 at the two open ocean stations SC and SK were near to the atmospheric equilibrium values (23.5 ‰) at the surface. The $\delta^{18}O$ of H_2O in the NEAS show a similar trend down the water column, between 0.4 ‰ to 0.9 ‰. The results are similar to the previously reported values for different oceanic waters (Craig and Weiss., 1970). Here also, as observed in the Pacific stations, $\delta^{15}N_{\alpha}$ was enriched at all depths with respect to $\delta^{15}N_{\beta}$, yielding a positive SP. SP values were nearly in equilibrium with respect to atmospheric values (18.7 ± 2.2 ‰) at SU, and slightly depleted at the surface with regards to that of the atmosphere at SC and SK.

In general, water column [N_2O] increased as [DO] decreased from the surface to the bottom, with highest N_2O concentration coincident with the lowest oxygen. However, in the bottom AAIW, a slight decrease in N_2O concentration was seen, with highest N_2O concentrations, of 48 ± 6.7 nM to 50.1 ± 7.0 nM in deep hypoxic waters. The N_2O saturation at the non-upwelling station SC was 418 ± 105 % in ICW and 358± 28 % in AAIW but higher at SK with saturation of 531± 98 % in ICW and 381±10 % in AAIW. At the OMZ enrichment was observed towards the bottom for the N_2O dual isotopes. $\delta^{18}O$ values followed the same trend as $\delta^{15}N_{bulk}$ while the values were enriched throughout with respect to atmospheric values. $\delta^{18}O$ of $O_{2(aq)}$ also increased to the bottom with increasing respiration, as O_2 consumption processes result in heavy isotope enrichment (Bender. M. L., 1990, Quay *et al.*, 1993). The $\delta^{18}O$ of H_2O did not show significant variation along the water column.

The positive correlation between ΔN_2O vs AOU and ΔN_2O vs nitrate suggests formation primarily via nitrification; however, the relationship also showed the possibility of existence for more than one pathway. The central waters (ICW) had a positive correlation (R^2=0.52) with a slope of 0.26 while AAIW had a slope of 0.18 (R^2=0.52). The values reported here for Arabian Sea AAIW is higher than that obtained for SWP (slope = 0.05) reflecting the higher N_2O and lower DO in

the carrying comparatively aged AAIW in the Arabian Sea (Piccard and Emery., 1990). The observed increase in ΔN_2O/AOU in the core of the OMZ is in accordance with earlier findings that the N_2O production rate increases at low concentrations of oxygen (Carlucci and McNally., 1969; Goreau *et al.*, 1980).

The $\delta^{15}N_{Bulk}$-N_2O and $\delta^{18}O$-N_2O in surface waters in the upwelling stations indicate formation by either nitrification alone, or via an additional contribution from advected N_2O from nitrifier denitrification. The non-upwelled SC shows dual isotopic characteristics closer to the mean tropospheric values, and so is more dominated by mixing with the overlying atmosphere with a lower supply of N_2O from deep water. The dual isotopic signals suggest a major role of nitrification in the OMZ. To understand further the mixing diagram was drawn for both $\delta^{15}N_{Bulk}$-N_2O and $\delta^{18}O$-N_2O. At the shallow station UC, the clusters of $\delta^{15}N_{Bulk}$ -N_2O and $\delta^{18}O$-N_2O are all in the same phase which is an indication of the same pathway of N_2O. At the SC and SK clusters of $\delta^{15}N$-N_2O and $\delta^{18}O$-N_2O are showing a moderate distribution and all are not in the same phase which shows the existence of different pathways at the surface and OMZ.

The $\delta^{18}O$ of O_2 had similar trends with depth as that of N_2O, while $\delta^{18}O$ of H_2O did not, indicating that N_2O is primarily derived via nitrification through the oxidation of NH_2OH/NO. The $\Delta^{18}O$ signatures and its variations along the depth show that nitrifier denitrification exists in the OMZ. ^{15}N in N_2O showed enriched $\delta^{15}N_\alpha$ with respect to the $\delta^{15}N_\beta$, yielding a positive ^{15}N S.P, with enrichment towards the bottom. In the mixed layer, $\Delta^{18}O$ and SP did not exhibit any indication of denitrification or nitrifier denitrification. However, SP showed a decreasing trend as $\Delta^{18}O$ from mixed layer up to the depth of 500-600 m (ICW) followed by an increase in the bottom layers. At the OMZ (75-500 m) SP and $\Delta^{18}O$ values indicate a combined N_2O source from both nitrification and nitrifier denitrification.

7.1.3. The regional differences and implications

This study reveals that N_2O has distinct features in its distribution, production mechanism, and role in marine N_2O cycling in the SWP and NEAS. Surface saturation in the NEAS are 2 – 4 times higher than the SWP waters, as the less oxic and nutrient-rich upwelled waters deliver more N_2O in the NEAS than the SWP waters. The non-upwelling open ocean surface waters had similar N_2O saturation (average 135 %) to that of the coastal SWP regions (highest surface values in SWP) but exceeded the open ocean SWP stations by a factor of 10. Increased N_2O fluxes toward the coast and their close relationship with average Chl-a (Chapter 3 and 4) is evidence of the relationship between N_2O production and productivity, with elevated organic matter production leading to high N_2O production. The relationship between organic matter production and N_2O production also reflects increased availability of reduced forms of labile nitrogen via organic matter remineralization by ammonium oxidizers.

This study also confirms that the yield of N_2O from nitrification strongly depends on the local DO and AOU, with O_2 a key factor in regulating N_2O production (and its emission to the atmosphere). Additionally, N_2O distributions in the ocean show a seasonal variability.

Regional flux estimates indicate a total annual N_2O emission of 1.85 Tg N_2O/yr from SWP. It is also estimated that the contributions to the global open ocean flux (3.2- 3.8 Tg N/yr, IPCC., 2007) is 29-34 % and to the global oceanic Flux (5.4 Tg N/yr, IPCC., 2007) is 24 % from the study regions. The contribution from the New Zealand Coastal regions to the global continental shelf emissions (1.5 Tg N/yr) were estimated to 6 %. The integrated N_2O flux to the atmosphere from Indian continental shelf regions of NEAS (area 2×10^5 km^2) based on the present study was calculated to 0.0009-0.49 Tg N_2O per year, in accordance with earlier estimates of 0.16 and 1.5 Tg N_2O per year (Law and Owens., 1990; Naqvi and Noronha., 1991; Bange et al., 2000). The contributions from Indian Continental

Shelf represent 0.2 to 10 % of the total global ocean N_2O budget. This research supports suggestions from previous studies (Naqvi *et al.*, 2005) that the gross production of oceanic N_2O has been underestimated in these waters.

N_2O emissions from the NEAS exceeds those from the SWP on a per unit area basis. There were also large discrepancies between the sea-to-air flux out of the mixed layer and the N_2O supply from upper thermocline due to diapycnal mixing in in the SWP. This infers N_2O production from nitrification within the mixed layer. In our study, the inferred surface layer nitrification rates responsible for this discrepancy are within the range of rates reported by earlier researchers from these regions (Law *et al.*, 2003). Calculated N_2O production rates are maximum in subsurface waters and are 4-6 times higher than the mixed layer production rates in SWP. In subsurface waters, an oxygen decrease and increased N_2O production from both nitrification and nitrifier-denitrification were inferred in the SWP except in subantarctic waters where AAIW was present as a subsurface water. Below the upper thermocline, regions dissolved oxygen concentration decreased and more N_2O was formed from nitrification in AAIW and CPDW.

In NEAS upwelling and non-upwelling zone, high N_2O production can be seen throughout the entire water column (especially in the OMZ, Figure 7.1). Wind-driven vertical mixing and offshore water transport make it difficult to evaluate separately the N_2O that is produced above or under the pycnocline. As an exercise, we estimated the cross thermocline flux, which suggests a surface N_2O source at all stations. The N_2O surface production mechanism was nitrification as inferred from the stable isotopes (Figure 7.1). However, a major contribution will be from the upwelling of subsurface waters. Below the mixed layer in the OMZ (ICW) nitrification and nitrifier denitrification was responsible for the production of N_2O and it was nitrification alone in the bottom AAIW.

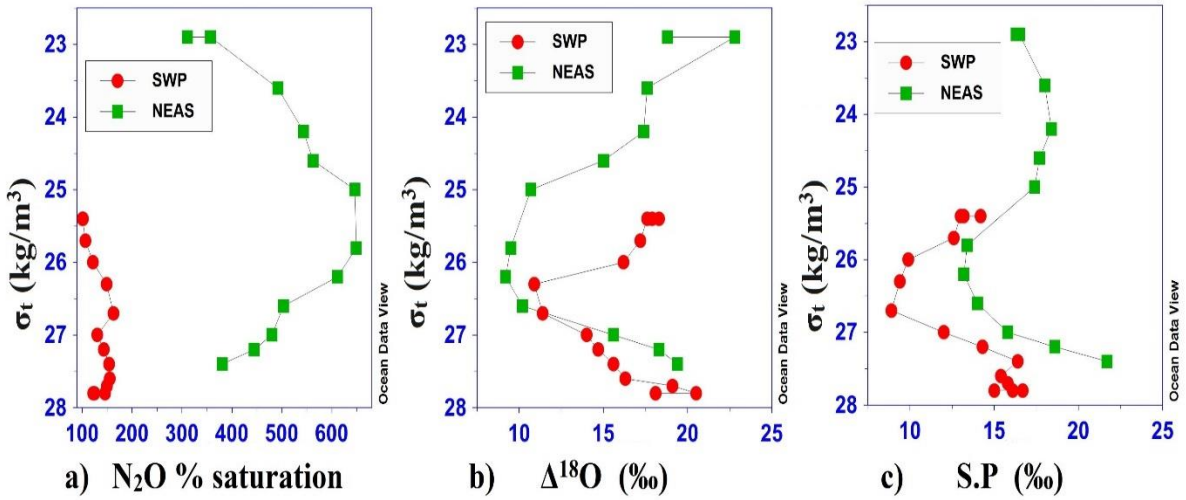

Figure 7.1: The water column profile of a) N_2O percentage saturation b) $\Delta^{18}O$ and c) S.P of N_2O for the selected stations from SWP and all the three NAS stations (The legends are same for all figures).

Figure 7.1 illustrates the existence of different pathways of nitrification and nitrifier denitrification in both regions. Although surface waters and the AAIW have relatively higher $\Delta^{18}O$ (20-25) as a result of nitrification in the NEAS. A reduced $\Delta^{18}O$ (below 10) is seen in the OMZ indicating nitrifier-denitrification. In the mixed layer or AAIW, SP (Figure 7.1c) did not show any signs of denitrification (above 40) or nitrifier denitrification (close to 10). However, SP has a decreasing trend similar to $\Delta^{18}O$ from the mixed layer to depths of 500-600 m (ICW) followed by an increase in the bottom waters. At the OMZ (75-600 m) SP and $\Delta^{18}O$ values indicate a combined N_2O source from both nitrification and nitrifier denitrification. This increase in SP and accompanying a decrease in [N_2O] in the bottom OMZ at SK when [DO] falls below 10 µM is again a strong evidence for nitrifier denitrification. The results also show that at SWP the major production pathway is nitrification via NH_2OH/NO except at the subsurface (200-500 m), where a combination of nitrification and nitrifier denitrification is responsible for the production.

This study suggests that due to the different oxygen concentrations in the OMZ between the two regions, significant differences in N_2O cycling occur that are reflected in N_2O saturations, isotopic signatures and emissions.

7.2. Suggestions for future work

Very few studies on oceanic N_2O have been reported, and hence there is a paucity of N_2O data available from for the world oceans. The present study has shown the importance of the OMZs for N_2O production; these regions are predicted to expand in the future in many parts of the ocean (Stramma *et al.*, 2008) hence N_2O production in the ocean will be enhanced (Naqvi *et al.*, 2010). The present work enabled the inter-hemispheric comparisons of oceanic N_2O distribution and production pathways incorporating stable isotopes and isotopomers. Yet studies on N_2O isotope and isotopomers, in particular, are still available only for few portions of the world oceans. So the major focus of the future oceanic research on N_2O will be to produce more spatial and temporal coverage of the concentration and isotopic data to track the N_2O changes in more detail according to the changing climate and ocean.

Detailed N_2O stable isotope measurements as explained in Chapter 5 and 6 signifies the importance of hydroxylamine (NH_2OH) in N_2O formation through nitrification. In 2011, Casciotti *et al.* suggested that the measurement of $\delta^{18}O$ in NH_2OH is necessary to understand the isotope effect for O incorporation by certain bacteria.

The next step related to the current research is, therefore, to successfully develop a method which will help to measure both concentration of NH_2OH and its stable isotope signatures. Some preliminary works have been already started towards the goal of method development.

Earlier it was suggested that Ammonia-Oxidizing Archaea (AOA) bacteria could also be a potential contributor to the N_2O formation during nitrification. Recently it is confirmed that AOA is able to produce N_2O both in suboxic and even in some of the oxic waters in 2012 (Santro *et al.*, 2011; Loscher *et al.*, 2012). It is also reported that AOA rather than AOB could be the key organisms for the oceanic production of the N_2O. Formation of N_2O through AOB and AOA will have a

significant difference in their pathways which can be traced through ^{18}O labelled H_2O, or ^{18}O labelled O_2 which will provide information about the mechanism of archaeal ammonia oxidation (Casciotti *et al*., 2011). So one of the future focuses on N_2O in Southwest Pacific, and Southern ocean regions will understand the role of AOA in its formation through culture experiments.

As reported the oceans are warming (Barnett *et al*., 2005; Levitus *et al*., 2005) and accompanying changes in the bacterial community structure will result in changes in N_2O production. Temperature changes in the oceans will affect the solubility of N_2O. Increase in ocean temperature will lead to the decrease in N_2O long-term storage capacity of the deep oceans. This effect will temporarily strengthen the N_2O source, which will eventually disappear again once the temperature change levels off and the system attains equilibrium. In addition, non-uniform warming will cause increased stratification in the water column which in effect will weaken the oceanic N_2O source (Freing *et al*., 2012). The ocean acidification due to the decrease in the oceanic pH resulting from the increase in atmospheric CO_2 will shift NH_3–NH_4^+ equilibrium towards NH_4^+. Beman *et al*. (2011) showed that nitrification rates and associated N_2O production during nitrification decreased when the pH was lowered to values expected to occur in the future ocean. However, laboratory experiments are required to verify the consequences of ocean acidification on N_2O production through nitrification. Otago Continental Shelf transect will be a perfect platform to conduct experiments on the effects of ocean warming and acidification. For more than one decade studies are being conducted in this bimonthly time series transect to study the warming-related changes. Ocean acidification experiments also started here in this transect very recently. So it will provide all the required background information that can be adapted for further work.

References

Abril, G. and Iversen, N. 2002, Methane dynamics in a shallow non-tidal estuary (Randers Fjord, Denmark), Mar. Ecol. Prog. Ser, 230: 171–181.

Albritton, D., Derwent, R., Isaksen, I., Lal, M. and Wuebbles, D. 1996, Trace gas radiative forcing indices in Climate Change 1995, The Science of Climate Change (ed. J. T. Houghton, L. G. Meira).

Alldredge, A. L. and Cohen, Y. 1987**,** Can microscale chemical patches persist in the sea Microelectrode study of marine snow, faecal pellets, Science, 235: 689-691.

Altabet, M. A., Higginson, M. J. and Murray, D. W. 2002, The effect of millennial-scale changes in Arabian Sea denitrification on atmospheric CO_2, Nature, 415(6868): 159-162.

Antia, A. N. 2005, Solubilization of particles in sediment traps: revising the stoichiometry of mixed layer export. Biogeosciences, 2: 189–204.

Arp, D. J. and Stein, L. Y. 2003, Metabolism of inorganic N compounds by ammonia-oxidizing bacteria. Crit. Rev. Biochem. Mol. Biol., 38: 471–495.

Baer Jones, K. N. 2012**,** Characterising the biological uptake of CO_2 across the Subtropical Frontal Zone (Thesis, Doctor of Philosophy), University of Otago, Retrieved from http://hdl.handle.net/10523/2355.

Bange, H. W., Rapsomanikis, S. and Andreae, M. O. 1996, Nitrous oxide emissions from the Arabian Sea, Geophys.Res. Lett., 23: 3175- 3178.

Bange, H. W. and Andreae, M. O. 1999, Nitrous oxide in the deep waters of the world‘s oceans. Global Biogeochemical Cycles, 13: 1127-1135.

Bange, H. W., Andreae, M. O., Lal, S., Law, C. S., Naqvi, S. W. A., Patra, P. K., Rixen, T. and Upstill-Goddard, R. C. 2001, Nitrous oxide emissions from the Arabian Sea: A synthesis, Atmospheric Chemistry and Physics, 1: 61-71.

Bange, H. W. 2004, Air-sea exchange of nitrous oxide and methane in the Arabian Sea: A simple model of the seasonal variability, Indian Journal of Marine Sciences, 33(1): 77–83.

Bange, H. W., Naqvi, S. W. A. and Codispoti, L. A. 2005, The nitrogen cycle in the Arabian Sea, Progress in Oceanography, 65: 145-158. 10.1016/j.pocean.2005.03.002

Bange, H.W. 2006, New directions: the importance of oceanic nitrous oxide emissions, Atmospheric Environment, 40: 198–199.

Bange, H. W. 2008, Gaseous nitrogen compounds (NO,N2O,N2,NH3) in the ocean, in: Nitrogen in the Marine Environment, 2 ed., edited by: Capone, D. G.,

Bronk, D. A., Mulholland, M. R., and Carpenter, E. J., Academic Press/Elsevier 51-94.

Bange, H. W., Freing, A., Kock, A. and Löscher, C. R.: Marine pathways to nitrous oxide, in: Nitrous Oxide and Climate Change, edited by: Smith, K., Earthscan, London, 36-62, 2010.

Bange, H. W., Bergmann, K., Hansen, H. P., Kock, A., Koppe, R., Malien, F.,and Ostrau, C. 2010, Dissolved methane during hypoxic events at the Boknis Eck time series station (Eckernforde Bay, SW Baltic Sea), Biogeosciences, 7, 1279-1284.

Barford, C. C., Montoya, J. P., Altabet, M. A. and Mitchell, R. 1999, Steady-state nitrogen isotope effects of N2 and N2O production in Paracoccusdenitrificans, Appl. Environ. Microbiol., 65(3): 989–994.

Barnard, R., Leadley, P. W. And Hungate, B. A. 2005, Global change, nitrification, and denitrification: A review, Global Biogeochem. Cycles, 19, GB1007, doi:10.1029/2004GB002282

Barnes, J. and Owens, N. J. P. 1998, Denitrification and nitrous oxide concentrations in the Humber estuary, UK, and adjacent coastal zones, Mar. Pollut. Bull., 37(3–7): 247–260.

Barth, J. A. C., Tait, A. and Bolshaw, M. 2004, Automated analyses of $^{18}O/^{16}O$ ratios in dissolved oxygen from 12-mL water samples, Limnol. Oceanogr. Method.

Bates, B. C., Kundzewics, Z. W., Wu, S., Palutikof, J. P. (eds), 2008,Climate Change and Water, IPPC Technical paper VI, IPCC Secretariat, Geneva, 210 pp.

Beal, L. M., Molinari, R. L., Chereskin, T. K. and Robbins, **P. E.** 2000, Reversing bottom circulation in the Somali basin, Geophys. Res. Lett., 27: 2565 – 2568.

Bender, M. L. and Grande, K. D. 1987, Production, respiration, and the isotope geochemistry of O_2 in the upper water column, Global Biogeochemical Cycles, 1: 49-59.

Bender, M. L. 1990, The $d^{18}O$ of dissolved O_2 in seawater: A unique tracer of circulation and respiration in the deep sea, Journal of Geophysical Research, 95: 22243-22252.

Benson, B. B. and Daniel Krause, Jr. 1980, The concentration and isotopic fractionation of gases dissolved in freshwater in equilibrium with the atmosphere, 1. Oxygen: Limnology and Oceanography, vol. 25, no. 4, p. 662-671.

Berounsky, V. M. and Nixon, S. W. 1990, Temperature and the annual cycle of nitrification in waters of Narragansett Bay. Limnology and Oceanography, 35: 1610-1617.

Bianchi, M., Feliatra, F., Treguer, P., Vincendeau, M. A. and Morvan, J. 1997, Nitrification rates, ammonium and nitrate distribution in upper layers of the water column and in sediments of the Indian sector of the Southern Ocean, Deep-Sea Res. II, 44(5): 1017– 1032.

Bostock, H. C., Sutton, P. J., Williams, M. J. M. and Opdyke, B. N. 2013, Reviewing the circulation and mixing of Antarctic Intermediate Water in the South Pacific using evidence from geochemical tracers and Argo float trajectories, Deep Sea Research Part I: Oceanographic Research Papers, 73: 84-98.

Bouwman, A. F. 1996, Direct emission of nitrous oxide from agricultural soils, Nutrient Cycling in Agroecosystems, 46: 53-70.

Boyd, P., LaRoche, J., Gall, M., Frew, R. and McKay, R. M. L. 1999, Role of iron, light, and silicate in controlling algal biomass in subantarctic waters SE of New Zealand, *J. Geophys. Res.*, 104(C6)**:** 13395-13408.

Boyd, P. W., Crossley, A. C., DiTullio, G. R., Griffiths, F. B., Hutchins, D. A., Queguiner, B., Sedwick, P. N. and Trull, T. W. 2001, Effects of iron supply and irradiance on phytoplankton processes in subantarctic waters south of Australia, *J. Geophys. Res*., 106(31): 573–84.

Boyd, P. W. 2002, Environmental factors controlling phytoplankton processes in the Southern Ocean, Journal of Phycology, 38(5)**:** 844-861.

Bradford, J. M. 1980, New Zealand region. Primary productivity surface. Oceanographic Institute Chart Miscellaneous Series, 42, Wellington, New Zealand.

Bradford, J. M. and Taylor, F. J. 1980, New Zealand region reactive phosphorus (October- April) surface. Oceanographic Institute Chart Miscellaneous Series, 46, New Zealand.

Bradford-Grieve, J., Chang, F. H., Gall, M., Pickmere, S. and Richards, F. 1998, Size-fractionated phytoplankton standing stocks and primary production during austral winter and spring 1993 in the Subtropical Convergence regions near New Zealand, New Zealand Journal of Marine and Freshwater Research, 31: 201-224.

Bremner, J. M. and Blackmer, A. M. 1981, Terrestrial nitrification as a source of atmospheric nitrous oxide, C.C. Delwiche, Editor, Denitrification, Nitrification, and Nitrous Oxide, Wiley, New York (1981), pp. 151–170

Bremner, J. M. and Mulvaney, C. S. 1982**,** Nitrogen-Total. In: A.L. Page, R.H. Miller (Eds). Methods of Soil Analysis. Part 2. 2nd ed. Agron. Monogr. 9. ASA and SSSA, Madison, WI, pp: 595-624.

Brenninkmeijer ,C. A. M. and Ro¨ckmann,T. 1999, Mass Spectrometry of the Intramolecular Nitrogen Isotope Distribution of Environmental Nitrous Oxide Using Fragment-ion Analysis, Rapid Commun. Mass Spectrom, 13: 2028–2033.

Brettar, I. and Rheinheimer, G. 1991, Denitrification in the central Baltic: Evidence for H_2S oxidation as motor of denitrification at the oxic–anoxic interface. Mar. Ecol. Prog. Ser. 77: 157–169.

Burling, R. W. 1961, Hydrology of Circumpolar Waters south of New Zealand, Bull. N.Z. Dep. scient. ind. Res. 143. 66 pp.

Butler, J. H., Elkins, J. W., Brunson, C. M., Egan, K. B., Thompson, T. M., Conway, T. J. and Hall, B. D. 1988, Trace gases in and over the west Pacific and east Indian Oceans during the El Nin˜o Southern Oscillation event of 1987, Data Rep. ERL ARL-16, Natl. Oceanic and Atmos. Admin., Silver Spring, Md., 104 pp

Butler, J. H., Elkins, J. W., Thompson, T. M. and Egan, K. B. 1989, Tropospheric and dissolved N_2O of the West Pacific and East Indian Oceans during the El Nin˜o Southern Oscillation event of 1987, J. Geophys. Res., 94(D12), 14: 865–14,877.

Butler, E. C. V., Butt, J. A., Lindstrom, E. J., Teldesley, P. C., Pickmere, S and Vincent, W. F. 1992, Oceanography of the Subtropical Convergence Zone around southern New Zealand. New Zealand Journal of Marine and Freshwater Research 26(2): 131- 154.

Cabello, P., Roldan, M. D. and Moreno, V. C. 2004, Nitrate reduction and the nitrogen cycle in archaea, Microbiology-SGM, 150: 3527–3546.

Canfield, D. E., Glazer, A. N., and Falkowski, P. G. 2010, The Evolution and Future of Earth's Nitrogen Cycle, Science, 330, 192-196, 10.1126/science.1186120.

Capone, D. 1996, A biologically constrained estimate of oceanic N2O flux. Mitteilungen, Internationale VereiningungfuerTheoretische und AngewandteLimnologie, 25: 105–113.

Casciotti K. L., Buchwald C., Santoro A. E. and Frame, C. 2011, Assessment of nitrogen and oxygen isotopic fractionation during nitrification and its expression in the marine environment, Methods Enzymol. 486: 253–280. 10.1016/B978-0-12-381294-0.00011-0

Carlucci, A. F., Mcnally, P. M. 1969, Nitrification by marine bacteria in low concentrations of substrate and oxygen. Limnology and Oceanography 14(5): 736–739.

Carton, J. A., Seidel, H. F. and Giese, B. S. 2012, Detecting historical ocean climate variability, *J. Geophys. Res.*, 117. C02023 DOI: 10.1029/2011JC007401.

Catalano, G. 1987**,** An improved method for the determination of ammonia in seawater, Mar Chem., 20: 289–295.

Charpentier, J., Farias, L., Yoshida, N., Boontanon, N. and Raimbault, P. 2007, Nitrous oxide distribution and its origin in the central and eastern South Pacific Subtropical Gyre, Biogeosciences, 4: 729–741.

Charpentier, J., Farias, L. and Pizarro, O. 2010, Nitrous oxide fluxes in the central and eastern South Pacific, Global Biogeochemical Cycles, 24. Artn Gb3011 Doi 10.1029/2008gb003388.

Chiswell, S. M., Bradford-Grieve, J., Hadfield M. G. and Kennan S. C. 2013, Climatology of surface chlorophyll-a, autumn-winter and spring blooms in the southwest Pacific Ocean. J. Geophys. Res. Oceans , 118, 1003–1018.

Christensen, P. B., Nielson, L. P., Sorensen, J. and Revsbech, N. P. 1990, Denitrification in nitrate-rich streams: Diel and seasonal variation related to benthic oxygen metabolism. Limnol. Oceanogr., 35: 640-651.

Clark, D. R., Rees, A. P. and Joint, **I**. 2008, Ammonium regeneration and nitrification rates in the oligotrophic Atlantic Ocean: Implications for new production estimates, Limnology and Oceanography, 53 (1): 52–62.

Cline, J. D., Wisegarver, D. P. and Kelly-Hansen, K. 1987, Nitrous oxide and vertical mixing in the equatorial Pacific during the 1982-1983 El Niño, Deep Sea Research Part A. Oceanographic Research Papers, 34: 857-873.

Codispoti, L. A. and Christensen, **J. P.** 1985, Nitrification, denitrification and nitrous oxide cycling in the eastern tropical South Pacific Ocean, Marine Chemistry, 16: 277-300.

Codispoti, L. A., Elkins, J., Yoshinari, T., Friederich, G. E., Sakamoto, C. M. and Packard, T. T. 1992, Nitrous oxide cycling in upwelling regions underlain by low oxygen waters. In ‘‘Oceanography of the Indian Ovean’’ (Desai, B. N., ed.). Oxford & IBH Publishing, New Delhi. pp. 271–284.

Codispoti, L. A., Brandes, J. A., Christensen, J. P., Devol, A. H., Naqvi, S. W. A., Paerl, H. W. and Yoshinari, T. 2001, The oceanic fixed nitrogen and nitrous oxide budgets: Moving targets as we enter the Anthropocene?, Sci. Mar., 65: 85–105.

Codispoti, L. A., Yoshinari, T. and Devol, A. H. 2005, Suboxic respiration in the oceanic water column, in: Respiration in Aquatic Ecosystems, edited by: del Giorgio, P. A. and Williams, P. J. Le B., Oxford University Press, 225–247.

Cohen, Y. and Gordon, **L. I**. 1978, Nitrous oxide in the oxygen minimum of the eastern tropical North Pacific: Evidence for its consumption during nitrification and possible mechanism for its production, Deep Sea Res., 25: 509-524.

Cohen, Y. and Gordon, **L. I.** 1979**,** Nitrous oxide production in the ocean, J. Geophys. Res., 8d: 347-353.

Cornejo, M. 2006, Temporal variability in N_2O water content and its air-sea exchange in an upwelling area off central Chile (36°S), *Mar. Chem.*, 101: 85–94, doi:10.1016/j.marchem.2006.01.004

Craig, H. and Gordon, **L. I.** 1963, Nitrous oxide in the ocean and marine atmosphere, Geochim.Cosmochim. Acta., 27: 949-955.

Craig, H. and Weiss, R. F. 1970, The GEOSECS 1969 inter calibration station: introduction and hydrographic features and total CO_2-O_2 relationships, Journal of Geophysical Research, 75: 7641-7647.

Crutzen, P. J. 1970, The influence of nitrogen oxides atmospheric ozone content, QJ.Roy.Meteor.Soc., 96: 320-325.

Currie, K. I. and Hunter, K. A. 1998, Surface water carbon dioxide in the waters associated with the subtropical convergence, east of New Zealand, Deep-Sea Research I, 45: 1765-77.

Currie, K. I. and Hunter, K. A. 1999, Seasonal variation of surface water CO2 partial pressure in the Southland current, east of New Zealand, Marine Freshwater Research, 50: 375-382.

Currie, K. I, Reid, M. and Hunter, K. A. 2009, Interannual variability of carbon dioxide drawdown by subantarctic surface water near New Zealand, Biogeochemistry, 104:23–34. doi:10.1007/s10533-009-9355-3

de Bie, M. J. M., Starink, M., Boschker, H. T. S., Peene, J. J. and Laanbroek, H. J. 2002, Nitrification in the Schelde estuary: Methodological aspects and factors influencing its activity, FEMS Microbiology Ecology, 42:99–107.

de Jong, J. T. M., den Das, J., Bathmann, U., Stoll, M. H. C., Kattner, G., Nolting, R. F. and de Baar, H. J. W. 1998, Dissolved iron at subnanomolar levels in the Southern Ocean as determined by ship-board analysis, Analytica Chimica Acta, **377**(2-3)**:** 113-124.

Deutsch, C., Gruber, N., Key, R. M. and Sarmiento, J. L., 2001, Denitrification and N_2 fixation in the Pacific Ocean, Global Biogeochemical Cycles, 15: 483–506.

Dore, J. E. and Karl, D. M. 1996, Nitrification in the euphotic zone as a source of nitrite, nitrate, and nitrous oxide at Station ALOHA, Limnol. Oceanogr., 41, 1619-1628.

Dore, J. E., Popp, B. N., Karl, D. M. and Sansone, F. J. 1998, A large source of atmospheric nitrous oxide from subtropical North Pacific surface waters, Nature, 396: 63–66.

Denman, K. L., Brasseur, G., Chidthaisong, A., Ciais, P., Cox, P. M., Dickinson, R. E., Hauglustaine, D., Heinze, C., Holland, E., Jacob, D., Lohmann, U., Ramachandran, S., Da Silva Dias, P. L., Wofsy, S. C. and Zhang, X. 2007. "'Coupling between changes in the climate system and biogeochemistry', in:". In *Climate Change 2007: The Physical Science Basis. Contribution of Working Group I to the Fourth Assessment Report of the Intergovernmental Panel on Climate Change* Edited by: Solomon, S., Qin, D., Manning, M., Chen, Z., Marquis, M., Averyt, K. B., Tignor, M. and Miller, B. R. 500–587. Cambridge, UK and New York, , US: Cambridge University Press

Devol, A. H. 2008. Denitrification including Anammox, in: Nitrogen in the Marine Environment, Capone, D., Bronk, D., Mulholland, M., and Carpenter, E. (Eds.), Academic Press 263-301.

De Wilde, H. P. J. and Helder, W. 1997, Nitrous oxide in the Somali Basin: The role of upwelling, Deep-Sea Res. II, 44(6–7): 1319–1340.

De Wilde, H. P. J. and de Bie, M. J. M. 2000, Nitrous oxide in the Schelde estuary: production by nitrification and emission to the atmosphere, Marine Chemistry, 69: 203-216.

Diaz, R. J. and Rosenberg. R. 2008, Spreading dead zones and consequences for marine ecosystems, Science, 321: 926-928.

Dua, R. D., Bhandari, B. and Nicholas, **D. J. D.** 1979, Stable isotope studies on the oxidation of ammonia to hydroxylamine by Nitrosomonaseuropaea, FEBS Lett., 106: 401– 404.

Duce, R. A., LaRoche, J., Altieri, K., Arrigo, K. R., Baker, A. R., Capone, D. G., Cornell, S., Dentener, F., Galloway, J., Ganeshram, R. S., Geider, R. J., Jickells, T., Kuypers, M. M., Langlois, R., Liss, P. S., Liu, S. M., Middelburg, J. J., Moore, C. M., Nickovic, S., Oschlies, A., Pedersen, T., Prospero, J., Schlitzer, R., Seitzinger, S., Sorensen, L. L., Uematsu, M., Ulloa, O., Voss, M., Ward, B. and Zamora,L. 2008, Impacts of anthropogenic atmospheric nitrogen on the open ocean, Science, 320: 893-897. DOI 10.1126/science.1150369.

Ekman, V. W. 1905, On the influence of the Earth's rotation on ocean-currents, Arkiv for Matematik, AstronomiochFysi, 2 (11): 1–52.

Elkins, J. W., Wofsy, S. C., McElroy, M. B., Kolb, C. E. and Kaplan, W. A. 1978, Aquatic Sources and Sinks for Nitrous-Oxide, Nature, 275 (5681): 602–606.

Falkowski, P. G. 1997, Evolution of the nitrogen cycle and its influence on the biological sequestration of CO_2 in the ocean, Nature, 387: 272-275.

Falkowski, P. G. and Godfrey, L. 2008, Electrons, life, and the evolution of Earth's oxygen cycle. Philosophical Transactions of the Royal Society of London, Series B, Biological Sciences, 363 (1504):2,705–2,716.

Farías, L., Paulmier, A. and Gallegos, M. 2007, Nitrous oxide and N-nutrient cycling in the oxygen minimum zone off northern Chile, Deep-Sea Research I, 54: 164-180.

Farias, L., Castro-Gonzalez, M., Cornejo, M., Charpentier, J., Faundez, J., Boontanon, N. and Yoshida, N. 2009, Denitrification and nitrous oxide cycling within the upper oxycline of the eastern tropical South Pacific oxygen minimum zone, Limnology and Oceanography, 54: 132-144.

Farias, L., Florez-Leiva, V., Besoain, V., Sarthou, G. and Fernández, C. 2015, Dissolved greenhouse gases (nitrous oxide and methane) associated with the naturally iron-fertilized Kerguelen region (KEOPS 2 cruise) in the Southern Ocean, Biogeosciences, 12: 1925–1940.

Feely, R. A., Sabine, C. L., Schlitzer, R., Mecking, S. and Greeley, **D.** 2004, Oxygen Utilization and Organic Carbon Remineralization in the Upper Water Column of the Pacific Ocean, Journal of Oceanography, 60: 45–52.

Fenchel, T. and Blackburn, T. H. (eds.) (1979). Mineral cycling. Academic Press, London.

Ferguson, S. J. 1994, Denitrification and its control, Antonie Van Leeuwenhoek, International Journal of General and Molecular Microbiology, 66: 89-110.

Firestone, M. K. and Tiedje, J. M. 1979, Temporal change in nitrous oxide and dinitrogen for denitrification following onset of anaerobiosis, Appl. Environ. Microbiol., 38: 673-679.

Firestone, M. K. and Davidson E. A. 1 9 8 9, Microbiological basis of NO and N_2Oproduction and consumption in soil . Pages 7–21 in Andreae MO,Schimel DS, eds. Exchange of Trace Gases between Terrestrial Ecosystems and the Atmosphere. New York : John Wiley & Son s .

Forster, G., Upstill-Goddard, R. C., Gist, N., Robinson, C., Uher, G. and Woodward, E. M. S. 2009, Nitrous oxide and methane in the Atlantic Ocean between 50 degrees N and 52 degrees S: Latitudinal distribution and sea-to-air flux, Deep-Sea Res Pt Ii, 56: 964-976, 10.1016/j.dsr2.2008.12.002.

Forster, P., Ramaswamy, V., Artaxo, P., Bernsten, T., Betts, R., Fahey, D. W., Haywood, J., Lean, J., Lowe, D. C., Myhre, G., Nganga, J., Prinn, R., Raga, G., Schulz, M. and Van Dorland, R. 2007, Changes in atmospheric constituents and in radiative forcing. In: Solomon, S.; Qin, D.; Manning, M.; Chen, Z.; Marquis, M.; Averyt, K.B.; Tignor, M.; Miller, H.L. (eds). Climate Change 2007: The Physical Science Basis. Contribution of Working Group I to the Fourth Assessment Report of the Intergovernmental Panel on Climate Change, pp. 129-234. Cambridge University Press, Cambridge, United Kingdom and New York, NY.

Frame C. H. and Casciotti K. L. 2010, Biogeochemical controls and isotopic signatures of nitrous oxide production by a marine ammonia-oxidizing bacterium, Biogeosci. Discuss. 7: 3019–3059.

Frame, C. H., Deal, E., Nevison, C.D. and Casciotti K.L. 2014, N_2O production in the eastern South Atlantic: Analysis of N_2O stable isotopic and concentration data, Global Biogeochem. Cycles, 28, 1262–1278, doi:10.1002/2013GB004790.

Francis, C. A., Beman, J. M. and Kuypers, M. M. M. 2007, New processes and players in the nitrogen cycle: the microbial ecology of anaerobic and archaeal ammonia oxidation, ISME J., 1: 19– 27.

Freing, A., Wallace, D. W. R., Tanhua, T., Walter, S. and Bange, H. W. 2009, North Atlantic production of nitrous oxide in the context of changing atmospheric levels, Global Biogeochem. Cycles, 23: GB4015, doi:10.1029/2009GB003472.

Freing, A., Wallace, D and Bange, H. W. 2012, Global oceanic production of nitrous oxide, Philos, T. R. Soc. Lon. B, in press, doi:10.1098/rstb.2011.0360.

Fuhrman, J. A. and Capone, D. G. 1991, Possible Biogeochemical Consequences of Ocean Fertilization. Limnology and Oceanography, 3 (8): 1951-1959.

Fujii, A., Toyoda, S., Yoshida, O., Watanabe, S., Sasaki, K and Yoshida, N. 2013, Distribution of nitrous oxide dissolved in water masses in the eastern subtropical North Pacific and its origin inferred from isotopomer analysis, J. Oceanogr., 69(2), 147–157, doi:10.1007/s10872-012-0162-4.

Galloway, J. N., Townsend, A. R., Erisman, J. W., Bekunda, M., Cai, Z. C, and Freney, J. R. 2008, Transformation of the nitrogen cycle: Recent trends, questions, and potential solutions, Science, 320: 889–892.

Ganachaud, A. 2007, Southwest Pacific ocean circulation and climate experiment (SPICE). part 1. scientific background, Tech. rep., NOAA.

Garcia, H. E., and Gordon, L. I. 1992, Oxygen solubility in seawater. Better fitting equations. Limnol. Oceanogr. 37, 1307–1312

Garner, D. M. 1959, The Subtropical Convergence in New Zealand surface Waters, N.Z. Jl Geol. Geophys., 2*:* 315-37.

Garner, D. M. 1961, Hydrology of New Zealand coastal waters Wellington, NZ Department of Scientific and Industrial Research Bulletin 138. 85 p

Goreau, T. J., Kaplan, W. A., Wofsy, S. C., McElroy, M. B., Valois, F. W. and Watson, S. W. 1980, Production of NO_2^- and N_2O by nitrifying bacteria at reduced concentrations of oxygen, Appl.Environ. Microbiol., 40: 526-532.

Grasshoff, K., Kremling, K. and Ehrhardt, M. 1999, Methods of seawater analysis, 3rd Edn., Wiley-VCH, Weinheim, Germany.

Groffman, P. M. 1991, Ecology of nitrification and denitrification in soil evaluated at scales relevant to atmospheric chemistry. In: Rogers, J.E., Whitman, W.B. (Eds.), Microbial production and consumption of greenhouse bases: Methane, nitrogen oxides, and halomethanes.American Society for Microbiology, Washington, DC.

Gruber, N. in *Carbon Climate Interactions* (edsOguz, T. & Follows, M.) 97–148 (Kluwer Academic, Dordrecht, 2004)

Gruber, N. 2008 The marine nitrogen cycle: overview and challenges, in: Nitrogen in the marine environment, 2 ed., edited by: Capone, D. G., Bronk, D. A., Mulholland, M. R., and Carpenter, E. J., Academic Press/Elsevier, 30-79.

Gruber, N. and Galloway, J. N. 2008, An Earth-system perspective of the global nitrogen cycle, Nature, 451: 293-296. 10.1038/nature06592.

Gupta, A. K., D. M. Anderson and Overpeck, J. T., 2003, Abrupt changes in the Asian southwest monsoon during the Holocene and their links to the North Atlantic Ocean, Nature, 421, 354 – 357

Gu¨ven, D., Dapena, A., Kartal, B., Schmidt, M., Maas, B., van de Pas-Schoonen, K., Sozen, S., Mendez, R., Op den Camp, H. J. M., Jetten, M. S. M., Strous, M. and Schmid, I. 2005, Propionate oxidation by and methanol inhibition of anaerobic ammonium-oxidizing bacteria, Appl. Environ. Microbiol., 71(2): 1066–1071.

Hall, S. J. and Matson, P. A. 1999, Nitrogen oxide emissions after nitrogen additions in tropical forests, Nature, 400: 152–155.

Hamersley, M. R., Lavik, G., Woebken, D., Rattray, J. E., Lam, P., Hopmans, E. C., SinninghеDamst´e, J. S., Kr¨uger, S., Graco, M., Guti´errez, D. and Kuypers, M. M. M. 2007, Anaerobic ammonium oxidation in the Peruvian oxygen minimum zone, Limnol. Oceanogr., 52: 923–933.

Hannig, M., Lavik, G., Kuypers, M. M. M., Woebken, D., Martens, H. W., and J¨urgens, K. 2007, Shift from denitrification to anammox after inflow events in the central Baltic Sea, Limnol. Oceanogr., 52, in press.

Hartmann, D. L., Klein Tank, A. M. G., Rusticucci, M., Alexander, L.V., Brönnimann, S., Charabi, Y., Dentener, F. J., Dlugokencky, E. J., Easterling, D. R, Kaplan, A., Soden, B. J., Thorne, P.W., Wild, M. and Zhai, P. M. 2013, Observations: Atmosphere and Surface. In: Climate Change 2013: The Physical Science Basis. Contribution of Working Group I to the Fifth Assessment Report of the Intergovernmental Panel on Climate Change [Stocker, T.F., D. Qin, G.-K. Plattner, M. Tignor, S.K. Allen, J. Boschung, A. Nauels, Y. Xia, V. Bex and P.M. Midgley (eds.)]. Cambridge University Press, Cambridge, United Kingdom and New York, NY, USA.

Hashimoto, L. K., Kaplan, W. A., Wofsy, S. C. and McElroy, M. B. 1983, Transformation of fixed nitrogen and N2O in the Cariaco Trench, Deep-Sea Res., 30(6A): 575–590.

Hashimoto, S., Gojo, K., Hikota, S., Sedai, N. and Otsuki, A. 1999, Nitrous oxide emissions from coastal waters in Tokyo Bay, *Mar. Environ. Res*, 47: 213–223. doi: 10.1016/S0141 1136(98)00118-4.

Hattori A., Goering, J. J. and Boisseau, D. B. 1978, Ammonium oxidation and its significance in the summer cycling of nitrogen in oxygen depleted Skan Bay, Unalaska Island, Alaska, Marine Science Communications, 4: 138-151.

Heath, R. A. 1976, Oceanic circulation in the head of the Hikurangi Trench, east of New Zealand, New Zealand Journal of Marine and Freshwater Research 10(4): 651- 674.

Heath, R. A., 1983, Observations on Chatham Rise currents, New Zealand Journal of Marine and Freshwater Research, 17: 321-330.

Heath, R. A. 1985a, A review of the physical oceanography of the seas around New Zealand-1982, New Zealand Journal of Marine and Freshwater Research, 19: 79-124.

Heath, R. A. 1985b, Large-scale influence of the New Zealand seafloor topography on western boundary currents of the South Pacific Ocean, Australian Journal of Marine and Freshwater Research, 36: 1-14.

Helland-Hansen, B. 1916, Nogenhydrografiskemetoder. Skand. Naturforskermate, 357 -359: Kristiana

Ho, D. T., Law, C. S., Smith, M. J., Schlosser, P., Harvey, M. and Hill, P. 2006, Measurements of air-sea gas exchange at high wind speeds in the Southern Ocean: Implications for global parameterizations, Geophys. Res. Lett., 33: L16611. doi:10.1029/2006GL026817.

Hollocher, T. C., Tate, M. E. and Nicholas, **D. J. D.** 1981, Oxidation of ammonia by Nitrosomonaseuropaea, J. Biol. Chem., 256: 10,834–10,836.

Hopkin, J., Shaw, A. G. P. and Challenor, P. G. 2010, The Southland Front, New Zealand: Variability and ENSO correlations, Continental Shelf Research, 30: 1535-1548.

Horrigan, S. G., Carlucci, A. F. and Williams, P. M. 1981, Light inhibition of nitrification in sea-surface films, Journal of Marine Research, 39: 557-565.

Houghton, J., G. Jenkins, and J. Ephraums (Eds.), Climate Change: The Intergovernmental Panel on Climate Change Scientific Assessment, 364 pp. pp., Cambridge University Press, Cambridge, United Kingdom and New York, NY, USA, 1990.

Houghton, J. T. et al. (eds) (2001) The scientific basis: contribution of working group I to the third assessment report of the intergovernmental panel on climate change. Climate Change, Cambridge University Press, pp 525–582.

Houtman, T. H. J. 1967, Water masses and fronts in the Southern Ocean south of New Zealand, Bull. N.Z. Dep. scient. ind. Res., 174: 39.

Howarth, R. W., Billen, G., Swaney, D., Townsend, A., Jaworkski, N., Lajtha, K., Downing, J. A., Elmgren, R., Caraco, N., Jordan, T., Berendse, F., Freney, J., Kudeyarov, V., Murdoch, P. and Zhu, Z. L. 1996, Regional nitrogen budgets and riverine N-and-P fluxes for the drainages to the North-Atlantic Ocean-Natural and human influences, Biogeochemistry, 35: 75-139.

Huesemann, M. H., Skillman, A. D. and Crecelius, E. A. 2002, The inhibition of marine nitrification by ocean disposal of carbon dioxide, Mar. Pollut. Bull., 44: 142–148.

Hynes, R. K. and Knowles, R. 1984, Production of nitrous oxide by Nitrosomonaseuropaea: Effects of acetylene, pH and oxygen, Canadian Journal of Microbiology, 30: 1397-1404.

IPCC, Intergovernmental Panel on Climate Change, IPCC First Assessment Report, 1996, Cambridge University Press, ISBN 0-521-56431-X (pb: 0-521-56437-9).

IPCC, 2001, Intergovernmental Panel on Climate Change, IPCC Third Assessment Report, Synthesis Report. Contribution of Working Groups I, II and III to the Third Assessment Report of the Intergovernmental Panel on Climate Change Cambridge Univ. Press, Cambridge, ISBN 0-521-80769-7.

IPCC, 2007, Climate Change: The Physical Science Basis. Contribution of Working Group I to the Fourth Assessment Report of the Intergovernmental Panel on Climate Change, Cambridge University Press, Cambridge, UK and New York, NY, USA.

IPCC, 2013, Climate Change: The Physical Science Basis. Contribution of Working Group I to the Fifth Assessment Report of the Intergovernmental Panel on Climate Change, Cambridge University Press, Cambridge, UK and New York, NY, USA.

Jain, A. K., Li, Z., Naik, V., Wuebbles, D. J., Good, D. A., J.C. Hanson, J. S. Francisco .2001.Evaluation of lifetime and radiative forcing on climate for 1,2,2,2-Tetrafluorethyl Trifluoromethyl Ether (CF3OCHFCF3), J. Geophys. Res., 106, 12,615-12,618

Jetten, M. S. M., Sliekers, O., Kuypers, M., Dalsgaard, T., van Niftrik, L., Cirpus, I., van de Pas- Schoonen, K., Lavik, G., Thamdrup, B., Le Paslier, D., Johannessen, O. M., G. Subbaraju, and Blindheim, J. 1987. Seasonal variations of the oceanographic conditions off the southwest coast of India during 1971–1975, Fisk Dir. Skr Hav Unders, 18, 247– 261

Op den Camp, H. J. M., Hulth, S. 2003, Anaerobic ammonium oxidation by marine and freshwater planctomycete-like bacteria, Appl. Microbiol. Biotechnol., 63(2): 107–114.

Jillett, J. B. 1969, Seasonal hydrology of waters of the Otago Penninsula, south-eastern New Zealand, New Zealand Journal of Marine and Freshwater Research, 3(3): 349-375.

Jillett, J. B. 1976, Zooplankton associations of Otago Peninsula, south-eastern New Zealand, related to different water masses, New Zealand Journal of Marine and Freshwater Research, 10: 543-557.

Jin, X. and Gruber, N. 2003, Offsetting the radiative benefit of ocean iron fertilization by enhancing N_2O emissions, Geophysical Research Letters, 30(24): 2249. doi:10.1029/2003GL018458.

Junge, C. and Hahn, J. 1971, N2O measurements in the North Atlantic, J. Geophys. Res., 76: 8143-8146.

Junge, C., Buckholt, B., Schutz, K. and Beck, **R.** 1971, N2O measurements in air and in seawater over the Atlantic, 'Meteor' Forschungsergebnisse, Reihe B, 6: 1-11.

Junk, G. and Svec, H. 1958, The absolute abundance of nitrogen isotopes in the atmosphere and compressed gas from various sources, GeochimicaetCosmochimicaActa, 14: 234-243.

Kaiser, J., Ro¨ckmann, T. and Brenninkmeijer, C. A. M. 2003, Complete and accurate mass spectrometric isotope analysis of tropospheric nitrous oxide, Journal of Geophysical Research, 108. doi: 10.1029/2003JD003613

Kaplan, W. A. and Wofsy, S. C. 1985, The biogeochemistry of nitrous oxide: A review. In: Jannasch, H.W., Williams, P.J.Leb (Eds.), Advances in aquatic microbiology, Volume 3. Academic, London, UK

Kara, A. B., Rochford, P. A. and Hurlburt, H. E. 2000, An optimal definition for ocean mixed layer depth, J. Geophys. Res., 105 (16): 803– 16, 821.

Karl, D. M., Knauer, G. A. and Martin, J. H. 1988, Downward flux of particulate organic matter in the ocean: A particle decomposition paradox, Nature, 332: 438-441.

Karl, D. M. 1999, A sea of change: Biogeochemical variability in the North Pacific Subtropical Gyre, Ecosystems, 2: 181.

Karl, D., Michaels, A., Bergman, B., Capone, D., Carpenter, E., Letelier, R., Lipschultz, F., Paerl, H., Sigman, D. and Stal, L. 2002, Dinitrogen fixation in the world's oceans, Biogeochemistry, 57: 47–98.

Kartal, B., Kuypers, M., Lavik, G., Schalk, J., Op den Camp, H. J. M., Jetten, M. S. M. and Strous, M. 2007, Anammox bacteria disguised as denitrifiers: nitrate reduction to dinitrogen gas via nitrite and ammonium, Environ. Microbiol., 9: 635–642.

Keeling, R., Najjar, R., M. Bender, and Tans, P. 1993, What atmospheric oxygen measurements can tell us about the global carbon cycle, Global Biogeochem. Cycles, 7: 37 – 67.

Keeney, D. R. and Nelson, D. W. 1982. Nitrogen in organic forms. Pages 643-698 in A. L. Page *et al.* , Eds. Methods of soil analysis. Part 2. Agronomy No. 9, American Society of Agronomy, Madison, WI.

Kessarkar, P. M., Rao, P. V., Naqvi, S. W. A., Chivas, A. R. and Saino, T., Fluctuations in productivity and denitrification in the southeastern Arabian Sea during the Late Quaternary, Current Science, VOL. 99, NO. 4, 2010. 485-491.

Khalil, M. A. K. and Rasmussen, R. A. 1992, The global sources of nitrous oxide, J. Geophys. Res. 97, 14651–14660.

Khalil, M. A. K., Rasmussen, R. A. and Shearer, M. J. 2002, Atmospheric nitrous oxide: Patterns of global change during recent decades and centuries, Chemosphere, 47: 807–821.

Kim, K. R. and Craig, H. 1990, Two-isotope characterization of N_2O in the Pacific Ocean and constraints on its origin in deep water, Nature, 347: 58-61.

Kim, K. R. and Craig, H. 1993, Nitrogen-15 and oxygen-18 characteristics of nitrous oxide: a global perspective, Science, 262: 1855-1857.

Knowles, R. 1982, Denitrification, Microbiol. Rev., 46(1): 43-70.

Kock, A., Schafstall, J., Dengler, M., Brandt, P. and Bange, H. W. 2011, Sea-to-air and diapycnal nitrous oxide fluxes in the eastern tropical North Atlantic Ocean, Biogeosciences Discuss., 8: 10229-10246. 10.5194/bgd-8-10229-2011.

Konneke, M., Bernhard, A. E., de la Torre, J. R., Walker, C. B., Waterbury, J. B. and Stahl, D. A. 2005, Isolation of an autotrophic ammonia-oxidizing marine archaeon, Nature, 437: 543–546. doi:10.1038/nature03911.

Kroeze, C., Mosier, A. R. and Bouwman, L. 1999, Closing the global N2O budget: a retrospective analysis 1500-1994, Global Biogeochemical Cycles, 13: 1-8.

Kroeze C. 1999, Closing the global N_2O budget: a retrospective analysis 1500–1994, Global Biogeochem. Cycles, 13: 1–8.

Kroopnick, P. and Craig, H. 1972, Atmospheric oxygen: isotopic composition and solubility fractionation, Science, 175: 54-55.

Kroopnick, P. and Craig, H., 1976, Oxygen isotope fractionation in dissolved oxygen in the deep sea, Earth and Planetary Science Letters, 32: 375- 388.

Kuypers, M. M., Lavik, G., Wo¨bken, D., Schmid, M., Fuchs, B. M., Amann, R., Jorgensen, B. B. and Jetten, M. S. M. 2005, Massive nitrogen loss from the Benguela upwelling system through anaerobic ammonium oxidation, Proc. Natl. Acad. Sci. U. S. A., 102(18): 6478–6483.

Kumar, S., Nicholas, D. J. D. and Williams, **E. H.** 1983, Definitive ^{15}N NMR evidence that water serves as a source of O during nitrite oxidation by Nitrobacteragilis, FEBS Lett., 152: 71– 74.

Kumar, P. S. And Prasad, T. G. 1999, Formation and spreading of Arabian Sea high salinity water mass, J. Geophys. Res., 104: 1455 – 1464.

Morrison, J. M. 1997, Inter-monsoonal changes in the ts properties of the near-surface waters of the northern Arabian Sea, Geophys. Res. Lett., 24: 2553 – 2556.

Lal, S. and Patra, **K. P.** 1998, Variabilities in the fluxes and annual emissions of nitrous oxide from the Arabian Sea, Global Biogeochem. Cycles., 12: 321-327.

Lal, S., Patra, K. P., Venkataramani, S. and Sarin, M. M. 1996, Distribution of nitrous oxide and methane in the Arabian Sea, Current Sci., 71: 894-899.

Lam, P., Lavik, G., Jensen, M. M., van de Vossenberg, J., Schmid, M., Woebken, D., Dimitri, G., Amann, R., Jetten, M. S. M. and Kuypers, M. M. M. 2009, Revising the nitrogen cycle in the Peruvian oxygen minimum zone, P. Natl. Acad. Sci. USA, 106: 4752– 4757. doi:10.1073/pnas.0812444106.

Law, C.S. and Owens, **N. J. P.** 1990, Significant flux of atmospheric nitrous oxide from the northwest Indian Ocean, Nature, 346: 826-828.

Law, C. and Ling, **R. D.** 2001, Nitrous oxide flux and response to increased iron availability in the Antarctic Circumpolar Current, Deep-Sea Research II, 48: 2509–2527.

Law, C. S., E. R. Abraham, A. J. Watson, and Liddicoat, M. I. 2003, Vertical eddy diffusion and nutrient supply to the surface mixed layer of the Antarctic Circumpolar Current, J. Geophys. Res., 108(C8), 3272, doi:10.1029/2002JC001604.

Liss, P. S. 1973, Processes of gas exchange across an air-water interface, Deep Sea Res., 20: 221-238.

Liss, P. S. 1983, Gas transfer: experiments and geochemical implications. In *Air-Sea Exchange of Gases and Particles*, ed. PS Liss, WG Slinn, pp. 241–99. Dordrecht, The Netherlands: Reidel

Liss, P. S. and Merlivat, L. 1986, Air– sea gas exchange rates: Introduction and synthesis, in The Role of Air– Sea Exchange in Geochemical Cycling, edited by P. Buat-Me´nard, pp. 113 – 127, Springer, New York.

Lobert, J. M., J. H. Butler, L. S. Geller, S. A. Yvon, S. A. Montzka, R. C. Myers, A. D. Clarke, and J. W. Elkins .1996. BLAST 94: Bromine Latitudinal Air/Sea Transect 1994: Report on oceanic measurements of methyl bromide and other compounds, NOAA Tech. Memo ERL CMDL-10, Natl. Oceanic and Atmos. Admin., Silver Spring, Md.

Loescher, C. R., Kock, A., Koenneke, M., LaRoche, J., Bange, H. W., Schmitz, R. A. 2012, Production of oceanic nitrous oxide by ammonia-oxidizing archaea, Biogeosci. Discuss., 9: 2095–2122.

Loscher, C. R.: Sensitivity to the biological oceanic nitrogen cycle ¨ to changes in dissolved oxygen, PhD, Microbiology, Christian Albrechts University, Kiel, Kiel, 120 pp., 2011.

Madhupratap, M., M. Gauns, N. Ramaiah, S. Prasanna Kumar, P. M. Muraleedharan, S. N. de Souza, S. Sardesai, and U. Muraleedharan, Biogeochemistry of the Bay of Bengal: Physical, chemical and primary Productivity characteristics of the central and western Bay of Bengal during summer monsoon, Deep-Sea Res. II.

Maheshwaran, P.A., G. Rajesh, C, Revichandran, and Nair. K. K. C. 1999, Upwelling and associated hydrography along the west coast of India during southwest monsoon. PORSEC Proceedings, Vol (2); 873-878.

Mantoura, R. F. C., Law, C. S., Owens, N. J. P., Burkill, P. H., Woodward, E. M. S., Howland, R. J. M. and Llewellyn, C. A. 1993, Nitrogen biogeochemical cycling in the north-western Indian Ocean, Deep Sea Res.,Part H, 40: 651-671.

Martens-Habbena, W., Berube, P. M., Urakawa, H., de la Torre, J. R. and Stahl, D. A. 2009, Ammonia oxidation kinetics determine niche separation of nitrifying Archaea and Bacteria, Nature, 461: 976–979. doi:10.1038/nature08465.

Matsumoto, K. 2007, Radiocarbon-based circulation age of the world oceans, Journal of Geophysical Research – Oceans, 112 (C9), doi:10.1029/2007JC004095.

Matthews, E. 1994, Nitrogenous fertilizers: Global distribution of consumption and associated emissions of nitrous oxide and ammonia, Global Biogeochem. Cycles, 8: 411-439. doi:10.1029/94GB01906.

McCartney, M. 1977, A voyage of discovery (Supplement to Deep-Sea Research, George Beacon 70th Anniversary Volume. ed). Pergamon, Oxford

McCreary, J. P., Kundu, P. K. and Molinari, R. L. 1993, A numerical investigation of dynamics, thermodynamics and mixed layer processes in the Indian Ocean, Prog. Oceanogr., 31: 18– 244. doi:10.1016/0079- 6611(93)90002-U

McGillis, W. R., Edson, J. B., Ware, J. D., Dacey, J. W. H., Hare, J. E., Fairall, C. W. and Wanninkhof, R. 2001, Carbon dioxide flux techniques performed during GasEx 98, Mar. Chem., 75: 267– 280.

McIlvin, M. R., Casciotti, K. L. 2010, Fully automated system for stable isotopic analyses of dissolved nitrous oxide at natural abundance levels, Limnol. Oceanogr., 8: 54–66.

Metz, B., Davidson, O. R., Bosch, P. R., Dave, R. and Meyer, L. A. (eds.) 2007. Climate change 2007. Mitigation of climate change: Contribution of Working Group III to the fourth assessment report of the Intergovernmental Panel on Climate Change. Cambridge: Cambridge University Press

Meybeck, M. 1993, C, N, P and S in rivers: from sources to global inputs. Interactions of C, N, P and S biogeochemical cycles and global change, Springer-Verlag, Berlin, 163–193.

Michotey, V. and Bonin, P. 1997, Evidence for anaerobic bacterial processes in the water column: denitrification and dissimilatory nitrate ammonification in the northwestern Mediterranean Sea, Mar. Ecol. Prog. Ser., 160: 47–56.

Millero Frank, J. *Chemical Oceanography (Third Edition)* CRC Press, 2005, 520 p, ISBN 0849322804.

Montzka, S. A., Dlugokencky, E. J. and Butler, J. H. 2011, Non-CO2 greenhouse gases and climate change, Nature, 476: 43–50.

Morell, J. M., Capella, J., Mercado, A., Bauz´a, J. and Corredor, **J. E.** 2001, Nitrous oxide fluxes in Carribean and tropical Atlantic waters: evidence for near surface production, Marine Chemistry, 74 (2-3): 131–143.

Morrison, J. M., Codispoti, L. A., Gaurin, S., Jones, B., Manghanani, V. and Zheng, Z. 1998, Seasonal variations of hydrographic and nutrient fields during the US JGOFS Arabian Sea Process Study, Deep-Sea Res. Pt. II, 45: 2053–2101.

Morrison, J. M., Codispoti, L. A., Gaurin, S., Jones, B., Manghanani, V. and Zheng, Z. 1998, Seasonal variation of hydrographic and nutrient fields during the US JGOFS Arabian Sea Process Study, Deep-Sea Res. II, 45: 2053–2101.

Morrison, J. M., Codispoti, L. A., Smith, S. L., Wishner, K., Flagg, C., Gardner, W. D., Gaurin, S., Naqvi, S. W. A., Manghnani, V., Prosperie, L., and Gundersen, J. S. 1999, The oxygen minimum zone in the Arabian Sea during 1995, Deep-Sea Res. Pt. II, 46: 1903– 1931.

Morrison, J. M. 1997, Inter-monsoonal changes in the ts properties of the near-surface waters of the northern Arabian Sea, Geophys. Res. Lett., 24: 2553 – 2556.

Mosier A., C. Kroeze, C. Nevison, O. Oenema, S. Seitzinger, and O. van Cleemput, 1998 , Closing the global N2O budget: nitrous oxide emissions through the agricultural nitrogen cycle - OECD/IPCC/IEA phase II development of IPCC guidelines for national greenhouse gas inventory methodology. Nutrient Cycling in Agroecosystems 52 (2-3): 225-248

Naik, H. and Naqvi S. W. A.: Sedimentary nitrogen cycling over the western continental shelf of India, EOS – Trans American Geophysical Union, 83, OSM Suppl., OS12I-05, 2002.

Naik, H., Naqvi, S. W. A., Suresh, T. and Narvekar, **P.V.,** 2008, Impact of tropical cyclone on biogeochemistry of the central Arabian Sea, Global Biogeochemical Cycles, 22: GB3020.

Naqvi, S. W. A. 1987, Some aspects of the oxygen deficient conditions and denitrification in the Arabian Sea, J. Mar. Rev., 45: 1049-1072.

Naqvi, S.W.A., R.J., Noronha, K., Somasundar, and Sengupta. R. 1990, Seasonal changes in the denitrification regime of the Arabian Sea. Deep- Sea Research, 37, 693-711

Naqvi, S. W. A. and Noronha, **R. J.** 1991, Nitrous oxide in the Arabian Sea, Deep Sea Res., Part A, 38: 871-890.

Naqvi, S. W. A. 1991, Geographical extent of denitrification in the Arabian Sea in relation to some physical processes, Oceanology. Acta, 14: 281-290.

Naqvi, S. W. A., Noronha, R. J., Shailaja, M. S., Somasundar, K. and Sen Gupta, R. 1992, Some aspects of the nitrogen cycling in the Arabian Sea; In: *Oceanography of the Indian Ocean* (ed) B N Desai (New Delhi: Oxford & IBH) pp. 285-311

Naqvi, S. W. A. and Shailaja, M. S. 1993, Activity of the respiratory electron transport system and respiration rates within the oxygen minimum layer of the Arabian Sea, Deep-Sea Res. I1, 40: 687-695.

Naqvi, S. W. A. 1994, Denitrification in the Arabian Sea , Proc. Indian Acad. Sc. (Earth Planet. Sci.), Vol. 1, No. 2. 279-300.

Naqvi, S. W. A., Jayakumar, D. A., Nair, M., Kumar, M. D. and George, M. D. 1994, Nitrous oxide in the western Bay of Bengal, Mar. Chem., 47: 269–278.

Naqvi, S. W. A., Yoshinari, T., Brandes, J. A., Devol, A. H., Jayakumar, D. A., Narvekar, P. V., Altabet, M. A. and Codispoti, L. A. 1998a, Nitrogen isotopic studies in the suboxic Arabian Sea, Proc. Indian Acad. Sci. (Earth Planet. Sci.), 107(4): 367–378.

Naqvi, S. W. A., Yoshinari, T., Jayakumar, D. A., Altabet, M. A., Narvekar, P. V., Devol, A. H., Brandes, J. A. and Codispoti L. A. 1998b, Budgetary and biogeochemical implications of N_2O isotope signatures in the Arabian Sea, Nature, 394: 462– 464.

Naqvi, S. W. A., Jayakumar, D. A., Narveka, P. V., Naik, H., Sarma, V. V. S. S., D'Souza, W., Joseph, S. and George, M. D. 2000, Increased marine production of N_2O due to intensifying anoxia on the Indian continental shelf, Nature, 408: 346-349.

Naqvi, S. W. A., Bange, H. W., Gibb, S. W., Goyet, C., Hatton, A. D. and Upstill-Goddard, R. C. 2005, Biogeochemical ocean atmosphere transfers in the Arabian Sea, Prog. Oceanogr., 65: 116–144.

Naqvi, S. W. A., Naik, H., Pratihary, A., D'Souza, W., Narvekar, P. V., Jayakumar, D. A., Devol, A. H., Yoshinari, T. and Saino, T. 2006, Coastal versus open-ocean denitrification in the Arabian Sea, Biogeosciences, 3: 621–633. doi:10.5194/bg-3-621-2006

Naqvi, S. W. A. and Unnikrishnan, A. S. 2009, Hydrography and biogeochemistry of the coastal ocean *In* "*Surface ocean – Lower atmosphere processes*. eds. by: Le Quere, C.; Saltzman, E.S.", 233-250p.

Naqvi, S. W. A., Naik, H., Jayakumar A., Pratihary A. K., Narvekar, G., Kurian S., Agnihotri, R., Shailaja, M. S. and Narvekar, P. 2009, Seasonal anoxia over the western continental shelf Indian Ocean Biogeochemical Processes and Ecological Variability, Geoph. Monog. Series, 185, 333–345.

Naqvi, S. W. A., Bange, H. W., Far´ıas, L., Monteiro, P. M. S., Scranton, M. I. and Zhang, J. 2010, Marine hypoxia/anoxia as a source of CH_4 and N_2O, Biogeosciences, 7: 2159–2190, doi:10.5194/bg- 7-2159-2010

Nevison, C., Weiss, R. F. and Erickson III, D. J. 1995, Global oceanic emissions of nitrous oxide, Journal of Geophysical Research, 100 (C8), 809–815.

Nevison, C., Butler, J. H., and Elkins, J. W. 2003**,** Global distribution of N_2O and the Delta N_2O-AOU yield in the subsurface ocean**,** Global Biogeochemical Cycles, 17: DOI: 10.1029/GB002110.

Nevison, C. D., Lueker, T. J. and Weiss, R. F. 2004, Quantifying the nitrous oxide source from coastal upwelling, Global Biogeochem. Cycles, 18: GB 1018. DOI: 10.1029/2003GB002110,

Nicol, G. W. and Schleper, C. 2006, Ammonia-oxidising crenarchaeota: important players in the nitrogen cycle, Trends Microbiol., 14: 207.

Nightingale, P. D., Liss, P. S. and Schlosser, P. 2000a, Measurements of air-sea gas transfer during an open ocean algal bloom, Geophys. Res. Lett., 27: 2117 – 2120.

Nightingale, P. D., Malin, G., Law, C. S., Watson, A. J., Liss, P. S., Liddicoat, M. I., Boutin, J. and Upstill-Goddard, R. C. 2000b, In situ evaluation of air-sea

gas exchange parameterizations using novel conservative and volatile tracers, Global Biogeochem. Cycles, 14: 373– 387.

Nightingale, P. D. 2009, Air-Sea Gas Transfer, in Lower Atmosphere Surface Ocean Interactions eds le Quere and Saltzman, AGU Monograph 187: 69-98.

NOAA National Climatic Data Center, State of the Climate: Global Analysis for September 2014, published online October 2014, retrieved on May 5, 2015, fromhttp://www.ncdc.noaa.gov/sotc/global/201409.

NOAA National Climatic Data Center, State of the Climate: Global Analysis for September 2014, published online October 2014, retrieved on June 10, 2017, fromhttp://www.ncdc.noaa.gov/sotc/global/201409

Nunn, P.D. 1999. Environmental Change in the Pacific Basin: chronologies, causes, consequences. Wiley, London.

Olivier, J. G. J., Bouwman, A. F., Van der Hoek, K. W., Berdowski, J. J. M. 1998, Global air emission inventories for anthropogenic sources of NO_x, NH_3, and N_2O in 1990, Environ. Poll., 102: 135–148.

Olson, R. J. 1981, Differential photoinhibition of marine nitrifying bacteria: A possible mechanism for the formation of the primary nitrite maximum, Journal of Marine Research, 39: 227–238.

Oschlies, A., Schulz, K. G., Riebesell, U. and Trimmer, M. 2008, Simulated 21st century's increase in oceanic suboxia by CO_2 –enhanced biotic carbon export, Global Biogeochemical Cycles, vol 22: GB4008. doi:10.1029/2007GB003147.

Ostrom, N. E., Russ, M. E., Popp, B., Rust, T. M. and Karl, D. M. 2000, Mechanisms of nitrous oxide production in the subtropical North Pacific based on determinations of the isotopic abundances of nitrous oxide and di-oxygen, Chemosphere Global Change Sci., 2(3– 4): 281– 290.

Oudot, C., Andrei, C. and Montel, Y. 1990, Nitrous oxide production in the tropical Atlantic Ocean, Deep Sea Research Part A, Oceanographic Research Papers, 37: 183-202. 10.1016/0198-0149(90)90123-D

Oudot, C., Jean-Baptiste, P., Fourre´, E., Mormiche, C., Guevel, M., Ternon, J. F. and Le Corre, P. 2002, Transatlantic equatorial distribution of nitrous oxide and methane, Deep-Sea Res. I, 49: 1175–1193.

Owens, N. J. P. 1993, Nitrate cycling in marine waters. Nitrate: Processes, Patterns and Management, Wiley press, 169-209.

Paerl, H. W. and Prufert, **L. E.** 1987, Oxygen-poor microzones as potential sites of N2 fixation in nitrogen-depleted aerobic marine waters, Appl. Environ. Microbiol., 53: 1078– 1087.

Pataki, D. E., Ehleringer, J. R., Flanagan, L. B., Yakir, D., Bowling, D. R., Still, C. J., Buchmann, N., Kaplan, J. O. and Berry, **J. A.** 2003, The application and interpretation of Keeling plots in terrestrial carbon cycle research, Global Biogeochem. Cycles, 17(1): 1022. doi:10.1029/2001GB001850.

Patra, P. K., Lal S., Venkataramani, S., de Dousa, S. N., Sarma, V. V. S. S., and Sardesai, S. 1999, Seasonal and spatial variability in N_2O distribution in the Arabian Sea, Deep-Sea Research I, 46: 529-543.

Patra, P. K., Maksyutov, S. and Nakazawa, T. 2004, Severe weather conditions in the Arabian Sea and their impact on atmospheric N_2O budget, Indian Journal of Marine Science, 33(1): 84-94.

Patra, P. K., Kumar, M. D., Mahowald, N. and Sarma, V. V. S. S. 2007, Atmospheric deposition and surface stratification as controls of contrasting chlorophyll abundance in the North Indian Ocean, J. Geophys. Res., 112: C05029. doi:10.1029/2006JC003885

Payne, W. J. 1973, Reduction of nitrogenous oxides by microorganisms, Bacteriol. Rev., 37: 409–452.

Pickard, G. L. and Emery, W. J. 1990, Descriptive Physical Oceanography, Pergamon Press.

Pierotti D. and Rasmussen, R. A. 1980, Nitrous oxide measurements in the eastern tropical Pacific Ocean, Tellus, 32: 56-72.

Popp, B. N., Westley, M. B., Toyoda, S., Miwa, T., Dore, J. E., Yoshida, N., Rust, T. M.,Sansone, F. J., Russ, M. E., Ostrom, N., and Ostrom, P. H. 2002, Nitrogen and oxygen isotopomeric constraints on the origins and sea-to-air flux of N_2O in the oligotrophic subtropical North Pacific gyre, Global Biogeochem. Cycles, 16(4), 1064, doi:10.1029/2001GB001806.

Poth, M. and Focht, D. D. 1985, 15N kinetic analysis of N_2O production by Nitrosomonaseuropea: An examination of nitrifier denitrification. Applied and Environmental Microbiology, 49: 1134-1141.

Prasad, T. G. and Ikeda, M. 2002a, The winter-time water mass formation in the northern Arabian Sea: A model study, J. Phys. Oceanogr., 32: 1028–1040.

Prasad, T. G. and M. Ikeda (2002b), A numerical study of the seasonal variability of Arabian Sea high-salinity water, J. Geophys. Res., 107(C11): 3197. doi:10.1029/2001JC001139

Prasad,T . G., Ikeda, M. and Prasanna K. S. 2001, Seasonal spreading of the Persian Gulf Water mass in the Arabian Sea, .J. Geophys. Res., 106: 17,059-17, 071.

Prasanna Kumar, S., Madhupratap, M., Dileep Kumar, M., Muraleedharan, P. M., de Souza, S. N., Gauns, M. and Sarma, V. V. S. S. 2001, High biological productivity in the central Arabian Sea during summer monsoon driven by Ekman pumping and lateral advection, Curr. Sci., 81: 1633–1638.

Prather, M., Ehhalt, D., Dentener, F., Derwent, R., Dlugokencky, E., Holland, E., Isaksen, I., Katima, J., Kirchhoff, V., Matson, P., Midgley, P., and Wang, M. 2001, Atmospheric chemistry and greenhouse gases. Climate change 2001: The scientific basis. Contribution of working group I to the third assessment report of the intergovernmental panel on climate change, (Houghton, J. T., Ding, Y., Griggs, D. J., Noguer, M., Van der Linden, P. J., Dai, X., Maskell, K., and Johnson, C. A., eds.). Cambridge University Press, Cambridge, UK. pp. 239–287

Prinn, R. G., Weiss, R. F., Fraser, P. J., Simmonds, P. G., Cunnold, D. M., Alyea, F. N., O'Doherty, S. O., Salameh, P., Miller, B. R., Huang, J., Wang, R. H. J., Hartley, D. E., 2000, A history of chemically and radiatively important gases in air deduced from ALE/GAGE/AGAGE, J. Geophys. Res., 105(D14): 17751–17792.

Punshon, S., and Moore, R. M. 2004, Nitrous oxide production and consumption in a eutrophic coastal embayment, Marine Chemistry, 91 (1-4), 37–51, doi:10.1016/ j.marchem.2004.04.003, 2004.

Qasim, S. Z. 1977, Biological productivity of the Indian Ocean, *Indian J Mar Sci*, 6, 122-137

Quay, P. D., Emerson, S., Wilbur, D. O., Stump, C. 1993, The $d^{18}O$ of dissolved O_2 in the surface waters of the subarctic Pacific: a tracer of biological productivity, Journal of Geophysical Research, 98: 8447-8458.

Rahn, T and Wahlen, M. 1997, Stable isotope enrichment in stratospheric nitrous oxide; Science 278 1776-1778

Rahn, T. and Wahlen, M. 2000, A reassessment of the global isotopic budget of atmospheric nitrous oxide, Global Biogeochem. Cycles, 14, 537–543.

Rao, G. D., Rao, V. D., Sarma, V. V. S. S. 2013, Distribution and air‐sea exchange of nitrous oxide in the coastal Bay of Bengal during peak discharge period (southwest monsoon), Mar. Chem., 155: 1‐9.

Ramaswamy, V. In Climate Change 2001: The ScientiÞc Basis (Working Group I to the Third Assessment Report of the IPCC, Cambridge Univ. Press, Cambridge, 2001), pp. 349-416.

Ravishankara, A. R., Daniel, J. S. and Portmann, **R. W.** 2009, Nitrous oxide (N2O): The dominant ozone-depleting substance emitted in the 21st century, Science, 326: 123–125. doi:10.1126/science.1176985

Redfield, A. C. 1958, The biological control of chemical factors in the environment, American Scientist, 46(3): 230A-221.

Rees, A. P., Brown, I. J., Clark, D. R. and Torres, R. 2011, The Lagrangian progression of nitrous oxide within filaments formed in the Mauritanian upwelling, Geophys. Res. Lett., in press, 10.1029/2011GL049322

Richards, F. A. 1965, Anoxic basins and Fjords: In: *Chemical Oceanography* vol. 1(eds) J P Riley and G Skirrow (New York: Academic Press) pp. 611-645.

Richardson, D. J. 2000, Bacterial respiration: a flexible process for a changing environment, Microbiology, 146: 551–571.

Riley, J. P. and Chester, R. 1971, Introduction to Marine Chemistry, Academic Press, London, 465.

Ritchie, G. A. F. and Nicholas, D. J. D. 1972, Identification of the sources of nitrous oxide produced by oxidative and reductive processes in Nitrosomonaseuropaea, Biochemical. Journal., 126: 1181–1191.

Rhee, T. S., Kettle, A. J. and Andreae, M. O. 2009, Methane and nitrous oxide emissions from the ocean: A reassessment using basin-wide observations in the Atlantic, J. Geophys. Res., 114: D12304. doi:10.1029/2008JD011662

Robinson, A. D., Nedwell, D. B., Harrison, R. M. And Ogilvie, B. G. 1998, Hypernutrified estuaries as sources of N2O emission to the atmosphere: the estuary of the River Colne, Essex, UK.

Rodhe, H. A. 1990, Comparison of the Contribution of Various Gases to the Greenhouse Effect. In Science, 248, Stockholm University Press, Sweden,1217-19

SanilKumar, V., Ashok Kumar, K. and Raju, N. S. N. 2004, Wave characteristics off Visakhapatnam coast during cyclone, Curr Sci., 86: 1524–1529.

Santoro, A. E., Casciotti, K. L. and Francis, C. A. 2010, Activity, abundance and diversity of nitrifying archaea and bacteria in the central California Current, Environ. Microbiol., 12: 1989–2006. doi:10.1111/j.1462-2920.2010.02205.x

Schleper, C., Jurgens, G. and Jonuscheit, M. , 2005**,** Genomic studies of uncultivated archaea, Nat. Rev. Microbiol., 3; 479–488. doi:10.1038/nrmicro1159

Schmidt, H. L., Werner, R. A., Yoshida, N. and Well, R. 2004, Is the isotopic composition of nitrous oxide an indicator for its origin from nitrification or denitrification? A theoretical approach from referred data and microbiological and enzyme kinetic aspects. Rapid Communication Mass Spectrometry, 18: 2036–2040.

Schmittner, A., Oschlies, A., Matthews, H. D. and Galbraith, E. D. 2008, Future changes in climate, ocean circulation, ecosystems, and biogeochemical cycling simulated for a business-as usual CO_2 emission scenario until year 4000 AD, Global Biogeochemical Cycles, 22: GB1013. doi:10.1029/2007GB002953.

Schropp, S. J. and Schwarz, J. R. 1983, Nitrous oxide production by denitrifying microorganisms from the Eastern Tropical North Pacific and the Caribbean Sea. Geomicrobiol. J., 3: 17-31.

Schulz, H., Von Rad, U. and Erlenkeuser, H. 1998, Correlation between Arabian Sea and Greenland climate oscillations of the past 110,000 years, Nature, 939: 54–57.

Seitzinger, S. P. and Nixon, S. W. 1985, Eutrophication and the rate of denitrification and N_2O production in coastal marine sediments, Limnology and Oceanography, 30:1332-1339.

Seitzinger, S. P.1990, Denitrification in aquatic sediments. In: N.P. Revsbech and J. Sorensen, (editors), Denitrification in soil and sediment. Plenum Press. pp. 301-322.

Seitzinger, S. P. and Kroeze, C. 1998, Global distribution of nitrous oxide production and N inputs in freshwater and coastal marine ecosystems, Global Biogeochemical Cycles, 12: 93-113.

Seitzinger, S. P., Kroeze, C., Styles, R. V., 2000, Global distribution of N_2O emissions from aquatic systems: natural emissions and anthropogenic effects, Chemosphere: Global Change Science, 2: 267-279.

Shankar, D. and S. R. Shetye 1997, On the dynamics of the Lakshadweep high and low in the southeastern Arabian Sea, J. Geophys. Res., 102: 12,551 – 12,562. doi:10.1029/97JC00465.

Shankar, D., P. N. Vinayachandran, Unnikrishnan, A. S. 2002. The monsoon currents in the North Indian Ocean. Progress in Oceanography, 52, 63–120.

Sharma, G. S. 1966, Thermocline as an indicator of upwelling. J. of Mar. Bio. Ass. India. 8(1); 8-19.

Shaw, L. J., Nicol, G. W., Smith, Z., Fear, J., Prosser, J. I. and Baggs, E. M. 2006, Nitrosospira spp. can produce nitrous oxide via a nitrifier denitrification pathway, Environmental Microbiology, 8: 214-222.

Shenoy, S.C., Shanker, D, Gopalakrishna V.V, Durand, F. 2005, Role of ocean in the genesis and annihilation of the core of the warm pool in the southeastern Arabian Sea. Mausam, 56, 1, 147-160.

Shenoy, D. M., Naik, H., Kurian, S. and Naqvi, S. W. A. 2011, Time Series Observations in the northern Indian Ocean, IMBER News Letter, new Delhi, Issue No. 9.

Shetye, S.R. and Shenoi, S.S.C. 1988, Seasonal cycle of surface circulation in the coastal north Indian Ocean. Proc. Ind. Acad. Of Sci. (Earth and Planetary Sci. 97:53-62.

Shoda, **M**. 2017, Heterotrophic Nitrification and Aerobic Denitrification by Alcaligenes faecalis No. 4, Ivan X. Zhu, ISBN 978-953-51-3300-1, Print ISBN 978-953-51, DOI: 10.5772/68052.

Siedler, G. and H. Peters 1986, Properties of seawater, in Oceanography, Landolt-Bo¨rnstein New Ser., vol. 3a, edited by J. Su¨ndermann, pp. 233 – 264, Springer-Verlag, New York

Signorini, S. R., Murtugudde, R. G., McClain, C. R., Christian, J. R., Picaut, J. and Busalacchi, A. J. 1999, Biological and physical signatures in the tropical and subtropical Atlantic, J. Geophys. Res. - Oceans, 104: 18367-18382.

Skiba, U. and Smith, K. A. 2000, The control of nitrous oxide emissions from agricultural and natural soils, Chemosphere**,** 23: 79–86.

Smith, M. S. and Zimmermann, K. 1981, Nitrous oxide production by nondenitrifying soil nitrate reducers, Soil Sci. Soc. Am. J., 45: 865-871.

Smith, L. C., de Klein, C. A. M., Monaghan, R. M., Catto, W. D. 2008, The effectiveness of DCD in reducing nitrous oxide emissions from cattle grazed winter forage crop in Southland, New Zealand, Australian Journal of Experimental Agriculture, 48: 160-164.

Sprintall, J. and Tomczak, M. 1993, On the formation of central water and thermocline ventilation in the southern hemisphere, Deep Sea Research Part I: Oceanographic Research Papers, 40(4): 827-848.

Stanton, B. R. and Ridgway, N. M. 1988, An oceanographic survey of the subtropical convergence zone in the Tasman Sea, New Zealand journal of Marine and Freshwater research, 22: 583-593.

Steffen, M. 1990, A simple method for monotonic interpolation in one dimension, Astronomy and Astrophysics, 239: 443–450.

Stein, L. Y. and Yung, Y. L. 2003, Production, isotopic composition, and atmospheric fate of biologically produced nitrous oxide, Ann. Rev Earth Planet. Sci., 31: 329–356.

Stephen, M., Chiswell, S. M., Bostock, H. C., Sutton, P. J. H. and Williams, M. J. M. Physical Oceanography of the deep seas around New Zealand-2014: a review, New Zealand Journal of Marine and Freshwater Research.

Stephen, P. and Robert, M. M. 2004, A stable isotope technique for measuring production and consumption rates of nitrous oxide in coastal waters, Marine Chemistry, 86: 159– 168.

Stramma, L., Fischer, J. and Schott, F. 1996, The flow field off southwest India at 8 N during the southwest monsoon of August 1993, J. Mar. Res., 54: 55–72.

Stramma, S., Brandt, P., Schott, F., Quadfasel, D. and Fisher, J. 2002, Winter and summer monsoon water mass, heat and freshwater transport changes in the Arabian Sea near 8N, Deep Sea Res., Part II, 49: 1173 – 1195.

Stramma, L., Johnson, G. C., Sprintall, J. and Mohrholz, V. 2008, Expanding oxygen-minimum zones in the tropical oceans, Science, 320: 655-658. DOI: 10.1126/science.1153847.

Strous, M., Fuerst, J. A., Kramer, E. H. M., Logemann, S., Muyzer, G., Van de Pas-schoonen, K. T., Webb, R., Kuenen, G. G. and Jetten, M. S. M. 1999, Missing lithotroph identified as new planctomycetes, Nature, 400: 446–449.

Suntharalingam, P. and Sarmiento, J. L. 2000, Factors governing the oceanic nitrous oxide distribution: Simulations with an ocean general circulation model. Global Biogeochemical Cycles 14(1): doi: 10.1029/1999GB900032. ISSN: 0886-6236

Sutka, R. L., Ostrom, N. E., Ostrom, P. H., Gandhi, H. and Breznak, J. A. 2003, Nitrogen isotopomer site preference of N_2O produced by Nitrosomonaseuropaea and Methylococcuscapsulatus Bath, Rapid Commun. Mass Spectrom., 17(7): 738– 745.

Sutka, R. L., Ostrom, N. E., Ostrom, P. H., Gandhi, H. and Breznak, J. A. 2004a, Erratum, Nitrogen isotopomer site preference of N_2O produced by Nitrosomonaseuropaea and Methylococcuscapsulatus Bath, Rapid Commun. Mass Spectrom., 18(12), 1411 –1412.

Sutka, R. L., Ostrom, N. E., Ostrom, P. H. and Phanikumar, M. S. 2004b, Stable nitrogen isotope dynamics of dissolved nitrate in a transect from the North

Pacific Subtropical Gyre to the Eastern Tropical North Pacific, Geochim. Cosmochim. Acta, 68: 517–527.

Sutka, R. L., Ostrom, N. E., Ostrom, P. H., Breznak, J. A., Gandhi, H., Pitt, A. J. and Li, F. 2006, Distinguishing nitrous oxide production from nitrification and denitrification on the basis of isotopomer abundances, Appl. Environ. Microbiol., 72: 638–644.

Sutton, P. J. H. 2003, The Southland Current: a Subantarctic current, New Zealand Journal of Marine and Freshwater Research, 37: 645-652.

Sverdrup, H. U., Johnson, M. W. and Fleming, R. H. 1942, The Oceans: Their Physics, Chemistry, and General Biology Englewood Cliffs, New Jersey, Prentice-Hall.

Swallow, J. C., Fieux, M. and Schott, F. 1988, The boundary currents east and north of Madagascar, Part I: Geostrophic currents and transports, Journal of Geophysical Research, 93: 4951–4962.

Thamdrup, B., Jensen, M. M., Dalsgaard, T., Ulloa, O., Farias, l. and Escribano, R. 2006, Anaerobic ammonium oxidation in the oxygen-deficient waters off northern Chile, Limnol. Oceanogr., 51: 2145–2156.

Thomas, H., Bozec, Y., Elkalay, K. and de Baar, H. J. W. 2004, Enhanced open ocean storage of co2 from shelf sea pumping, Science, 304: 1005–1008.

Tomczak, M. and Godfrey, J. S. 1994, Regional Oceanography: An introduction. Oxford, Pergamon. 422 p.

Tomczak, M. and Godfrey, J. S. 2001, Regional Oceanography: An introduction.(http://www.geo.unibremen.de/~apau/proper3/library/tomczak_godfrey_994.pdf).

Tomczak, Matthias and J Stuart Godfrey: Regional Oceanography: an Introduction 2nd edition (2003), Daya Publishing House, Delhi. ISBN: 8170353068.

Toyoda, S. and Yoshida 1999, Determination of nitrogen isotopomers of nitrous oxide on a modified isotope ratio mass spectrometer, Anal. Chem., 71(20): 4711 –4718.

Toyoda, S., Yoshida, N., Miwa, T., Matsui, Y., Yamagishi, H., Tsunogai, U., Nojiri, Y. and Tsurushima, N. 2002, Production mechanism and global budget of N_2O inferred from its isotopomers in the western North Pacific, Geophys. Res. Lett., 29(3): 1037. doi:10.1029/2001GL014311.

Toyoda, S., Mutobe, H., Yamagishi, H., Yoshida, N. and Tanji, Y. 2005, Fractionation of N_2O isotopomers during production by denitrifier, Soil Biol. Biochem., 37(8): 1535–1545. doi:10.1016/j.soilbio.2005.01.009

Treusch, A. H., Leininger, S., Kletzin, A., Schuster, S. C., Klenk, H. P. and Schleper, C. 2005, Novel genes for nitrite reductase and amorelated proteins indicate a role of uncultivated mesophilic crenarchaeota in nitrogen cycling, Environ. Microbiol., 7: 1985–1995. doi:10.1111/j.1462-2920.2005.00906.

UNEP(United Nations Environment Programme). 2004, Global Environment Outlook Year Book 2003,UNEP, Nairobi.

Upstill-Goddard, R. C., Barnes, J. and Owens, N. J. P. 1999, Nitrous oxide and methane during the 1994 SW monsoon in the Arabian Sea/northwestern Indian Ocean, J. Geophys. Res., 104: 30067– 30084.

vanNiftrik, L., Fuerst, J., SinninghDamste, J. S., Kuenen, G., Jetten, M. S. M., and Strous, M. 2004, The anammoxasome: an intracytoplasmic compartment in anammox bacteria, FEMS Microb. Lett., 233: 7–13.

Vincent, W. F., Howard-Williams, C., Tildesley, P. and Butler, E., 1991, Distribution and biological properties of oceanic water masses around the South Island, New Zealand, New Zealand Journal of Marine and Freshwater Research, 25: 21-42.

Vincent, W. F. 1992, Oceanography of the subtropical convergence zone around southern New Zealand, New Zealand Journal of Marine and Freshwater Research, 26: 131-154.

Van Hale, R. and Russell, D. F. 2010, Rayleigh distillation equations applied to isotopic evolution of organic nitrogen across a continental shelf, *Marine and Freshwater Research*, 61: 369–378.

Walker, C. B., de la Torre, J. R., Klotz, M. G., Urakawa, H., Pinel, N., Arp, D. J., Brochier-Armanet, C., Chain, P. S. G., Chan, P. P., Gollabgir, A., Hemp, J., Hugler, M., Karr, E. A., Konneke, M., Shin, M., Lawton, T. J., Lowe, T., Martens Habbena, W., Sayavedra-Soto, L. A., Lang, D., Sievert, S. M., Rosenzweig, A. C., Manning, G. and Stahl, D. A. 2010, Nitrosopumilusmaritimus genome reveals unique mechanisms for nitrification and autotrophy in globally distributed marine crenarchaea, Proceedings of the National Academy of Sciences of the United States of America, 107, 8818-8823, 10.1073/pnas.0913533107.

Walter, S., Peeken, I., Lochte, K., Webb, A., and Bange, H. W. 2005, Nitrous oxide measurements during EIFEX, the European Iron Fertilization Experiment, in the subpolar South Atlantic Ocean, Geophys. Res. Lett., 32: L 23613. doi:10.1029/2005GL024619

Walter, S., Bange, H. W., Breitenbach, U. and Wallace, D. W. R. 2006, Nitrous oxide in the North Atlantic Ocean, Biogeosciences, 3: 607–619.

Walter, S., Breitenbach, U., Bange, H. W., Nausch, G. and Wallace, D. W. R. 2006b, Distribution of N2O in the Baltic Sea during transition from anoxic to oxic conditions, Biogeosciences, 3: 557–570.

Wanninkhof, R., Ledwell, J. R. and Broecker, W. S. 1985, Gas exchange wind speed relationship measured with sulfur hexafluoride on a lake, Science, 227: 1224-1226.

Wanninkhof, R. 1992, Relationship between gas exchange and wind speed over the ocean, J. Geophys. Res., 97: 7373– 7381.

Wanninkhof, R. and McGillis, W. R. 1999, A cubic relationship between air-sea CO_2 exchange and wind speed, Geophys. Res. Lett., 26(13): 1889– 1892.

Wanninkhof, R., Asher, W., Weppernig, R., Chen, H., Schlosser, P., Langdon, C. and Sambrotto, R. 1993, Gas transfer experiment on Georges Bank using two volatile deliberate tracers, J. Geophys. Res., 98: 20, 237– 20, 248.

Wanninkhof, R. (1997), Gas exchange, dispersion, and biological productivity on the west Florida shelf: Results from a Lagrangian tracer study, Geophys. Res. Lett., 24(14), 1767– 1770.

Wanninkhof, R., Sullivan, K. F. and Top, Z. 200, Air-sea gas transfer in the Southern Ocean, J. Geophys. Res., 109: C08S19.. doi:10.1029/ 2003JC001767.

Wanninkhof, R., Asher, W. E., Ho, D. T., Sweeney, C. and McGillis, W. R. 2009, Advances in Quantifying Air-Sea Gas Exchange and Environmental Forcing, Annu. Rev. Mar. Sci., 1: 213-244. 10.1146/annurev.marine.010908.163742.

Ward, B. B. 2008, Nitrogen in the Marine Environment, eds Capone D, Bronk D, Mulholland M, Carpenter E (Elsevier, Amsterdam), 2nd ed, pp 199–262

Watson, A. J. and Ledwell, **J. R.** 2000, Oceanographic tracer release experiments using sulphur hexafluoride, Journal of Geophysical Research, 105 (C6): 14,325–14,337.

Weiss, R. F. and Price, B. A. 1980, Nitrous oxide solubility in water and seawater. Mar. Chem. 8, 347–359.

Weiss, R., F. A. Van Woy, and P. K. Salameh, Surface water and atmospheric carbon dioxide and nitrous oxide observations by shipboard automated gas chromatography: Results from expeditions between 1977 and 1999, Report – Scripps Institution of Oceanography, Reference 92-11, 1992

Westley, M. B., Yamagishi, H., Popp, B. N. and Yoshida, N. 2006, Nitrous oxide cycling in the Black Sea inferred from stable isotope and isotopomer distributions, Deep Sea Res., Part, 53: 1802. doi:10.1016/j.dsr2.2006.03.012.

Whiting, G. J. and J. P. Chanton, 2001, Greenhouse carbon balance of wetlands: Methane emission versus carbon sequestration, Tellus, 53B: 521–528.

Wollast, R. 1983, Interactions in estuaries and coastal waters,p. 385-407. In B. Bolin and R. B. Cook [eds.], The major biogeochemical cycles and their interactions. SCOPE 2 1. Wiley-Inter.science.

Wrage, N., Velthof, G. L., Van Beusichem, M. L., and Oenema, O. 2001, Role of nitrifier denitrification in the production of nitrous oxide, Soil Biol. Biochem., 33: 1723–1732.

Wuchter, C., Abbas, B., Coolen, M. J. L., Herfort, L., van Bleijswijk, J., Timmers, P., Strous, M., Teira, E., Herndl, G. H., Middelburg, J. J., Schouten, S. and Damste, J. S. S. 2006, Archaeal nitrification in the ocean, Proceedings of the National Academy of Sciences of the United States of America 103: 12317–12322.

Wyrtki, K. 1971, Oceanographic Atlas of the International Indian Ocean Expedition, National Science Foundation, Washington DC. pp. 531

Yamagishi, H. 2007, Role of nitrification and denitrification on the nitrous oxide cycle in the eastern tropical North Pacific and Gulf of California, J. Geophys. Res. Biogeosci., 112 ARTN G02015.

Yamagishi, H., Yoshida, N., Toyoda, S., Popp, B. N., Westley, M. B. and Watanabe, S. 2005, Contributions of denitrification and mixing on the distribution of nitrous oxide in the North Pacific, Geophys. Res. Lett., 32: L04603, doi:10.1029/2004GL021458.

Yamazaki, T., Yoshida, N., Wada, E. and Matsuo, S. 1987, N_2O reduction by Azotobactervinelandii with emphasis on kinetic nitrogen isotope effects, Plant Cell Physiol., 28: 263– 271.

Yamulki, S., Toyoda, S., Yoshida, N., Veldkamp, E., Grant, B. and Bol, R. 2001, Diurnal fluxes and the isotopomer ratios of N_2O in a temperate grassland following urine amendment, Rapid Commun. Mass Spectrom., 15: 1263–1269.

Yool, A., Martin, A. P., Fernandez, C., and Clark, D. R. 2007**,** The significance of nitrification for oceanic new production, Nature, 447, 999–1002, doi:10.1038/nature05885.

Yoshida, N. 1988, 15N-depleted N_2O as a product of nitrification, Nature, 335: 528– 529.

Yoshida, T. and Alexander, M. 1970, Nitrous oxide formation by Nitrosomonaseuropae and heterotrophic microorganisms, Soil Society of America. Proceedings, 34: 880-882.

Yoshida, N. and Matsuo, **S.** 1983, Nitrogen isotope ratio of atmospheric N_2O as a key to the global cycle of N_2O, Geochem. J., 17: 231– 239.

Yoshida, N., Wada, E., Hattori, A., Saino, T. and Matsuo, S. 1984, $^{15}N/^{14}N$ ratio of dissolved N_2O in the eastern tropical Pacific Ocean, Nature, 307: 442– 444.

Yoshida, N., Morimoto, H., Hirano, M., Koike, I., Matsuo, S., Wada, E., Saino, T. and Hattori, A. 1989, Nitrification rates and ^{15}N abundances of N_2O and NO_3^- in the western North Pacific, Nature, 342: 895–897.

Yoshida, N. and Toyoda, S. 2000, Constraining the atmospheric N_2O budget from intramolecular site preference in N_2O isotopomers, Nature, 405: 330– 334.

Yoshinari, T. 1976, Nitrous oxide in the sea, Mar. Chem., 4: 189– 202.

Yoshinari, T. 1990, Emissions of N_2O from various environments: The use of stable isotope compositions of N_2O as a tracer for studies of N_2O biogeochemical cycling, in Denitrification in Soils and Sediments, edited by N. P. Revsbech and J. Sorensen, pp. 195–215, Plenum, New York.

Yoshinari, T. and Wahlen, M. 1985, Oxygen isotope ratios in N_2O from nitrification at a wastewater treatment facility, Nature, 317: 349– 350.

Yoshinari, T. and Koike, I. 1994, The use of stable isotopes for the studies of gaseous nitrogen species in the marine environment. In ‘‘Stable isotopes in ecology and environmental science’’ (Lajtha, K., Michener, R. H., eds.). Blackwell Scientific, Oxford. pp. 114–137

Yoshinari, T., Altabet, M. A., Naqvi, S. W. A., Codispoti, L., Jayakumar, A., Kuhland, M. and Devol, A. 1997, Nitrogen and oxygen isotopic composition of N_2O from suboxic waters of the eastern tropical North Pacific and the Arabian Sea – measurement by continuous-flow isotope-ratio monitoring, Mar. Chem., 56: 253– 264.

Yung, Y. L. and Miller, **C. E.** 1997, Isotopic fractionation of stratospheric nitrous oxide, Science, 278: 1778– 1780.

Zhang, G. L., Zhang, J., Ren, J. L., Li, J. B. and Liu, S. M. 2008, Distributions and sea to air fluxes of Methane and Nitrous Oxide in the North East China Sea in Summer, Mar. Chem., 110(1/2): 42–55.

Zehr, J. P. and Ward, B. B. 2002, Nitrogen cycling in the ocean: New perspectives on processes and paradigms, Appl. Environ. Microbiol., 68(3): 1015–1024.

Zumft, W. G. and Ko¨rner, H. 1997, Enzyme diversity and mosaic gene organization in denitrification, Antonie Leeuwenhoek, 71: 43–58.